

MaNEP
SWITZERLAND

Materials with **N**ovel **E**lectronic **P**roperties

NATIONAL CENTRE OF COMPETENCE IN RESEARCH

PROGRESS REPORT

Year 9

April 1st 2009 – March 31st 2010

FNSNF

FONDS NATIONAL SUISSE
SCHWEIZERISCHER NATIONALFONDS
FONDO NAZIONALE SVIZZERO
SWISS NATIONAL SCIENCE FOUNDATION

Die Nationalen Forschungsschwerpunkte (NFS) sind ein Förderinstrument des Schweizerischen Nationalfonds.
Les Pôles de recherche nationaux (PRN) sont un instrument d'encouragement du Fonds national suisse.
The National Centres of Competence in Research (NCCR) are a research instrument of the Swiss National Science Foundation.

NCCR: 9th Progress Report - Cover Sheet

Title of the NCCR	Materials with Novel Electronic Properties (MaNEP)
NCCR Director	
Name, first name	Prof. Øystein Fischer
Institution address	UNIVERSITE DE GENEVE, Faculté des Sciences Département de Physique de la Matière Condensée 24 quai Ernest-Ansermet, CH-1211 Genève 4
Office phone number	022 379 62 70
E-mail	Oystein.Fischer@unige.ch

1. Executive summary [1]
2. Research
 - 2.1 Structure of the NCCR and status of integration [2]
 - 2.2 Results since the last progress report [3]
3. Knowledge and technology transfer [4]
4. Education/training and advancement of women [5]
5. Communication [6]
6. Structural aspects [7]
7. Management
 - 7.1 Activities [8]
 - 7.2 Experiences, recommendations to the SNSF
8. Reaction to the recommendations of the review panel
9. Lists
 - 9.1 Overview of personnel and functions [9]
 - 9.2 Education and training [9]
 - 9.3 Publications [9]
 - 9.4 Lectures at congresses etc. [9]
 - 9.5 Services, patents, licences, start-up companies etc. [9]
 - 9.6 Cooperation with third parties [9]
10. Statistical output data [9]
11. Finance
 - 11.1 Finance NCCR Overview [10]
 - 11.2 Funding sources [10]
 - 11.3 Allocation to projects [10]
 - 11.4 Expenditures [10]
 - 11.5 Comments on finances [11]

Contents

1	Executive summary	3
2	Research	5
2.1	Structure of the NCCR and status of integration	5
2.2	Results since the last progress report	9
	Project 1	9
	Project 2	28
	Project 3	41
	Project 4	58
	Project 5	80
	Project 6	92
	Project 7	100
	Project 8	110
	Techniques and know-how	118
3	Knowledge and technology transfer	127
4	Education, training and advancement of women	131
5	Communication & outreach	137
6	Structural aspects	141
7	Management	143
7.1	Activities	143
7.2	Experiences, recommendations to the SNSF	144
8	Reaction to the recommendations of the review panel	145
9	Lists	147
9.3	Publications	147
11	Finance	177
11.1	Finance NCCR Overview	178
11.2	Funding sources	182
11.3	Allocation to projects	183
11.4	Expenditures	186
11.5	Comments on finances	190
12	Appendix: milestones of the MaNEP projects	191

1 Executive summary

MaNEP was established in 2001 and entered into its third 4-year phase on July 1, 2009. The structure for this phase was completely changed and 8 new collaborative projects established. We also added a large number of new full members to the MaNEP Forum, whereas some earlier members either left MaNEP or continue as associated members. This report covers formally the period from July 1, 2009 until March 31, 2010. However, for the members who continue from Phase II, results obtained between April 1, 2009 and June 30, 2009 are also included. Below we summarize the most important results obtained in this first period of Phase III.

Research

Project 1. This project addresses novel properties arising at interfaces and in superlattices. The $\text{LaAlO}_3/\text{SrTiO}_3$ interface is a model system because of the superconductivity discovered earlier by MaNEP researchers. We have continued to probe this interface with several techniques resulting in a number of striking observations. Superconductivity, magnetism and ferroelectricity have been investigated in oxide multilayers and charge transfer interfaces have been studied in organic compounds.

Project 2. Here we use oxide materials and carbon based systems, such as graphene and organic semiconductors, for the realization of new nano-electronic devices. In this first period, significant progress has been made on nanoscale patterning of $\text{LaAlO}_3/\text{SrTiO}_3$ heterostructures and in integrating carbon nanotubes and ferroelectric materials. Research on graphene has resulted in several remarkable results.

Project 3. This project focuses on applied projects in collaboration with industry. In the field of superconductivity we have achieved record high values of critical currents in MgB_2 wires. In the domain of MEMS and energy harvesting, we have produced epitaxial ferroelectric layers on Si-membranes for novel transducers. An important step in the development of neutron supermirrors has been achieved. First investigations of intermetallic hydrides for hydrogen detectors have been carried out and giant piezoresistance devices have been investigated. A new surface treatment device for marking technology has been developed.

Project 4. Although the so-called classical low-temperature superconductors are well understood, since the discovery of the high-temperature superconductors 24 years ago, the field of superconductivity is confronted with a huge challenge: how to understand the cuprate superconductors and other superconducting compounds like the pnictides. This project aims at exploring the striking properties of these novel superconductors. During the first period of Phase III a number of important results are reported.

Project 5. Whereas Project 4 focuses on the most striking classes of high-temperature superconductors, Project 5 studies numerous compounds with non-conventional superconductivity and other unusual electronic phases. Among these are heavy fermion compounds and non-centro-symmetric crystals. We have started to explore this very rich field resulting in a harvest of exceptional results.

Project 6. The aim of this project is to apply a variety of complementary techniques to address some of the most intriguing problems in the modern field of quantum magnetism. The focus this year was on specific structural features: low-dimensionality geometric frustration, quenched disorder and magneto-electric coupling. What we discovered is the emergence of several qualitatively new and previously inaccessible quantum magnetic phases.

Project 7. This project aims at studying the various electronic instabilities in low-dimensional materials and their competition in stabilizing the ground state of the system. A highlight among many striking results is the finding of a fingerprint of an excitonic condensate in $1T\text{-TiSe}_2$ and the stabilization of super-

conductivity by pressure in the region of the phase diagram where the excitonic order parameters show strong fluctuations.

Project 8. Here MaNEP introduces a project where issues common to cold atomic gases and condensed matter physics are studied. During this first year, progress has been made in several directions, especially in using the cold atoms as quantum simulators for fermionic and bosonic systems. As an example, we can mention that for fermions an excellent agreement has been obtained between theory and experiment on measurements of the double occupation, allowing for a very precise determination of the temperature and entropy in the fermionic Hubbard model.

Knowledge and technology transfer

In Phase III, Project 3 represents a close collaboration with six different industrial companies. We have furthermore formalized collaboration with three other companies. This reflects a strong increase in our technology transfer efforts. Last year, MaNEP proposed to establish a new collaboration, the Geneva Creativity Center (GCC), between MaNEP and the Physics section of the University of Geneva, the engineering school, Hepia, a part of HES-SO, and the industry in Geneva. This idea is now in the phase of implementation and GCC shall probably start its activity in the fall of 2010, adding a new stimulus for technology transfer in the Lake Geneva region.

Education, training and advancement of women

The MaNEP doctoral school in Geneva entered now its second year and has become a new approach to the doctoral studies in MaNEP. This year MaNEP started collaboration with the 3^{ème} *Cycle de la Physique en Suisse Romande*. As a result MaNEP has participated in the establishment of the new doctoral program for physics of the CUSO. With this program MaNEP doctoral courses will become available to all physics students in the 3^{ème} *Cycle* and conversely our students will benefit from a larger choice of courses.

The PhysiScope has continued its successful story this year. Highlights were the participation in the 450 year anniversary of the University of Geneva.

MaNEP continues to offer to female students summer internships. These internships are highly appreciated by those who choose to take advantage of them.

Communication

During this year we have continued to participate to a number of outreach activities. This was especially the case in relation with the 450 year anniversary of UniGE. We are also actively working with artists and the use of superconductivity in the field of art. We collaborate with the Swiss sculptor Etienne Krähenbühl to propose and create an artwork based on superconductivity. On the other hand the artistic company Exos is elaborating performances featuring superconducting levitation. We are working on this towards the 100 year superconductivity anniversary in 2011.

2.1 Structure of the NCCR and status of integration

2.1.1 Structure of the NCCR

This section provides an up-to-date summary of the organization of MaNEP, the Swiss National Centre of Competence in Research (NCCR) on Materials with Novel Electronic Properties.

Academic institutions members of MaNEP

- University of Geneva (UniGE), home institution
- University of Fribourg (UniFR)
- University of Berne (UniBE)
- University of Zurich (UniZH)
- Federal Institute of Technology, Lausanne (EPFL)
- Federal Institute of Technology, Zurich (ETHZ)
- Paul Scherrer Institute (PSI)
- Materials Science and Technology Research Institute (Empa)
- Haute école de paysage, d'ingénierie et d'architecture, Genève (Hepia)

Industrial Partners

- ABB, Baden
- AgieCharmilles, Meyrin
- Asulab (a member of Swatch Group), Marin
- Bruker BioSpin, Fällanden
- Nirva Industries, Genève
- Phasis, Geneva
- Sécheron, Meyrin
- SwissNeutronics, Klingnau
- Vacheron Constantin, Geneva

Scientific Committee

- Leonardo Degiorgi, ETHZ
- Øystein Fischer, UniGE, director
- László Forró, EPFL
- Thierry Giamarchi, UniGE
- Dirk van der Marel, UniGE, deputy director

- Frédéric Mila, EPFL
- Alberto Morpurgo, UniGE
- Christoph Renner, UniGE, deputy director
- Manfred Sigrist, ETHZ
- Jean-Marc Triscone, UniGE
- Urs Staub, PSI
- Andrey Zheludev, PSI and ETHZ

MaNEP Forum

Full members:

- Markus Abplanalp, ABB
- Philipp Aebi, UniFR
- Dionys Baeriswyl, UniFR
- Bertram Batlogg, ETHZ
- Christian Bernhard, UniFR
- Gianni Blatter, ETHZ
- Markus Büttiker, UniGE
- Michel Decroux, UniGE
- Leonardo Degiorgi, ETHZ
- Daniel Eckert, Bruker BioSpin
- Tilman Esslinger, ETHZ
- Øystein Fischer, UniGE
- René Flükiger, UniGE
- László Forró, EPFL
- Thierry Giamarchi, UniGE
- Enrico Giannini, UniGE
- Marco Gioni, EPFL
- Didier Jaccard, UniGE
- Janusz Karpinski, ETHZ
- Hugo Keller, UniZH
- Michel Kenzelmann, PSI
- Dirk van der Marel, UniGE
- Joël Mesot, PSI and ETHZ
- Frédéric Mila, EPFL
- Elvezio Morenzoni, PSI

- Alberto Morpurgo, UniGE
- Christof Niedermayer, PSI
- Hans-Rudolf Ott, ETHZ
- Patrycja Paruch, UniGE
- Greta Patzke, UniZH
- Christoph Renner, UniGE
- T. Maurice Rice, ETHZ
- Nico de Rooij, EPFL
- Henrik M. Rønnow, EPFL
- Manfred Sigrist, ETHZ
- Urs Staub, PSI
- Gilles Triscone, Hepia
- Jean-Marc Triscone, UniGE
- Matthias Troyer, ETHZ
- Anke Weidenkaff, Empa and UniBE
- Philip Willmott, PSI
- Klaus Yvon, UniGE
- Andrey Zheludev, PSI and ETHZ

Associate members:

- Christophe Berthod, UniGE
- Harald Brune, EPFL
- Kazimierz Conder, PSI
- Jorge Cors, UniGE and Phasis
- Bernard Delley, PSI
- Bertrand Dutoit, EPFL
- Vladimir Gritsev, UniFR
- Hans-Joseph Hug, Empa
- Jürg Hulliger, UniBE
- Ivan Maggio-Aprile, UniGE
- Reinhard Nesper, ETHZ
- Frithjof Nolting, PSI
- Davor Pavuna, EPFL
- Andreas Schilling, UniZH
- Louis Schlapbach
- Philipp Werner, ETHZ
- Oksana Zaharko, PSI

Advisory Board

- Dave Blank, University of Twente, Netherlands
- Robert J. Cava, Princeton University, USA
- Antoine Georges, Ecole Normale Supérieure, France
- Denis Jérôme, University Paris Sud, Orsay, France
- Andrew Millis, Columbia University, USA
- George Sawatzky, University of British Columbia, Canada

Management (UniGE)

- Øystein Fischer, director
- Dirk van der Marel, deputy director
- Christoph Renner, deputy director
- Marie Bagnoud, administrative manager
- Christophe Berthod, education
- Adriana Bonito Aleman, communication and, *ad interim*, knowledge and technology transfer
- Pascal Cugny, accountant
- Michel Decroux, scientific manager, education and training, advancement of women
- Lidia Favre-Quattropani, scientific manager
- Elizabeth Gueniat, management secretary
- Ivan Maggio-Aprile, computer and internet resources
- Greg Manfrini, technical organization

Collaborative projects

1. Novel phenomena at interfaces and in superlattices

Project leader:

- J.-M. Triscone (UniGE)

Members:

- Ph. Aebi (UniFR)
- C. Bernhard (UniFR)
- D. Jaccard (UniGE)
- E. Morenzoni (PSI)
- A. Morpurgo (UniGE)
- P. Paruch (UniGE)
- J.-M. Triscone (UniGE)
- Ph. Willmott (PSI)

2. Materials for future electronics

Project leader:

- A. Morpurgo (UniGE)

Members:

- M. Büttiker (UniGE)
- T. Giamarchi (UniGE)
- D. van der Marel (UniGE)
- A. Morpurgo (UniGE)
- P. Paruch (UniGE)
- C. Renner (UniGE)
- M. Sigrist (ETHZ)
- J.-M. Triscone (UniGE)

3. Electronic materials for energy systems and other applications

Project leader:

- Ø. Fischer (UniGE)

Members:

- M. Abplanalp (ABB)
- J. Cors (UniGE and Phasis)
- M. Decroux (UniGE)
- D. Eckert (Bruker Biospin)
- Ø. Fischer (UniGE)
- R. Flükiger (UniGE)
- M. Kenzelmann (PSI)
- G. Patzke (UniZH)
- C. Renner (UniGE)
- N. de Rooij (EPFL)
- G. Triscone (Hepia)
- J.-M. Triscone (UniGE)
- A. Weidenkaff (Empa and UniBE)
- K. Yvon (UniGE)
- This project is carried out with six participating industries

4. Electronic properties of oxide superconductors and related materials

Project leader:

- D. van der Marel (UniGE)

Members:

- D. Baeriswyl (UniFR)
- B. Batlogg (ETHZ)
- L. Degiorgi (ETHZ)
- Ø. Fischer (UniGE)
- E. Giannini (UniGE)
- J. Karpinski (ETHZ)
- H. Keller (UniZH)
- M. Kenzelmann (PSI)
- D. van der Marel (UniGE)
- J. Mesot (PSI and ETHZ)
- E. Morenzoni (PSI)
- C. Niedermayer (PSI)
- T. M. Rice (ETHZ)
- M. Sgrist (ETHZ)

5. Novel electronic phases in strongly correlated electron systems

Project leader:

- M. Sgrist (ETHZ)

Members:

- D. Baeriswyl (UniFR)

- G. Blatter (ETHZ)
- E. Giannini (UniGE)
- D. Jaccard (UniGE)
- M. Kenzelmann (PSI)
- D. van der Marel (UniGE)
- M. Sgrist (ETHZ)
- M. Troyer (ETHZ)

6. Magnetism and competing interactions in bulk materials

Project leaders:

- F. Mila (EPFL)
- A. Zheludev (PSI and ETHZ)

Members:

- T. Giamarchi (UniGE)
- J. Mesot (PSI and ETHZ)
- F. Mila (EPFL)
- H.-R. Ott (ETHZ)
- H. M. Rønnow (EPFL)
- U. Staub (PSI)
- M. Troyer (ETHZ)
- A. Zheludev (PSI and ETHZ)

7. Electronic materials with reduced dimensionality

Project leader:

- L. Forró (EPFL)

Members:

- Ph. Aebi (UniFR)
- L. Degiorgi (ETHZ)
- Ø. Fischer (UniGE)
- L. Forró (EPFL)
- T. Giamarchi (UniGE)
- M. Grioni (EPFL)

8. Cold atomic gases as novel quantum simulators for condensed matter

Project leader:

- T. Giamarchi (UniGE)

Members:

- G. Blatter (ETHZ)
- T. Esslinger (ETHZ)
- T. Giamarchi (UniGE)
- V. Gritsev (UniFR)
- M. Troyer (ETHZ)

2.1.2 Status of integration

The passage from Phase I to Phase II was marked by a passage from individual projects to collaborative projects. When passing from Phase II to Phase III we have adjusted the collaborative projects to make them more focused and balanced. This resulted in 8 new collaborative projects. Between January 26 and January 29, 2010 we had the first MaNEP Internal Workshops in Phase III, during which each of the 8 projects were discussed among the group leaders (members of the Forum). This is the opportunity to mutually inform about the progress in each group participating in a project and to adjust research goals according to the latest results from our research. Thus this event is each year improving contacts and synergies between groups. The milestones are systematically discussed at these meetings as well and this is a very useful tool to boost integration.

As announced we have opened up for new collaborations to financially further stimulate the interactions between groups. A call was sent out in October 2009. Many groups took this opportunity to reinforce their collaborations with groups in other institutions. The proposals were discussed in the meeting of the scientific committee on December 15, 2009 and it was decided to give financial support to 8 new collaborations.

1. MaNEP collaborative project on thermoelectric $[\text{Ca}_2\text{CoO}_3]^{\text{RS}}\text{CoO}_2$ (P. Aebi (UniFR), J. Hulliger (UniBE), A. Weidenkaff (Empa and UniBE)).
2. Low energy excitations of pressure tuned correlated matter (L. Forró (EPFL), D. van der Marel (UniGE)).
3. Synthesis and investigations of single-crystals and polycrystalline samples of FeAs based superconductors (B. Batlogg (ETHZ), Ø. Fischer (UniGE), J. Karpinski (ETHZ), H. Keller (UniZH)).
4. Numerical simulations of frustrated correlated systems (F. Mila (EPFL), M. Troyer (ETHZ)).

5. Topological properties of electronic states of matter (D. van der Marel (UniGE), A. Morpurgo (UniGE), M. Sigrist (ETHZ)).
6. Excitations of the orbital and spin degree of freedom in quasi-one-dimensional cuprates and multiferroic materials (F. Nolting (PSI), H. M. Rønnow (EPFL), U. Staub (PSI)).
7. High pressure phases in pure and doped quantum antiferromagnets (M. Kenzelmann (PSI), H. M. Rønnow (EPFL)).
8. One-dimensional quantum magnets with bond randomness: μSR and neutron scattering (B. Batlogg (ETHZ), E. Morenzoni (PSI), A. Zheludev (PSI and ETHZ)).

A significant indication of the importance of the integration within the MaNEP network is the fact that a large number of new members wanted strongly to join the network in Phase III. This was the case in spite of the fact that the amount of yearly grant per group amounts on the average only to about half a doctoral student. Thus the membership counts clearly much more than the financial support. This sign of integration is also seen in the strong participation to the MaNEP meetings. The SWM meeting at les Diablerets gathers every second year 200 MaNEP researchers and the MaNEP participation to the Swiss Physical Society continues to attract the largest group at that meeting. About 130 participants are so far registered for the upcoming meeting in Basel on June 21 – 22, 2010.

During the last year, we have continued to work on the integration and stabilization of MaNEP Geneva into the Geneva University. A brainstorming event took place on March 7, 2010 between some members of MaNEP in Geneva and other senior scientists from other parts of physics at the University, in order to discuss how to structure future research in Geneva. This was one important step among many which will take place over the next year to ensure the integration of MaNEP Geneva in the official university structure.

2.2 Results since the last progress report

This section reports on the research performed in the eight MaNEP projects for the period from April 1st 2009 to March 31st 2010.

Project 1 Novel phenomena at interfaces and in superlattices

Project leader: J.-M. Triscone (UniGE)

Participating members: Ph. Aebi (UniFR), C. Bernhard (UniFR), D. Jaccard (UniGE), E. Morenzoni (PSI), A. Morpurgo (UniGE), P. Paruch (UniGE), J.-M. Triscone (UniGE), Ph. Willmott (PSI)

Introduction: Interfaces are not simply the place where two distinct materials meet, with each of them retaining their own distinct and bulklike properties. There are abrupt changes in both chemical and electrostatic potentials, which can lead to an amazing variety of new physical properties and phenomena including, for instance, novel spin, charge, or orbital orders and possible new phases. It is the aim of this project to study existing exciting interface systems and try discovering new properties.

Summary and highlights

We list here very briefly some of the achievements obtained last year which are more detailed below in the present report.

- Using the technique of infrared ellipsometry we determined the depth profile of the carrier concentration of the electrons that are confined to the interface of LaAlO₃/SrTiO₃ heterostructures.
- Still at the LaAlO₃/SrTiO₃ interface, we have shown that a large, tunable, spin-orbit coupling takes place which correlates the system phase diagram.
- A multiprobe experiment has been designed to explore electric and thermoelectric properties of the LaAlO₃/SrTiO₃ interface at ambient and high pressures. This study revealed a very large Nernst coefficient in the superconducting region and a strong pressure dependence of the superconducting critical temperature T_c .
- With neutron reflectometry we observed an interesting superconductivity-induced modification of the ferromagnetic order in multilayers consisting of cuprate high- T_c superconductors and ferromagnetic manganites.
- Using low-energy- μ SR, we have investigated the magnetic structure of La₂CuO₄/La_{1.56}Sr_{0.44}CuO₄ superlattices and shown that the insulating part of the structure (12 CuO₂ layers thick) is partially antiferromagnetic.
- In artificially layered ferroelectrics, such as PbTiO₃/SrTiO₃ superlattices, we have discovered a periodic ferroelectric domain structure and we show that this system might be ideal for studying the dynamics of ferroelectric nano-domains in ultrathin films under uniform applied fields.
- We have used photoemission to characterize thin oxide films of the nickelate family. For a 100 Å thick NdNiO₃ film, photoelectron diffraction patterns have been recorded to study the crystallographic arrangement. Both, the resistivity of the film and the valence band spectral weight have also been measured.
- We have realized charge-transfer interfaces using TTF, TMTSF, and BEDT-TTF as electron donors, and TCNQ as acceptors. Whereas TTF/TCNQ interfaces are metallic, with a transferred charge estimated to be in the order of 0.5 carrier/molecule, TMTSF/TCNQ and BEDT-TTF/TCNQ behave as small gap semiconductors.
- We used surface X-ray diffraction to study the detailed structures of ultrathin heteroepitaxial perovskite-like thin films, including the interface to the substrate and surface relaxations and/or reconstructions, and therefore provide invaluable information about the possible physi-

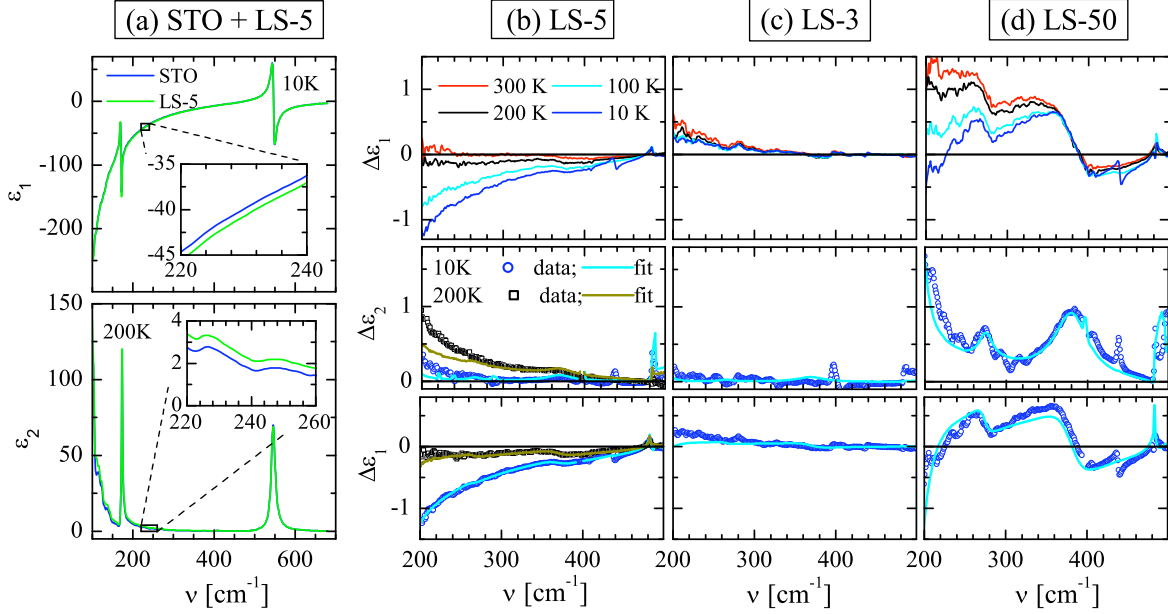


Figure 1: (a) Spectra of ϵ_1 at 10 K and ϵ_2 at 200 K for a sample with five unit cells of LaAlO_3 on SrTiO_3 (LS-5, green lines) and bare SrTiO_3 (blue lines). Inset: magnification of the differences. The corresponding spectra of $\Delta\epsilon_{1,2} = \epsilon_{1,2} - \epsilon_{1,2}(\text{STO})$ are shown in (b)–(d) for the samples with 5, 3, and 50 unit cells of LaAlO_3 , respectively. In agreement with the transport data, a clear Drude response occurs for LS-5 (b) but not for LS-3 (c). Top panels show the T -dependence of ϵ_1 , middle and bottom panels show ϵ_1 and ϵ_2 as obtained from the experiment (symbols) and model calculations (lines), respectively.

cal mechanisms at play in these systems.

- We have used piezoresponse force microscopy and related techniques to probe new functionalities at ferroelectric domain walls, and their behavior as elastic interfaces in disordered media. We have observed a lateral shear at 180° domain walls in epitaxial $\text{Pb}(\text{Zr}_{0.2}\text{Ti}_{0.8})\text{O}_3$ thin films,

forbidden by tetragonal symmetry in a uniformly polarized region, but possible specifically at the position of the domain walls. We have also investigated the switching dynamics in BiFeO_3 films under electric field applied by an atomic force microscopy tip.

1 Conducting interfaces (C. Bernhard, J.-M. Triscone, D. Jaccard)

Since its discovery in 2004, the conducting interface between LaAlO_3 and SrTiO_3 has generated a lot of interest and has been the subject of intense investigation [27]. More generally, the physics of oxide interfaces has become a very active field of research. We summarize below our investigations on the $\text{LaAlO}_3/\text{SrTiO}_3$ and the $\text{LaAlO}_3/\text{LaTiO}_3$ systems.

1.1 Charge transfer at oxide interfaces (C. Bernhard)

a) *Infrared ellipsometry on $\text{LaAlO}_3/\text{SrTiO}_3$ heterostructures* We have performed infrared ellipsometry and transport measurements on $\text{LaAlO}_3/\text{SrTiO}_3$ heterostructures to investigate the electrons at the interface which are supposed to arise from a charge transfer between these two band-insulators. With the optical

technique we were able to directly observe the Drude-like response of the confined charge carriers (Fig. 1) and from the comparison with the Hall-effect data (taken on the same sample) we obtained a sheet carrier concentration of $N_s \approx 5 - 9 \cdot 10^{13} \text{ cm}^{-2}$, an effective mass of $m^* = 3.2(\pm 0.4)m_e$, and a strongly frequency dependent mobility.

The latter are similar to bulk $\text{SrTi}_{1-x}\text{Nb}_x\text{O}_3$ and therefore suggestive of polaronic correlations. From the analysis of a so-called Berreman-mode (Fig. 2), which in parts arises from the plasma-oscillation of the electron gas in the vicinity of the interface, we were also able to determine the vertical concentration profile which has a strongly asymmetric shape with a rapid initial decay over the first 2 nm and a pronounced tail that extends to about 11 nm [1].

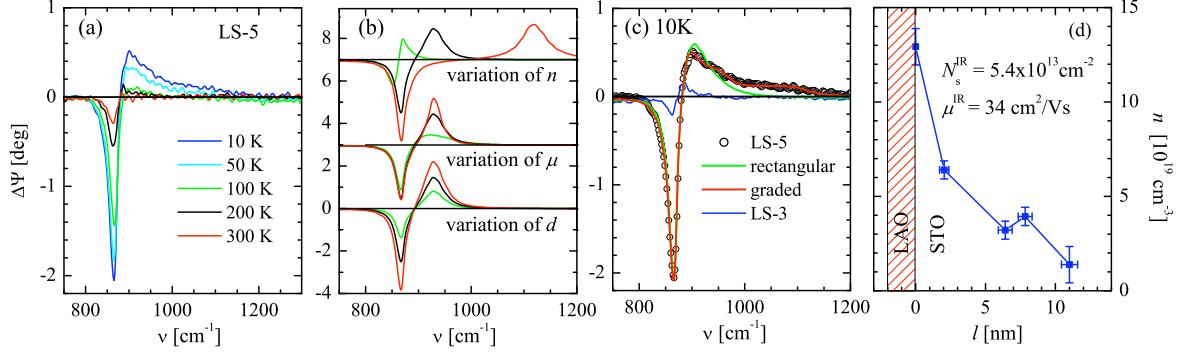


Figure 2: (a) Difference spectra of the ellipsometric angle $\Delta\Psi = \Psi(\text{LS-5}) - \Psi(\text{STO})$, showing the Berreman mode in the vicinity of the highest LO phonon of STO. (b) Simulations of $\Delta\Psi$ with a block-like carrier concentration profile showing the variation with carrier concentration n , mobility μ , and thickness d , in increasing order for green to red lines. (c) Comparison between the data of LS-5 at 10 K (open circles) and calculations with a rectangular (green line) and a graded profile (red lines). Data for LS-3 are shown as blue line. (d) Depth profile of n as obtained from the fit (red line) in (c).

b) *Spectral ellipsometry on electronic anisotropy of $\text{LaTiO}_3/\text{LaAlO}_3$ superlattices* In addition we have used the technique of spectroscopic ellipsometry at variable angles of incidence to investigate the anisotropy of the interband transitions parallel and perpendicular to the planes of $\text{LaTiO}_3/\text{LaAlO}_3$ multilayers (Fig. 3). Our measurements provide direct information about the electronic structure of the two-dimensional $3d^1$ state of the Ti ions near the interfaces. In combination with local density approximation, including Hubbard U calcula-

tions, our data suggest that the confinement in the TiO_2 slabs lifts the degeneracy of the t_{2g} states leaving only planar d_{xy} orbitals occupied.

Our results demonstrate the unique potential of the spectroscopic ellipsometry technique for the investigation of the electronic properties of interface states in oxide based heterostructures [2].

1.2 Tuning the electronic properties at the $\text{LaAlO}_3/\text{SrTiO}_3$ interface (J.-M. Triscone)

It has been recently demonstrated by transport experiments [3] and conductive AFM imaging [28, 29] that the electron gas present in $\text{LaAlO}_3/\text{SrTiO}_3$ heterostructures grown using appropriate conditions is confined within a few nanometers from the interface. This structural configuration clearly breaks inversion symmetry and, as a result, the electron gas confined in the vicinity of a polar interface will experience a strong electric field directed perpendicular to the conduction plane. A new class of physical phenomena occurring because of the presence of this effective electric field are captured by the Rashba Hamiltonian [30]

$$H_R = \alpha(\hat{n} \times \mathbf{k}) \cdot \mathbf{S} \quad (2.1)$$

where \mathbf{S} are the Pauli matrices, \mathbf{k} is the electron wave-vector and \hat{n} is a unit vector perpendicular to the interface. One important consequence of this interaction is that the dispersion relation of the electrons divides into two branches separated at the Fermi surface by a spin splitting $\Delta = 2\alpha k_F$, k_F being the Fermi wave-vector and α the strength of the spin-orbit coupling. Perhaps the most appealing feature of this interaction is that its coupling

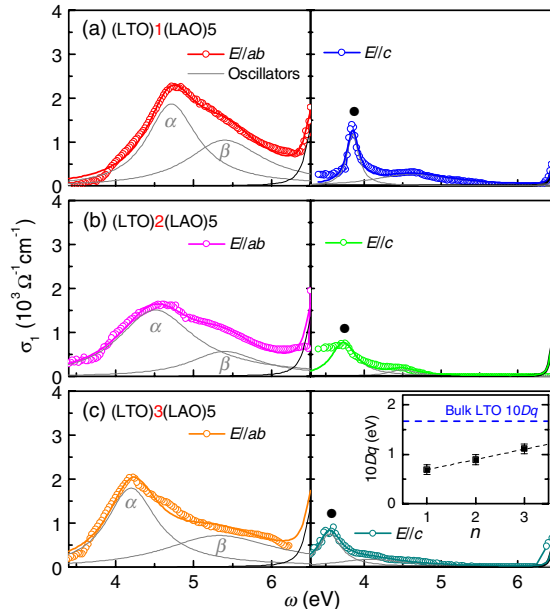


Figure 3: In-plane (left) and out-of-plane (right) components of the optical conductivity spectra of $(\text{LTO})_n/(\text{LAO})_5$ multilayers with (a) $n = 1$, (b) $n = 2$, and (c) $n = 3$. Inset of (c): obtained crystal field splitting, $10 Dq$, of Ti^{3+} as a function of n . The dashed (blue) line gives the value in bulk LTO.

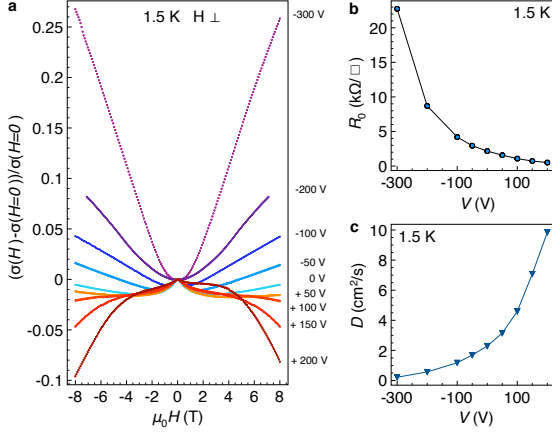


Figure 4: Modulation of the transport properties of the $\text{LaAlO}_3/\text{SrTiO}_3$ interface under electric and magnetic fields. (a) Magneto-conductance $[\sigma(H) - \sigma(H = 0)]/\sigma(H = 0)$ (σ being the sheet conductance, and H the applied magnetic field) measured at 1.5 K in perpendicular magnetic field for different applied gate voltages. (b) Sheet resistance (R_0) modulation resulting from the field effect measured at 1.5 K. (c) Field effect modulation of the diffusion coefficient D estimated at 1.5 K.

constant is defined by the total electric field experienced by the electrons and can be therefore tuned by applying an external gate voltage. Aiming to explore this phenomenon in $\text{LaAlO}_3/\text{SrTiO}_3$ interfaces, we fabricated field effect devices [4].

The intriguing coupling between spin dynamics and transport manifests in the magnetic field dependence of the conductance. Fig. 4a shows the magneto-conductance $[\sigma(H) - \sigma(H = 0)]/\sigma(H = 0)$ (σ being the sheet conductance and H the applied magnetic field), measured in a magnetic field applied perpendicular to the $\text{LaAlO}_3/\text{SrTiO}_3$ interface at a temperature $T = 1.5$ K for gate voltages V between -300 V and $+200$ V. For large negative gate voltages we observe a large positive magneto-conductance that reaches more than +25% at 8 T and -300 V. As we increase the voltage ($V > -200$ V), a low-field regime characterized by a negative magneto-conductance appears. Increasing the gate voltage further, we observe that the negative magneto-conductance regime widens out. For the largest applied electric field, we observe that the magneto-conductance remains negative up to the largest accessible magnetic field (8 T). Similar modulations of magneto-conductance have already been observed in metallic thin films [31] and semiconductor heterostructures [32]. Here, the large electrostatic tunability of the magneto-conductance observed in $\text{LaAlO}_3/\text{SrTiO}_3$

heterostructures is an explicit example of a transport phenomenon occurring at an oxide interface, never observed in its constituent materials. A possible interpretation of this phenomenon is based on the presence of a strong spin-orbit interaction in a diffusive system, which counteracts weak localization.

In a diffusive system the magneto-conductivity can be described by the Maekawa-Fukuyama (MF) theory [33] which takes into account the Zeeman and spin-orbit effects on weak localization. The parameters of the theory are $H_i = \hbar/4eD\tau_i$, $H_{so} = \hbar/4eD\tau_{so}$ and the electrons g -factor g which enters into the Zeeman correction $\gamma = g\mu_B H/4eDH_{so}$. D is the diffusion coefficient, e the elementary charge, μ_B the Bohr magneton, τ_i is the inelastic scattering time and τ_{so} is the spin-orbit relaxation time. In a magneto-transport experiment we can then quantify the two relevant time scales of the problem, namely τ_{so} and τ_i . In the Rashba scenario, the coupling constant α and the spin relaxation time τ_{so} are related through

$$\tau_{so} = \frac{\hbar^4}{4\alpha^2 m^2 2D} \quad (2.2)$$

The MF theory has been used to fit the experimental data of Fig. 4a in terms of variation of conductance with respect to $e^2/\pi h \simeq 1.2 \cdot 10^{-5}$ S. Since the effective mass (the elastic scattering time) is one to two orders of magnitude larger (smaller) than the corresponding quantities for typical semiconductors, the diffusive regime holds for fields up to 4 T. As the MF theory is based on a perturbative expansion, we have also checked that the magneto-resistance and magneto-conductance are still equal in absolute value up to 4 T. For the range of fields and gate voltages (up to 100 V) that we analyzed, weak localization corrections dominate Coulomb interaction contributions. The best fits are presented in Fig. 5a, where we observe a remarkable agreement between theory and experiments. This analysis allows us to trace the electric field dependence of the parameters $H_{i,so}$, presented in Fig. 5b, and γ . To extract from these parameters the relaxation times $\tau_{i,so}$ and the electrons g -factor, we need to determine the electric field dependence of the diffusion coefficient. For this purpose we measured the electric field modulation of the sheet carrier concentration n_{2D} by means of Hall effect and by capacitance measurements [5]. An estimate of the Fermi velocity v_F and of the elastic scattering time using a parabolic dispersion relation with an effective mass $m^* = 3m_e$ (m_e is the bare electron mass) and data collected at the temperature $T = 1.5$ K allows us then to

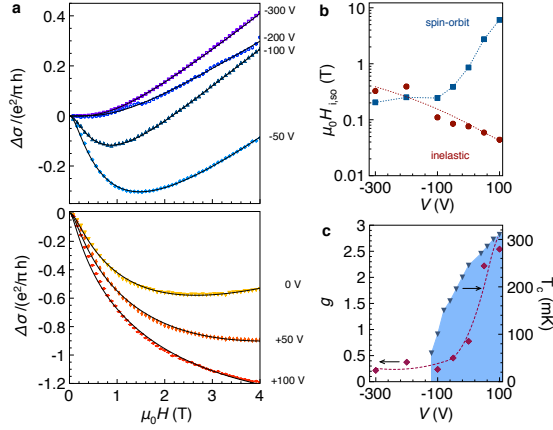


Figure 5: Analysis of the magneto-conductivity of the $\text{LaAlO}_3/\text{SrTiO}_3$ interface. (a) Best fits according to the Maekawa-Fukuyama theory of the variation of conductance $\Delta\sigma$, normalized with respect to $e^2/\pi h$, for different gate voltages. (b) Gate voltage dependence of the fitting parameters H_i (red dots) and H_{so} (blue squares). The lines are a guide to the eye. (c) Left axis, purple diamonds: gate voltage dependence of the electrons g -factor g . The line is a guide to the eye. Right axis, blue triangles: superconducting critical temperature T_c as a function of gate voltage for the same sample.

derive the diffusion coefficient as $D = v_F^2\tau/2$ (τ being the elastic scattering time). Using this approach we can plot D as a function of V as shown in Fig. 4c. The steady rise of the diffusion coefficient as the gate voltage is increased signals an insulator to metal transition and, as discussed below, correlates with the increase of the spin-orbit coupling.

The gate voltage dependence of the g -factor is presented in Fig. 5c. One observes a large increase from a small value, around 0.5 for negative voltages, towards the typical value of 2 for bare electrons at positive voltages. We now turn to the issue of the gate voltage dependence of the parameters $H_{i,so}$ that will allow us to discern the modulation of spin-orbit coupling brought about by the electric field.

The relaxation times $\tau_{i,so}$ are plotted against gate voltage in Fig. 6a. For large negative gate voltages we observe that the inelastic scattering time is shorter than the spin relaxation time, indicating that the effect of the spin-orbit interaction is weak compared with the orbital effect of the magnetic field. In this regime, the quantum correction to the conductivity can be ascribed to weak localization, in agreement with the observed temperature evolution of the conductivity [5]. Above a critical voltage the spin relaxation time becomes shorter than the inelastic scattering time and decreases sharply, by three orders of magnitude, as the voltage

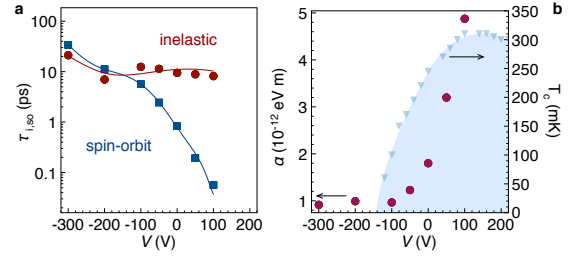


Figure 6: Rashba control of the $\text{LaAlO}_3/\text{SrTiO}_3$ interface electronic phase diagram. (a) Inelastic relaxation time τ_i (red circles) and spin relaxation time τ_{so} (blue squares) plotted on a logarithmic time scale as a function of gate voltage. The lines are a guide to the eye. (b) Left axis, red dots: field effect modulation of the spin-orbit coupling α . Right axis, blue triangles: superconducting critical temperature T_c as a function of gate voltage for the same sample.

is increased. On the other hand, the inelastic scattering time remains fairly constant as we increase the voltage. Here a weak antilocalization regime appears, characterized by a strong spin-orbit interaction. A detailed analysis of the relation of τ_{so} with τ reveals that the spin-orbit coupling stems from a Rashba-like mechanism. These observations indicate that the unusually strong and tunable spin-orbit interaction found in $\text{LaAlO}_3/\text{SrTiO}_3$ heterostructures arises from the interfacial breaking of inversion symmetry.

A remarkable correlation between the onset of strong spin fluctuations and the emergence of superconductivity is evident looking at Fig. 6b, where we notice that the superconducting dome, measured on the same sample, develops as soon as the spin relaxation time becomes significantly smaller than the inelastic scattering time. In Fig. 6b we can appreciate the sharp increase of the spin-orbit coupling constant α , calculated using equation 2.2, as we move across the quantum critical point. The spin-orbit coupling strength keeps increasing as the voltage is increased up to optimal doping. This remarkable correlation between the critical temperature and the intensity of spin-orbit coupling is probably indicative of an unconventional superconducting order parameter at the $\text{LaAlO}_3/\text{SrTiO}_3$ interface. We note that the spin splitting values are much higher than the superconducting gap (which is of the order of $40 \mu\text{eV}$ at optimal doping) and comparable to the Fermi energy (which is of the order of 20meV). Hence the spin-orbit coupling turns out to be an essential ingredient to describe the electronic properties of the $\text{LaAlO}_3/\text{SrTiO}_3$ interface, both in the normal and superconducting state.

1.3 The $\text{LaAlO}_3/\text{SrTiO}_3$ interface under pressure (D. Jaccard, J.-M. Triscone)

The low carrier concentration and the confinement of the electron gas at the interface make the $\text{LaAlO}_3/\text{SrTiO}_3$ heterostructure an interesting system for doping the electron gas by field effect [34][5]. A different tool for tuning the properties of a solid is the application of high pressures, which can also change the carrier density n . The question arises therefore, how the tuning of the interface properties by an electric field would compare to the tuning of these same properties by pressure. For answering this question a multiprobe study combining electric and thermoelectric probes was designed. The set-up allows us to measure on a single sample resistivity, the Hall and Nernst effects, and the thermopower, and to study their dependencies on four control parameters, namely temperature, pressure, magnetic field and electric field. The measurements are performed on the same sample at ambient pressure and subsequently at high pressures. An extensive report on this study can be found in [6].

The first thermoelectric measurements of the $\text{LaAlO}_3/\text{SrTiO}_3$ interface at ambient pressure and low temperature are presented. The thermopower at ambient pressure and 4.2 K is $S \simeq -100 \mu\text{V}/\text{K}$, which is a very large value compared to the thermopower of a simple metal with the same low carrier concentration. The Nernst coefficient ν in the superconducting state at ambient pressure is of the order of several hundred $\mu\text{V}/\text{KT}$ (Fig. 7). This is two orders of magnitude higher than in the high-temperature superconductors and a sign for extremely mobile vortices. Under pressure the residual sheet resistance increases due to an increase of the pressure-induced disorder. As

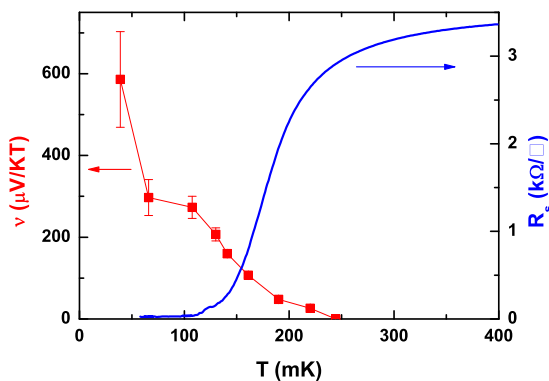


Figure 7: The Nernst coefficient and the sheet resistance as a function of temperature of the $\text{LaAlO}_3/\text{SrTiO}_3$ interface.

shown in Fig. 8, the sheet resistance at 4.2 K, $R_s(4.2 \text{ K})$, which characterizes the amount of disorder, is a smooth function of pressure and the ambient pressure data is a nice extrapolation of the high-pressure data. We therefore have a proof for the good quality of the pressure measurements and know that pressure does not introduce a qualitative change of the disorder. The high-pressure experiments reveal that superconductivity is already suppressed at the lowest investigated pressure of 0.8 GPa. It is assumed that superconductivity is destroyed by the pressure-induced disorder.

The above multiprobe study has provided an overview on a wide measurement space and has given many interesting results. These findings must however be confirmed and investigated in more detail. For this we focus on the two most promising results, namely the Nernst effect at ambient pressure and the pressure dependence of T_c . This allows us to optimize the sample geometry for the specific physical property. Since the Nernst effect is only measured at ambient pressure, a bigger sample can be used. Nevertheless, not only for the $T_c(p)$ but also for the Nernst measurements, a small sample must be cut-out from the $5 \times 5 \text{ mm}$ raw sample and the SrTiO_3 substrate must be thinned. A new method was developed for thinning evenly a relatively large sample down to about $100 \mu\text{m}$.

The influence of the sample preparation was then studied. For this, contacts are placed on the raw sample at the correct positions with respect to the later cut-out small sample and $R_s(T)$ is measured. In a second step the small

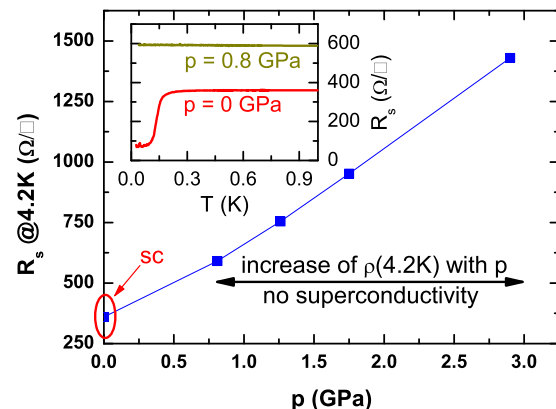


Figure 8: The sheet resistance R_s of the $\text{LaAlO}_3/\text{SrTiO}_3$ interface at 4.2 K as a function of pressure. Its smooth dependence on pressure is a proof for the quality of the pressure measurements. Inset: $R_s(T)$ at low temperature at ambient pressure and the lowest investigated pressure, where superconductivity is already suppressed.

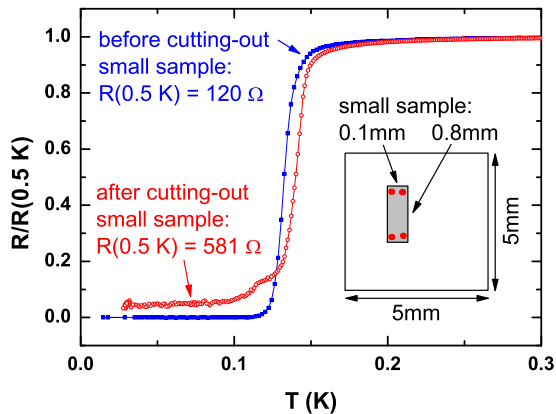


Figure 9: Normalized resistance of a $\text{LaAlO}_3/\text{SrTiO}_3$ interface as a function of T . The resistance is measured two times with the same contacts, before and after having cut-out the small sample.

sample is cut-out (around the existing contacts) and the $R_s(T)$ curve is again measured with the same contacts. We found that the sample preparation does not qualitatively influence the temperature dependence of the sheet resistance in the normal state. In the superconducting state T_c can be slightly shifted and the zero-resistance state can be lost (Fig. 9). The latter could however also be due to sample inhomogeneities and the fact that the current is now forced to keep within the small cut-out sample. As mentioned above, important efforts have been undertaken to improve the quality of the Nernst measurements at ambient pressure. A new sample geometry specially adapted for this measurement was developed. This sample geometry increases the resolution by about one order of magnitude in comparison with the previous multiprobe study. In the latter study, the thermal gradient was measured with a thermocouple, since it had to fit inside a pressure cell. Thermocouples have a limited precision, particularly at very low temperatures. For the forthcoming experiment the resolution of the measurement of the thermal gradient will be greatly increased by using a RuO_2 resistive thermometer. The dimensions of this thermometer were adapted to the sample size and it was calibrated in a separate measurement run. Since it is important to measure the Nernst effect well below T_c and since the dependence of the Nernst effect on the gate voltage will be studied, it is important to select a sample with the highest possible T_c and a large response to an applied electric field. The testing of potential samples is now under way.

2 Magnetic/SC interfaces (C. Bernhard, E. Morenzoni)

2.1 Competing orders at complex oxide interfaces (C. Bernhard)

Extensive work has been performed on superlattices consisting of cuprate high- T_c superconductors and colossal magneto-resistance (CMR) manganites of the composition $\text{Y}_{0.6}\text{Pr}_{0.4}\text{Ba}_2\text{Cu}_3\text{O}_7$ (100Å) / $\text{La}_{2/3}\text{Ca}_{1/3}\text{MnO}_3$ (100Å) $\times 10$ that were grown on (001) oriented surfaces of SrTiO_3 substrates. Previously we had investigated by synchrotron X-ray diffraction and reflectometry how the various kinds of structural phase transitions of the SrTiO_3 substrates affect the multilayers that are grown on top. These experiments have been performed at the Material-beamline at the Swiss Synchrotron Light Source (SLS) at PSI in Villigen. We found that below 65 K a surprisingly strong tilting of the substrate surfaces occurs which gives rise to the formation of anisotropic micrometer sized domains that are tilted with respect to each other by up to 0.5° . This tilting was found to be translated into the multilayer that is grown on top.

In addition, we investigated by means of neutron reflectometry measurements which influence these tilt domains have on the magnetic and superconducting properties of these superlattices. In particular, we studied how they affect the superconductivity-induced formation of a fractional-order Bragg peak which is indicative of a giant superconductivity-induced modulation of the ferromagnetic order in the $\text{La}_{2/3}\text{Ca}_{1/3}\text{MnO}_3$ (LCMO) layers. We had previously suspected that the observed drastic changes in the magnetization density of the LCMO layers are enabled by the near degeneracy of ferromagnetic and non-ferromagnetic domains that are stabilized by the double exchange mechanism and the Jahn-Teller distortion, respectively. In order to test this hypothesis, we performed neutron reflectivity measurements while applying uniaxial pressure to the substrate. This enabled us to control the orientation and the ordering of the structural tilt domains of the SrTiO_3 substrate. As shown in Fig. 10, this allowed us to switch on and off (by external pressure) the superconductivity-induced modulation of the ferromagnetic magnetization density which shows up due to an additional Bragg peak at the fractional-order position [7]. The neutron experiments have been mainly performed at the SINQ source of the PSI in Villigen. These results demonstrate a fascinating interplay between superconducting and ferromagnetic order which strongly

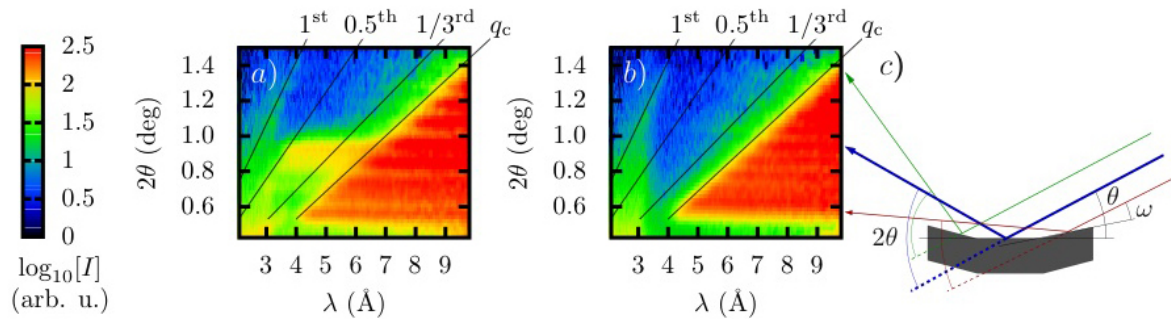


Figure 10: Influence of the uniaxial pressure on the fractional-order Bragg peak and the structural and magnetic domains in polarized neutron reflectivity data: (a) and (b) off-specular maps of the R-channel collected with an area detector in time-of-flight mode at $T = 8$ K with the sample mounted under different uniaxial pressures of 0.4 MPa and 0.1 MPa, respectively. The signals from the different facets of the sample appear here on straight horizontal lines at different values of 2θ , where θ is the angle of incidence of the neutrons with respect to the facets as sketched in (c). At 0.4 MPa (a) a fractional-order superlattice Bragg peak appears for several facets which is entirely absent at 0.1 MPa.

depends on the lattice strain that is transmitted from the substrate.

2.2 Superconductivity and magnetism in $\text{La}_{2-x}\text{Sr}_x\text{CuO}_4$ superlattices (E. Morenzoni)

Interfacial layers of oxide heterostructures can display electronic states different from the ground state of the constituents [8]. A recent example is a metal-insulator bilayer of (214) cuprates, which displays a superconducting transition with $T_c \sim 30$ K related to the presence of interface superconductivity on the insulator side [35, 36].

So far complex-oxide heterostructures have been studied by probes that are either macroscopic (e.g. transport measurements) and/or not spin sensitive (X-ray, electron, and ion scattering). Low-energy (LE)- μ SR is sensitive to the microscopic magnetic state (either static or fluctuating) and can characterize and quantify superconductivity (e.g. superfluid density) even in ultrathin layers. For instance, although it has been shown that a unit cell thick La_2CuO_4 (LCO) layer is insulating, nothing is known about magnetic properties of very thin LCO layers.

a) *Magnetic properties* For the present work, we synthesized superlattices in which we digitally varied the thickness of insulating LCO layers alternating with metallic $\text{La}_{1.56}\text{Sr}_{0.44}\text{CuO}_4$ (LSCO) layers. Counting in $\frac{1}{2}$ unit cell (UC) increments, each of which contains a single CuO_2 plane, the investigated superlattices have the repeated structure [3LSCO + 6LCO], [3LSCO + 9LCO], and [3LSCO + 12LCO], respectively. The total film thickness was kept at about 85 nm.

The main results from zero field measurements are as follows. In [3LSCO + 12LCO] we observe static antiferromagnetic (AF) order, evident from the precession signal (Fig. 11). The internal field is equal to what is observed in single-phase LCO films and bulk samples, thus showing that the full electron magnetic moment is present. However, the magnetic volume fraction estimated from the oscillatory amplitude of the muon polarization signal indicates that the magnetic layer thickness corresponds to only 4 – 5 CuO_2 layers, i.e. about 1/3 of the nominal number of insulating planes. This re-

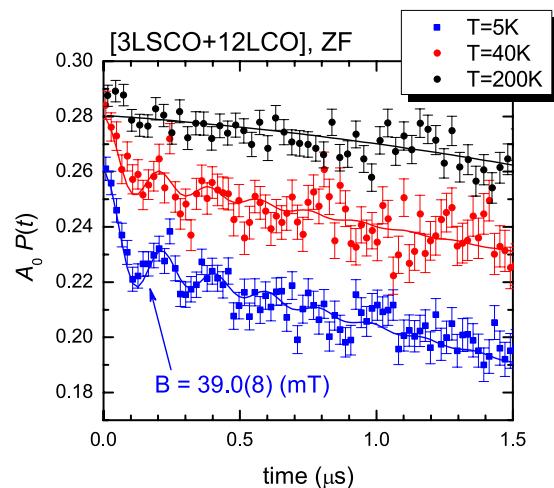


Figure 11: Muon spin depolarization function, $A_0P(t)$, for zero applied magnetic field for the [3LSCO + 12LCO] superlattice. A_0 is an instrumental number. The spontaneous precession signal implies that the internal magnetic field B_{int} is static on the muon time scale. The inferred value for B_{int} is very close to what is found in antiferromagnetic LCO single films and bulk. The $T = 40$ K and $T = 200$ K curves are shifted up by 0.02 for clarity.

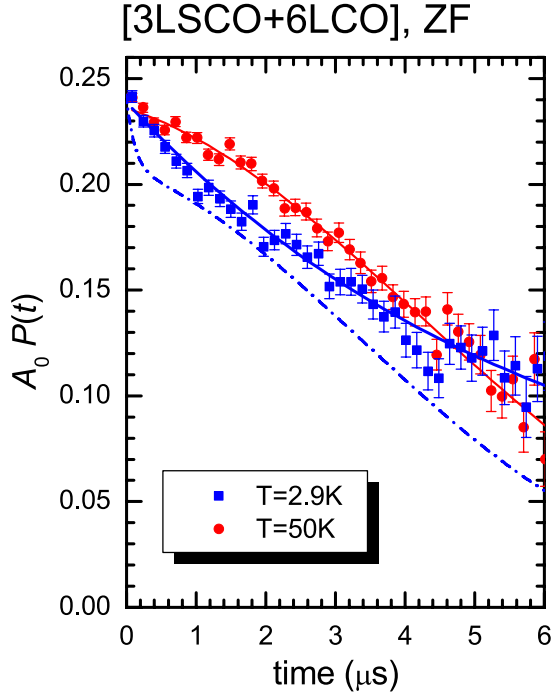


Figure 12: $A_0 P(t)$ for the $[3\text{LSCO} + 6\text{LCO}]$ superlattice. The dash-dotted curve shows the expected polarization at $T = 2.9\text{ K}$ if one assumes the doping level to be equal to that obtained from the charge-transfer model and using parameters obtained from single-phase film measurements.

duction reflects charge transfer with hole depletion/accumulation at the metal/insulator interface, as confirmed by model calculations taking into account the chemical potential mismatch (0.3 eV) between the metal and insulating layers [37, 38]. In superlattices with thinner insulating layers ($[3\text{LSCO} + 6\text{LCO}]$, $[3\text{LSCO} + 9\text{LCO}]$), magnetic long range order is absent, even with the μSR spatial resolution of $\sim 5\text{ nm}$. Although the exact nature of this state requires further investigations the data suggest a highly fluctuating, soft magnetic state combined with residual small static magnetic moments. Such a state is not simply expected on the basis of the above charge transfer model and is also different from the so-called “spin cluster glass state” (Fig. 12).

b) *Superconducting properties* The absence of Meissner shielding for $T < T_c$ when a field is applied parallel to the ab -planes and the broadening of the field distribution when the field is applied perpendicular to the planes reflects the formation of a vortex state restricted to the interface in a thickness $d \approx 1 - 2\text{ nm}$. From the field broadening we can deduce the effective magnetic penetration depth λ_{\parallel} , where $1/\lambda_{\parallel}^2$ is directly proportional to the sheet superfluid density $n_{2\text{D}}$ [39]. We find the sheet superfluid

density equal in all investigated heterostructures with values corresponding to an average density within d , $n_{3\text{D}} \simeq n_{2\text{D}}/d$ of the same order of magnitude as optimally doped bulk LSCO.

3 Improper ferroelectricity and domain structure in $\text{PbTiO}_3/\text{SrTiO}_3$ superlattices (J.-M. Triscone)

3.1 Introduction

Continued investigations of $\text{PbTiO}_3/\text{SrTiO}_3$ superlattices have revealed new complexities in this seemingly simple two-component system. Artificial layering of the ferroelectric and paraelectric constituents results in novel materials with electrical and structural properties that can be tuned in a very controlled and predictable fashion [9]. One surprise came from the “third” component – the interfaces between the layers. Here a local breaking of symmetry allows for the coupling of different structural instabilities that results in a qualitatively new type of interfacial ferroelectricity [10]. More recently, we have focused our attention on a different aspect of the superlattices – the behavior of ferroelectric nano-domains. The continuing technological drive for device miniaturization is pushing towards nano-scale dimensions where the intrinsic domain structures of ferroelectrics are becoming increasingly denser. The structure and dynamics of such nano-domains will thus play a crucial role in device performance. Here we show that artificially layered ferroelectrics give unique access to the physics of ultrathin ferroelectric films allowing their behavior to be studied using uniform electric field with simultaneous imaging through X-ray diffraction.

3.2 Dielectric response of superlattices

Ferroelectrics can rarely be considered in isolation. Electrical characterization requires intimate contact with metallic electrodes and hence the minimal system is generally a metal-ferroelectric-metal sandwich. The choice of electrode material often has a dramatic effect on the observable properties of the ferroelectric. As an illustration consider the two series of superlattices shown in Fig. 13: one grown on conducting Nb-doped SrTiO_3 substrates (with Pt top electrodes), the other, sandwiched between SrRuO_3 (SRO) electrodes. While structurally the two series are the same (as illustrated by their identical tetragonality in part (a) of the figure), they display markedly different electrical behavior. In particular, the remanent

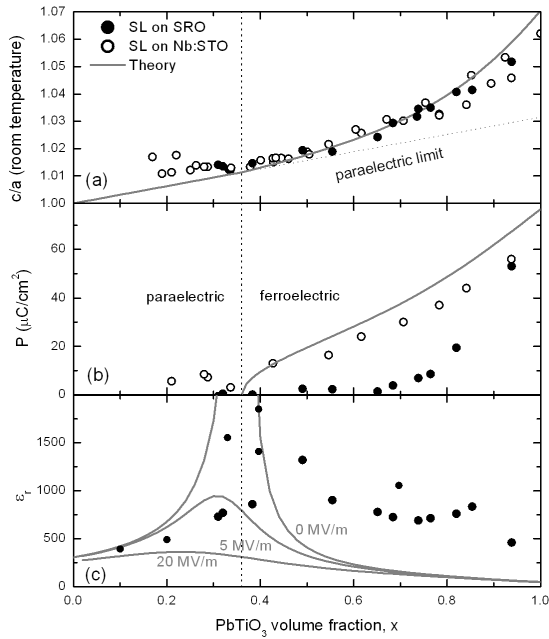


Figure 13: (a) Ratio of *c* to *a* lattice parameters for two superlattice series with different electrodes as a function of PbTiO₃ volume fraction, showing similar structural properties. (b) Polarization suppression in superlattices with SRO electrodes as compared to those grown on conducting Nb:STO substrates. (c) The dielectric constants are in good agreement with phenomenological theory predictions for paraelectric (low *x*) superlattices, but show significant enhancement due to domain wall motion in the ferroelectric phase.

polarization of samples with SRO electrodes seems to be unstable compared with that of samples grown on Nb:SrTiO₃ (Fig. 13b). A clue to understanding this apparent discrepancy is provided by the dielectric data shown in part (c) of the figure. While the response of paraelectric samples is well described by a Landau-Devonshire theory based model, a large enhancement in the dielectric response is observed for the ferroelectric compositions, indicating that domain wall motion is playing a role. It thus appears that samples with SRO electrodes are in a polydomain state with zero (or small) net polarization.

3.3 180° nano-domains

The presence of domains was confirmed with X-ray diffraction (XRD). Fig. 14 shows diffuse satellites around the superlattice reflections arising from an ordered array of 180° ferroelectric domains. The domain period is estimated at approximately 6 nm, i.e. neighboring domain walls are separated by only about 3 nm. Similar domains have been previously observed in ultrathin films of PbTiO₃.

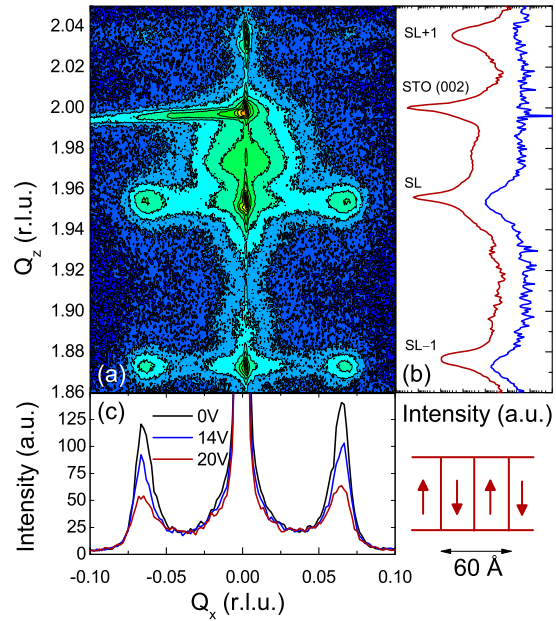


Figure 14: Reciprocal space map (a), crystal truncation rod (b) and in-plane line scans (c) around the (002) main superlattice (SL) reflection showing the substrate (002) peak (STO), and two diffuse in-plane satellites around each of the superlattice peaks. These satellites arise from the regular 180° stripe domain structure. Part (c) also shows the changes in intensities of the satellite peaks under applied electric field, as the domain walls move, causing the increased dielectric response. The domain period is approximately 60 Å.

A study of their response to externally applied electric fields, however, has so far been elusive due to the large conductivity of the very thin films. Scanning probe techniques such as piezoresponse force microscopy (PFM), which have been invaluable to our understanding of switching phenomena and domain dynamics in ferroelectric thin films, are also powerless as these domain structures are finer than the resolution limit of PFM. It is here that PbTiO₃/SrTiO₃ superlattices offer a unique opportunity to probe ultrathin film physics in structures with total thicknesses that can be hundreds of nanometers, allowing large and uniform electric fields to be applied over large areas of the sample.

We illustrate the power of this approach by fabricating a 500 nm thick superlattice, which still exhibits the striped nano-domains of PbTiO₃ films that are only a few unit cells thick, and apply a uniform field through an electrode that covers the whole 2 × 2 mm² sample surface. At the same time we are able to observe with XRD the changes in the intensity of the in-plane domain satellites due to the movement of domain walls as the sample is poled. Taking care to ex-

clude the effects of heating due to leakage, we have been able to show that the observed intensity changes are consistent with the changing relative sizes of up and down ferroelectric domains, which were determined from the electrical data and hence were able to reconcile the structural data with the observed enhanced permittivities reported in Fig. 13c. Note that the intensities of the satellite peaks were observed to recover to their original value upon removal of the field, indicating a return to the polydomain state with approximately equal sizes of the up and down domains and consistent with the absence of macroscopically measurable remanent polarization, as observed in Fig. 13b. A surprising finding was that despite exceeding the thermodynamic coercive field (as predicted by the phenomenological model) the sample never reached a saturated monodomain state.

4 RNiO₃ thin film oxides: a photoemission study (Ph. Aebi, J.-M. Triscone)

4.1 Introduction

Transition-metal oxides, exhibiting perovskite-like structures, are very interesting. In such materials, e.g. the nickelates, manganites or cobaltites, the metal d orbitals overlap with the oxygen p orbitals forming energy bands. The bandwidth in transition-metal oxides is generally narrow and in these systems the Coulomb repulsion plays an important role. Small perturbations can dramatically influence the balance between metallic and insulating properties leading to a metal-insulator transition.

In this scenario, the nickelate family RNiO₃, where R is a trivalent rare-earth ion, is a very interesting case. LaNiO₃ shows metallic conductivity without extra doping, and for $R \neq \text{La}$ a metal to insulator transition appears that requires neither electron nor hole doping. The metal-insulator (MI) transition temperature T_{MI} depends on the rare-earth atomic size [40, 41] and it was observed for the heaviest rare-earth nickelates a charge disproportionation and a crystal structure transition from orthorhombic to monoclinic, taking place at this same temperature.

Although the nickelates is a family that has been extensively studied during the last two decades and very comprehensive reviews can be found in the literature (see for instance Medarde [42] or Catalan [43]), recent results and the emergence of thin film research have caused that, far from fading away, the interest on this type of materials has increased. Indeed, since high-quality large single-crystals

of RNiO₃ are not available to date, the research on thin films increases the experimental possibilities. Also thin films of these materials have potential for various applications such as electrode material in oxide electronics, thermochromatic coatings or non-volatile memory.

Some examples of challenging open questions on RNiO₃ are: to provide a correct detailed structural description that allows the comparison with the smaller rare-earths and check whether this structural description holds for thin films, or to clarify the precise mechanism for the gap opening which is still under debate. Very recent data shows that charge disproportionation of Ni accompanied by a symmetry change from orthorhombic to monoclinic could be the driving force of the MI transition for the entire RNiO₃ family [44, 45].

A very recent paper from Scherwitzl *et al.* [11] has shown that epitaxial LaNiO₃ thin films grown coherently on (001) SrTiO₃ exhibit a MI transition as the film thickness is reduced below 8 unit cells. It follows from this work that a study on a possible gap opening at this transition would be an important issue to clarify. Also it would be compelling to determine the crystal structure of these LaNiO₃ ultrathin films and compare it to the rhombohedral structure exhibited by the bulk material.

For this purpose, angle-resolved photoemission (ARPES) and X-ray photoemission spectroscopy (XPS) are ideal experimental techniques since they are sensitive to material properties in an area close to the surface defined by the escape depth of the electrons. Our experimental setup allows us to operate in two distinct energy regimes: we can study the valence band and the Fermi surface by the use of ultraviolet photons and the core electrons by using soft X-rays. Local, real-space information on the geometrical structure around the emitting atom can be also obtained by performing X-ray photoelectron diffraction (XPD).

4.2 First results

A high-quality epitaxial film of NdNiO₃ of 100 Å thickness has been grown on a [001]-oriented NdGaO₃ substrate ($Pbnm$) by pulsed laser deposition. The details can be found in [12]. The quality of the sample was tested by resistivity measurements and X-ray diffraction. The resistivity of the sample as a function of temperature can be seen in the inset of Fig. 15. The data was collected with the conventional four probe technique. A clear hysteresis can be observed which shows the first order character of the MI transition. It should also be noted that

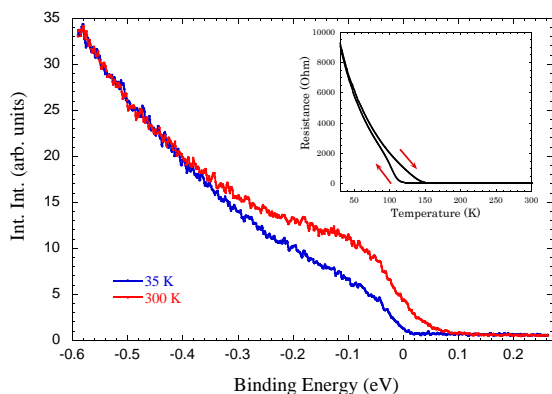


Figure 15: Photoemission spectra in the vicinity of the Fermi level measured at 35 and 300 K on a thin NdNiO_3 film. The inset shows the resistivity of the thin NdNiO_3 film.

T_{MI} is about 20 K lower than in polycrystalline NdNiO_3 probably due to epitaxial strain.

Photoemission spectra were recorded using a He resonance lamp in conjunction with an upgraded Scienta SES-200 hemispherical analyzer with energy resolution of $\Delta E = 10$ meV and integrated in angle. The NdNiO_3 thin film was glued onto a copper sample holder mounted on a He flow cryostat, which achieves temperatures between 18 K and 400 K. The surface was treated with O_2 plasma, and its cleanliness was monitored by XPS. The Fermi energy and instrumental energy resolution were calibrated by measuring a polycrystalline copper sample. Fig. 15 shows the comparison between UPS spectra measured on NdNiO_3 at temperatures above and below the MI transition, i.e. 35 K and 300 K. The change in the density of states (DOS) across the MI transition indicates a gap opening at E_{F} . A noticeable hysteresis in analogy to the resistivity measurements could also be observed.

Measurements on distorted NdNiO_3 thin films with *in situ* photoemission have also been shown recently by Eguchi *et al.* [46]. However, the strain effect on those films was very large, causing T_{MI} to be 50 K higher than in the bulk material and the unit cell parameters to be closer to those on bulk SmNiO_3 .

Our data shows that plasma treatment of the surface of these oxide thin films also allows us to carry out photoemission studies on this type of materials *ex situ*.

5 Organic charge transfer interfaces (A. Morpurgo)

We recently discovered that a large charge transfer occurs at the interface between single-crystals of the organic molecules TTF and

TCNQ (acting as donor and acceptor, respectively) [13]. This charge transfer results in the accumulation of a large density of electrons at the surface of the TCNQ crystal and of holes at the surface of the TTF crystal (larger than 10^{14} cm^{-2}). The electrons and holes are mobile, and cause the interface to be in a metallic state. Remarkably, the fabrication techniques needed for the realization of these TTF/TCNQ systems are extremely simple: for the interface assembly it is sufficient to laminate two thin (less than $1 \mu\text{m}$ thick) crystals on top of each other. This simplicity enables, at least in principle, a much broader class of molecular materials to be used for the preparation of similar systems. This project focuses on the exploration of charge-transfer interfaces based on new materials, with the ultimate goal of gaining control of the electronic properties of the interfacial electron/hole conductor, through the selection of specific organic molecules.

Our work has so far concentrated on exploring different organic donor molecules to be used in place of TTF. To this end, we have realized interfaces between TMTSF and BEDT-TTF crystals, and TCNQ, and analyzed their transport properties as a function of temperature (Fig. 16). We found that both TMTSF/TCNQ and BEDT-TTF/TCNQ interfaces exhibit an electrical conduction that is much larger than that of the constituent materials (that being large gap, undoped semiconductors are virtually insulating). This electrical conductivity, however, is three-to-four orders of magnitude

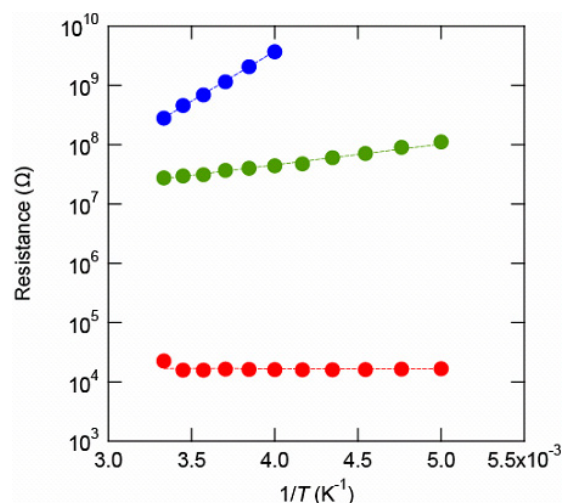


Figure 16: Temperature dependence of the resistance measured in TTF/TCNQ (red circles), TMTSF/TCNQ (green circles), and BEDT-TTF/TCNQ (blue circles) interfaces. The data show the activated behavior of the TMTSF/TCNQ and BEDT-TTF/TCNQ systems.

less in TMTSF/TCNQ than in TTF/TCNQ (the conductivity is even smaller in BEDT-TTF/TCNQ). In addition, in these new interfaces the conductivity decreases with lowering temperature, exhibiting a thermally activated behavior, indicating that these interfaces behave as small gap semiconductors. The measured activation energies are approximately 100 meV for TMTSF/TCNQ and 300 meV for BEDT-TTF/TCNQ.

In the simplest possible scenario, the measured activation energy should correspond to the difference between the energy of the lowest unoccupied molecular orbital (LUMO) level in TCNQ and the energy of the highest occupied molecular orbital (HOMO) in the donor molecules. The relative position (in energy) of these molecular levels can be estimated from cyclic voltametry measurements, even though the absolute precision of this technique is limited (for instance, the values estimated depend on the specific solvent used in the measurements). These experiments indeed show that the TMTSF HOMO level is lower than that of TTF by 100 meV, and that the BEDT-TTF HOMO level is between 200 and 400 meV lower than the level of TTF, which corresponds well to the activation energies measured in transport for both TMTSF/TCNQ and BEDT-TTF/TCNQ. This finding is important, because it gives the clear indication that molecular materials with a higher HOMO level needs to be found in order to achieve metallicity at an interface in conjunction with TCNQ.

6 Advanced techniques to study oxide and organic interfaces (Ph. Willmott)

As mentioned above, the discovery in 2004 of a conducting interface between LaAlO_3 and SrTiO_3 has generated intense activities to try understanding this system and more broadly oxide interface physics. An important aspect of such studies is a detailed structural study of such interfaces [47]. Efforts in this direction are presented below.

In the period under review, work related to Project 1 of the MaNEP network has concentrated on four systems, namely the interface of LaAlO_3 with SrTiO_3 ; the detailed structure of ultrathin $\text{YBa}_2\text{Cu}_3\text{O}_7$ thin films on SrTiO_3 and $(\text{La}_{1-x}\text{Sr}_x)(\text{Al}_y\text{Ta}_{1-y})\text{O}_3$, including studies on the efficacy of a new direct-method structural solution technique, DCAF; the interface between under- and overdoped $\text{La}_{2-x}\text{Sr}_x\text{CuO}_4$; and the structure of nano-templates based on single-layer graphene and *h*-BN on transition-metal surfaces.

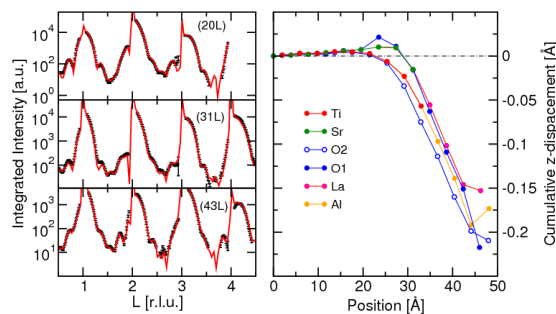


Figure 17: Left: sample SXR of a 5 ML LAO film on STO. Right: the out-of-plane positions of the constituent atoms emerging from the SXR analysis.

6.1 The interface between LaAlO_3 and SrTiO_3

a) *SXR studies* One of the most fascinating properties of this system is the fact that conductivity only appears for LaAlO_3 (LAO) layers thicker or equal to four monolayers (MLs) [34]. In addition, density-functional theory (DFT) calculations by Pentcheva and Pickett have predicted that the LAO film contains layers in which the Oxygen–cation chains become buckled in response to the polar interface [48]. With these and other phenomena in mind, the structure of these systems with picometer accuracy are investigated using surface X-ray diffraction (SXR).

LAO films grown on STO with thicknesses of 2, 3, 4, and 5 MLs were obtained from the group of Prof. Jochen Mannhart, at the University of Augsburg. For each film, a complete SXR data set was recorded and subsequently data-mined and analyzed using the three different methods, DCAF [49], FIT, and COBRA [50].

The emerging atomic structures show that (a) the interface is intermixed for all the investigated films, and (b) there is no significant buckling of the layers. A typical result is shown in Fig. 17.

b) *Hard X-ray photoelectron spectroscopy* In a collaborative project with the group of Prof. Ralf Claessen from the University of Würzburg, the depth profile of the Ti^{3+} concentration was investigated using hard X-ray photoelectron spectroscopy at the BESSY synchrotron [14]. By using hard X-rays, the photoelectron escape depth becomes larger, allowing one to probe embedded interfaces. From the data, an upper limit of 10 nm could be inferred, compatible with recent results using ellipsometry from the group of C. Bernhard (UniFR) [1] and transport anisotropy analyses performed at UniGE [3].

6.2 Ultrathin layers of $\text{YBa}_2\text{Cu}_3\text{O}_7$ and DCAF

The physical processes responsible for high-temperature superconductivity in the cuprates remains unresolved more than twenty years after their discovery. One of the most powerful tools available to condensed-matter physicists to probe the electronic structure of these materials is angle-resolved photoelectron spectroscopy (ARPES). The validity of ARPES data depends intimately on the assumption that the topmost region of the sample down to the photoelectron escape depth of only one or two nanometers is also representative of the bulk properties. As the surface can often be radically different from the bulk, this assumption was tested for ultrathin films of $\text{YBa}_2\text{Cu}_3\text{O}_7$ (YBCO) using SXRD.

Films grown on both $\text{SrTiO}_3(001)$ (STO) and $(\text{La}_{1-x}\text{Sr}_x)(\text{Al}_y\text{Ta}_{1-y})\text{O}_3(001)$ (LSAT) exhibit perfect pseudomorphic strain, that is the films are tetragonal. Despite this, they show good superconducting properties. Importantly, the films all begin growth with the stacking sequence

substrate | $\text{BaO-CuO}_2\text{-Y-CuO}_2\text{-BaO-CuO}\dots$. The cumulative out-of-plane positions of the film atoms are all within ± 5 pm of the known bulk values. This result should improve the confidence in interpretation of ARPES data.

In obtaining these results, the direct method ‘‘DCAF’’ was used. The advantage of direct (phase-retrieval) methods over conventional fitting techniques is twofold. First, one can avoid becoming trapped in local minima in parameter space, and thereby find the global minimum. Secondly, the technique is model-independent – no input information is given regarding the film structure [49]. That bulklike YBCO emerges from our data and DCAF is a stunning confirmation of the efficacy of this analytical technique (Fig. 18).

6.3 The interface between under- and overdoped $\text{La}_{2-x}\text{Sr}_x\text{CuO}_4$

In 2008, Gozar *et al.* reported on the formation of high-temperature superconductivity between under- and overdoped thin films of $\text{La}_{2-x}\text{Sr}_x\text{CuO}_4$ (LSCO) [35], whereby the critical temperature is enhanced compared to that of optimally doped bulk LSCO.

In a collaborative project with the groups of Professors Ivan Bozovic and Ron Pindak, both of Brookhaven National Laboratories (BNL), the structure of the interface was investigated using SXRD. The resulting data was then independently analyzed using COBRA (at BNL) and DCAF (at PSI). Until now, the structures

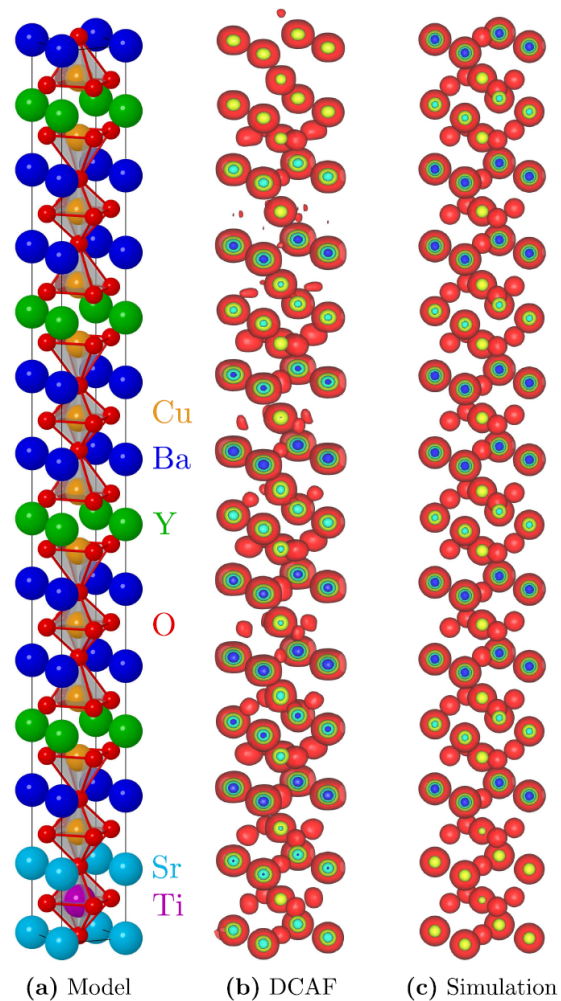


Figure 18: DCAF results compared to bulk YBCO: (a) ball-and-stick model; (b) isosurfaces of the DCAF-retrieved electron-density map; (c) isosurfaces of a simulated electron-density map based on (a).

that emerge are very similar, except in one critical aspect, the distance of the apical Oxygen at the interface. The DCAF results seem to indicate that the apical Oxygen is essentially bulklike, while from COBRA, an increase in the apical Oxygen position is seen, which could explain the enhanced superconducting properties. The relative merits and degree of confidence in these techniques is being investigated to try and resolve this apparent contradiction.

6.4 Structural studies of *h*-BN and graphene on transition metals

Graphene has provoked enormous interest since its discovery in 2004 [51], due mainly to its potential in electronic applications. On the other hand, both graphene and its isoelectronic cousin, single-layer hexagonal boron nitride (*h*-BN), show fascinating structural fea-

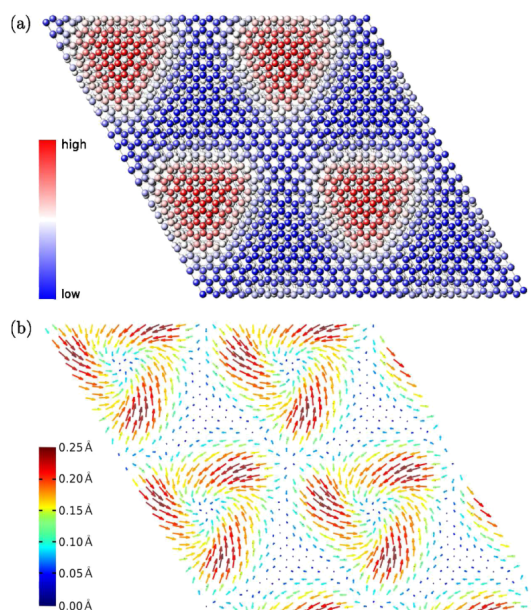


Figure 19: Graphene on Ru(0001) – a corrugated and chiral structure. (a) the out-of-plane islands and valleys produced by the moiré-like bonding of graphene to Ru(0001). (b) map of the in-plane movements of the same system.

tures when deposited on certain transition-metal surfaces, particularly rhodium(111) and ruthenium(0001). In these systems, the sp^2 -hybridized layer (be it graphene or h -BN) bonds relatively strongly to the metal surface, whereby the slight differences in the lattice constants cause the bonding strength to “beat” causing the formation of a corrugated superstructure with a periodicity of the order of 30 Å [52, 53][15, 16, 17].

SXRD has proven to be exceptionally well suited to study the detailed structures of these systems, and has resolved open issues regarding the periodicity of the superstructures and the amplitude of the corrugation. Perhaps the most exciting result to emerge, however, has been the evidence of chiral twisting of the graphene layer when grown on Ru(0001) (Fig. 19) [15]. Very recent and unpublished results using the highest resolution scanning tunneling microscopy have confirmed the chirality.

7 Domain walls in ferroelectric/multiferroic systems (P. Paruch)

7.1 Introduction

The delicate balance of long and short-range interactions giving rise to ferroic ordering in many complex oxide compounds have made them fascinating objects of fundamental study, as well as goldmines for present and future

technological applications using the different physical properties (ferroelectric polarization, magnetization, ferroelastic ordering, piezo- and pyro-electricity) of these materials. Recent interest in the field has focused on single-phase or composite oxide thin films with two or more coexisting and, ideally, coupled ferroic orders (with the definition often broadened to include different types of magnetic ordering, and not just ferromagnetism) [54]. In particular, magneto-electric multiferroics in which (anti)ferromagnetic ordering can be controlled by applied electric fields, and the ferroelectric polarization by applied magnetic fields, show great promise for spintronic applications and multiple-state memories [55, 56]. However, the specific mechanisms behind magneto-electric coupling in nano-composites [57], or its effects on the switching dynamics [58] and domain structure [18] in the one widely-studied, naturally occurring room-temperature multiferroic, BiFeO₃ (BFO) remain a little understood theoretical and experimental challenge.

A large part of our research effort is focused specifically on domain walls in (multi)ferroic materials, an intrinsically nano-scale multifunctional system, which can be quantitatively probed using the high resolution of different atomic force microscopy (AFM) techniques. Fundamentally, domain walls provide a useful model elastic disordered system: their behavior is governed by the competition between their elastic energy, which tends to minimize the domain wall surface, and the randomly varying potential landscape due to disorder present in the samples, which allows pinning [19]. The domain walls present a characteristic static roughness, and a complex dynamic response when subjected to a driving force (applied field), with non-linear creep observed for small forces, as has been shown in pure ferromagnetic and ferroelectric systems [59][20, 21]. In addition, as a result of different symmetries and electronic structures, as well as possible defect migration, these intrinsically nano-scale interfaces often show additional properties, beyond those of their already multifunctional parent material, such as conduction [60] or possibly ferromagnetism [61] at certain ferroelectric domain walls in BFO, or polar behavior at ferroelastic domain walls in SrTiO₃ [62], opening new perspectives for device applications [22]. Our studies, using a combination of piezoresponse force microscopy (PFM), magnetic and electric force microscopies (MFM and EFM, respectively), address these two aspects of domain wall behavior in a variety of perovskite oxide systems.

7.2 Shear effects in lateral piezoresponse force microscopy at 180° ferroelectric domain walls

Piezoresponse force microscopy is the primary tool for nano-scale characterization of ferroelectric domains, with the vertical (VPFM) and lateral (LPFM) components of the piezoresponse, given by the vertical deflection and lateral torsion of the AFM cantilever, respectively, linked to the out-of-plane and in-plane polarization. In the case of uniformly polarized tetragonal ferroelectrics, the response to an out-of-plane electric field is determined by the d_{33} piezoelectric coefficient, leading to a VPFM signal, while the d_{35} and d_{34} coefficients, corresponding to a lateral shear response, are zero by symmetry. However, studies on such materials have shown non-zero LPFM signal at 180° domain walls, generally seen as an artifact attributable to either surface tilting [63, 64] or electrostatic effects [65]. Only recently, theoretical work has shown that a local symmetry lowering at these walls can lead to a non-zero d_{35} coefficient [66], thus allowing local shear and an LPFM signal.

In PFM measurements of domains in epitaxial thin films of $\text{Pb}(\text{Zr}_{0.2}\text{Ti}_{0.8})\text{O}_3$ (PZT) (001) films grown by rf-magnetron sputtering on SrTiO_3 substrates with SrRuO_3 electrodes, we observed a clear LPFM signal at 180° domain walls, as shown in Fig. 20.

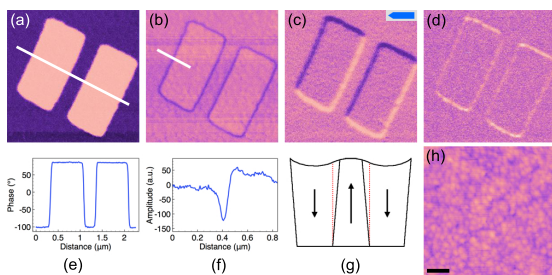


Figure 20: PFM measurement of rectangular ferroelectric domains written on PZT by applying +12 V to the scanning tip in an as grown monodomain region (scale bar is $0.5 \mu\text{m}$). Each domain structure shows a 180° contrast in the vertical phase (a), (e) with a corresponding minimal vertical amplitude at the domain wall (b), (f). Two opposite non-zero signals (dark and bright colors) are observed in the lateral phase (c) perpendicularly to the AFM cantilever at the position of these domain walls, with a corresponding rise in the lateral amplitude (d). The orientation of the AFM cantilever is indicated by the blue arrow in (c). (g) Schematic representation of domain wall shear deformation due to locally non-zero d_{35} coefficient (dashed red lines show the initial domain wall positions). (h) Topography of the region, showing a 4 \AA rms surface roughness [23].

To investigate the mechanism behind the observed response, we carried out electric force microscopy studies of the electrostatic surface effects, which we found to diminish strongly over time, while both the vertical and lateral PFM signals remained close to their initial values, demonstrating that electrostatic effects do not significantly contribute to the observed LPFM response. From topographical measurements across the domain walls, compared with numerical models of surface tilting, we also eliminate this latter mechanism as a significant contribution, and conclude that the observed response is indeed due to the non-zero effective d_{35} coefficient present only at domain walls [23]. We also show that a lateral shear response is observed in systems such as 71 , 180 and 109° domain walls in BiFeO_3 and 90° domain walls in PZT films with both a and c -axis domains, where it is superimposed on the signal due to in-plane polarization [24].

7.3 Ferroelectric switching dynamics in epitaxial BiFeO_3 thin films

A promising candidate for room temperature devices is BiFeO_3 (BFO), presenting magnetoelectrically coupled antiferromagnetic and ferroelectric ordering up to high temperatures [25]. However, extensive quantitative studies have been rendered challenging in part by the complex ferroelectric structure of BFO, with eight equivalent polarization variants giving rise to domains separated by three different types of domain walls (71 , 109 and 180°). One important aspect is control over the switching path from one domain configuration to another under an applied electric field [58], since this may bring about a rotation of the antiferromagnetic plane in the case of 109 and 71° switching. To investigate switching in the combined vertical and (very small) horizontal electric field provided by the AFM tip, we carried out PFM measurements of domains in epitaxial BFO (001) films grown on SrTiO_3 with SrRuO_3 electrodes by pulsed laser deposition [26]. Using polydomain films presenting all eight polarization variants, we prepolarized wide horizontal domains with alternating positive and negative voltage, then wrote lines sweeping the tip along either $[010]$ or $[0\bar{1}0]$.

In VPFM, as expected, the domains written with negative voltage (“up” polarization) show a dark contrast (Fig. 21b), while the positive-voltage-written domains are bright. In LPFM along $[100]$ (Fig. 21c), we observe that the negatively-written rectangles (1) show bright contrast indicating an in-plane polariza-

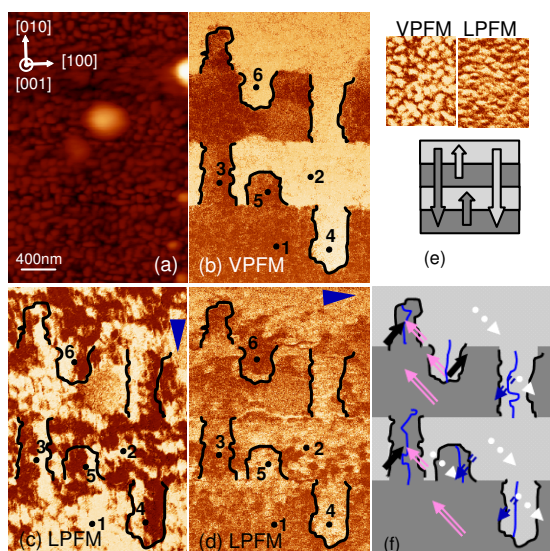


Figure 21: (a) Topography, (b) VPFM, (c) and (d) LPFM after writing large horizontal rectangles with negative and positive voltages and then sweeping the tip vertically. The blue triangles indicate the orientation of the cantilever during LPFM measurements. As grown VPFM and LPFM images and the written pattern are indicated in upper part of (e). Lower part of (e): dark gray corresponds to -12 V, light gray to $+12$ V, and the arrows indicate the sweeping direction. For the rectangles, the slow scan axis was along $[0\bar{1}0]$. The black lines correspond to domain walls written during vertical tip sweeps (b). (f) Out-of-plane (bright and dark colors) and in-plane orientation of polarization (arrows) determined from the PFM measurements. The black lines follow those of (b). For the numbers, see text [26].

tion component along $[\bar{1}00]$, while positively written rectangles (2) show a predominantly dark contrast (in-plane polarization component along $[100]$). In the subsequently written lines, the in-plane component of the polarization was also modified, but only in the specific regions in which the out-of-plane polarization was concurrently reversed (outlined in black in Fig. 21b–d). The characteristic pattern observed in these regions (dark LPFM contrast on the right and bright on the left for the negative-voltage-written lines (3, 5), and the opposite for positive-voltage-written lines (4, 6), correlates with the horizontal component of the electric field perpendicular to the cantilever axis during writing. In LPFM along $[010]$ (Fig. 21d), we again observe in-plane switching only where the out-of-plane polarization component is switched (outlined in black). In these measurements, however, the LPFM contrast depends on both the voltage polarity and the tip sweeping direction during writing. For lines negatively written along $[0\bar{1}0]$ (3) dark

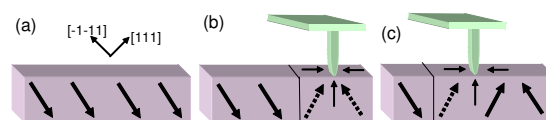


Figure 22: Schematic representation of the switching mechanism: starting with (a) a homogeneous polarization along $[11\bar{1}]$ (wide arrows), a negative voltage applied to the tip switches the polarization (dashed wide arrows) to $[11\bar{1}]$ leftwards, and $[\bar{1}11]$ rightwards, following the direction of both vertical and horizontal electric field components (small narrow arrows) (b). When the negative-voltage tip is swept leftwards the in-plane polarization will be modified only if the out-of-plane component of the polarization is switched, i.e. to the left of the cantilever (c). In the end, the in-plane component of the polarization will thus present a thin stripe with polarization oriented along $[\bar{1}11]$ in the initial switching region and then along $[11\bar{1}]$ in the rest of the area swept by the tip, giving an in-plane component opposite to the tip sweeping direction, as experimentally observed (Fig. 21f) [26].

contrast is observed whereas while for lines negatively written along $[010]$, the contrast is bright (5). For positively-written lines, the opposite is observed: along $[0\bar{1}0]$, the contrast is bright (4), along $[010]$, the contrast is dark (6). The in-plane polarization switching under a bi-ased tip is thus assisted by the out-of-plane polarization switching in this range of fields and reproduces the horizontal electric field distribution, as schematically described in Fig. 22.

8 Collaborative efforts

As can be seen from this report, several collaborations are ongoing and new ones are starting between the MaNEP members of Project 1. Let us mention here the new collaboration on nickelate thin films where growth, standard characterization and transport measurements will be complemented by photoemission and surface X-ray diffraction studies (Aebi, Triscone, Willmott). A new collaboration will also start on the LAO/STO interface where high pressure, optical studies, and nano-lithography will be used to try better understanding the properties of this fascinating interface (Bernhard, Jaccard, Morpurgo, Triscone). Finally, on PTO/STO superlattices, X-ray photoelectron diffraction and surface X-ray diffraction will be used to better understand the structural properties at interfaces, in particular for samples displaying improper ferroelectricity (Aebi, Triscone, Willmott).

MaNEP-related publications

- [1] A. Dubroka, M. Rössle, K. W. Kim, V. K. Malik, L. Schulz, S. Thiel, C. W. Schneider, J. Mannhart, G. Herranz, O. Copie, M. Bibes, A. Barthélémy, and C. Bernhard, *to be published in Physical Review Letters* (2010).
- [2] S. S. A. Seo, M. J. Han, G. W. J. Hassink, W. S. Choi, S. J. Moon, J. S. Kim, T. Susaki, Y. S. Lee, J. Yu, C. Bernhard, H. Y. Hwang, G. Rijnders, D. H. A. Blank, B. Keimer, and T. W. Noh, *Physical Review Letters* **104**, 036401 (2010).
- [3] N. Reyren, S. Gariglio, A. D. Caviglia, D. Jaccard, T. Schneider, and J.-M. Triscone, *Applied Physics Letters* **94**, 112506 (2009).
- [4] A. D. Caviglia, M. Gabay, S. Gariglio, N. Reyren, C. Cancellieri, and J.-M. Triscone, *Physical Review Letters* **104**, 126803 (2010).
- [5] A. D. Caviglia, S. Gariglio, N. Reyren, D. Jaccard, T. Schneider, M. Gabay, S. Thiel, G. Hammerl, J. Mannhart, and J.-M. Triscone, *Nature* **456**, 624 (2008).
- [6] A.-S. Rüetschi, High Pressure, Quasi-Hydrostaticity and Multiprobes: Instrumental Development and Studies of Organic Conductors and the LaAlO₃/SrTiO₃ Interface, Ph.D. thesis, Université de Genève (2009).
- [7] J. Hoppler, J. Stahn, C. Niedermayer, V. K. Malik, H. Bouyanfif, A. J. Drew, M. Rössle, A. Buzdin, G. Cristiani, H.-U. Habermeier, B. Keimer, and C. Bernhard, *Nature Materials* **8**, 315 (2009).
- [8] N. Reyren, S. Thiel, A. D. Caviglia, L. F. Kourkoutis, G. Hammerl, C. Richter, C. W. Schneider, T. Kopp, A.-S. Ruetschi, D. Jaccard, M. Gabay, D. A. Muller, J.-M. Triscone, and J. Mannhart, *Science* **317**, 1196 (2007).
- [9] M. Dawber, N. Stucki, C. Lichtensteiger, S. Gariglio, P. Ghosez, and J.-M. Triscone, *Advanced Materials* **19**, 4153 (2007).
- [10] E. Bousquet, M. Dawber, N. Stucki, C. Lichtensteiger, P. Hermet, S. Gariglio, J.-M. Triscone, and P. Ghosez, *Nature* **452**, 732 (2008).
- [11] R. Scherwitzl, P. Zubko, C. Lichtensteiger, and J.-M. Triscone, *Applied Physics Letters* **95**, 222114 (2009).
- [12] V. Scagnoli, U. Staub, M. Janousch, A. M. Mulders, M. Shi, G. I. Meijer, S. Rosenkranz, S. B. Wilkins, L. Paolasini, J. Karpinski, S. M. Kazakov, and S. W. Lovesey, *Physical Review B* **72**, 155111 (2005).
- [13] H. Alves, A. S. Molinari, H. Xie, and A. F. Morpurgo, *Nature Materials* **7**, 574 (2008).
- [14] M. Sing, G. Berner, K. Goß, A. Müller, A. Ruff, A. Wetscherek, S. Thiel, J. Mannhart, S. A. Pauli, C. W. Schneider, P. R. Willmott, M. Gorgoi, F. Schäfers, and R. Claessen, *Physical Review Letters* **102**, 176805 (2009).
- [15] D. Martoccia, M. Björck, C. M. Schlepütz, T. Brugger, S. A. Pauli, B. D. Patterson, T. Greber, and P. R. Willmott, arXiv:0908.4517 (2009).
- [16] D. Martoccia, S. A. Pauli, T. Brugger, T. Greber, B. D. Patterson, and P. R. Willmott, *Surface Science* **604**, L9 (2010).
- [17] D. Martoccia, T. Brugger, M. Björck, C. M. Schlepütz, S. A. Pauli, T. Greber, B. D. Patterson, and P. R. Willmott, *Surface Science* **604**, L16 (2010).
- [18] G. Catalan, H. Béa, S. Fusil, M. Bibes, P. Paruch, A. Barthélémy, and J. F. Scott, *Physical Review Letters* **100**, 027602 (2008).
- [19] T. Giamarchi, A. B. Kolton, and A. Rosso, in *Jamming, Yielding and Irreversible Deformation in Condensed Matter*, M. C. Miguel and J. M. Rubi, eds. (Springer-Verlag, Berlin, 2006), vol. 688 of *Lecture Notes in Physics*, p. 91.
- [20] T. Tybell, P. Paruch, T. Giamarchi, and J.-M. Triscone, *Physical Review Letters* **89**, 097601 (2002).
- [21] P. Paruch, T. Giamarchi, and J.-M. Triscone, *Physical Review Letters* **94**, 197601 (2005).
- [22] H. Béa and P. Paruch, *Nature Materials* **8**, 168 (2009).
- [23] J. Guyonnet, H. Béa, F. Guy, S. Gariglio, S. Fusil, K. Bouzehouane, J.-M. Triscone, and P. Paruch, *Applied Physics Letters* **95**, 132902 (2009).
- [24] J. Guyonnet, H. Béa, and P. Paruch, *to be published in Journal of Applied Physics* (2010).
- [25] G. Catalan and J. F. Scott, *Advanced Materials* **21**, 2463 (2009).
- [26] H. Béa, P. Paruch, M. Bibes, and A. Barthélémy, arXiv:0907.4568 (2009).

Other references

- [27] A. Ohtomo and H. Y. Hwang, *Nature* **427**, 423 (2004).
- [28] M. Basletic, J. L. Maurice, C. Carrétéro, G. Herranz, O. Copie, M. Bibes, É. Jacquet, K. Bouzehouane, S. Fusil, and A. Barthélémy, *Nature Materials* **7**, 621 (2008).
- [29] O. Copie, V. Garcia, C. Bödefeld, C. Carrétéro, M. Bibes, G. Herranz, E. Jacquet, J.-L. Maurice, B. Vinter, S. Fusil, K. Bouzehouane, H. Jaffrès, and A. Barthélémy, *Physical Review Letters* **102**, 216804 (2009).
- [30] Y. A. Bychkov and R. E. I., *Journal of Physics C: Solid State Physics* **17**, 6039 (1984).
- [31] G. Bergmann, *Physics Reports* **107**, 1 (1984).
- [32] J. Nitta, T. Akazaki, H. Takayanagi, and T. Enoki, *Physical Review Letters* **78**, 1335 (1997).
- [33] S. Maekawa and H. Fukuyama, *Journal of the Physical Society of Japan* **50**, 2516 (1981).
- [34] S. Thiel, G. Hammerl, A. Schmehl, C. W. Schneider, and J. Mannhart, *Science* **313**, 1942 (2006).
- [35] A. Gozar, G. Logvenov, L. Fitting-Kourkoutis, A. T. Bollinger, L. A. Giannuzzi, D. A. Muller, and I. Bozovic, *Nature* **455**, 782 (2008).
- [36] G. Logvenov, A. Gozar, and I. Bozovic, *Science* **326**, 699 (2009).
- [37] A. Ino, T. Mizokawa, K. Kobayashi, A. Fujimori, T. Sasagawa, T. Kimura, K. Kishio, K. Tamasaku, H. Eisaki, and S. Uchida, *Physical Review Letters* **81**, 2124 (1998).
- [38] V. M. Loktev and Y. G. Pogorelov, *Physical Review B* **78**, 180501 (2008).
- [39] J. R. Clem, *Physical Review B* **43**, 7837 (1991).
- [40] P. Lacorre, J. B. Torrance, J. Pannetier, A. I. Nazzal, P. W. Wang, and T. C. Huang, *Journal of Solid State Chemistry* **91**, 225 (1991).
- [41] J. B. Torrance, P. Lacorre, A. I. Nazzal, E. J. Ansaldo, and C. Niedermayer, *Physical Review B* **45**, 8209 (1992).
- [42] M. L. Medarde, *Journal of Physics: Condensed Matter* **9**, 1679 (1997).
- [43] G. Catalan, *Phase Transitions* **81**, 729 (2008).
- [44] M. Medarde, M. T. Fernández-Díaz, and P. Lacorre, *Physical Review B* **78**, 212101 (2008).

- [45] J. A. Alonso, J. L. García-Muñoz, M. T. Fernández-Díaz, M. A. G. Aranda, M. J. Martínez-Lope, and M. T. Casais, *Physical Review Letters* **82**, 3871 (1999).
- [46] R. Eguchi, Y. Okamoto, Z. Hiroi, S. Shin, A. Chainani, Y. Tanaka, M. Matsunami, Y. Takata, Y. Nishino, K. Tamasaku, M. Yabashi, and T. Ishikawa, *Journal of Applied Physics* **105**, 056103 (2009).
- [47] P. R. Willmott, S. A. Pauli, R. Herger, C. M. Schlepütz, D. Martoccia, B. D. Patterson, B. Delley, R. Clarke, D. Kumah, C. Cionca, and Y. Yacoby, *Physical Review Letters* **99**, 155502 (2007).
- [48] R. Pentcheva and W. E. Pickett, *Physical Review Letters* **102**, 107602 (2009).
- [49] M. Björck, C. M. Schlepütz, S. A. Pauli, D. Martoccia, R. Herger, and P. R. Willmott, *Journal of Physics: Condensed Matter* **20**, 445006 (2008).
- [50] Y. Yacoby, M. Sowwan, E. Stern, J. Cross, D. Brewe, R. Pindak, J. Pitney, E. B. Dufresne, and R. Clarke, *Physica B* **336**, 39 (2003).
- [51] K. S. Novoselov, A. K. Geim, S. V. Morozov, D. Jiang, Y. Zhang, S. V. Dubonos, I. V. Grigorieva, and A. A. Firsov, *Science* **306**, 666 (2004).
- [52] M. Corso, W. Auwärter, M. Muntwiler, A. Tamai, T. Greber, and J. Osterwalder, *Science* **303**, 217 (2004).
- [53] D. Martoccia, P. R. Willmott, T. Brugger, M. Björck, S. Günther, C. M. Schlepütz, A. Cervellino, S. A. Pauli, B. D. Patterson, S. Marchini, J. Wintterlin, W. Moritz, and T. Greber, *Physical Review Letters* **101**, 126102 (2008).
- [54] W. Eerenstein, N. D. Mathur, and J. F. Scott, *Nature* **442**, 759 (2006).
- [55] M. Fiebig, T. Lottermoser, D. Frölich, A. V. Goltsev, and R. V. Pisarev, *Nature* **419**, 818 (2002).
- [56] M. Bibes and A. Barthélémy, *Nature Materials* **7**, 425 (2008).
- [57] F. Zavaliche, T. Zhao, H. Zheng, F. Straub, M. P. Cruz, P.-L. Yang, D. Hao, and R. Ramesh, *Nano Letters* **7**, 1586 (2007).
- [58] S. Lisenkov, D. Rahmedov, and L. Bellaiche, *Physical Review Letters* **103**, 047204 (2009).
- [59] S. Lemerle, J. Ferré, C. Chappert, V. Mathet, T. Giamarchi, and P. Le Doussal, *Physical Review Letters* **80**, 849 (1998).
- [60] J. Seidel, L. W. Martin, Q. He, Q. Zhan, Y.-H. Chu, A. Rother, M. E. Hawkrigde, P. Maksymovych, P. Yu, M. Gajek, N. Balke, S. V. Kalinin, S. Gemming, F. Want, G. Catalan, J. F. Scott, N. A. Spaldin, J. Orenstein, and R. Ramesh, *Nature Materials* **8**, 229 (2009).
- [61] J. Přivratská and V. Janovec, *Ferroelectrics* **222**, 281 (1999).
- [62] P. Zubko, G. Catalan, A. Buckley, P. R. L. Welche, and J. F. Scott, *Physical Review Letters* **99**, 167601 (2007).
- [63] J. Wittborn, C. Canalias, K. V. Rao, R. Clemens, H. Karlsson, and F. Laurell, *Applied Physics Letters* **80**, 1622 (2002).
- [64] D. A. Scrymgeour and V. Gopalan, *Physical Review B* **72**, 024103 (2005).
- [65] T. Jungk, Á. Hoffman, and E. Soergel, *Applied Physics Letters* **89**, 042901 (2006).
- [66] A. N. Morozovska, E. A. Eliseev, S. L. Bravina, and S. V. Kalinin, *Physical Review B* **75**, 174109 (2007).

Project **2****Materials for future electronics**

Project leader: A. Morpurgo (UniGE)

Participating members: M. Büttiker (UniGE), T. Giamarchi (UniGE), D. van der Marel (UniGE), A. Morpurgo (UniGE), P. Paruch (UniGE), C. Renner (UniGE), M. Sigrist (ETHZ), J.-M. Triscone (UniGE)

Introduction: The development of novel materials with sufficiently well-controlled properties opens the possibility to fabricate electronic devices that are useful for fundamental physics and have potential for future applications. According to a strategy typical of mesoscopic physics, these devices enable focused experiments to probe specific microscopic electronic processes not accessible in bulk systems. In this project we focus on classes of novel materials that are sufficiently under control to enable the realization of new nano-structures. The materials investigated include oxide heterostructures and thin films, carbon-based materials such as graphene and organic molecular crystals, and their combinations. In the spirit of mesoscopic physics, the experimental program proceeds in conjunction with a theoretical effort, that is needed to provide assistance in designing specific devices and experiments, as well as in the interpretation of the experimental results.

Summary and highlights

We use oxide materials and carbon-based systems such as graphene and organic semiconductors for the realization of new nano-electronic devices that are of interest for fundamental studies, and have potential for possible future electronics applications. On oxide materials, we have developed a technology for the nano-scale patterning of $\text{LaAlO}_3/\text{SrTiO}_3$ heterostructures (which are superconducting and possess strong spin-orbit interaction), and we have successfully created gate-tunable conducting channels with 100 nm lateral dimension. Significant progress has also been made in integrating carbon nanotubes and ferroelectric materials, with the twofold goal of gaining nano-scale control of the electrical polarization of the ferroelectric, and of integrating new electronic functionalities in nanotube devices. Research on graphene-based materials has advanced in several directions. These include the understanding of trilayer-graphene (previously unexplored), the detailed study of optical spectroscopy of gated bilayer devices – that have enabled a complete understanding of the basic band structure parameters, the

use of SrTiO_3 as substrate, which provide a very high dielectric constant environment for charge carriers. Furthermore, first devices have been fabricated to test a scanning probe facility, which will be used to investigate local properties of graphene edges by means of combined AFM/STM spectroscopy. The experimental work has proceeded in parallel to theoretical studies of the same problems. Graphene edges have been investigated in the ideal disorder-free case, to analyze the possible occurrence of a Peierls transition in a temperature range accessible experimentally. The effects of edge disorder have been studied for gapped bilayers – which have properties similar to those of the newly discovered topological insulators. This has led to the conclusion that edge states of topological origin are robust against non-idealities, and can give a dominant contribution to the conductance of actual devices under realistic conditions. Finally, the analysis of quasi-one-dimensional superconductivity has shown that weak coupling to a normal state conducting channel increases the stability of the superconducting state, a conclusion that may be relevant for future work on $\text{LaAlO}_3/\text{SrTiO}_3$ channels.

1 Nano-structures with oxide materials

A variety of different oxide materials have become available in heterostructure and thin-film form, with quality and reproducibility sufficient to explore their nano-scale properties by means of different experimental techniques. Contrary to the case of more conven-

tional semiconductors like gallium arsenide or silicon, oxide-based nano-electronics is a new emerging field, and research has a truly exploratory character. It offers the potential to make unexpected discoveries and to identify new phenomena potentially relevant for elec-

tronic applications.

1.1 Nano-structuring $\text{LaAlO}_3/\text{SrTiO}_3$ conducting interfaces (J.-M. Triscone and A. Morpurgo)

The use of electron beam lithography (EBL) makes it possible to fabricate solid state devices with small lateral dimensions, on the scale of different characteristic lengths of electronic systems. This possibility has enabled the study of fascinating physical phenomena in conventional semiconductor devices. To date, however, the use of nano-fabrication techniques to create nano-structures based on conducting materials with novel electronic properties such as complex oxides has been very limited.

In this collaborative project between the groups of J.-M. Triscone and A. Morpurgo, we explore the possibility to realize nano-scale structures in the electron gas present at the $\text{LaAlO}_3/\text{SrTiO}_3$ interface. This electronic system displays a rich phase diagram [1], with a superconducting phase separated by a quantum critical point from a conducting phase, which displays signatures of phase-coherent transport phenomena (i.e. weak localization). In addition, strong spin-orbit interaction is also present and it was shown that both interface superconductivity and spin-orbit coupling can be tuned using the electric field effect [2]. Combining the ability to tune the electronic properties of the system with an electric field together with the capability of the electron beam lithography to pattern small structures should allow the fabrication of devices where the interplay between spin-orbit and superconductivity can be probed.

Different devices were fabricated, whose lat-

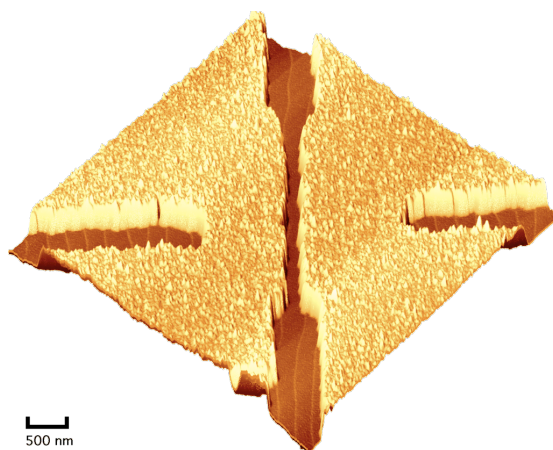


Figure 1: AFM topography of a side gate field effect device based on the $\text{LaAlO}_3/\text{SrTiO}_3$ interface with lateral dimension of the order of 150 nm.

eral dimension (around 100 nm) is comparable to the electronic mean free path and to the superconducting coherence length. Patterning relies on a sophisticated combination of lift-off processes with material re-growth. Specifically, a mask defining a field effect device with a narrow transport channel is patterned on the surface of a single-crystal of TiO_2 -terminated SrTiO_3 , using the electron sensitive negative resist mr-EBL 6000 (produced by Micro Resist Technology). After development, a 20 nm thick layer of amorphous SrTiO_3 is deposited by room-temperature pulsed laser deposition (PLD). The resist is then lifted-off, resulting in the nano-structuring of the substrate as depicted in Fig. 1, where we can distinguish regions where the amorphous STO is present (thick and relatively rough) from a transport channel and two side gate electrodes (atomically flat with a step and terrace structure). The last step of the process consists in depositing a thin film of LaAlO_3 by high-temperature PLD. Only in the regions of the substrate where the amorphous SrTiO_3 layer is absent, the LaAlO_3 thin film grows epitaxially and an electron gas is formed. These devices have been characterized by transport measurements from room temperature down to 20 mK. The samples exhibit metallic behavior and superconductivity, as shown in Fig. 2. These observations demonstrate the appropriateness of the fabrication technology. As a next step, we will study the effects of the reduced lateral size on the superconducting properties of the system, and subsequently we will try to fabricate more complex device structures, such as Aharonov-Bohm rings and electrostatically gated geometries.

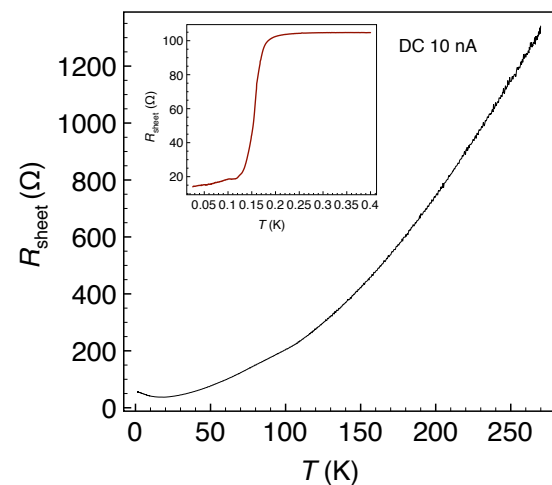


Figure 2: Resistance versus temperature of a 150 nm wide channel based on the $\text{LaAlO}_3/\text{SrTiO}_3$ interface measured using a 4 points dc technique.

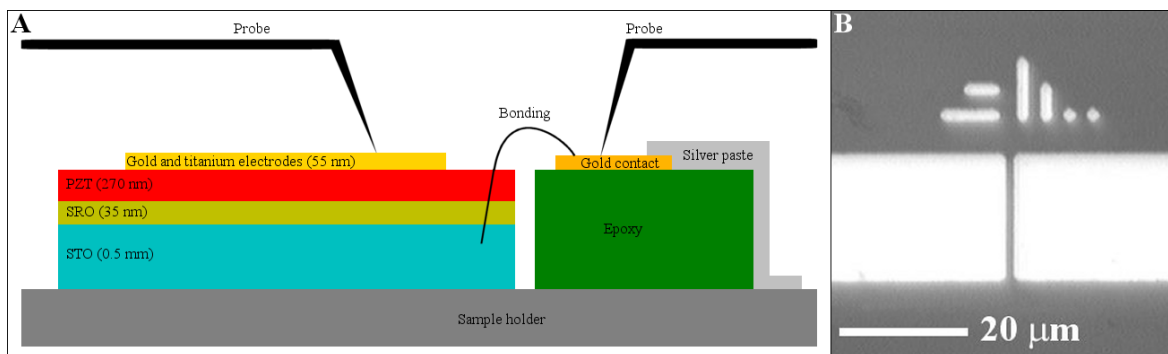


Figure 3: (A) Schematic side view of the experimental device. (B) Optical microscope view (1000 \times) of the central part of the electrodes and the position markers.

1.2 Hybrid ferroelectric/carbon nanotubes structures (P. Paruch)

Ferroelectric thin films and carbon nanotubes (CNTs) both possess unique properties, such as (reversible) spontaneous polarization, pyroelectric and piezoelectric behavior for the former, and extremely high-mechanical strength together with quasi-one-dimensional insulating, semi-conducting, and metallic behavior for the latter. The properties of these individual systems are relatively well understood, but their combination has remained virtually unexplored, despite the potential for new multifunctional devices. Indeed, CNTs can be used to control the polarization of ferroelectrics, ideally on a nanometer scale [3], since single-wall CNTs have diameters of ~ 2 nm, an order of magnitude smaller than the sharpest atomic force microscope (AFM) tips. Conversely, a ferroelectric substrate can be used to inject or deplete charge carriers in an overlying CNT through field effect [4], by accumulating densities of carriers well beyond what can be achieved with more conventional gated devices, and potentially with nano-scale resolution [5]. From the technological side, the main challenge is to obtain a clean interface between defect-free single-wall CNTs and an undamaged ferroelectric surface. In previous work, we found that devices fabricated by direct growth of CNT on BaTiO_3 allowed polarization switching, but deteriorated the ferroelectric surface, leading to charge injection rather than ferroelectric field effect [6]. The opposite strategy – i.e. the growth of ferroelectric onto existing CNTs done by Kawasaki *et al.* – resulted in deterioration of the CNTs during the high-temperature oxygen annealing necessary for ferroelectric crystallization [23].

The present project aims at going beyond state-of-the-art, by realizing single-wall CNT/ferroelectric interfaces suitable for both

nano-scale polarization control and clear ferroelectric field effect modulation. To this end, we spin-coated CNTs onto a 270 nm PZT thin film, grown by radio frequency magnetron sputtering on SrTiO_3 (001) single-crystals (with a 35 nm conducting top SrRuO_3 (SRO) layer). Ti (5 nm)–Au (50 nm) electrodes were fabricated using photolithography, e-beam evaporation, and lift-off. The single-wall CNTs, with nominal lengths between 5 and 15 μm , were purchased in powder form (SES Research), and subsequently suspended in deionized water using a long, low-power sonication (24 h, 30 W, 45 kHz) with sodium dodecylbenzenesulfonate as surfactant (the resulting suspension was completely opaque and stable for months). After multiple spin-coating runs (4000 rpm), we found a density of about 10'000 nanotubes/ mm^2 on the PZT surface, whose length ranged between 1 and 5 μm . Individual CNTs in contact with the Au-Ti electrodes were located and characterized by AFM tapping mode measurements. To study the growth of ferroelectric domains under and beside these CNTs, a voltage was applied between the top Au-Ti electrode and the SRO layer (see scheme in Fig. 3). Conducting CNTs in contact with the Au-Ti electrode exhibit a uniform potential difference with respect to the SRO bottom electrode, and thus act as well-defined local electric field sources for polarization switching. The ferroelectric domain structure induced in this way could be imaged by piezoresponse force microscopy (PFM), and compared to the initial tapping mode topographical scans.

We reproduced the results of CNT-mediated switching of the polarization from the as grown “UP” direction, by applying single 10 V, 10 s pulses (much shorter than in previous studies). These pulses resulted in “DOWN”-polarized domains whose shape exactly followed the CNT position determined by AFM

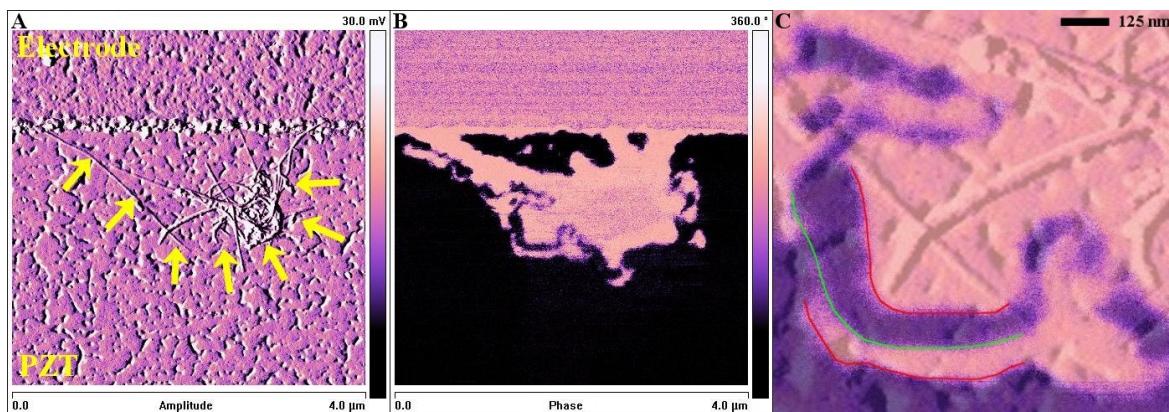


Figure 4: (A) An AFM tapping mode image of a cluster of nanotubes touching the side of an electrode. (B) A PFM image of the same area after the successive application of three different voltages (10 V , -10 V , 10 V) on the electrode. (C) A close up on the superposition of both previous images demonstrating the writing of “DOWN”, “UP”, and “DOWN”-polarized domains whose outlines follow the positions of the CNT present in the cluster.

topography. We then investigated the reversibility of the CNT-controlled polarization switching, by successively applying a positive and negative voltage. Our previous work has shown that the size of AFM-written domains depends linearly on writing voltage, and logarithmically on writing time. Both these parameters can be varied to try to obtain the desired domain size. Based on this knowledge, we developed an empirical approach, applying $+10\text{ V}$ for 1 minute, followed by -12 V for 150 minutes, which only partially erase the domain grown during the application of the positive voltage. In Fig. 4 we show the result of this procedure, followed by a third application of a voltage ($+10\text{ V}$ during 1 minute): all three switching steps are clearly visible in Fig. 4C, illustrating our current level of control of the domain size. We are currently measuring the transport properties of these PZT–CNT devices, to understand whether ferroelectric field effect modulation of charge carrier density in the CNT can be achieved.

1.3 Carbon Nanotube growth for hybrid devices (P. Paruch)

Since the deposition of water-suspended CNTs can result in the presence of surfactant molecules between the CNTs and the ferroelectric surface, decreasing the quality of their interface, we have also started working on a different technique for the deposition of CNTs. In this case, CNTs grown by means of chemical vapor deposition (CVD) over trenches on a substrate (Fig. 5 left), are subsequently transferred onto a pristine ferroelectric surface [24]. The substrate used for the CVD growth consists of Si wafers with low-stress Si_3N_4 and

SiO_2 layers, and trenches were realized by lithographic patterning and different etching steps. CNTs are grown by chemical vapor deposition from ferrihydrite nanoparticle-based catalysts. So far, our main efforts have focused on the optimization of the CNT growth by adjustment of the feed source, reductive and carrier gases (CH_4 , C_2H_4 , H_2 and Ar, respectively), flow rates, and different catalysts. We found that both an iron and molybdenum salt based catalyst, supported on alumina nanoparticles and suspended in water [25], as well as ferrihydrite nanoparticles synthesized by following the standard procedure described by Schwertmann [26] work well. The former results in dense growth of CNTs over trenches $\leq 50\ \mu\text{m}$ wide, while the latter is more suitable for the growth of CNTs over wider trenches (up to $150\ \mu\text{m}$), as determined by characterization based on scanning electron microscopy (SEM) imaging. Analysis of the as grown CNTs by AFM and Raman spectroscopy, aiming at determining their structural and electronic properties, is under way, and future work will focus on the transfer and micro-scale placement of the CNTs onto the ferroelectric surfaces.

Finally, we have performed preliminary studies of the CVD growth of CNTs onto AFM Si probes (either uncoated, or Co/Cr-coated). This activity currently overlaps, in goals and techniques used, with the work done to realize CNT devices on top of ferroelectric substrates (the CNT probes can be used to bias the ferroelectric substrates with nanometer resolution), but a much broader scope can be envisioned once the technology will be fully under control (e.g. AFM tips could be used as nano-scale intracellular probes). At this initial stage, the as grown CNTs are too long to be used as probes

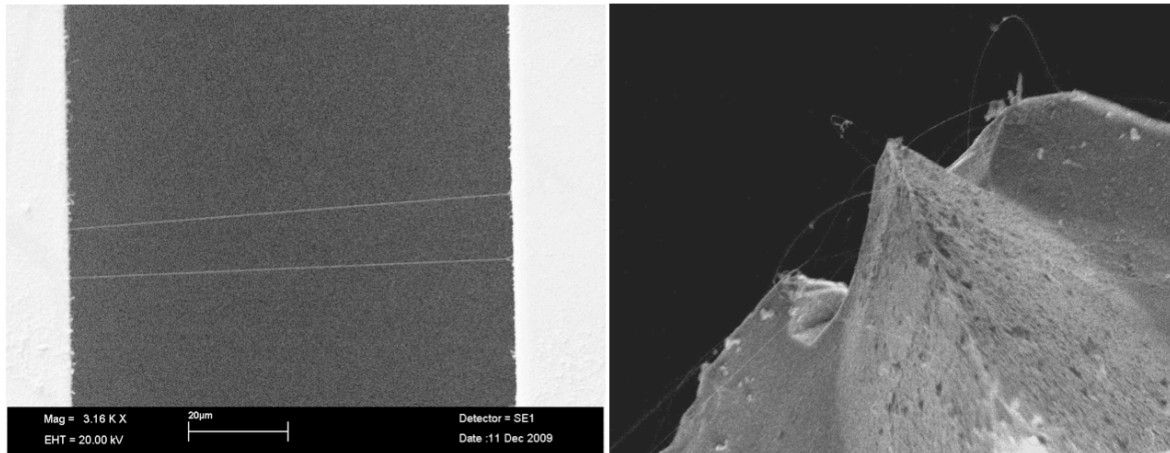


Figure 5: Left: SEM image of CNTs grown by chemical vapor deposition across an 80 μm wide trench etched into a $\text{Si-SiO}_2\text{-Si}_3\text{N}_4$ substrate. Right: SEM image of CNTs grown by chemical vapor deposition from ferrihydrite nanocrystal catalyst deposited on a commercial Si etched AFM tip (Nanosensors).

for AFM scanning, and their random orientation (Fig. 5 right) also poses problems. As a next step, we will focus on the etching and alignment of CNTs by different means, including the application of external electric fields between the tip and a rough conductive substrate.

2 Carbon-based electronics

The activity on carbon electronics mainly focuses on graphene-based systems, with part of the research also addressing organic single-crystal transistors. The work on graphene benefits from the complementary techniques made available by the different participants. Morpurgo's group brings in nano-fabrication capabilities and specializes on low-temperature dc transport measurements on nano-structures, the group of van der Marel contributes with state-of-the-art optical spectroscopy measurements, and in the group of Renner the focus is on scanning probe spectroscopy. These experimental activities are well supported by theoretical efforts (Sigrist, Büttiker) described in the next section.

2.1 Trilayer graphene as a semimetal with tunable band overlap (A. Morpurgo)

Since the discovery of graphene [27, 28], most studies have focused on single-layer materials, in which electrons behave as relativistic massless particles. Bilayers are also subject to an increasing number of investigations, because they possess very interesting properties as well. For instance, the system is a zero-gap semiconductor with quadratically dispersing, chiral quasi-particles [29]; the quantum

Hall effect is anomalous [30]; the band structure can be tuned by applying a perpendicular electric field, that causes the opening of a gap between valence and conduction bands [7]. These unique phenomena indicate that bilayer graphene is a new material system, clearly distinct from single-layers. The question arises as to whether thicker layers also are "unique" material systems, or if their properties simply start to resemble those of graphite (Fig. 6 shows an optical microscope image of single-, double-, and triple-layer graphene). We have addressed this issue by performing the first systematic investigation of transport through trilayer graphene. Trilayer graphene had not been investigated experimentally before, and band structure calculations had given conflicting results for its low-energy electronic

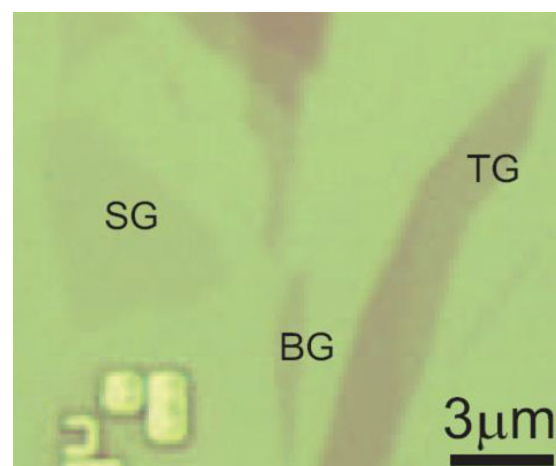


Figure 6: Optical microscope images of graphene flakes of different thicknesses. The contrast observed under the microscope is sufficient to determine the layer thickness reliably.

properties. Our work has relied on the use of double-gated devices, in which the carrier density and the electric field perpendicular to the material can be tuned independently. The response of trilayer graphene to a perpendicular electric field is strikingly different from that of bilayers, and provide considerable information on the microscopic electronic structure. Magneto-resistance measurements, consistently with the temperature dependence of the resistance, clearly indicate that trilayer graphene is a semi-metal with a band overlap of approximately 30 meV. Upon applying a perpendicular electric field, the resistance of trilayers decreases. We performed a theoretical analysis of the data to show that the effect originates from a large increase in the band overlap, which can be doubled by applying an electric field of fairly moderate strength ($E \approx 2 \cdot 10^6$ V/cm). The analysis of the electric field dependence of the resistance and of its temperature dependence also enables the determination of the effective mass of charge carriers. We find it to be approximately 0.05 the free-electron mass, in agreement with theory. These results have been published in Nature Nanotechnology [8].

2.2 Optical conductivity of gate-tunable bilayer graphene (*D. van der Marel*)

It was predicted [29] that in gated bilayer graphene (sketched in Fig. 7a) an applied gate

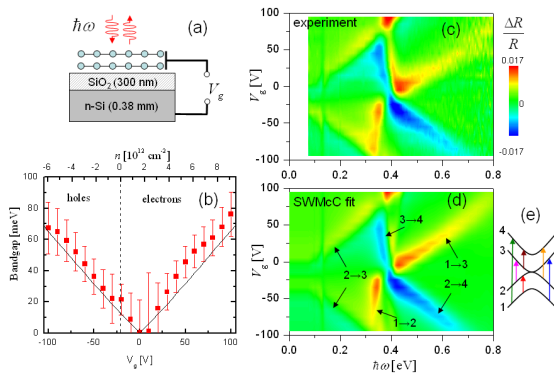


Figure 7: (a) A sketch of the gated bilayer graphene and of the reflectivity experiment. (b) The gate voltage dependence of the bandgap obtained by fitting of the infrared spectra. The calculated bandgap obtained using *ab initio* methods (that involve the self-screening effects) is shown as a solid line. (c) The measured differential reflectivity spectra. (d) The fit of the measured spectra using the tight-binding model. The assignments of the interband transitions are given. (e) The four electronic bands of bilayer graphene. The gap opens between the bands 2 and 3.

voltage does not only shift the chemical potential, but also opens a bandgap due to the induced interlayer difference in electrostatic potential. Indeed, an insulating state could be achieved in [7], although the size of the bandgap could not be extracted from dc electrical transport measurements. We measured reflectivity spectra of bottom gated exfoliated bilayer graphene using an infrared microscope coupled to a Fourier transform spectrometer [9, 10]. The gate voltage dependent value of the gap was extracted (Fig. 7b) by fitting the gate-modulated spectra, using a tight-binding model and the Kubo formula. We find that the self-screening effect is crucial to explain the actual size of the bandgap. A close quantitative agreement between the experimental and model spectra is achieved (Fig. 7c and d), allowing us to determine self-consistently the full set of tight-binding parameters, including the ones responsible for the electron-hole band asymmetry. All the interband optical transitions (Fig. 7e) are identified in the spectra as specified in Fig. 7d. There are certain mismatches between the tight-binding model and the data, which can be related to electron-electron and electron-phonon interactions. Our work amounts to demonstrating the possibility to directly fit infrared spectra using microscopic, physically meaningful parameters, instead of the conventional phenomenological Drude-Lorentz model. This result also shows how the combination of electrostatic gating and optical spectroscopy is able to provide detailed information about the material band structure.

An unexpected and surprising result of our study is the observation of a giant increase of the infrared intensity of the in-plane E_u phonon mode (~ 0.2 eV), as a function of the gate-induced doping (Fig. 8) [11]. This phonon peak was found to have a pronounced Fano-like asymmetry, indicating that it is coupled to a continuum of electronic excitations. We suggest that the intensity growth and the softening originate from the coupling of the phonon mode to the narrow electronic transition between parallel bands of the same character ($1 \rightarrow 2$ and $3 \rightarrow 4$ in Fig. 7e), while the asymmetry is due to the interaction with the continuum of transitions between the lowest hole and electron bands ($2 \rightarrow 3$). The growth of the peak can be interpreted as a “charged-phonon” effect [31] observed previously in organic chain conductors [32] and doped C_{60} [33]. It is remarkable that in graphene this effect can be tuned with the gate voltage, which opens new possibilities for the use of this ma-

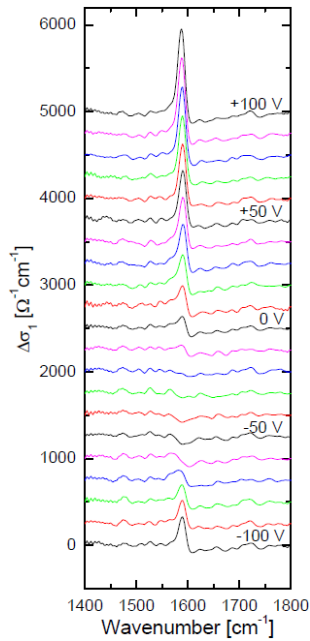


Figure 8: The real part of the optical conductivity of bilayer graphene at different gate voltages in the vicinity of the E_u phonon peak. The electronic baseline is subtracted.

terial in electro-optical applications.

2.3 Graphene on SrTiO_3 substrates (A. Morpurgo)

The dominant source of disorder in graphene is represented by charged impurities present in the supporting substrate. These impurities are responsible for rather large potential fluctuations in the graphene layer, which scatter charge carriers and, when the system is close to charge neutrality, cause the formation of regions where the Fermi level is either in the conduction or in the valence band (the so-called “puddles”). These effects affect the low-energy properties of graphene and often prevent the observation of its intrinsic properties. It has been proposed to use high-dielectric constant environments (e.g. substrates with high-dielectric constant) to screen potential fluctuations and suppress disorder due to electrostatic potential fluctuations. Several groups have performed experiments based on different strategies, and reported contrasting results. As a consequence, it is currently unclear what really are the main effects caused by a high-dielectric constant substrate.

To address this point, we have started the investigation of transport through graphene on SrTiO_3 substrates. These substrates have a relative dielectric constant of 300 at room temperature, reaching values in excess of 10'000

at liquid helium temperature. This is up to three orders of magnitude higher than the value for SiO_2 substrates that have been routinely used in the past (the relative dielectric constant of SiO_2 is about 4). We have developed the needed technology to realize nano-devices, and performed first systematic magneto-transport measurements. The results show both similarities and differences with the behavior of graphene on the commonly used SiO_2 substrates. In particular, the mobility of graphene on SrTiO_3 is comparable to that of graphene on SiO_2 , indicating that the high-dielectric constant of the substrate is not sufficient to suppress disorder. In addition, in contrast to what is observed for graphene on SiO_2 substrates, graphene on SrTiO_3 shows a pronounced, insulating-like temperature dependence of the conductivity. A first analysis of the measurements appears to indicate that the phenomenon is due to the effect of short range scattering, which is stronger for graphene layers on SrTiO_3 . When completed, this study will clarify the mechanism responsible for the effect of the dielectric environment on the properties of graphene.

We have also performed first measurements on devices consisting of nano-ribbons on SrTiO_3 substrates. In this case the experimental results are very different from the case of graphene on SiO_2 . In particular, differently from SiO_2 substrates, no transport gap is observed. The effect is likely due to the suppression of charging energy in the electronic “islands” that are formed in the nano-ribbons (due to electron localization caused by disorder) by the high-dielectric constant of the substrate. More devices need to be measured to draw a definitive conclusion. If confirmed, these results will provide clear indication as to the nature of transport through graphene nano-ribbons, which is currently under debate.

2.4 Scanning tunneling spectroscopy of graphene-based systems: edges and intercalated layers (C. Renner)

Two distinct aspects of graphite are motivating our work: i) the peculiar electronic structure of graphene and ii) the superconductivity at remarkably high temperature discovered a few years ago [34] in intercalated graphite compounds (GIC). On the first topic, our aim is to characterize edge states using scanning tunneling microscopy, both on single and multi-layer exfoliated graphene flakes. The second topic is building on our experimental capabilities to decorate single and stacked graphene

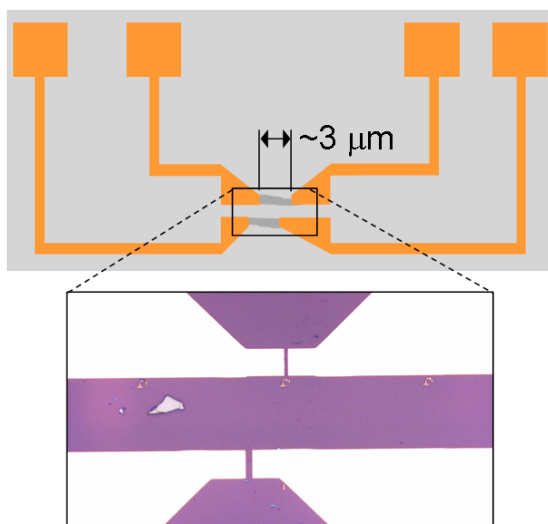


Figure 9: Gold contact layout to enable STM studies of two graphene flakes on SiO₂ (top) and photograph of its first implementation (bottom).

layers with selected atomic species. The goal is to unveil key ingredients of superconductivity observed in GIC's using scanning tunneling spectroscopy.

Both experiments introduced above require the ability to safely position the tip of our scanning probe over tiny graphene flakes obtained by exfoliation. The graphene flakes are deposited on an insulating substrate, SiO₂, making it impossible to safely find a flake and its edge atoms using scanning tunneling microscopy (STM) alone: the STM tip would irreparably crash into the substrate if we were to miss the edge atoms by as little as an angstrom. Consequently, we need to use combined STM and atomic force microscopy (AFM). Electron tunneling spectroscopy will be carried out using the STM while the AFM safely maintains the tip within tunneling distance of the surface, whether it is conducting or not.

We are using a very recently commissioned commercial scanning probe instrument featuring combined STM/AFM capabilities in ultra-high vacuum and operating in the temperature range from 4.8 K to about 330 K. The system is located in a dedicated Faraday cage and is equipped with RHEED, LEED, XPS and a range of evaporators allowing *in situ* deposition of submonolayer amounts of selected materials. The base pressure in the STM chamber, with the system cold, reaches into the mid 10⁻¹² mbar range.

The STM has outstanding performance, with demonstrated 5 pm vertical imaging resolution. To study exfoliated graphene flakes with the STM, a special electrode configuration was

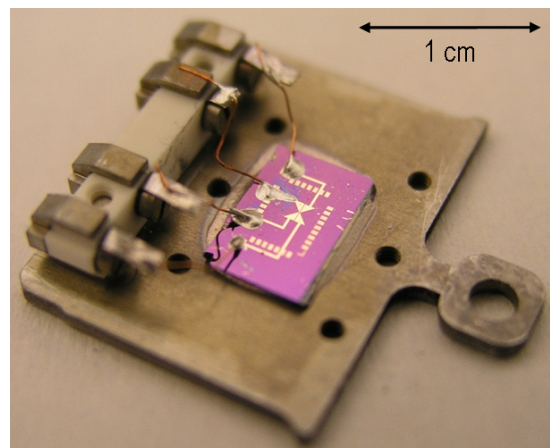


Figure 10: Two graphene flakes mounted on the STM sample plate. The arrow configuration of the gold contacts pointing at the graphene flakes is clearly visible to the naked eye.

designed to contact the sample and to assist in the positioning the tip within close proximity of the flake (Fig. 9). The arrow shape of the contact pads near the samples provide a clear landmark visible to the naked eye to locate the flake to be studied (Fig. 10). Imaging the oblique edge using AFM shall further enable to steer the tip precisely onto the graphene flake. We have tested the functionality of the above setup, demonstrating the possibility to position the tip over a selected graphene flake. We will proceed with the planned experiments after a few technical difficulties that we have encountered at this stage (with the electronics of the controller unit, and with the sample holder – which is currently being modified (Fig. 10)) are solved.

2.5 Organic single-crystal transistors (A. Morpurgo)

The use of organic field-effect transistors (FETs) for the investigation of the intrinsic transport properties of organic semiconductors relies on devices fabricated on crystals of the highest possible quality, to minimize the influence of disorder (originating from chemical impurities and structural defects). An unambiguous manifestation of the intrinsic transport properties is the increase of carrier mobility with lowering temperature, over a sufficiently broad temperature interval. Until now, such a systematic increase in mobility in a FET configuration has only been reported for devices realized with rubrene single-crystals, which is why this material has been extensively studied over the past few years. However, the identification of a broader class of materials whose quality is suf-

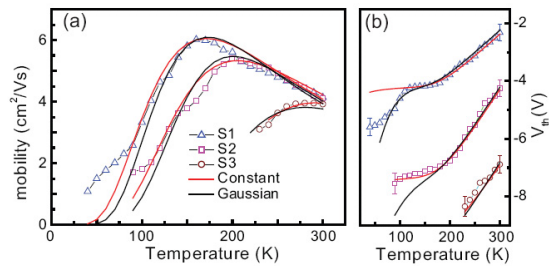


Figure 11: Temperature dependence of mobility and threshold voltage in three different TMTSF single-crystal FETs. The symbols represent the experimental data and the lines are fit based on our model (red and black lines correspond to different energy distributions of shallow traps, with the same total trap density and characteristic energy).

ficient to reveal the intrinsic transport properties is clearly essential to reach a true understanding of organic semiconductors. Indeed, only comparative studies of different materials can indicate which of the properties that are observed experimentally are generic to all organic semiconductors, and which are specific to a given molecule.

To address this issue, we have realized organic FETs made with single-crystals of many different molecules, and we have found new materials exhibiting a mobility increase upon cooling. These are crystals of TMTSF (*p*-type) and PDIF-CN₂ (*n*-type; this is the first electron conducting organic material exhibiting a metallic-like mobility in FET measurements). We discuss here the case of TMTSF that we have already analyzed in quite some detail. The experiment consists in the measurement of the FET electrical characteristics as a function temperature, from which we extract the main FET parameters, such as the carrier mobility and the threshold voltage. The results are shown in Fig. 11 for three different devices, together with theoretical curves that we have calculated from a simple – but microscopically well-defined – phenomenological model. The model has as input parameters the density of deep and shallow trap states and the corresponding energy scales. By comparing the model predictions and the experiments we can extract quantitative values for all these parameters, in the different devices. The consistency of the model can be checked by analyzing the measured density dependence of the FETs characteristics, that can be calculated in terms of the quantities extracted by the analysis of the temperature dependence, without the need to introduce additional parameters. We conclude that the model allows a reliable determination of deep and shallow trap density. These results

also give an indication as to the origin of the shallow traps (currently unknown in organic FETs), which appears to be due in large part to electrostatic potential fluctuations caused by carriers trapped in the deep traps [12].

Finally, we have also investigated charge transfer at metal/organic interfaces, using short channel rubrene single-crystal FETs of different length. In these devices, charge transfer from the metal to the organic semiconductor results in a length dependent threshold voltage shift, which can be accurately measured and modeled (using Poisson’s equation, under the assumption that the density of states in rubrene is that of a conventional semiconductor). Remarkably, all quantities involved in the theoretical expression for the length dependence of the threshold voltage shift are either known from previous experiments, or can be measured, and we find an excellent quantitative agreement between data and model without the need to introduce any unknown fitting parameter. This result provides a clear indication of the internal consistency of the physical picture on which our description of organic semiconductors is currently based [13].

3 Theory

The theoretical activities in this project proceed in close connection with the topics investigated experimentally. The work of Giamarchi’s group on superconducting quantum wires is relevant for the transport experiments that are being performed on LaAlO₃/SrTiO₃ nano-structures. The analysis of the electronic properties of graphene edges (Sigrist, Büttiker) is directly related to experiments performed in Morpurgo’s group, on transport through graphene nano-ribbons and electrostatically gapped bilayer graphene.

3.1 Superconducting quantum wires coupled to a dissipative systems (*T. Giamarchi*)

Narrow superconducting (SC) wires with a diameter $d \ll \xi_0$ (where ξ_0 is the bulk superconducting coherence length) are low-dimensional systems in which strong fluctuations of the order parameter inhibit long-range order (LRO), and only quasi-LRO (i.e. power-law decay of the order-parameter correlation function) can exist [35]. Recent advances in nanofabrication have enabled the realization of ultranarrow SC wires, in which quantum fluctuations completely dominate the physics at low temperatures, allowing to address fundamental questions in low-dimensional superconductivity [36]. Particularly, in the group of J.-M.

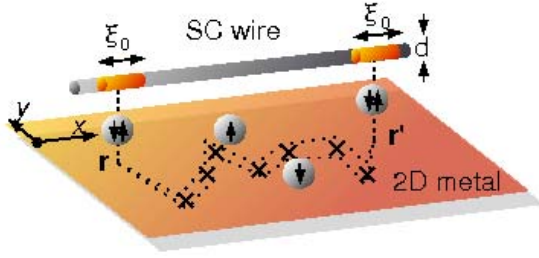


Figure 12: A superconducting wire coupled to a dissipative environment; paradoxically the dissipative environment reinforces the superconductivity in the wire.

Triscone it was suggested recently the possibility to fabricate (among other nano-structures) narrow SC wires embedded in a normal metallic matrix by the means of the ferroelectric field effect, in experiments done on SC Nb-doped SrTiO_3 films covered with ferroelectric $\text{Pb}(\text{Zr,Ti})\text{O}_3$ [14]. While ideally isolated 1D SC systems have been thoroughly studied in the past [15], the complete understanding of systems coupled to the environment is still an open issue. In particular, the interplay between fluctuations and dissipation induced by the environment in quantum systems is at present under intensive research [37, 38].

In this project, we concentrate on the study of thin SC wires coupled to a diffusive metallic film as shown in Fig. 12. In a BCS description at $T \ll T_c$, where T_c is the bulk SC transition temperature, the SC order parameter can be expressed as $\Delta(\mathbf{x}) = \Delta_0 e^{i\theta(\mathbf{x})}$, where Δ_0 is the BCS gap parameter, and $\mathbf{x} \equiv (x, \tau)$, with x the coordinate along the wire and τ the imaginary-time. The “phase-only” description of the coupled SC wire/2D diffusive metal system writes $S[\theta] = S_0[\theta] + S_E[\theta]$, where $S_0[\theta]$ is the action of the isolated wire, which follows a Luttinger liquid description [15]. On the other hand, the effects of the environment are embedded in the term

$$S_E \propto - \int dx dx' P_c(\mathbf{x} - \mathbf{x}') \cos[\theta(\mathbf{x}) - \theta(\mathbf{x}')] \quad (2.1)$$

where the kernel $P_c(\mathbf{r} - \mathbf{r}', \tau - \tau')$ is the Cooperon propagator of an electronic pair in the 2D diffusive metal. Interestingly, we have found that the term S_E of Eq. (2.1) induces a quantum phase transition towards a phase with true SC LRO in the wire at $T = 0$ [16]. This is possible due to the long-range coupling in τ -space introduced by the kernel $P_c(\mathbf{r} - \mathbf{r}', \tau - \tau') \sim \delta(\mathbf{r} - \mathbf{r}') / (\tau - \tau')^2$ on the field $\theta(\mathbf{x})$. At finite temperatures $T \ll T_c$, this coupling translates into a higher effective SC stiffness of the wire. Indeed, our results show

that the resistivity due to phase slip processes (vortices in 1 + 1 dimensions) is smaller in the case of the wire/2D metal system than in the isolated case [16].

3.2 Electron phonon coupling in graphene nano-ribbons (M. Sigrist)

Electronic properties near the boundary of graphene sheets are strongly influenced by the type of edges. It has been shown that zigzag edges give rise to zero-energy bound states of non-bonding character which live only on one sublattice. In narrow graphene ribbons, so-called nano-graphene ribbons (NGR), these bound states acquire a dispersion through the overlap of edge states from the two ribbon sides. It had been speculated early on that the large density of states at the zero-energy could give rise to instabilities of these edge states. In our study, we investigated how susceptible the graphene ribbons are against a lattice instability [17]. At half-filling ($\mu = 0$) the non-bonding character of the edge states protects them against a Peierls instability, despite the diverging density of states. For finite chemical potentials the overlap for non-bonding states from both edges (both belonging to opposite

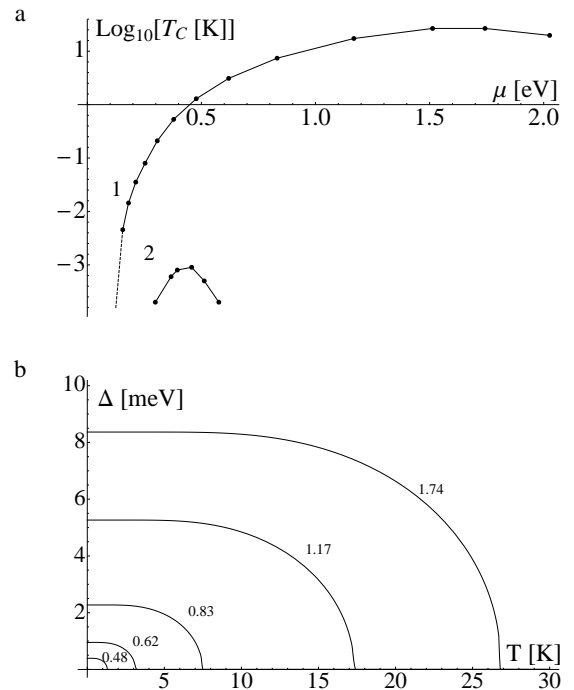


Figure 13: Peierls instability in nano-graphene ribbons. (a) The mean field critical temperature of NGR of width 1 and 2 as a function of chemical potential. Note that T_c vanishes as $\mu = 0$ is approached. (b) Temperature dependence of the quasi-particle gap at the Fermi energy for NGR of width 1 and different values of μ .

sublattices) yields a finite electron-phonon coupling which leads to a Peierls deformation with $Q = 2k_F$. The fact that the electron-phonon coupling relies on the overlap of two edge states leads to a very low energy scale for the instability which shrinks dramatically with growing ribbon width. The estimates by Staar *et al.* [17] give a critical temperature of order 10–20 K for the most narrow NGR of width 1 and show that this temperature drops by 2 orders of magnitude for a width of 2 (Fig. 13). Thus, although doped NGR can undergo a Peierls deformation which opens a gap in the electron spectrum and leads to insulating behavior, the critical temperatures are extremely low and would most likely not affect the transport properties of ideal zigzag-NGR.

3.3 Topological insulators (*M. Büttiker*)

Topological insulators are a new class of materials, for which today only a few realizations exist. Three-dimensional topological insulators are predicted to have conducting surface states and two-dimensional topological insulators support edge states. Thus, even if these materials are insulators in their bulk, they are in fact conducting due to their surface or edge states. Edge states are known from the quantum Hall effect where they explain the quantization of conductance. To see conductance quantization due to the quantum Hall effect, typically magnetic fields of the order of Tesla need to be applied. In contrast, in topological insulators, edge states exist in the absence of a magnetic field. However, different from the case of the quantum Hall effect, in topological insulators, edge states come in pairs. The edge states are helical in nature: spin and momentum are coupled such that at an edge spin up

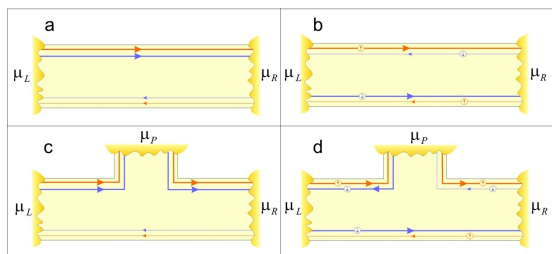


Figure 14: Topological insulator (a and c) compared to a quantum Hall conductor (b and d) at filling factor 2. The direction of carrier motion in the edge states is indicated with arrows. A voltage probe (c) changes the conductance of a topological insulator by half a conductance quantum. In contrast, the quantized Hall conductance (d) remains unaffected by the presence of a probe. After [18].

electrons travel to the left and spin down electrons to the right. Fig. 14, taken from [18], compares a topological insulator (b) with a quantum Hall conductor at filling factor 2 (a). A recent experiment [39] tests the existence of edge states by attaching additional contacts serving as voltage probes along an edge. For a topological insulator (Fig 14d) a voltage probe has the effect that half of the current which flows into the probe is sent back to the contact from which the probe is fed. Only half of the current leaves the probe in the forward direction to the next contact. As a consequence the conductance is reduced by half a conductance quantum. In contrast the quantum Hall sample (Fig 14c) is immune to the presence of a voltage probe.

The experiment mentioned above [39] is performed in a mercury telluride heterostructure. It is interesting to ask whether more readily available materials are topological insulators. An important candidate is bilayer graphene which can be gapped with the help of gates [19]. There are two experiments which have measured this gap; one by Morpurgo *et al.* [7] investigates transport and another measures the gap optically [40]. The gaps observed in these two experiments are rather different. In recent work, Jian Li, Ivar Martin and Alberto Morpurgo (unpublished) have examined edge states in bilayer graphene and suggest that the existence of these states explains the difference between the two experiments.

It turns out that electrostatically gapped bilayer graphene is not a true topological insulator, or at best only a weak one. In contrast to

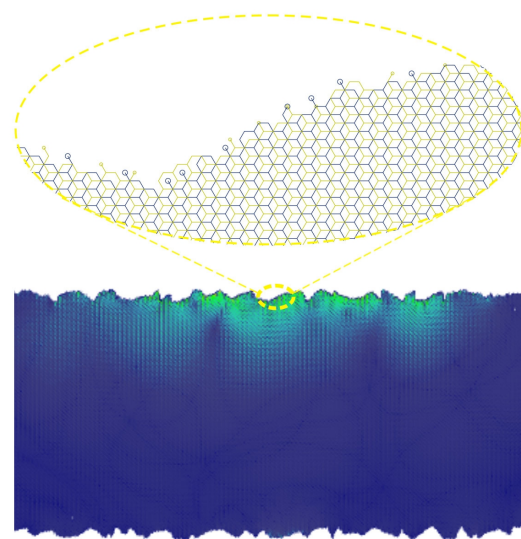


Figure 15: Edge state in a gapped bilayer graphene ribbon. Lower panel: light colors indicate a high electron density. Upper panel: disordered edge. After Li, Martin and Morpurgo (unpublished).

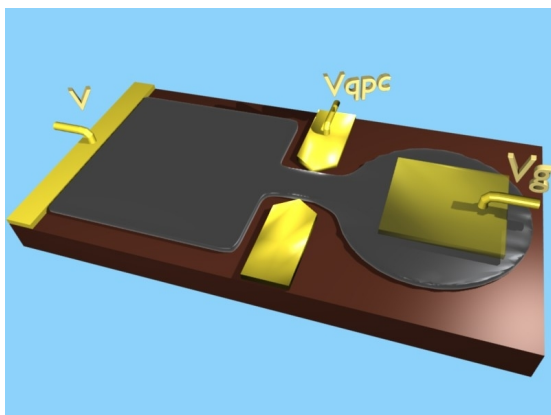


Figure 16: Mesoscopic capacitor. After [20].

a true topological insulator, surface roughness leads to localization of the edge states. Fig 15 shows an example of a numerical simulation of such a localized edge state. Thus at zero temperature bilayer graphene is strictly speaking an insulator. However, at some elevated temperature, as it exists in an experiment, there is variable range hopping along the edge which at even higher temperature changes to nearest neighbor hopping. In this way the localized edge states provide a contribution to transport.

3.4 Quantum coherent electronics with single-particle emitters (*M. Büttiker*)

Recent experiments have demonstrated that it is possible to use mesoscopic capacitors (Fig. 16) to emit a single-electron and a single-hole into a conductor in each cycle of a periodic voltage applied to the capacitor [41]. Such sources represent a novel tool for the investigation of electrical transport and might revolutionize electronics in a similar way that lasers revolutionized optics. The experiment realizes single-electron and hole emission at high frequencies in the GHz range. We have examined the use of mesoscopic capacitors as charge detectors [20]. We have shown that with the help of two single-particle emitters we can realize two-particle Aharonov-Bohm oscillations, generating shot noise which depends on the Aharonov-Bohm flux through two distant interferometers [21]. In addition, we have examined the heat production and noise of a single-particle emitter [22].

4 Collaborative efforts

Within this project, several collaborative efforts are ongoing, and others are likely to be established in the near future. On oxides, the collaboration between the groups of

Triscone and Morpurgo is making it possible to combine new materials ($\text{LaAlO}_3/\text{SrTiO}_3$ heterostructures) with nano-fabrication for the realization of devices. The collaboration between Paruch's and Triscone's groups is important for the study of nano-scale domains in ferroelectrics. On graphene-based electronics, collaborations are active between the groups of Morpurgo, Renner, and Büttiker, focusing on different experimental and theoretical topics. Additional collaborative work – combining device nano-fabrication with experimental techniques like optical spectroscopy – is currently being discussed.

MaNEP-related publications

- [1] A. D. Caviglia, S. Gariglio, N. Reyren, D. Jaccard, T. Schneider, M. Gabay, S. Thiel, G. Hammerl, J. Mannhart, and J.-M. Triscone, *Nature* **456**, 624 (2008).
- ▶ [2] A. D. Caviglia, M. Gabay, S. Gariglio, N. Reyren, C. Cancellieri, and J.-M. Triscone, *Physical Review Letters* **104**, 126803 (2010).
- [3] P. Paruch, T. Tybell, and J.-M. Triscone, *Proceedings of the 10th International Ceramics Congress CIMTEC 2002 D*, 675 (2002).
- [4] C. H. Ahn, J.-M. Triscone, and J. Mannhart, *Nature* **424**, 1015 (2003).
- [5] P. Paruch, T. Tybell, and J.-M. Triscone, *Applied Physics Letters* **79**, 530 (2001).
- [6] P. Paruch, A.-B. Posadas, M. Dawber, C. H. Ahn, and P. L. McEuen, *Applied Physics Letters* **93**, 132901 (2008).
- [7] J. B. Oostinga, H. B. Heersche, X. Liu, A. F. Morpurgo, and L. M. K. Vandersypen, *Nature Materials* **7**, 151 (2008).
- ▶ [8] M. F. Craciun, S. Russo, M. Yamamoto, J. B. Oostinga, A. F. Morpurgo, and S. Tarucha, *Nature Nanotechnology* **4**, 383 (2009).
- ▶ [9] A. B. Kuzmenko, E. van Heumen, D. van der Marel, P. Lerch, P. Blake, K. S. Novoselov, and A. K. Geim, *Physical Review B* **79**, 115441 (2009).
- ▶ [10] A. B. Kuzmenko, I. Crassee, D. van der Marel, P. Blake, and K. S. Novoselov, *Physical Review B* **80**, 165406 (2009).
- ▶ [11] A. B. Kuzmenko, L. Benfatto, E. Cappelluti, I. Crassee, D. van der Marel, P. Blake, K. S. Novoselov, and A. K. Geim, *Physical Review Letters* **103**, 116804 (2009).
- ▶ [12] H. Xie, H. Alves, and A. F. Morpurgo, *Physical Review B* **80**, 245305 (2009).
- ▶ [13] I. Gutiérrez Lezama and A. F. Morpurgo, *Physical Review Letters* **103**, 066803 (2009).
- [14] K. S. Takahashi, M. Gabay, D. Jaccard, K. Shibuya, T. Ohnishi, M. Lippmaa, and J.-M. Triscone, *Nature* **441**, 195 (2006).
- [15] T. Giamarchi, *Quantum Physics in One Dimension* (Oxford University Press, Oxford, 2004).
- ▶ [16] A. M. Lobos, A. Iucci, M. Müller, and T. Giamarchi, *Physical Review B* **80**, 214515 (2009).
- [17] P. Staar, K. Wakabayashi, and M. Sgrist, *submitted* (2009).
- [18] M. Büttiker, *Science* **325**, 278 (2009).

- [19] I. Martin, Y. M. Blanter, and A. F. Morpurgo, *Physical Review Letters* **100**, 036804 (2008).
- [20] S. E. Nigg and M. Büttiker, *Physical Review Letters* **102**, 236801 (2009).
- [21] J. Splettstoesser, M. Moskalets, and M. Büttiker, *Physical Review Letters* **103**, 076804 (2009).
- [22] M. Moskalets and M. Büttiker, *Physical Review B* **80**, 081302 (2009).
- ### Other references
- [23] S. Kawasaki, G. Catalan, H. J. Fan, M. M. Saad, J. M. Gregg, M. A. Correa-Duarte, J. Rybczynski, F. D. Morrison, T. Tatsuta, O. Tsuji, and J. F. Scott, *Applied Physics Letters* **92**, 053109 (2008).
- [24] X. M. H. Huang, R. Caldwell, L. Huang, S. C. Jun, M. Huang, M. Y. Sfeir, S. P. O'Brien, and J. Hone, *Nano Letters* **5**, 1515 (2005).
- [25] J. Kong, H. T. Soh, A. M. Cassell, C. F. Quate, and H. Dai, *Nature* **395**, 878 (1998).
- [26] U. Schwertmann and R. M. Cornell, *Iron Oxides in the Laboratory: Preparation and Characterization* (Wiley-VCH, Weinheim, 1991).
- [27] K. S. Novoselov, A. K. Geim, S. V. Morozov, D. Jiang, M. I. Katsnelson, I. V. Grigorieva, S. V. Dubonos, and A. A. Firsov, *Nature* **438**, 197 (2005).
- [28] Y. Zhang, Y.-W. Tan, H. L. Stormer, and P. Kim, *Nature* **438**, 201 (2005).
- [29] E. McCann and V. I. Fal'ko, *Physical Review Letters* **96**, 086805 (2006).
- [30] K. S. Novoselov, E. McCann, S. V. Morozov, V. I. Fal'ko, M. I. Katsnelson, U. Zeitler, D. Jiang, F. Schedin, and A. K. Geim, *Nature Physics* **2**, 177 (2006).
- [31] M. J. Rice, N. O. Lipari, and S. Strässler, *Physical Review Letters* **39**, 1359 (1977).
- [32] D. B. Tanner, C. S. Jacobsen, A. A. Bright, and A. J. Heeger, *Physical Review B* **16**, 3283 (1977).
- [33] K.-J. Fu, W. L. Karney, O. L. Chapman, S.-M. Huang, R. B. Kaner, F. Diederich, K. Holczer, and R. L. Whetten, *Physical Review B* **46**, 1937 (1992).
- [34] T. E. Weller, M. Ellerby, S. S. Saxena, R. P. Smith, and N. T. Skipper, *Nature Physics* **1**, 39 (2005).
- [35] N. D. Mermin and H. Wagner, *Physical Review Letters* **17**, 1133 (1966).
- [36] A. Bezryadin, C. N. Lau, and M. Tinkham, *Nature* **404**, 971 (2000).
- [37] G. Schön and A. D. Zaikin, *Physics Reports* **198**, 237 (1990).
- [38] R. Fazio and H. van der Zant, *Physics Reports* **355**, 235 (2001).
- [39] A. Roth, C. Brüne, H. Buhmann, L. W. Molenkamp, J. Maciejko, X.-L. Qi, and S.-C. Zhang, *Science* **325**, 294 (2009).
- [40] Y. Zhang, T. Tang, C. Girit, Z. Hao, M. C. Martin, A. Zettl, M. F. Crommie, Y. R. Shen, and F. Wang, *Nature* **459**, 820 (2009).
- [41] G. Fève, A. Mahé, J.-M. Berroir, T. Kontos, B. Plaçais, D. C. Glattli, A. Cavanna, B. Etienne, and Y. Jin, *Science* **316**, 1169 (2007).

Project 3 Electronic materials for energy systems and other applications

Project leader: Ø. Fischer (UniGE)

Participating members: M. Abplanalp (ABB), J. Cors (UniGE and Phasis), M. Decroux (UniGE), D. Eckert (Bruker-Biospin), Ø. Fischer (UniGE), R. Flükiger (UniGE), M. Kenzelmann (PSI), G. Patzke (UniZH), C. Renner (UniGE), N. de Rooij (EPFL), G. Triscone (Hepia), J.-M. Triscone (UniGE), A. Weidenkaff (Empa and UniBE), K. Yvon (UniGE),

Introduction and highlights: This project continues the effort carried out in Project 6 of Phase II. The goal is to develop applications based on the research carried out in MaNEP. Compared to Phase II some of the successful projects continue and many new projects have been added. In the field of superconductivity, a distinct highlight is that we have achieved record values of critical currents in industrial *in situ* MgB₂ wires at high magnetic fields. We have started a new project on “Oxides for energy harvesting”. The first part of this subproject aims at developing the technique to deposit epitaxial ferroelectric thin films on silicon wafers. Here we report on the realization of PZT epitaxial films and on further optimization of the deposition process. Furthermore we have successfully fabricated epitaxial PZT transducers in the form of membranes and cantilevers. This represents a first important step towards the use of such structures in energy harvesting devices and other MEMS applications. Our project on applications of artificial superlattices focuses on the use of metallic superlattices in neutron mirrors. A key result of this research is that we have demonstrated the fabrication of metallic substrates with extraordinarily low surface roughness allowing even better neutron mirrors opening up an avenue towards advanced neutron optical devices. Another new set of projects is contained in the subproject “Hydrogen detectors and other sensors”. In this part we report in particular on progress in our search for an optimal material for which the metal-insulator transition resulting from hydrogen uptake of an intermetallic compound can be used as a hydrogen selective gas detector. Finally the subproject “New surface treatments for microcomponents” represents a novel development in which nano-powder-printed marks can be written into a surface. This new technology opens up the door for a number of different applications, in particular in the watch industry.

Summary

Applied superconductivity

1. Very high J_c and B_{irr} values in densified *in situ* MgB₂ wires: by means of the cold high pressure densification (CHPD) method developed in Geneva, we have improved the J_c value of industrial *in situ* MgB₂ wires to the world’s highest values of $J_c(4.2\text{ K}) = 10^4\text{ A/cm}^2$ at 13.4 T and 6.0 T for 4.2 and 20 K, respectively. The value of B_{irr} has been enhanced by 2 T: solenoids producing fields of $\sim 5\text{ T}$ at 20 K are now possible.
2. Impact of steel reinforcement on Nb₃Sn internal tin wires under tensile strain: the behavior of J_c of a multifilamentary Nb₃Sn wire has been measured up to 19 T as a function of applied tensile stress, showing a strong improvement compared to the behavior of unsheathed wires. The analysis of the results shows the effect of three-dimensional stresses.
3. Synchrotron radiation for the characterization of Nb₃Sn wires under transverse com-

pression: high resolution synchrotron diffraction measurements were performed for the first time on Nb₃Sn wires at 4.2 K simultaneously to the application of transverse compressive stresses. The elastic strain in powder in tube (PIT) Nb₃Sn wires is higher than for other wire types, in agreement with the higher sensitivity of J_c with respect to transverse stresses.

4. Towards understanding thermal properties of coated conductors for fault current limiters: we have characterized the electrical and the thermal properties of coated conductors (CC). We have determined the local electric field in the CC at the beginning of the short-circuit. The heat propagation velocity in the substrate has been measured thank to the development of a special structure on CC. We confirm that this heat propagation velocity is of the order of few cm/s. For the measurement of the thermal conductivity of the CC a new probe has been built.

Oxides for energy harvesting

This subproject aims at investigating the use of oxides in either mechanical or thermoelectric energy harvesting. Oxides with their large spectrum of different properties open up a rich field of investigation in this domain. In the first part of this subproject we aim at developing the technique to deposit epitaxial ferroelectric thin films on silicon wafers. This approach will open up the door to electromechanical MEMS devices. Here we report on the realization of PZT epitaxial films on Si and on further optimization of the deposition process. Furthermore we have successfully fabricated epitaxial PZT transducers in the form of membranes and cantilevers. The resonance behavior of these structures have been studied. This represents a first important step towards of the use of such structures in energy harvesting devices and other MEMS applications. On the other hand, in order to explore the potential of oxides for use in thermoelectric devices we have studied Nb doped CaMnO_3 . This material was synthesized and characterized for a possible application as n -type conductor in all oxide thermoelectric converters. This compound has a very high Seebeck coefficient but also a very high electrical resistivity and thermal conductivity. Doping this compound and producing it in a granular form has a potential for improved thermoelectric figure of merit.

Applications of artificial superlattices

We have developed a process for polishing metallic substrates to produce an extraordinarily low surface roughness compared to high-quality float glass. In a first step, we produced neutron supermirror coatings on aluminum substrates with a reflectivity $R \approx 91\%$ at the critical angle of reflection of $m = 2$, demonstrating the excellent quality of the aluminum surface. In a second step, we succeeded to coat $m = 3.6$ supermirror on aluminum and steel substrates with $R \approx 77\%$. These supermirrors on metallic substrates open new options for advanced neutron optical devices. A prerequisite for the development of the metallic substrates for neutron mirrors was an adequate method to measure the surface roughness. We performed measurements with atomic force microscopy (AFM) in order to determine the surface roughness for supermirror substrates. We find that AFM provides a valuable tool for quality control of the neutron supermirror production. This project is carried out with Swiss-neutronics.

Hydrogen detectors and other sensors

Members of the metal-hydrogen series $LnMg_2T-H_x$ ($Ln = \text{La, Ce, Pr, Nd}$; $T = \text{Ni, Pd, Pt}$) were further characterized with respect to structure, electric resistivity and hydrogen sorption properties. The systems are metallic for $x < 7$ and insulating for $x = 7$. No major structural reconstruction occurs during the metal-insulator transition, and the transitions are reversible. All systems display an intermediate hydride phase of approximate composition $LnMg_2T-H_{\sim 3}$. Hydrogen absorption/desorption plateau pressures of the palladium members ($Ln = \text{La, Ce, Pr, Nd}$) increase in the sequence $\text{La} < \text{Ce} < \text{Pr} < \text{Nd}$ and scale with cell volume. This shows that the MI transitions can be “tuned” to suit given hydrogen pressure-temperature conditions. This project is developed in the framework of a CTI project with Asulab (a member of Swatch group).

Over the past months, we have successfully implemented nano-structured alkali W/Mo-oxides for ammonia sensing. The sensitivity of the W/Mo-oxide nano-materials depends on the alkali cation that is incorporated into the hexagonal channel structure and thereby also on the different nano-scale morphologies that range from nano-wires to hierarchical arrangements. Furthermore, we have hydrothermally synthesized and characterized novel bismuth oxysulfate, $\text{Bi}_6\text{S}_2\text{O}_{15}$, nano-wires with high aspect ratio. Their humidity sensing properties are quite promising for environmental applications.

We made significant progress in understanding the giant piezoresistance observed in metal-semiconductor hybrids (MSH) and depleted silicon nano-structures. A couple of companies have expressed interest in this work and a white paper has been written to explore pressure sensors based on MSH with Freescale Semiconductors Inc. Depleted silicon nano-structures have been fabricated in an attempt to demonstrate the supposed electrostatic origin of a giant piezoresistance recently observed in silicon nano-wires. To date however, the measured piezoresistances are small compared to that previously measured in silicon nano-wires.

New surface treatments for microcomponents

In this new subproject we are developing a novel technology using an STM inspired device to write marks on a microscopic scale into a metallic surface. The marks consist of small dots of *in situ* synthesized surface alloys. This

is achieved using ultrashort sparks across a composite dielectric containing nano-powders. A system has been developed to write any form and any material onto the surface. A first

1 Applied superconductivity

1.1 Enhanced superconducting properties of *in situ* MgB₂ wires after Cold High Pressure Densification (R. Flukiger, D. Eckert; Bruker-Biospin)

The cold high pressure densification technique (CHPD) recently developed in Geneva has led to a considerable improvement of the in-field critical current density J_c in *in situ* binary and alloyed MgB₂ wires and tapes [1, 2]. For wires alloyed with malic acid (C₄H₆O₅), the highest J_c values reported so far for *in situ* wires were found after applying CHPD at 1.5 GPa, reaching at 4.2 K the value 10^4 A/cm² at 13.4 T [2]. These densified wires exhibit a considerably higher MgB₂ mass density and a lower electrical resistivity, thus reflecting an improved grain connectivity (Fig. 1). A common feature observed in binary as well as in the alloyed MgB₂ wires is the enhancement of B_{irr} with increasing CHPD pressures.

Specific heat measurements show a considerably narrower T_c distribution for densified MgB₂ filaments (Fig. 2): the onset T_c value remains unchanged, while the downset value is shifted to higher temperatures. This shift of the average T_c to higher values for densified wires is correlated to the increase of the average B_{c2} and thus of B_{irr} , with B_{irr} up to 2 T higher. At the same applied field, the value of J_c for densified wires is increased by a factor 2.

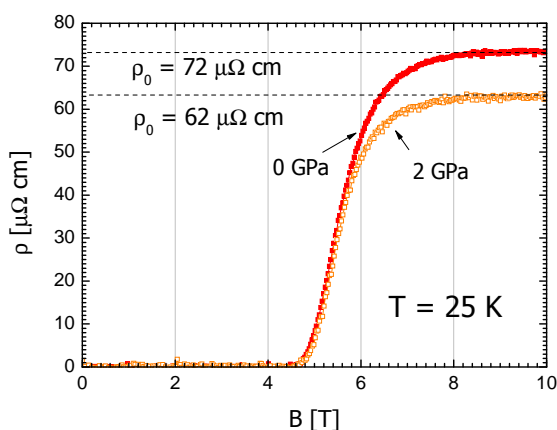


Figure 1: Resistivity vs magnetic field at 25 K for the non-pressed MgB₂ wire (red symbols) and for the wire densified at 2 GPa (orange symbols).

application has been developed for marking against counterfeiting and a CTI project with Vacheron Constantin has been awarded.

1.2 Impact of steel reinforcement on Nb₃Sn internal tin wires under tensile strain (R. Flukiger, D. Eckert; Bruker-Biospin)

In large magnets, as for example the ITER toroidal coils (TF), the Lorentz forces at 12 T become very large, with strong consequences for the I_c in the Nb₃Sn wires. In order to get further information about the behavior of cable-in-conduit (CIC) superconductors, we have studied the behavior of I_c of a steel jacketed Nb₃Sn wire produced by Oxford Instruments (OST, ITER type-I) as a function of the applied compressive stress. The strain dependence of I_c was measured with a Walters spring probe (WASP) in magnetic fields up to 19 T (Fig. 3).

As a consequence of the higher thermal pre-compression of the A15 layer induced by the stainless steel (SS) jacket, the strain value corresponding to the maximum of I_c , ϵ_m , is shifted by 0.31% with respect to the bare wire (Fig. 3). The SS reinforced wire does not exhibit any degradation of I_c after releasing the tensile force from applied strains values as high as 1.03%. The irreversibility limit, ϵ_{irr} , for the bare wire has been raised by more than 0.50%. The strain behavior of I_c in Fig. 3 shows a three-dimensional characteristics, not only for high compressive strains, but also for high tensile strains.

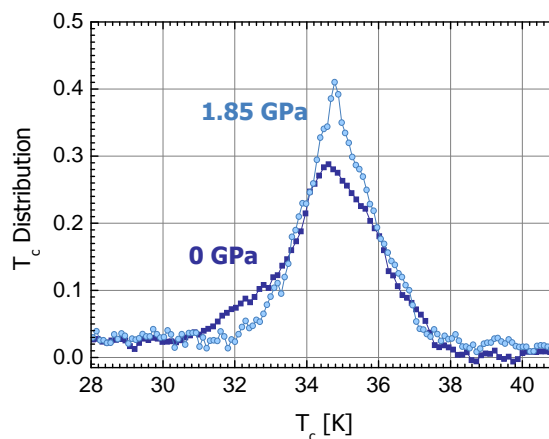


Figure 2: Distribution of T_c for the non-pressed MgB₂ wire (dark blue symbols) and for the wire densified at 2 GPa (light blue symbols).

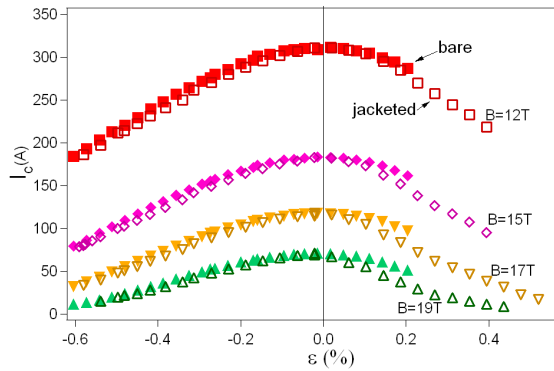


Figure 3: I_c vs intrinsic strain for both bare (solid symbols) and SS reinforced samples (open symbols), at $T = 4.2$ K and for four different applied fields.

1.3 Synchrotron radiation techniques for the characterization of Nb_3Sn wires under transverse compression (R. Flukiger, D. Eckert; Bruker-Biospin)

The high flux of X-rays in high-energy synchrotron beam lines has enabled a variety of new experiments with the highly absorbing Nb_3Sn superconductors [3]. Until recently the materials characterization of multifilamentary wires has been performed almost entirely by destructive methods, apart from studies performed with neutron techniques. In contrast to laboratory X-ray sources, high-energy X-rays from synchrotron sources allow *in situ* diffraction measurements in transmission geometry. In the present work, high-resolution synchrotron X-ray diffraction measurements were performed *in situ* at 4.2 K during the transverse compression of individual, bare Nb_3Sn wire samples. Three types of strands were studied: powder in tube (PIT), restack rod processed (RRP) internal Sn, and bronze route. Below a certain threshold stress, the strain in RRP and bronze route wires depends very little on the applied stress, suggesting that the matrix may initially protect the filaments. The elastic strain in the Nb_3Sn filaments at equivalent stresses is higher in the PIT than in the RRP and the bronze route wires (Fig. 4). This is consistent with the I_c measurements on bare PIT wires showing a stronger sensitivity to transverse compression.

1.4 Superconducting fault current limiter (M. Decroux, M. Abplanalp; ABB)

a) *Introduction* The superconducting fault current limiter (SFCL) is a device which limits the current in the electrical network during a short-circuit. Thanks to the fast superconducting to normal transition, the SFCL can limit the

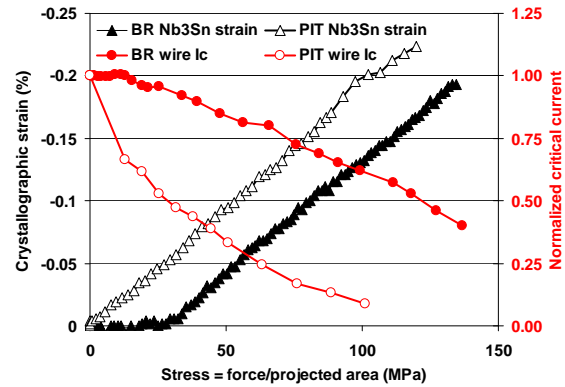


Figure 4: Crystallographic strain vs compressive stress (left axis) and I_c vs compressive stress (right axis) for a bronze route Nb_3Sn wire (solid symbols) and a PIT Nb_3Sn wire (open symbols).

current in less than a ms. We are now focusing on SFCL made of superconducting thin films grown onto a metallic substrate (Hastelloy) known as coated conductors (CC). We have already reported on the behavior of CC during a short-circuit and we have highlighted some weaknesses of these CC [4]. The first one is the low mean electric field they can sustain (<1 V/cm) and the second is the low propagation velocities of the switched region (of the order of few cm/s compared to 20 m/s in films grown onto sapphire wafer) [4]. These low propagation velocities are related to the poor thermal properties of the structure, i.e the thermal properties of the superconducting/buffer layer, of the substrate and the thermal coupling between them. Therefore during this year we have both studied the electric field in CC at the beginning of a short-circuit and we have started the thermal characterization of the CC by the study of the substrate.

b) *Electric field in coated conductors* In CC, at the beginning of a short-circuit, only a part of the superconducting line is switching into the normal state. The applied voltage appears on this normal region and therefore the local electric field E_{local} is higher than the mean electric field E_{mean} (= applied voltage divided by the length of the line). This leads to a local power density which can be higher than a threshold value and therefore damaging the sample. It is then important to have an idea of the value of this local electric field. We have then carefully measured the behavior of a superconducting line during short constant voltage pulses. The resistance of the line at the beginning of the voltage pulse is shown on Fig. 5.

This graph shows that the resistance increases linearly with E_{mean} until a kink appears at the total resistance of the line in the normal state.

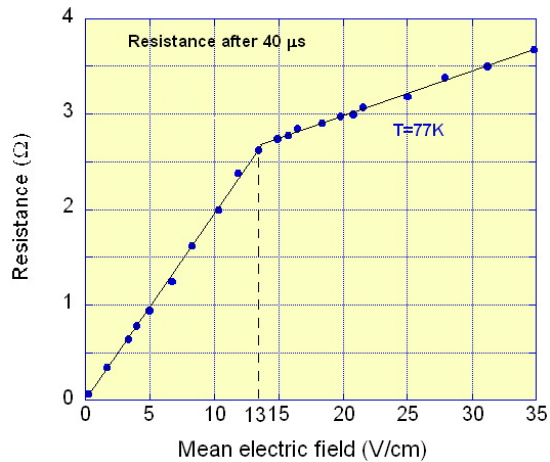


Figure 5: Resistance of a 1.2 cm long line 40 μs after the beginning of a constant voltage pulse as a function of the applied mean field.

This indicates that the whole line has switched for an applied field of 13 V/cm. This means that if one applied a low E_{mean} ($\ll 13$ V/cm) to this CC (produced by Theva with $d_{\text{YBCO}} = 300$ nm) the local electric field in the switched region will be 13 V/cm, i.e. E_{local} can be much higher than E_{mean} .

c) *Heat propagation within the substrate* The propagation of the heat in the Hastelloy substrate certainly plays a role in the propagation velocity of the normal zone. It is then interesting to determine what the heat propagation velocity in this substrate is. For this measurement we have developed a special structure made of several parallel superconducting strips along the tape on which we can record the propagation of the temperature front within the substrate as shown on Fig. 6 (inset). The heat is generated by applying a current pulse ($J > J_c$) on a heater strip. The switching sequence of these stripes is reported on Fig. 6.

From these measurements we can estimate that the heat propagation velocities in the substrate are around 1–3 cm/s. These velocities are lower than the measured propagation velocities of the normal zone along the CC (8 – 15 cm/s) and further studies are needed to determine if the difference is coming from the propagation of the heat in the superconducting/buffer bilayer.

d) *Thermal conductivity of thin films* One important parameters which play a crucial role in the propagation of the normal zone is the thermal conductivity of the different layers of the CC's structure. We have then developed a new probe which allows us to measure the thermal conductivity of thin films as shown on Fig. 7.

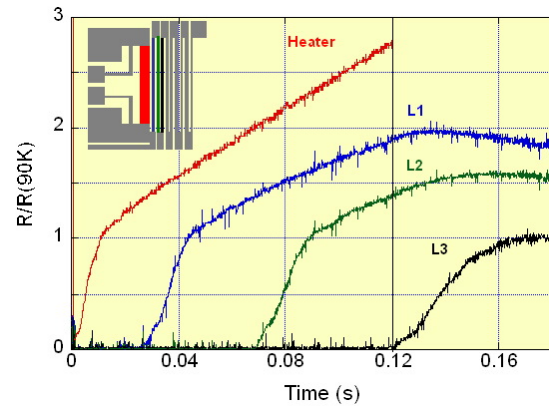


Figure 6: Resistance of the heater and the thermometer stripes during a 120 ms constant current pulse applied to the heater line. The space between the thermometer stripes (L1, L2, L3) is 200 μm . The inset shows the structure used for this measurement.

The heat, on the CC, is generated by a current biased strain gauge. We are now calibrating the setup and we have already measured, by a steady-state technique, the thermal conductivity of an Hastelloy/MgO structure. The thermal conductivity we measured is close to the value reported in the literature.

2 Oxides for energy harvesting

2.1 MEMS based on epitaxial oxides on silicon (J.-M. Triscone, G. Triscone, N. de Rooij)

a) *Oxide growth and characterization* Si microfabrication technology has demonstrated its huge potential and success with microelectromechanical systems (MEMS) such as accelerometers or digital light processing devices, widely used in commercial applications. Providing new and/or improved functionalities to MEMS with crystalline complex oxides is the scope of this collaborative project. In particular, we aim to integrate epitaxial piezoelectric thin films with silicon microfabrication techniques to realize deflecting membranes and cantilevers for sensing, actuation and energy harvesting.

The main challenges for the integration of oxides on silicon are the control of the silicon/oxide interface at the atomic level, the growth of high quality epitaxial oxide films and the choice of microfabrication processes, allowing the excellent properties of the oxide layers to be retained, in order to maximize the performance of fabricated devices.

Our all-epitaxial MEMS are based on a piezoelectric $\text{Pb}(\text{Zr}_{0.2}\text{Ti}_{0.8})\text{O}_3$ (PZT) layer grown on a silicon substrate through two oxide layers: SrTiO_3 used as structural buffer and metal-

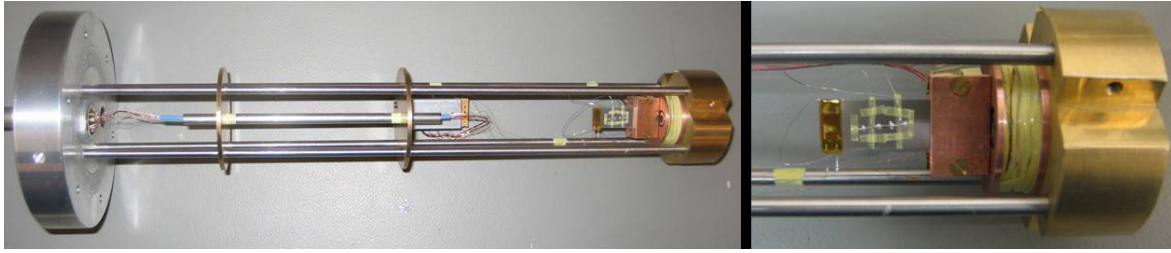


Figure 7: Probe for the measurements of the thermal conductivity of thin films.

lic SrRuO_3 (SRO) used as bottom electrode. A few unit cell thick epitaxial (001) SrTiO_3 film is initially grown by molecular beam epitaxy on 2" (001) silicon wafers, providing the structural interface between the silicon and the perovskite structure [14]. We then employ off-axis magnetron sputtering to deposit a 30 nm thick metallic SrRuO_3 and a ferroelectric $\text{Pb}(\text{Zr}_{0.2}\text{Ti}_{0.8})\text{O}_3$ layer, typically 150 nm thick [5].

X-ray $\theta - 2\theta$ diffractograms confirm the c -axis orientation of the oxide stack (see MaNEP Progress Report, Year 8). Local measurements of the d_{33} piezoelectric coefficient, performed with an atomic force microscope, permit to estimate a d_{33} value of the order of 50 pm/V and a coercive field of ~ 100 kV/cm. Current-voltage ($I - V$) and polarization-electric field ($P - E$) measurements realized on test structures (surface area $100 \times 100 \mu\text{m}^2$) show clear ferroelectric switching peaks without a significant presence of leakage currents up to 20 V, indicating a robust ferroelectric response of the epi-piezo thin film on silicon. The estimated remnant polarization is around $70 \mu\text{C}/\text{cm}^2$.

Different tests have been performed to evaluate the influence of the microfabrication steps on the properties of the piezoelectric layer. We have investigated the role of different materials suitable as top electrodes. Au/Cr, Pt/Ta and Pt/Ti have been tested. The results show that the degradation in the remnant polarization is least severe for PZT thin films with Au/Cr top electrode. The thermal budget of the heterostructures during the patterning process was also studied. It was found that high processing temperatures can degrade the properties of piezoelectric thin films. We have realized test structures with Au/Cr top electrodes for $P - E$ measurements. The samples have been heated in an oven in ambient atmosphere at different temperatures for 30 minutes and then characterized at room temperature. Ferroelectric properties remain robust up to an annealing temperature of 250°C , as shown in Fig. 8; at 300°C , $I - V$ curves reveal the appearance of a large leakage component, mask-

ing the ferroelectric switching current.

b) *Processing and characterization of devices* Epitaxial PZT transducers (membranes and cantilevers) are fabricated using micro-patterning techniques optimized for these oxide layers [6]. The front-side processing is a combination of wet etching for the PZT layer and dry etching for the SRO electrode. For the Si back-side etching, a deep reactive ion etching technique has been used to obtain membranes with a thickness of the order of $10 \mu\text{m}$. To release the cantilever structures from the wafer, a direct laser cutting technology has been employed.

Circular membranes fully covered by an electrode with different diameters of 1000, 1500 and $2000 \mu\text{m}$ with a silicon thickness of $20 \mu\text{m}$, as shown in Fig. 9, and cantilever beams with different sizes have been fabricated.

The static and dynamic behavior of these structures has been investigated by optical probes. The resonant frequencies have been identified by exciting the structure with a white noise signal. These resonant frequencies, observed in

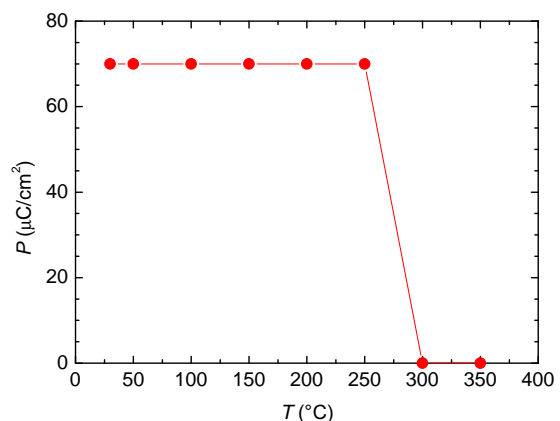


Figure 8: Remnant polarization measured at room temperature versus the annealing temperature T . $P - E$ loop of an as grown sample reveals a remnant polarization of $70 \mu\text{C}/\text{cm}^2$, which is maintained up to an annealing temperature of 250°C . For annealing temperatures above 300°C , the leakage becomes important.

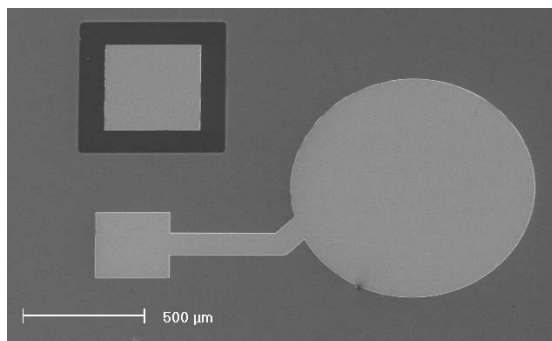


Figure 9: Optical microscope view of the front-side of a 1000 μm circular membrane. The Cr/Au metalization (light gray area) covers the PZT layer of the membrane and works as top electrode. The access to the SrRuO₃ bottom electrode is visible in the left top corner.

Fig. 10 for a 2000 μm membrane, are in agreement with theoretical simulations.

Successively, the quality factor (Q factor) of the first resonance mode has been measured with an excitation signal of 1 V ac, in atmospheric pressure and under vacuum. The Q factor, calculated as the ratio between the resonant frequency and the full width half maximum of the resonant peak is an important parameter in resonant applications, since it determines the sensitivity of the device. Fig. 11 shows the frequency spectra for a 1500 μm diameter membrane under atmospheric and 0.1 mbar pressures. We observe that the resonant peak increases in intensity and shifts to higher frequency with decreasing pressure. This phenomenon is due to the reduction of air damping around the structures. In the case of the membrane, the Q factor is 50 at atmospheric

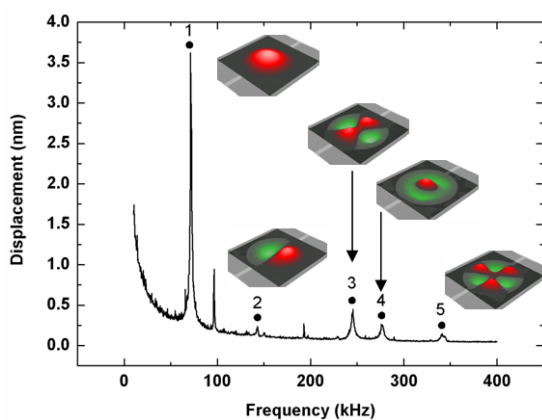


Figure 10: Resonance frequencies for a 2000 μm membrane excited by a white noise signal. The different deformation modes have been theoretically calculated and are shown for each resonance frequency.

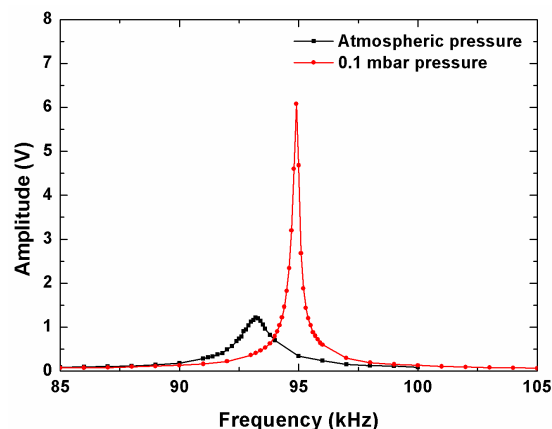


Figure 11: Frequency spectra for a 1500 μm diameter membrane under atmospheric and 0.1 mbar pressures.

pressure and increases markedly to 323 when the pressure is reduced to 0.1 mbar.

2.2 Controlling the structure and thermoelectric properties of perovskite-type manganates (A. Weidenkaff)

a) *Identification of promising thermoelectric oxides* Thermoelectric (TE) materials are used for the direct conversion of heat into electricity. If a temperature gradient is imposed on two sides of the thermoelectric module, a voltage gradient will form in response via the Seebeck effect. The value of the voltage generated for the temperature drop of 1 K is characterized by the Seebeck coefficient and depends on the electronic structure of the compounds. CaMnO₃ exhibits a large thermoelectric coefficient ($S_{(T=300\text{ K})} = -800 \mu\text{V/K}$), which is essential for the application in thermoelectric converters. As described by the so-called dimensionless figure of merit $ZT = S^2T/\rho\kappa$, high S needs to be combined with low electrical resistivity ρ and thermal conductivity κ . Although CaMnO₃ does not fill the low- ρ requirement, a better n -type conductivity can be introduced through substitution of Mn with cations having higher stable oxidation numbers. This principle was applied when synthesizing improved n -type thermoelectrics with a nominal composition of CaMn_{0.98}Nb_{0.02}O_{3- δ} . The theoretical Seebeck coefficient values were calculated by applying the extended Heikes formula taking spin entropy terms into account. The results were confirmed with Seebeck measurements and a detailed error calculation. With increasing Nb substitution, the resistivity is lowered as expected and confirmed by theoretical evaluations. Nevertheless, it was found that the density and morphology of the

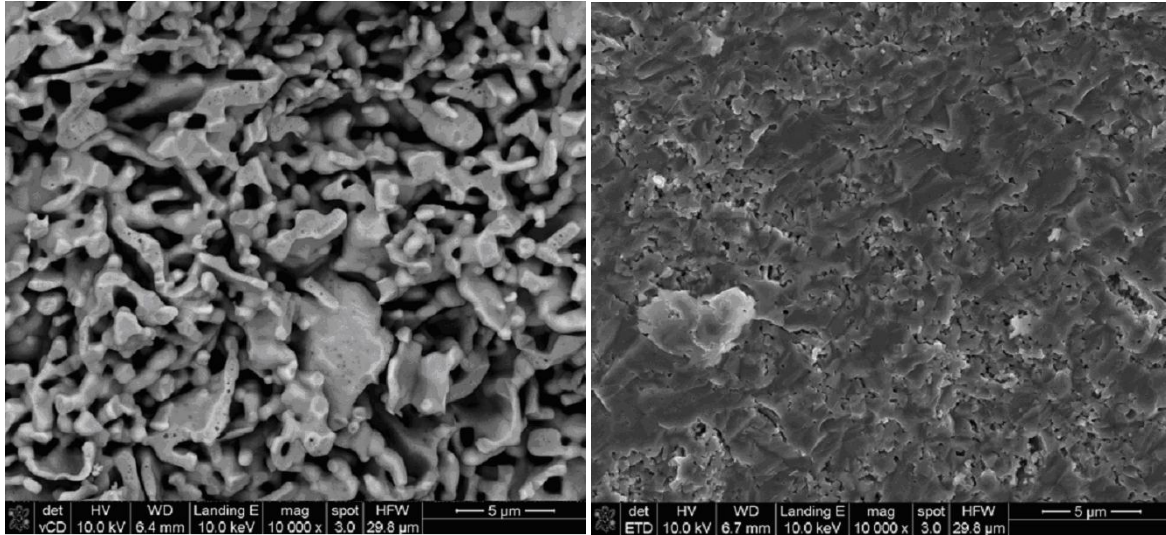


Figure 12: The nano-structures of high-ZT (left) and low-ZT (right) $\text{CaMn}_{0.98}\text{Nb}_{0.02}\text{O}_3$ materials.

samples on the thermoelectric performance ZT has to be determined very accurately, since the deviation in reproducibility can be up to one order of magnitude. This finding led to a critical review of the available literature data on the most promising new materials and was unfortunately confirmed for all published data on thermoelectric oxides.

For further systematic studies $\text{CaMn}_{0.98}\text{Nb}_{0.02}\text{O}_3$ phases with different densities (60% – 100%) and morphologies are being produced and characterized (fig 12). Samples with smaller grain size and lower density show extremely low thermal conductivity. The grain boundaries work effectively as phonon scatterers and together with pores provide higher ZT values having impact on the efficiency of the thermoelectric conversion.

b) *Finite element modeling* The efficient usage of energy at all stages along the energy supply chain and the utilization of waste heat are very important for a sustainable energy supply system. Thus, thermoelectric modules need to be modeled to be optimized according to the operating temperature gradients between hot T_h and cold T_c sides of the module. The required output voltage V , current I , and generated power output P is evaluated by using the acquired input parameters, i.e. the thermoelectric properties S , ρ and κ , and validated with experimental values from thermoelectric modules. The equations governing the multi-dimensional temperature and electrical potential distributions in TE materials, under steady-state conditions and in the absence of an applied magnetic field, can be presented as the

energy equations:

$$\nabla(\lambda \nabla T) - T \cdot J \frac{\partial \alpha}{\partial T} \nabla T + \rho J^2 = 0 \quad (2.1)$$

and current flow:

$$J + \sigma(\nabla V + \alpha \nabla T) = 0 \quad (2.2)$$

$$\nabla J = 0 \quad (2.3)$$

$$q = \alpha T J - \lambda \nabla T \quad (2.4)$$

where the vector J is the electric current per unit area, the vector q is the heat transfer rate per unit area, T is the temperature, λ is the thermal conductivity at zero current, $\sigma = 1/\rho$ is electrical conductivity, ρ is electrical resistivity, α is the absolute Seebeck coefficient (thermoelectric power) and V is the voltage. All the materials properties are functions of temperature. These functions are based here on interpolation of measured data. The equations above form a system of two direct coupled partial differential equations with two dependent variables the temperature T and the electrical potential V . In COMSOL Multiphysics the geometry is modeled by using the internal CAD tool.

3 Applications of artificial superlattices – development of neutron guides (M. Kenzelmann; Swissneutronics)

3.1 Introduction

It is well known that decreasing the roughness of the substrate surface and/or of the layer interfaces can substantially increase the reflectivity of neutron supermirrors. However, in the

process of neutron mirror deposition, the interface roughness is usually increased. This effect can be minimized by appropriate deposition parameters. In particular, recent developments of the coating process for neutron supermirrors [7][15] showed that a high reflectivity can be achieved if the supermirrors are deposited on ultrasmooth surfaces.

During recent years, supermirrors became an essential component at most neutron scattering instruments and are widely used for the efficient transport and manipulation of neutron beams. Present neutron guides and optics are usually assembled from flat glass substrates. The natural surface of floated glass provides an extremely small roughness, and this allows the deposition of supermirrors with high reflectivity for very large angles of reflection, i.e. up to $m = 7$ times the critical angle of Ni. For example, reflectivities $R \geq 80\%$, 70% , 60% , and 50% are regularly obtained for $m = 4, 5, 6$, and 7 , respectively [7]. Unfortunately, glass has limited stability against irradiation, temperature, and mechanical stress. Hence metal substrates of a similarly high quality are desired for demanding application [8].

3.2 metallic substrates

We developed processes to refine the surface on aluminum substrates and monitored the results by AFM. The roughness is quantified by the vertical deviations of the surface from its ideal form. The simplest description of surface or interfacial roughness is the root mean square (RMS) value Sq (areal roughness). The surface of floated glass served as the reference because borated or non-borated glass has been proven to be the best substrate for supermirror coatings when prepared properly. Fig. 13a shows a typical image of the topography of a float glass [8]. The analysis results in a RMS roughness of $Sq \approx 1.8 \text{ \AA}$. We also succeeded to adapt the refining process to steel substrates.

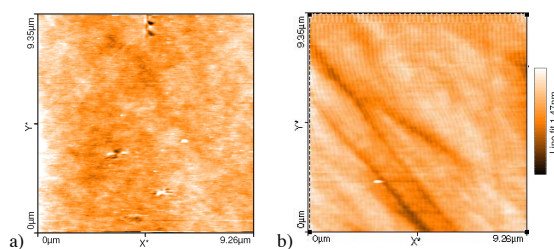


Figure 13: AFM images of the surface of (a) float glass and (b) steel substrate. The surface of the steel substrate exhibits fine scratches from the polishing process. The color code is identical for both images.

Fig. 13b displays the AFM image of the steel surface as obtained from a state-of-the-art refinement process. A roughness of $Sq \approx 2.1 \text{ \AA}$ is obtained, which approaches the typical value of floated glass. Measurements on various locations confirm the homogeneity of the quality, indicating that the refinement process is constant across the complete substrate area of $70 \text{ mm} \times 180 \text{ mm}$.

The aluminum substrates were coated with a Ni/Ti supermirror $m = 2$ and 3.6 . The measured reflectivity profiles are presented in Fig. 14 showing $R = 91\%$ at $m = 2.1$ and $R = 77\%$ at $m = 3.6$. For comparison, the reflectivity of a similar supermirror on float glass is included, reaching $R = 94\%$ and $R = 82\%$ at the respective edge of the supermirrors. The reflectivity of the supermirror $m = 3.6$ on a steel substrate is also included in Fig. 14 reaching $R \approx 77\%$ at $m = 3.6$. The excellent neutron reflectivity of the supermirror on aluminum and steel substrates confirms the excellent smooth surface. However, it is also clear that the float glass is still slightly superior compared with the refined metallic substrates. This is in agreement with our AFM measurements.

With this study, we also demonstrated the importance of AFM measurements for the determination of the surface roughness of supermirror substrates. We succeeded to correlate the RMS roughness from AFM and the reflectivity data of the coated substrates consistently. This method thus provides a valuable tool for the

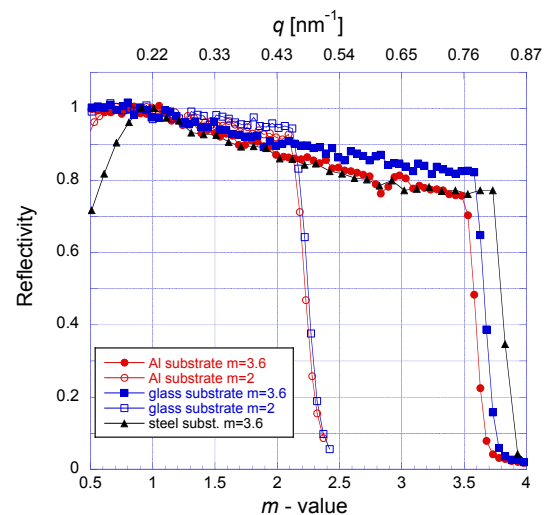


Figure 14: Neutron reflectivity of a $m_{\text{nominal}} = 2$ resp. $m_{\text{nominal}} = 3.6$ supermirror deposited on refined aluminum (circles) and steel substrates (triangle) and on float glass (squares). The m -values differ slightly from the targeted value due to a small deviation of the thickness calibration of the deposition process.

quality control of the neutron supermirror production.

It is not clear how reliable the absolute roughness values Sq are, which are obtained from our AFM measurements [16]. The AFM has a few drawbacks in relation to the quantitative measurement of surface roughness. One of the undesirable shortcomings is the coupling of the tip geometry with the scanned image. Due to the finite size of the tip, the image scanned by an AFM is a convolution of the tip geometry and sample topography [16]. Our AFM measurements were carried out in air using a Nanosurf easyscan II operated in the tapping mode. Images were acquired on $9.26 \mu\text{m} \times 9.26 \mu\text{m}$ areas having 256×256 data points. This area is approximately complying with the lateral coherence length of the neutron beam. We plan to include further AFM features such as the skewness to overcome present limitations of the RMS roughness.

In summary, using AFM characterization of substrate surfaces, we developed a polishing process to refine the surface of aluminum and steel substrates, which enable the growth of supermirrors with a high reflectivity $R \approx 91\%$ at $m = 2.1$ and $R \approx 77\%$ at $m = 3.6$. Metallic substrates are required for neutron optics in order to overcome limitations implied by glass. Benefits are: i) increased durability against large changes in temperature and intense irradiation, ii) enhanced mechanical deformation to impose more complicated geometrical designs of guides, e.g. for focusing, and iii) robustness against mechanical damages and implosions. Dedicated applications of neutron guides with metallic substrates are initial guide sections very close to the moderator to reduce streaming of neutrons.

4 Hydrogen detectors and other sensors

4.1 Progress towards a solid-state hydrogen detector (K. Yvon, J. Cors, Ø. Fischer; Asulab (Swatch group))

a) *Aim of project* Hydrogen fuel cells and electrolyzers play a key role in future energy scenarios. Mass markets such as hydrogen powered vehicles and hydrogen production units for residential areas require hydrogen detectors and sensors on a very large scale. The devices must be cheap, sensitive, selective, and require little energy. The project aims at developing such devices by using thin films technologies on novel materials undergoing hydrogen-induced metal-insulator transitions. Here we report on further results concerning the material's issue of the project. The

	La	Ce	Pr	Nd	Sm
Ni	x		x	x	
Pd	x	x	x	x	x
Pt	x				

Table 2.1: Known $LnMg_2TH_7$ analogues.

work is performed within the framework of a CTI project and benefits from support by an industrial partner.

b) *Materials available* Among the metal-hydrogen systems showing hydrogen induced metal-insulator (MI) transitions, the $LnMg_2T-H_x$ systems are of particular interest because they undergo no major structural reconstruction during the MI transition and the transitions are reversible within a useful favorable hydrogen pressure-temperature range. Members were previously found for $Ln = La, Ce, Pr, Nd$ and $T = Ni, Pd, Pt$ (see MaNEP Progress Report, Year 8). The palladium member with $Ln = La$ was found to be metallic at $x < 3$ and insulating at $x = 7$. At 50°C the material was found to absorb hydrogen in the pressure range $0 - 0.1$ bar, i.e. the MI transition presumably occurs under these conditions, at least in the bulk.

c) *Work performed* A search for new $LnMg_2TH_7$ representatives revealed the existence of the previously unknown palladium-samarium member $SmMg_2PdH_7$. An updated list of known $LnMg_2TH_7$ representatives is given in Table 2.1.

Pressure-composition isotherms for hydrogen absorption/desorption were measured for the palladium systems $LnMg_2Pd-H$ ($Ln = La, Ce, Pr, Nd$). As shown in Fig 15, all four systems

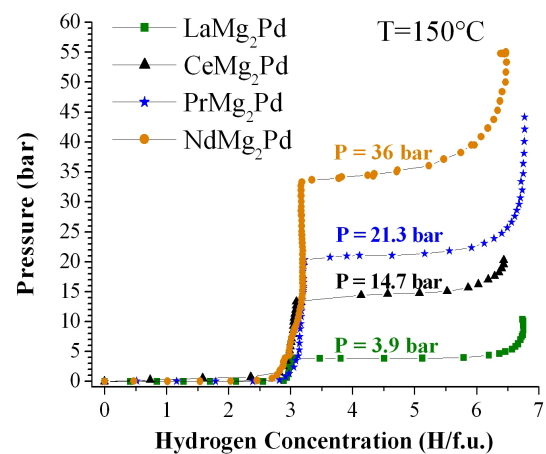


Figure 15: Hydrogen plateau pressures of $LnMg_2Pd-H$ systems ($Ln = La, Ce, Pr, Nd$) at 150°C during absorption.

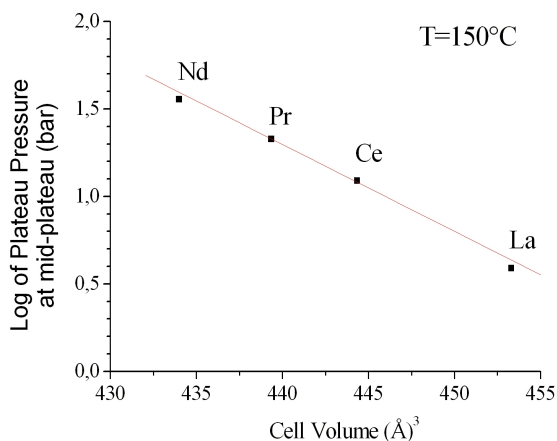


Figure 16: Log of hydrogen plateau pressures for $LnMg_2Pd-H$ analogues ($Ln = La, Ce, Pr, Nd$) at $150^\circ C$ during absorption versus cell volume.

display a second plateau consistent with the formation of an intermediate hydride phase of approximate composition $LnMg_2PdH_{\sim 3}$. Consequently, the hydrogen induced metal-insulator transition is expected to occur at or near this composition. Clearly, *in situ* resistance measurements are required to substantiate this expectation. Furthermore, it can be seen from Figs. 15 and 16 that the hydrogen absorption plateau pressures increase in the sequence $La < Ce < Pr < Nd$ and scale with cell volume: the larger the cell volume the lower the plateau pressure at a given temperature. These findings are important because they allow one to “tune” the plateau pressures and thus the hydrogen induced MI transitions.

d) *Conclusions and perspectives* The hydrogen absorption/desorption pressures and MI transitions in the $LnMg_2T-H$ systems can be conveniently “tuned” by lanthanide substitution. *In situ* resistance measurements on bulk and thin film samples, as well as sputtering tests are under way. While the pressure-temperature conditions for hydrogen absorption in these systems appear to be in a useful range for hydrogen detectors/sensors, additional efforts appear to be necessary to decrease the hydrogen equilibrium pressures. For that purpose, exploring the potential of other materials showing hydrogen induced MI transitions is desirable.

4.2 Development of novel sensors based on oxide nano-wires (G. Patzke, J. Cors; Phasis)

a) *Construction of the experimental sensor setup* We focus on enhancing the sensitivity and improving the selectivity of oxide-based gas sensors starting from MoO_3 nano-rods and nano-

structured W/Mo-oxides wires [9] as well as from Bi-containing oxides [10]. Further oxide materials are tuned with respect to morphology and composition via hydrothermal synthesis [11]. Semiconducting sensors based on gas-sensing metal-oxide layers detect in principle the impedance change on the metal-oxide surface before and after contact with the target gases [17]. The sensor signal is induced by surface redox reactions and can be measured at operating temperatures usually over $200^\circ C$. The following experimental setup is now being constructed in our laboratory:

- the measurement takes place in a chamber made of steel with exchangeable gas flow;
- the heater with 150 W power can be operated up to $400^\circ C$ and it is regulated by an external temperature regulator;
- a glass pane is fixed as a substrate on the bronze over the heater and the effective working temperature is measured by an external temperature controller;
- two gold electrodes are fixed on the glass pane with a distance around $20 \mu m$ for measuring the electrical properties (to be fabricated at FIRST Center for Micro- and Nanoscience, ETHZ);
- several drops of ethanol with dissolved nano-powders are put in between the electrodes on the substrate.

b) *NH_3 sensing properties of nano-structured W/Mo oxides* As our setup for sensing measurements is just being installed, additional sensing investigations were performed in collaboration with the group of Prof. G. Chen, Department of Materials Science, Fudan University, China¹. In our previous studies, we demonstrated how the alkali chlorides can strongly influence the morphologies of mixed W/Mo-oxides [9, 12]: whereas the smaller alkali cations (Li, Na) favor the formation of nano-rods, the larger cations (K, Rb, Cs) support hierarchical arrangements of nano-rods into spherical architectures. Our NH_3 sensing study revealed that their sensor properties are strongly dependent on the cations incorporated into the hexagonal channel structure. Fig. 17 shows the sensitivity versus operating temperature of the gas sensors for 100 ppm NH_3 diluted in pure Ar. Here, the sensitivity S was defined as the relative resistance: $S = R_{Ar}/R_{ammonia}$. Generally, the resistance of the W/Mo-oxide-based sensors decreases in the presence of NH_3 , which is characteristic

¹Supported by the Sino Swiss Science and Technology Cooperation, SSSTC, EG05-092008

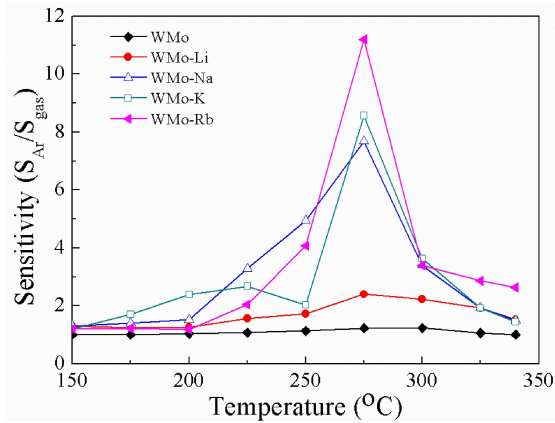


Figure 17: Sensitivity S vs operating temperature for 100 ppm NH_3 sensing among the WMo-oxide series.

for n -type semiconductors. All investigated alkali-containing nano-structured oxides of the W/Mo-series reach their maximum sensitivities around 275°C and they exhibit higher sensitivities than the reference alkali-free W/Mo-oxide. Furthermore, the sensitivity of the WMo-sensors increases with the size of alkali cations, i.e. $S_{\text{WMo-Rb}} > S_{\text{WMo-K}} > S_{\text{WMo-Na}} > S_{\text{WMo-Li}}$.

An analogous trend of sensitivity versus gas concentration can be observed at 275°C as shown in Fig. 18. The sensitivity increases rapidly and saturation is achieved for high gas concentrations. The measurement data fitted well with the power law of the semiconducting oxide gas sensor defined as follows:

$$S = 1 + A_g(P_g)^\beta \quad (2.5)$$

where P_g is the target gas partial pressure, which is proportional to the gas concentration, A_g is a prefactor, and β is the exponent on

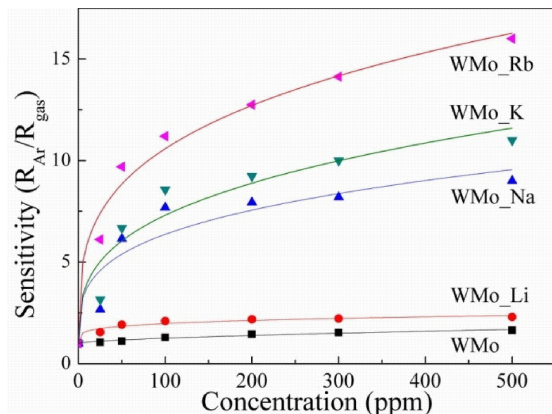


Figure 18: Sensitivities of the alkali W/Mo-oxides versus different NH_3 concentrations (operating $T = 275^\circ\text{C}$).

P_g . Our results clearly demonstrate that the sensitivity of W/Mo-oxides towards NH_3 can be remarkably enhanced through incorporating different alkali cations into the oxide channel structure and thereby shaping the particle morphology.

c) *Humidity sensing properties of new $\text{Bi}_6\text{S}_2\text{O}_{15}$ nano-wires* Humidity sensors are very important for practical applications in environmental monitoring, industrial process control and in daily life. We studied the humidity sensing properties of new $\text{Bi}_6\text{S}_2\text{O}_{15}$ nano-wires that were obtained from hydrothermal synthesis. Fig. 19 shows the characteristic humidity hysteresis of a model humidity sensor constructed from $\text{Bi}_6\text{S}_2\text{O}_{15}$ nano-wires. The upper line is corresponding to the adsorption process, while the lower one represents the desorption process: the resistance changes from about $10^7 \Omega$ to $10^4 \Omega$ when the relative humidity (RH) increases from 11% to 95%. This resistance change of three orders of magnitude over the RH range points to a very high sensitivity of the $\text{Bi}_6\text{S}_2\text{O}_{15}$ nano-wire sensor. Further dynamic testing procedures were performed which provide more information such as response, recovery time and reproducibility of the sensor. The response and recovery times, defined as the time required for sample conductance variation to reach 90% of the equilibrium and return to 10% above the original conductance, were about 6 s and 40 s with RH values from 11% to 85%, respectively. These results indicate that $\text{Bi}_6\text{S}_2\text{O}_{15}$ nano-wires display a promising application potential regarding environmental monitoring and electronic devices for humidity control.

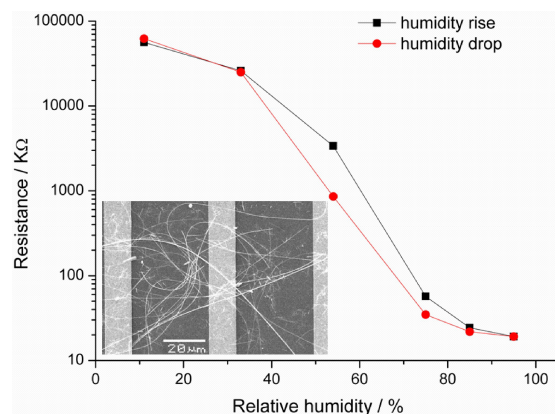


Figure 19: Humidity hysteresis of the $\text{Bi}_6\text{S}_2\text{O}_{15}$ nano-wire sensors (inset: SEM image of the nano-wire sensor chip, scale bar = $20 \mu\text{m}$).

4.3 Giant piezoresistance silicon cantilever (C. Renner)

a) *Introduction* The focus of this project is on understanding and exploiting unusually large piezoresistances observed in custom designed silicon devices. The goal is to develop very sensitive gauges capable of measuring minute strains that occur, for example, in atomic force microscopy cantilever. The interest for such gauges is not only driven by achieving the ultimate sensitivity. Indeed, very sensitive piezoresistive strain gauges offer better signal-to-noise ratio than standard gauges when operated at low currents. This is a decisive advantage for applications where power consumption is the defining parameter, like in mobile (one reason why Freescale Semiconductors Inc. is interested) and distributed sensor network applications.

We have been working on two distinct implementations. A metal-silicon hybrid (MSH), where the piezoresistance is controlled by a metal shunt evaporated along a doped silicon strip, and a depleted silicon nano-structure where the piezoresistance is supposed to stem from an electrostatic effect. The results have been presented at international professional fairs, attracting the interest of several companies. Two patents were filed in 2009, and we have received one of the two first UniGAP awards to build a functional MEMS cantilever using these novel strain gauges. A white paper has been drafted to explore the potential of MSH in the area of pressure gauges with Freescale Semiconductors Inc.

b) *Metal-Semiconductor Hybrid* Metal-semiconductor hybrid (MSH) strain gauges are planar devices (Fig. 20) fabricated using standard lithography from a boron implanted ($p = 1 \cdot 10^{17} \text{cm}^{-3}$) silicon (001) wafer. Giant piezoresistance observed in MSH devices [13] is a purely geometrical effect controlled

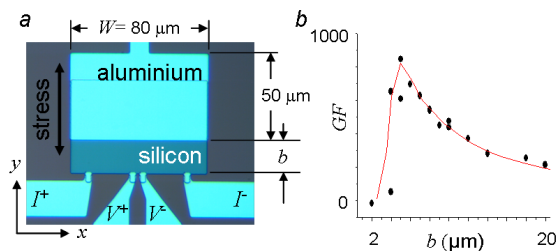


Figure 20: (a) False color SEM picture of a metal semiconductor hybrid strain gauge. x and y point along the $[1\bar{1}0]$ and $[110]$ silicon crystal axes, respectively. (b) Measured gauge factor GF as a function of distance b .

by the distance b separating the metal shunt (aluminum in our case) from the four ohmic contacts to the silicon strip for a given ohmic width W . In p -type silicon, the maximum response is obtained for stresses X applied along the $[110]$ direction, corresponding to the y axis in Fig. 20. The gauge factor $GF = \frac{\Delta R}{R_0} / \frac{\Delta \ell}{\ell_0}$ was measured using the four terminal configuration shown in Fig. 20a. Although this configuration, with the voltage leads positioned very close together, yields very high GF , it turned out to be inadequate for applications due to low signal-to-noise ratio. This experimental observation was subsequently confirmed theoretically by Hansen *et al.* [18]. Unfortunately, this result implies that four terminal MSH are not suitable to monitor the deflection of an AFM or biomechanical assays cantilever.

Large gauge factors translate into greater sensitivity only for two terminal devices [18]. Upon inspection of the simplified conductivity tensor $\bar{\sigma} = \sigma_0 \begin{pmatrix} 1 + \delta & 0 \\ 0 & 1 - \delta \end{pmatrix}$ (where $\delta \approx \frac{X}{2} \pi_{44}$, X is the stress applied along $[110]$ and $\pi_{44} = 138.1 \times 10^{-11} \text{Pa}^{-1}$) describing the transport property of the MSH depicted in Fig. 20, one finds a critical stress $X_c \approx \frac{2}{\pi_{44}}$ for which the conductance along the y direction can be switched off, thereby generating a large GF . Hence, to achieve large GF , a two-terminal MSH requires an offset stress. We are confident that for some applications it will be possible to comply with the required offset stress. This is a very promising prospect, since a two-terminal (piezo-)resistor is much easier to integrate into an electronic circuit than a four terminal component.

c) *Piezopinich strain gauge* A very large and non-linear piezoresistance observed in Si nano-wires [19] prompted us to explore a different avenue to achieve large gauge factors. The piezoresistance in these nano-wires was shown to result from a stress-induced modulation of

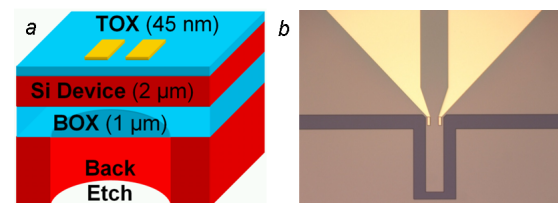


Figure 21: (a) Model view of a depleted silicon piezopinich device. (b) False color SEM picture of a cantilever with an integrated piezopinich gauge at its base.

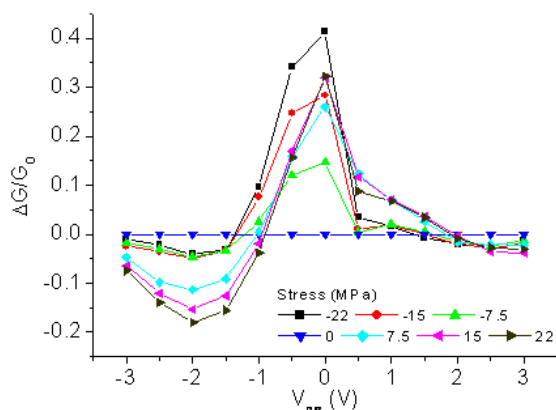


Figure 22: Relative conductance changes of a piezopinched strain gauge measured as a function of bias voltage for different applied stresses. The response in the vicinity of 0 V and -2 V is consistent with large GF.

the surface depletion region width ω [20]. This model predicts that tensile stress applied to a silicon slab with at least one dimension transverse to the current flow smaller than 2ω , would reduce the carrier density enough to ultimately pinch off the current flow. Based on this quantitative understanding, we fabricated depleted silicon nano-structures (Fig. 21a), including on-cantilever devices (Fig. 21b), to demonstrate the supposed electrostatic origin of the giant piezoresistance. We have encountered a number of experimental difficulties in measuring these so-called piezopinched devices. Initial experiments showing very large piezoresistances (Fig. 22), consistent with the measurements made on silicon nano-wires [19], were subsequently found to be totally independent of applied stress. These difficulties have now been overcome, however to date, the piezoresistances measured in our devices are small compared to the values previously measured in silicon nano-wires. We are currently pursuing a number of possibilities to better understand the absence of a giant piezoresistance in our structures. It should be noted that the results on silicon nano-wires [19], although largely cited, have not yet been reproduced and the community is still waiting for a convincing experimental demonstration.

5 New surface treatments for micro-components (J. Cors, J.-M. Triscione, Ø. Fischer; Vacheron Constantin)

5.1 Scope of the project

This work uses a STM-inspired experimental setup to mark metal objects at the microscopic scale. The marks consist of small dots

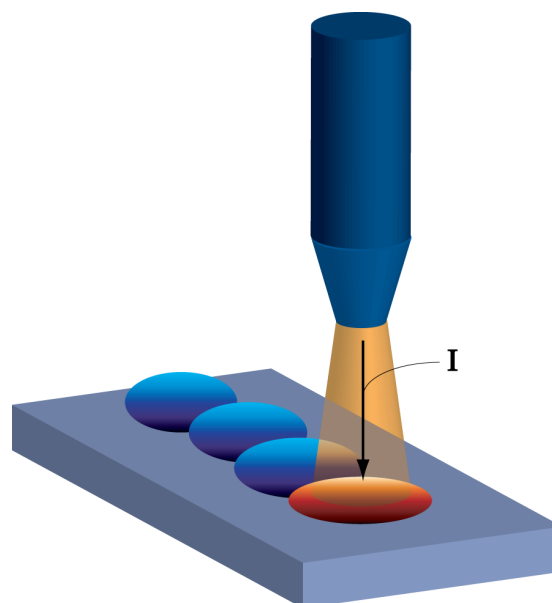


Figure 23: A metal tip is brought to a well-defined distance of the surface of the sample. The process leaves a nano-powder printed mark on the surface. Numerical control software allows for the transfer of pre-defined patterns.

of *in situ* synthesized surface alloys. This is achieved by promoting ultrashort sparks across a composite dielectric containing selected nano-powders. Hair-thin transient plasma channels occur in the gap between the tip and the surface of the sample (Fig. 23). The energy settings (voltage, current shape) are optimized to produce plasma masses containing volatilized nano-powder material.

The process leaves surface dots displaying a tailored composition that acts as a chemical fingerprint². The STM-like configuration allows for the precise control of the spark locations and for the use of viscous liquids. Applications for this technique range from part traceability in quality control to anti-counterfeiting and even decorative engravings. First application tests were carried out in the framework of a CTI feasibility grant³. At that exploratory stage, several potential industrial partners were approached who confirmed their keen interest in the technology. The main results of that exploratory phase showed that the technology can be used in a wide range of applications and markets. Technical alloys, hard metals, or precious metals could be marked successfully showing the potential for applications in fields as diverse as jewelry, medical and aerospace industries, among others.

²International Patent Application WO 2008/010044 A3

³CTI feasibility project N° 8897.1

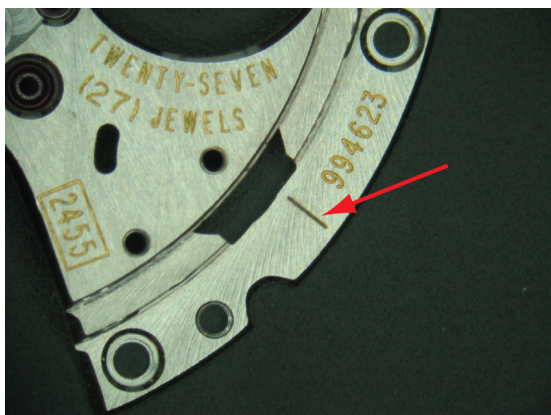


Figure 24: A rhodiated, decorated watch barrel marked with a 70 microns wide tungsten line.

5.2 Watch industry applications

Counterfeiting is a serious threat for the Swiss watch industry. Together with Vacheron Constantin, a prestigious watch manufacturer, we have now started a focused, product-specific project. The non-contact nature of the present marking method makes it extremely attractive for the microscopic marking of finished, delicate watch parts. We have obtained a regular CTI grant⁴ for a project whose main goals are 1) to achieve marks of metallurgical quality compatible with the highest standards of watchmaking and 2) to develop the required peripheral automation technology for batch processing thousands of watch parts.

Finished watch parts bring the additional challenge of the presence of galvanic coatings and decorative structures on the surface (Fig. 24). The main parameters of the marking process, like the spark energies and the servo-control constants for the accurate vertical motion of the tip have been investigated. Dedicated technologies for marking the watch parts have been prepared. Numerical control software has been developed to “write” structured patterns, symbols and logos in 2D (Fig. 25).

The chemical signature is incorporated in the fine engravings as a security feature. Refractory alloys and hard ceramics (nitrides, carbides) can be blended together with other metals and compounds. The former provide robustness to the marks while the latter act as chemical taggants. Also, visually attractive effects can be achieved with macroscopic marks. Continuous paths of “printed” surface alloys have a large potential for decorative applications as well.

⁴CTI project N° 10281.2

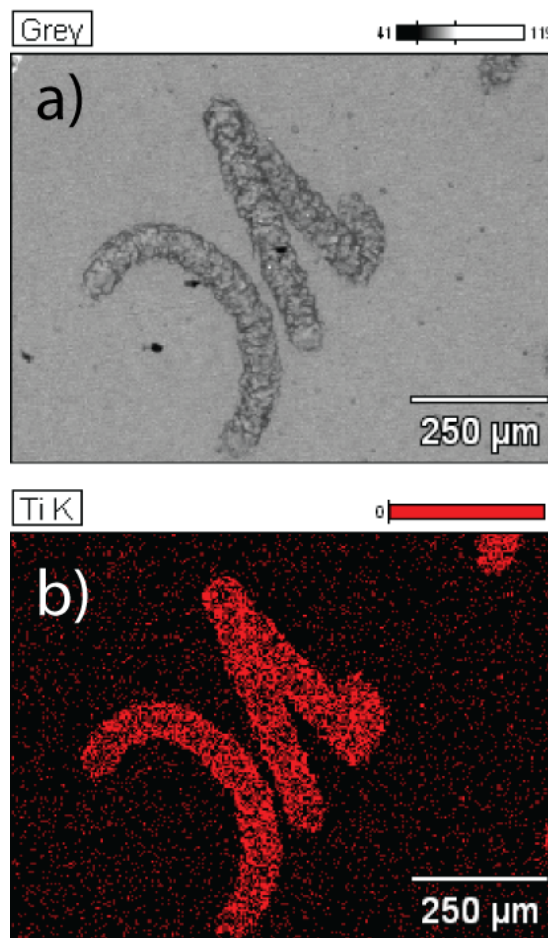


Figure 25: Fine titanium engravings on a stainless steel surface. (a) SEM image, (b) EDX mapping showing the presence of Ti on the marks. The displacement of the tip is software-driven and follows a pre-defined pattern.

5.3 Towards local probe metallurgy

Local alloying is achieved by the interaction of a dense, radiating transient plasma channel with the substrate surface. Encapsulated by the viscous dielectric between the tip and the surface, the spark plasma has a high energy density. Its physical properties (temperature, pressure, mass and composition) can be adjusted by the electronics setup (pulse duration, current level, gap size) and the composition of the dielectric. This configuration provides to the material scientist a flexible setup to synthesize alloys at a “local” scale. Polarity and current pulse shape effects are shown in Fig. 26. By switching the polarity and the current pulse shapes, a dot-matrix symbol has been written using one single composite dielectric. This shows that electronically controlled selective alloying is possible. Moreover, the composition of the dielectric can be tuned to achieve a very large range of mark compositions. This is pos-

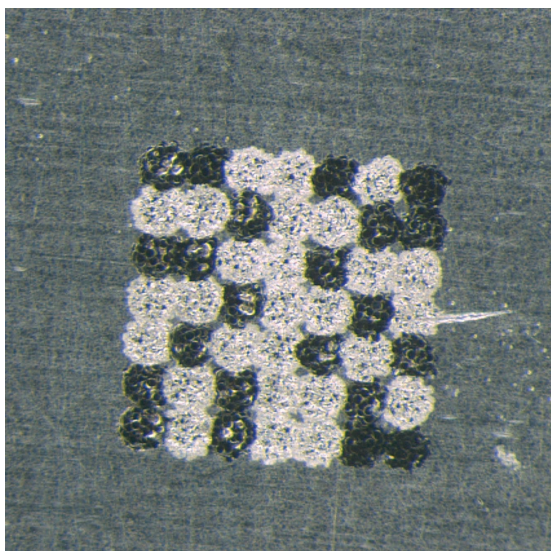


Figure 26: Dot-matrix structure printed on a steel surface. Dark and bright dots have a different metallurgical composition. Identification data is encoded into the 2D symbol of lateral dimensions 1 mm×1 mm.

sible since only very small amounts of metallic impurities are required to dramatically reduce the breakdown strength of the dielectric [21]. This means that a large number of materials, including semiconductors and insulators, can be used as taggants. Also, surface active impurities like S or Te are known to affect surface tension gradients in melt pools [22]. For instance, inward radial flow of the molten metal is suitable to achieve smaller and deeper marks. While smaller marks are suitable for better covertness, deeper marks are more robust against wear and operations like polishing.

Technical blending of precise micro-positioning, high-speed electronics and nano-powder-based metallurgy offers exciting perspectives for surface alloys science and engineering.

6 Collaborative efforts

In view of Phase III we have made a considerable effort to establish collaborations between MaNEP groups and industrial companies as well as between two or more research groups. Within Project 3 the collaborative efforts can be summarized as follows:

Applied superconductivity

Superconducting wires: René Flukiger (UniGE) with Carmine Senatore (UniGE) and Daniel Eckert (Bruker Biospin).

Fault current limiters: Michel Decroux (UniGE) with Markus Abplanalp (ABB).

Oxides for energy harvesting

A close collaboration has been established between Jean-Marc Triscone (UniGE), Nico de Rooij (EPFL) and Gilles Triscone (Hepia-Geneva) to develop silicon membranes and cantilevers with an epitaxial layer of a ferroelectric oxide.

First meetings have taken place between Anke Weidenkaff (Empa and UniBE), Manfred Sigrist (ETHZ) and Jean-Marc Triscone (UniGE) concerning thermoelectricity.

Application of artificial superlattices

The close collaboration between PSI (Michel Kenzelmann) and Swissneutronics (Peter Böni) continues in view of the development of supermirrors for neutron guides.

Hydrogen detectors and other sensors

A close collaboration between Klaus Yvon (UniGE), Øystein Fischer (UniGE), Jorge Cors (UniGE) and Asulab SA to develop hydrogen sensors has been further strengthened this year. Furthermore Greta Patzke (UniZH), Jorge Cors (UniGE) and Phasis continue to develop their collaboration on the use of nano-material for gas sensors.

New surface treatment for microcomponents

A new collaboration has been started this year between Jorge Cors (UniGE), Øystein Fischer (UniGE), J.-M. Triscone (UniGE) and the watch company Vacheron Constantin.

MaNEP-related publications

- ▶ [1] R. Flükiger, M. S. A. Hossain, and C. Senatore, *Superconductor Science & Technology* **22**, 085002 (2009).
- ▶ [2] M. S. A. Hossain, C. Senatore, R. Flükiger, M. A. Rindfleisch, M. J. Tomsic, J. H. Kim, and S. X. Dou, *Superconductor Science & Technology* **22**, 095004 (2009).
- [3] C. Scheuerlein, M. Di Michiel, and F. Buta, *IEEE Transactions on Applied Superconductivity* **19**, 2653 (2009).
- ▶ [4] L. Antognazza, M. Therasse, M. Decroux, F. Roy, B. Dutoit, M. Abplanalp, and Ø. Fischer, *IEEE Transactions on Applied Superconductivity* **19**, 1960 (2009).
- [5] S. Gariglio, N. Stucki, J.-M. Triscone, and G. Triscone, *Applied Physics Letters* **90**, 202905 (2007).
- [6] D. Isarakorn, D. Briand, S. Gariglio, A. Sambri, N. Stucki, J.-M. Triscone, F. Guy, S.-H. Baek, C.-B. Eom, J. W. Reiner, C. H. Ahn, and N. F. de Rooij, in *Proceedings of EUROSENSORS 2008, Dresden, Germany* (2008), p. 819.
- [7] www.swissneutronics.ch.
- [8] C. Schanzer, P. Böni, and M. Schneider, *to be published in Journal of Physics: Conference Series* (2010).
- ▶ [9] Y. Zhou, N. Pienack, W. Bensch, and G. R. Patzke, *Small* **5**, 1978 (2009).
- ▶ [10] Y. Zhou, K. Vuille, A. Heel, and G. R. Patzke, *Zeitschrift für Anorganische und Allgemeine Chemie* **635**, 1848 (2009).

- [11] Y. Zhou, K. Vuille, A. Heel, B. Probst, R. Kontic, and G. R. Patzke, *Applied Catalysis A* **375**, 140 (2010).
- [12] R. Kiebach, N. Pienack, W. Bensch, J.-D. Grunwaldt, A. Michailovski, A. Baiker, T. Fox, Y. Zhou, and G. R. Patzke, *Chemistry of Materials* **20**, 3022 (2008).
- [13] A. C. H. Rowe, A. Donoso-Barrera, C. Renner, and S. Arscott, *Physical Review Letters* **100**, 145501 (2008).
- [14] J. W. Reiner, K. F. Garrity, F. J. Walker, S. Ismail-Beigi, and C. H. Ahn, *Physical Review Letters* **101**, 105503 (2008).
- [15] M. Hino, H. Sunohara, Y. Yoshimura, R. Maruyama, S. Tasaki, H. Yoshino, and Y. Kawabata, *Nuclear Instruments and Methods in Physics Research A* **529**, 54 (2004).
- [16] D. L. Sedin and K. L. Rowlen, *Applied Surface Science* **182**, 40 (2001).
- [17] N. Barsan, D. Koziej, and U. Weimar, *Sensors and Actuators B: Chemical* **121**, 18 (2007).
- [18] O. Hansen, K. Reck, and E. V. Thomsen, *Journal of Applied Physics* **104**, 114510 (2008).
- [19] H. Rongrui and Y. Peidong, *Nature Nanotechnology* **1**, 42 (2006).
- [20] A. C. H. Rowe, *Nature Nanotechnology* **3**, 311 (2008).
- [21] P. D. Beale and P. M. Duxbury, *Physical Review B* **37**, 2785 (1988).
- [22] S. Z. Beer, ed., *Liquid metals, chemistry and physics* (Marcel Dekker, New York, 1972).

Other references

Project 4

Electronic properties of oxide superconductors and related materials

Project leader: D. van der Marel (UniGE)

Participating members: D. Baeriswyl (UniFR), B. Batlogg (ETHZ), L. Degiorgi (ETHZ), Ø. Fischer (UniGE), E. Giannini (UniGE), J. Karpinski (ETHZ), H. Keller (UniZH), M. Kenzelmann (PSI), D. van der Marel (UniGE), J. Mesot (PSI and ETHZ), E. Morenzoni (PSI), C. Niedermayer (PSI), T. M. Rice (ETHZ), M. Sigrist (ETHZ)

Introduction: Superconductivity is the phenomenon of electric current flow without any loss of energy. Indeed, superconducting coils in persistent mode can generate magnetic fields which do not decay on a time scale of the age of the universe or longer. Superconducting electro-magnets large enough to contain an entire human body are routinely used in hospitals for the purpose of scanning NMR. At present no materials are known which exhibit superconductivity at ambient temperatures. In fact, almost all superconducting applications require cooling to liquid helium temperatures. One of the important goals of the research in Project 4 is to understand superconductivity and to develop novel materials exhibiting superconductivity at higher temperatures requiring no cooling with liquid helium. Actually cuprate superconductors can already be used at liquid nitrogen temperature. The strong progress in the microscopic understanding of high- T_c superconductivity obtained in the context of MaNEP invites us to reach toward novel superconducting materials with strongly improved properties.

Summary and highlights

Strong progress has been made in the microscopic theory of the electronic structure and phase diagram of the cuprates. The Yang-Rice-Zhang (YRZ) phenomenological ansatz [1] for the single-particle propagator is evolving into a useful theoretical formulation that can be used to integrate the anomalous results from a wide range of experiments into a consistent description of the pseudogap phase of underdoped cuprates. It explains the anomalous Fermi surfaces seen in angle resolved photoemission (ARPES) from underdoped with its apparent Fermi arcs to a full Fermi surface for overdoped samples. In the past year this ansatz has been demonstrated to also explain recent STM experiments on the Fermi arcs underlying the coherent Bogoliubov quasi-particle spectrum and many features of the checkerboard patterns seen with STM [2]. The YRZ model was furthermore shown to predict the particle-hole asymmetry in underdoped samples as one moves along the Fermi arc away from the nodal direction observed by ARPES, and angle integrated photoelectron spectra on underdoped cuprates, confirming that the hole density of states is described by doping a valence band with a Dirac spectrum at its maximum [3]. Based on the variational ansatz by Baeriswyl [4], a coherent picture of the superconducting phase diagram as a function of carrier concentration is emerging for the repulsive

Hubbard model in two dimensions.

ARPES was used to investigate electronic excitations in various hole-doped cuprates. The results on underdoped $\text{La}_{2-x}\text{Sr}_x\text{CuO}_4$ (LSCO) reveal that in the pseudogap phase, the dispersion has two branches located above and below the Fermi level with a minimum at the underlying k_F [5, 6]. This is the characteristic of the Bogoliubov dispersion in the superconducting state. ARPES of $\text{Bi}_2\text{Sr}_2\text{CaCu}_2\text{O}_{8-\delta}$ (Bi-2212) displayed a smooth evolution of the excitation spectrum, along with the appearance of coherent quasi-particles, as one goes through the insulator-to-superconductor transition as a function of doping [7]. Inelastic neutron-scattering experiments on the high-temperature superconductor $\text{La}_{1.855}\text{Sr}_{0.145}\text{CuO}_4$ reveal a magnetic excitation gap that decreases continuously upon application of a magnetic field perpendicular to the CuO_2 planes. The gap vanishes at the critical field required to induce long-range incommensurate antiferromagnetic order, providing compelling evidence for a field-induced soft-mode driven quantum phase transition [8]. In Bi-2201 doping dependent STM measurements show the unambiguous signature of the Van Hove singularity (VHS). The VHS approaches – and even crosses – the Fermi energy as doping increases progressively from underdoped to strongly overdoped [9].

Optical spectra and ARPES of electron doped

SrTiO₃ show the manifestation of moderate electron-phonon interaction, as revealed by mid-infrared features and a moderate (factor ~ 2) mass enhancement, and is shown to agree quantitatively with the many-body large-polaron theory of Devreese [10]. In pyrochlores, the phonon density of states extracted from the spectra of K-based and Rb-based compounds using STM reveal low-energy modes which may account for the surprisingly high surface T_c observed in the STS measurements

In the past year a concentrated effort has been made within Project 4 on the so-called “11” family of Fe-based chalcogenides FeCh ($Ch = Te, Se, S$). It represents the simplest system for investigating the interplay between superconductivity and magnetism in the class of Fe-based superconductors with the PbO-based crystal structure. By reducing the Fe excess and increasing the Se substitution for Te in Fe_{1+x}Te_{1-y}Se_y crystals, the antiferromagnetic order is modified, the spin localization is weakened, and a superconducting ground state is favored over a wide range of compositions ($y > 0.1$) [11]. Using magnetic susceptibility, muon-spin rotation (μ SR) and neutron diffraction, three regimes of behavior are found: (i) commensurate magnetic order for $x \leq 0.1$, (ii) bulk superconductivity for $x \sim 0.5$, and (iii) a range $x \approx 0.25 - 0.45$ in which superconductivity coexists with incommensurate magnetic order [12]. In the Fe-Se system, a stable phase exhibiting superconductivity at $T_c \simeq 8$ K was discovered in a narrow range of selenium concentration (FeSe_{0.974±0.005}) [13]. At a pressure $\simeq 0.8$ GPa the non-magnetic and superconducting FeSe_{1-x} enters a region where static magnetic order is realized above T_c , and bulk superconductivity coexists and competes on short length scales with the magnetic order below T_c . For even higher pressures an enhancement of both the magnetic and the superconducting transition temperatures as well as

of the corresponding order parameters is observed. For FeTe the RIXS spectra exhibit edge-singularity behavior predicted for metals by Nozières and Abrahams, and reported experimentally for the first time [14].

Two new superconductors with crystal structure similar to the iron-pnictide high- T_c materials have been discovered: (i) BiOCuS with $T_c = 5.8$ K when hole-doped by introducing Cu-vacancies [15], and (ii) RbFe₂As₂ with $T_c = 2.6$ K [16].

Superconductivity in SmFeAsO has been generated by Th and P substitution for Sm and As respectively. A new NaAs flux has been used successfully for SmFeAsO single-crystal growth. Large superconducting single-crystals of CaFe_{2-x}Co_xAs₂ and EuFe_{2-x}Co_xAs₂ have been grown. The transport properties of SmFeAsO_{0.7}F_{0.25} single-crystals were found to reveal a promising combination of high ($> 2 \cdot 10^6$ A/cm²) and nearly isotropic critical current densities along all crystal directions. The pinning forces have been characterized by scaling the magnetically measured peak effect of j_c . Muon-spin rotation of SmFeAsO_{1-x}F_x shows that static magnetism persists well into the superconducting regime [17].

The spin-density wave (SDW) metal BaFe₂As₂ has a depletion in the far-infrared energy interval of the optical conductivity below T_{SDW} , ascribed to the formation of a pseudogap-like feature in the excitation spectrum. This is accompanied by the narrowing of the Drude term consistent with the dc transport results and suggestive of suppression of scattering channels in the SDW state [18]. Infrared spectra of optimally doped BaFe_{2-x}Co_xAs₂ reveal two superconducting gaps, $2\Delta = 6.2$ meV and $2\Delta = 14$ meV [19]. Further support for the two-gap scenario for Fe-based superconductors is obtained by employing the complementarity of μ SR and ARPES in superconducting Ba_{1-x}K_xFe₂As₂ ($T_c \simeq 32$ K) [20].

1 Microscopic properties of the cuprates

1.1 Checkerboard pattern in underdoped cuprate superconductors (*T. M. Rice and M. Sigrist*)

Understanding the anomalous properties of the pseudogapped phase of underdoped cuprate high-temperature superconductors has long been considered a key to constructing a microscopic theory for these materials. Several years back Yang, Rice and Zhang (YRZ) proposed a phenomenological ansatz for the single-particle propagator based on the

resonant valence bond (RVB) model. The goal was to combine the insights from earlier functional renormalization group calculations at weak to moderate coupling and renormalized mean field theories of a RVB description of strong coupling, into a tractable form for the propagator. At that time they showed how this YRZ form for the propagator gave a very good description of the evolution of the anomalous Fermi surfaces seen in angle resolved photoemission (ARPES), from underdoped with its

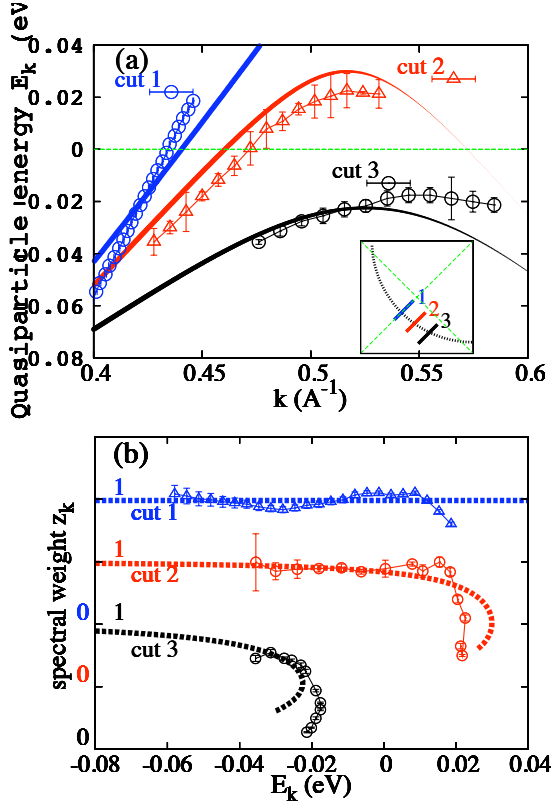


Figure 1: Comparisons between (a) Quasi-particle dispersion E_k , (b) spectral weight z_k , from the YRZ propagator, and the values obtained from the ARPES results. Error bars reflect the uncertainties in the fitting procedures; z_k at low energies in cuts 2 and 3 have large error bars due to uncertainties in the choice of the rising background.

apparent Fermi arcs to a full Fermi surface at overdoped. Since then more detailed ARPES results have emerged. We could show that the particle-hole asymmetry observed by the ARPES group at Brookhaven [40] in underdoped samples as one moves along the Fermi arc away from the nodal direction, which is unexpected in simple pairing scenarios, fits nicely with the YRZ form [3]. A separate set of angle integrated spectra on underdoped cuprates is also fitted nicely by the YRZ form and confirms that the hole density of states is described by doping a valence band with a Dirac spectrum at its maximum (Fig. 1).

More recently we have put a great deal of effort into a careful analysis of the scanning tunneling microscopy (STM) results by the Seamus Davis group [41]. Their results, which find Fermi arcs underlying the coherent Bogoliubov quasi-particle spectrum which ends at the diamond connecting the antinodal points, fit nicely to the YRZ propagator. However the higher voltage STM spectra, which probe the localized states near anti-

nodal, are harder to interpret. We spent considerable effort trying to determine the conditions in these highly disordered underdoped $\text{Bi}_2\text{Sr}_2\text{CaCu}_2\text{O}_{8-\delta}$ (Bi-2212) samples that lead to a locally prominent checkerboard pattern which breaks the square C_4 -symmetry, but without convincing success [2]. So, while we could explain many features of these STM patterns, which have attracted so much attention, there are still some important questions unresolved about the correct interpretation of these STM results. The YRZ phenomenology is used also to interpret the strong local fluctuations in the magnitude of the antinodal energy gap in underdoped Bi-2212 as a consequence of a spatially varying hole density in this compound which is randomly doped with acceptors.

The YRZ form conforms to the widely discussed two-gap description of the underdoped cuprates which distinguishes the antinodal and superconducting energy gaps. Carbotte, Nicol and coworkers in a series of papers have used the YRZ ansatz to successfully analyze the doping and temperature dependence of many basic properties of the pseudogap phase, i.e. specific heat, London penetration depth, infrared conductivity and Raman scattering spectra [42]. The YRZ ansatz is evolving into a useful theoretical formulation that can be used to integrate the anomalous results from a wide range of experiments into a consistent description of the pseudogap phase of underdoped cuprates.

1.2 Superconductivity in the repulsive Hubbard model (D. Baeriswyl)

The question of superconductivity out of purely repulsive interactions remains an interesting, heavily debated issue. The PhD thesis of David Eichenberger has produced detailed variational results for the ground state of the repulsive two-dimensional Hubbard model [21, 22]. More recently, the comparison of our results with those of other studies gave a rather coherent picture [4]. Fig. 2 shows the d -wave order parameter for the simple Hubbard model (only hopping t to nearest neighbors), as obtained with four different methods. The early calculations by Giamarchi and Lhuillier [43] and more recent results by Paramekanti *et al.* [44] appear to predict superconductivity in a very large doping range, but both results should be taken with caution for $x > 0.2$. In fact, in [43] the correlation length exceeds the system size in this range, while the data of [44] have been obtained for the t - J Hamiltonian, which can be used at most close to half filling,

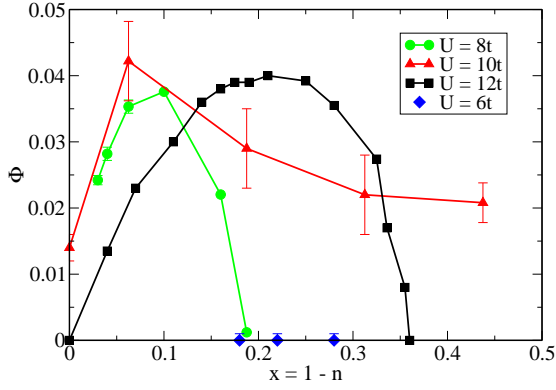


Figure 2: Comparison of superconducting order parameters for the simple Hubbard model. Black squares: Paramakanti, red triangles: Giamarchi, green circles: Eichenberger, blue diamonds: Aimi and Imada.

say, for $x < 0.2$ (and for very large U). Our own results, which predict superconductivity only below a doping of about 18%, agree with the finite-size analysis of Aimi and Imada [45], who did not find superconductivity above 18% (but did not provide a corresponding analysis for smaller dopings). In the more realistic case, where hopping to next-nearest neighbors is included, our variational results agree very nicely with quantum cluster calculations and also with the experimental values for the critical dopant concentrations, both for electron and hole doping [4].

1.3 Ground state fidelity for the reduced BCS Hamiltonian (*D. Baeriswyl*)

The PhD thesis of Bruno Gut was concerned with crossover problems in many-body systems. It turned out that the ground state fidelity, a quantity used frequently for characterizing quantum phase transitions, does also provide a valid criterion for a crossover, as exemplified for superconductivity as a function of system size and/or coupling strength. Consider a Hamiltonian $H(\lambda)$, where λ is some parameter, such as $|U|/t$ in the attractive Hubbard model. The ground state fidelity is defined as

$$F = \langle \Psi_0(\lambda) | \Psi_0(\lambda + d\lambda) \rangle, \quad (2.1)$$

where $|\Psi_0(\lambda)\rangle$ is the ground state of $H(\lambda)$. For $d\lambda \rightarrow 0$, F can be expressed as

$$F^2 = 1 - \chi_F(d\lambda)^2, \quad (2.2)$$

where χ_F is referred to as fidelity susceptibility. We have considered the reduced BCS Hamiltonian

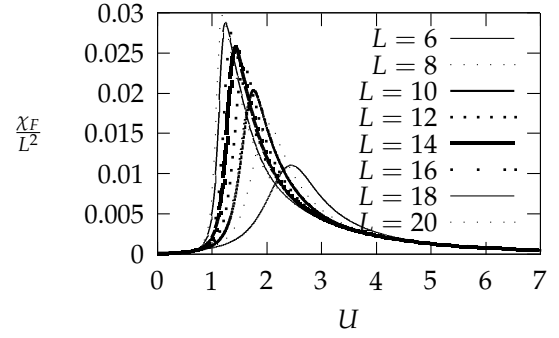


Figure 3: Fidelity susceptibility per site for the half-filled reduced BCS Hamiltonian on the square lattice for the following system sizes, starting from the lowest peak upwards: $L = 6$, $L = 8$, $L = 10$, $L = 12$, $L = 14$, $L = 16$, $L = 18$ and $L = 20$.

of the attractive Hubbard model,

$$H = \sum_{\mathbf{k}\sigma} \varepsilon_{\mathbf{k}} n_{\mathbf{k}\sigma} - \frac{|U|}{L^2} \sum_{\mathbf{k}, \mathbf{k}'} b_{\mathbf{k}}^\dagger b_{\mathbf{k}'}, \quad (2.3)$$

where $n_{\mathbf{k}\sigma} = c_{\mathbf{k}\sigma}^\dagger c_{\mathbf{k}\sigma}$ is the occupation number and $b_{\mathbf{k}}^\dagger = c_{\mathbf{k}\uparrow}^\dagger c_{-\mathbf{k}\downarrow}^\dagger$ creates a pair of electrons with momentum zero. This model is soluble thanks to Richardson's solution of a related BCS model [46]. We have calculated χ_F for a square lattice of size $L \times L$ for various values of L . The results of Fig. 3, obtained with a tight-binding spectrum $\varepsilon_{\mathbf{k}}$ at half filling, exhibit a pronounced peak, which shifts slowly to smaller values of $|U|$ with increasing system size and at the same time becomes sharper. It is tempting to identify the location of the peak with the onset of superconductivity for small L and with the BCS-BEC crossover at large L . A paper on these results is in preparation.

1.4 Evidence for preformed Cooper pairs in the pseudogap phase of cuprates (*J. Mesot*)

What is the relationship between the pseudogap and the superconducting gap in the underdoped cuprates is still shrouded in mystery. Using ARPES we have performed a systematic study of electronic excitations in the pseudogap phase of moderately underdoped $\text{La}_{2-x}\text{Sr}_x\text{CuO}_4$ (LSCO) [5, 6]. Our main experimental findings are: 1) beyond the gapless Fermi arc, the pseudogap above T_c has the same simple d -wave form as the superconducting gap below T_c , 2) above T_c there exists a Bogoliubov-like dispersion near the underlying k_F where the spectra are gapped (Fig. 4), and 3) the same underlying Fermi surface was obtained both in the superconducting state and in the pseudogap phase. The

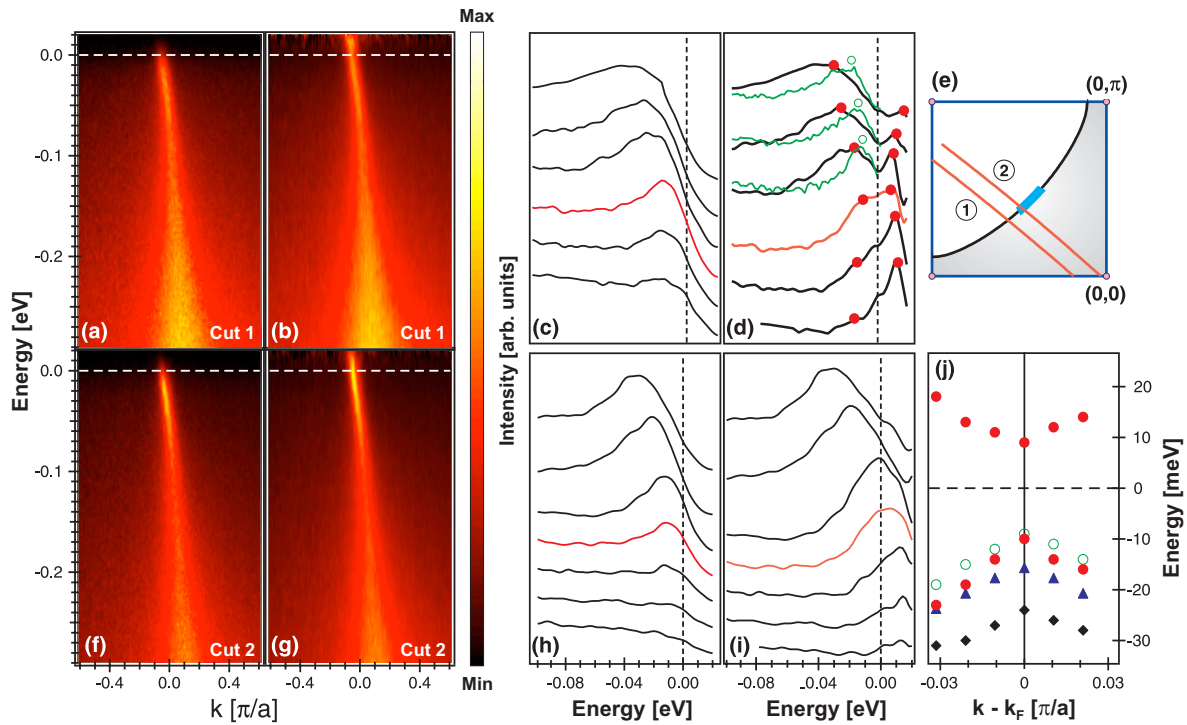


Figure 4: ARPES spectra for underdoped LSCO ($T_c = 30$ K) at 49 K. (a)–(d) The spectra along cut 1 in (e). (a) The intensity, (b) the intensity divided by Fermi function, (c) the spectra in the vicinity of k_F , and (d) the Fermi function divided spectra. The thick and thin lines in (d) are spectra at 49 K and 12 K, respectively. (e) Fermi surface; the thick line centered at the node indicates the gapless Fermi arc. (f)–(i) Same as (a)–(d), but the spectra are along cut 2 in (e). (j) The dispersions in the gapped region of the zone obtained from the Fermi function divided spectra. The pair of closed circles are the two branches of the dispersion derived from (d) at 49 K.

similarity between the Bogoliubov-like dispersion in the pseudogap phase of underdoped LSCO and the dispersion of Bogoliubov quasiparticles in the superconducting state of heavily overdoped Bi-2212 provides direct evidence that the pseudogap in underdoped cuprates arises from pairing of electrons, and thus the pseudogap phase is a state precursor to superconductivity [5].

1.5 Observation of a d -wave nodal liquid in highly underdoped Bi-2212 (*J. Mesot*)

A key question in condensed matter physics is to understand how high-temperature superconductivity emerges on adding mobile charged carriers to an antiferromagnetic Mott-insulator. We address this question using ARPES to probe the electronic excitations of the non-superconducting state that exists between the Mott-insulator and the d -wave superconductor in $\text{Bi}_2\text{Sr}_2\text{CaCu}_2\text{O}_{8-\delta}$. We observe that the sharp quasi-particles of the superconducting state exist down to the lowest doping levels while rapidly losing spectral weight (Fig. 5), but are no longer visible on the insulating side. Nonetheless, a low-energy d -wave like gap survives the phase-disordering transi-

tion. The simplest picture consistent with our data is that the nodal liquid is just a phase-incoherent version of the d -wave superconductor, and adding charged carriers to this liquid establishes phase coherence, leading to high- T_c superconductivity [7].

1.6 The Ortho II band folding in Y123 films (*J. Mesot*)

By combining two well established experimental techniques, pulsed laser deposition (PLD) and ARPES, we have been able for the first time to grow and study the electronic structure of the Ortho II ordered surface of $\text{YBa}_2\text{Cu}_3\text{O}_{7-\delta}$ films without any sample cleaving. Through a careful control of the growth, we successfully produced underdoped surfaces with ordered oxygen vacancies within the CuO chains. The resulting Fermi surface displays a clear Ortho II band folding (Fig. 6), in good agreement with theoretical predictions/calculations, but in contradiction to previous ARPES results from the potassium treated surface. This clearly highlights the importance of having not only the correct carrier-concentration, but also a very well ordered and clean surface to facilitate ARPES data representative of the com-

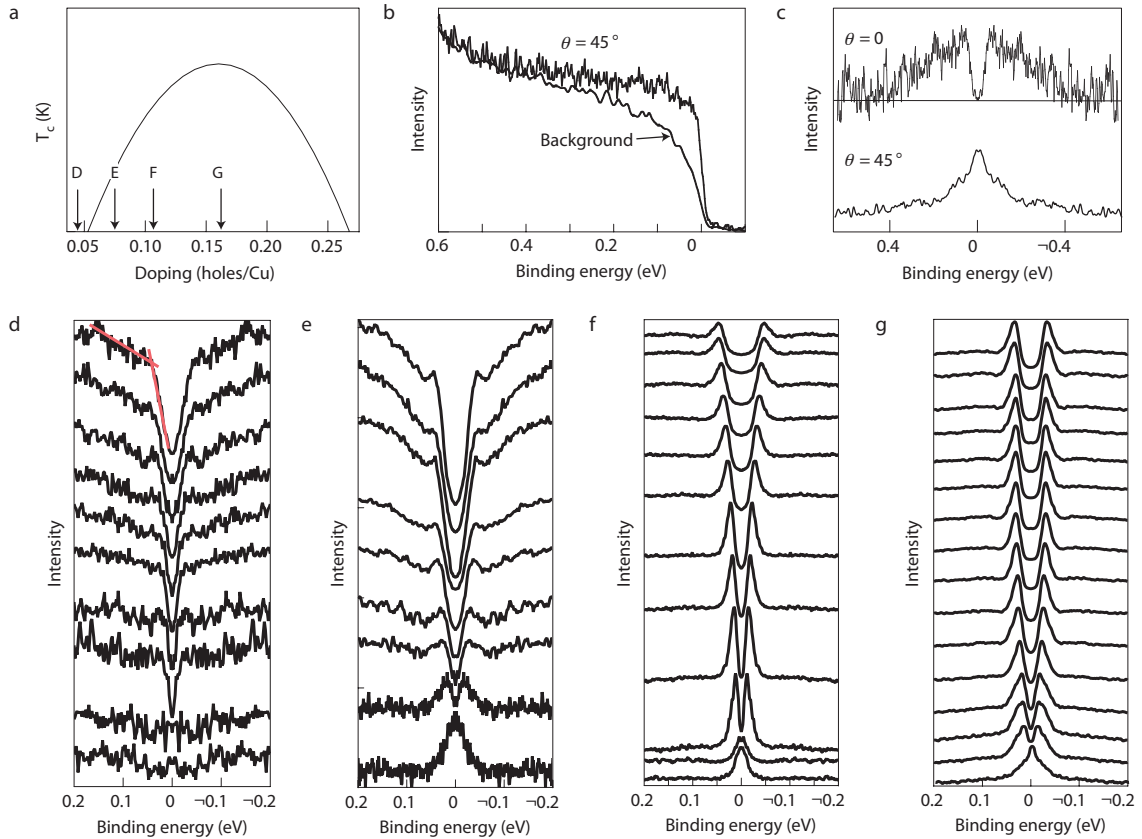


Figure 5: Spectral function versus doping for Bi-2212. (a) Doping levels of four samples for which spectra are plotted in (d)–(g). (b) Insulator nodal spectrum and background (D in (a)) at $T = 16$ K. (c) Background-subtracted, symmetrized intensity for sample D, showing a gap at the antinode and zero gap at the node. (d)–(g) Symmetrized energy distribution curves for an insulating film at $T = 16$ K (d), a $T_c = 33$ K film at $T = 16$ K (e), a $T_c = 69$ K crystal (f) and a $T_c = 80$ K film at $T = 40$ K (g); the spectra are plotted from the antinode (top) to the node (bottom). The intersection of the red lines in (d) defines the gap in the insulator.

pound’s true nature [23]. We emphasize that it is difficult to obtain a very well ordered surface by cleaving a single-crystal of YBCO cuprates [24], because their crystal structures lack natural cleavage plane.

1.7 Magnetic field induced soft-mode quantum phase transition in the high-temperature superconductor $\text{La}_{1.855}\text{Sr}_{0.145}\text{CuO}_4$ (C. Niedermayer)

We performed an inelastic neutron scattering study of the low-energy spin fluctuations in slightly underdoped $\text{La}_{1.855}\text{Sr}_{0.145}\text{CuO}_4$, which in the absence of a magnetic field is a homogeneous, magnetically disordered superconductor with an excitation gap. The gap decreases on approaching a field-induced transition to a magnetically ordered state, that coexists with superconductivity, and vanishes at the point where spin-density wave (SDW) order sets in (Fig. 7) [8]. These observations follow the expectations for a continuous soft-mode driven quantum phase transition [47] and suggest the

existence of a line of such transitions in the doping-field phase diagram of $\text{La}_{2-x}\text{Sr}_x\text{CuO}_4$.

Closure of the excitation gap appears to be a universal phenomenon in cuprates hosting quantum phases in which superconductivity can coexist with magnetic order. In $\text{YBa}_2\text{Cu}_3\text{O}_{6+p}$, the gap collapses abruptly for $p \sim 0.5$ [48], and a robust superconducting phase with incommensurate, quasi-static fluctuations (an electronic nematic) emerges at lower doping levels ($\text{YBa}_2\text{Cu}_3\text{O}_{6.45}$) [25]. Static incommensurate magnetic order develops at even lower temperatures. Application of a magnetic field strongly enhances this order and induces a spectral-weight shift in the magnetic-excitation spectrum [26].

Further work is needed to clarify precisely how the closure of an excitation gap and appearance of incommensurate magnetic order relate to the reconstruction of the Fermi surface into small pockets as revealed by recent quantum oscillation experiments in $\text{YBa}_2\text{Cu}_3\text{O}_{6+p}$ with $p \sim 0.5$ [49].

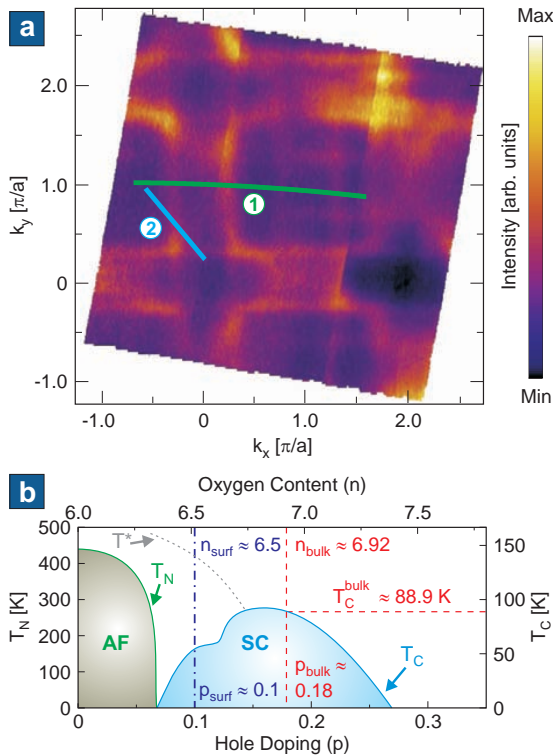


Figure 6: (a) Fermi surface of $\text{YBa}_2\text{Cu}_3\text{O}_{6.5}$, obtained by energy integration of ARPES spectra over a 35 meV window about E_F . (b) Phase diagram of $\text{YBa}_2\text{Cu}_3\text{O}_{7-\delta}$ as function of hole doping and oxygen content. The doping level p_{surf} was extracted from the Fermi surface volume.

1.8 First direct observation of the Van Hove singularity in the tunneling spectra of cuprate (Ø. Fischer)

In two-dimensional lattices the electronic levels are unevenly spaced and the density of states (DOS) displays a logarithmic divergence known as the Van Hove singularity (VHS) [50]. This issue is particularly relevant in the study of high-temperature cuprate superconductors. The scanning tunneling microscope (STM) probes the DOS and is therefore the ideal tool to observe the VHS. However no STM study of cuprate superconductors has reported such an observation. A popular interpretation is that the DOS is canceled in the tunneling spectra just as in ideal planar tunnel junctions. An alternative is that the VHS peak is suppressed due to the interaction of electrons with collective excitations. One then expects to recover the VHS peak on reducing the coupling to collective modes, i.e. on reducing the critical temperature (T_c). Among the cuprates, $\text{Bi}_2\text{Sr}_2\text{CuO}_{6+\delta}$ (Bi-2201) combines several properties required for an optimal scanning tunneling spectroscopy (STS) investigation of the VHS: it is nearly two-

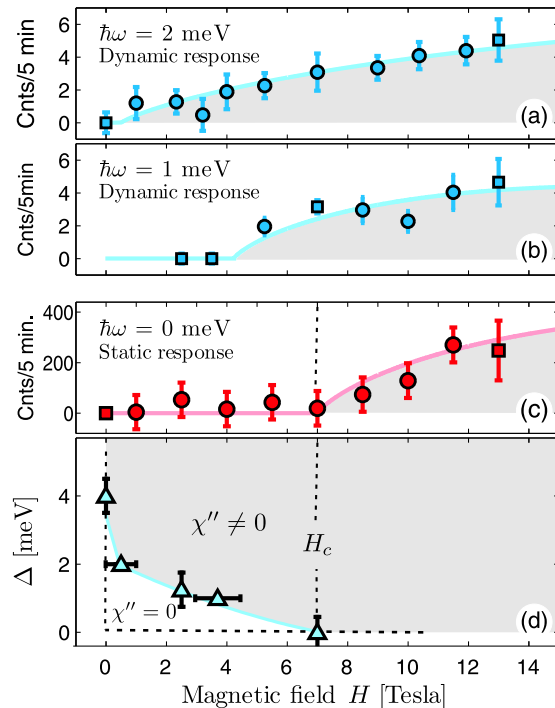


Figure 7: (a) and (b) Magnetic field dependence of the inelastic neutron response at $Q_{IC} = (0.63, 0.5, 0)$ with $\hbar\omega = 2$ and 1 meV, respectively. (c) Elastic neutron response at Q_{IC} as a function magnetic field. (d) Field dependence of the excitation gap Δ . The gap is extremely sensitive to the application of a magnetic field: following an initial dramatic drop, Δ subsequently softens more slowly and finally vanishes at the critical field $H_c \ll H_{c2}$ which marks the onset of long range incommensurate magnetic order.

dimensional and has a low maximal T_c of around 12 K [27] giving access to the normal state at low temperature. Our doping dependent STM measurements on this compound show unambiguously and for the first time in a cuprate the VHS [9].

As seen in Fig. 8(a) some of the spectra obtained in Bi-2201 only show a single and high peak at negative energies. We attribute this feature to the VHS. Other spectra are gapped, suggesting an interplay of the VHS with superconductivity. Fig. 8(b) shows how the spectra are distributed over the sample surface. The differences between the spectra are due to variations of the local doping level. This is supported by the fact that in extremely overdoped samples it is possible to obtain single peaked spectra at positive energy such as seen in Fig. 8(c). As it was previously done in parental Bi-based superconducting cuprates [28, 29, 30], we have performed accurate fits to the experimental spectra obtained in Bi-2201 (Fig. 8(d)). This has confirmed our interpretation of the tunneling

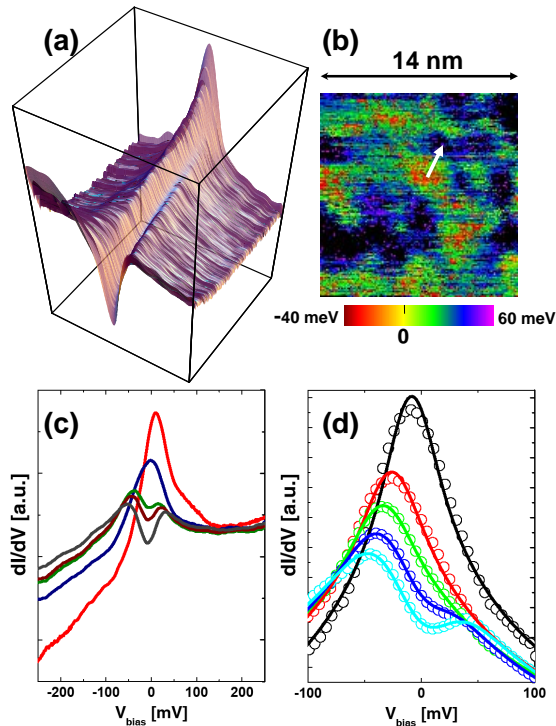


Figure 8: Low-temperature STS of Bi-2201 ($T_c = 11$ K). (a) Evolution of the tunneling spectra along the white arrow drawn on figure (b) which is a 14×14 nm² map of the gap value (positive) and the VHS position (negative). (c) Spectra of a strongly overdoped sample ($T_c < 1.8$ K) showing a VHS at positive energy (red). (d) dI/dV experimental curves (circles) and fits based on a VHS + BCS model (lines).

spectra as being the result of an interplay between a d -wave superconducting gap, a realistic band structure exhibiting a strong VHS, and a coupling of the electrons with collective excitations. Our study proves that the STM tunneling conductance is proportional to the full electron DOS, not only the superconducting DOS. This must be taken seriously for the interpretation of tunneling spectra in materials with singularities in the electron dispersion.

1.9 Modelling the tunneling spectra of Y-123 single-crystals (Ø. Fischer)

In striking similarity with Bi-based compounds, tunneling spectra of YBa₂Cu₃O₇ (Y-123) single-crystals systematically reveal the presence of a “dip-hump” feature. We showed in previous studies [28, 29, 30] that this spectroscopic feature can be identified as the signature of the collective bosonic mode revealed by neutron scattering experiments [51, 52, 53]. For Y-123 as well, this mode is locally anticorrelated with the superconducting gap (Fig. 9a and b). On the other hand the tunneling spec-

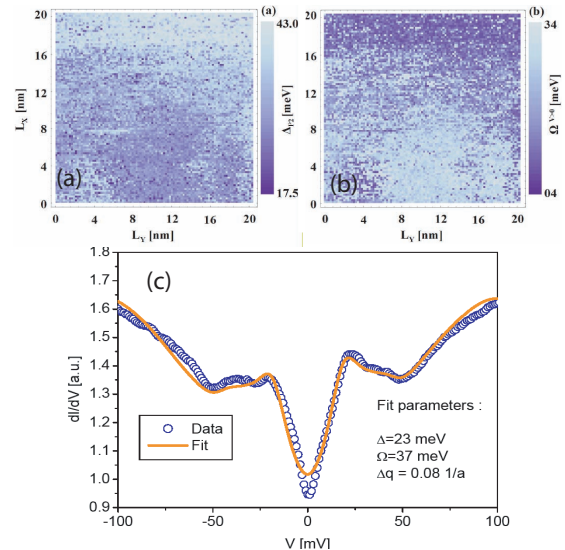


Figure 9: 20×20 nm² spectroscopic maps of the local superconducting gap (a) and the mode energy (b). (c) Experimental tunneling spectrum (blue) and calculated spectrum fitted using a strong coupling model (orange).

tra of Y-123 reveal a number of differences compared to those measured on Bi-2212 with similar T_c : the zero-bias conductance is always high and the conductance at high bias is strongly energy-dependent; the main coherence peaks define a gap of ~ 20 meV, much closer to the value expected for a BCS d -wave superconductor than the gap observed in the Bi-based cuprates; weak shoulders flank the main peaks at higher energy. This multiple peak structure does not correspond to the simple d -wave expectation. We followed the procedure applied to fit the tunneling spectra of Bi-based cuprates, using the strong-coupling model taking into account the two-dimensional band structure of the Cu-O planes and an interaction of the quasi-particles with the (π, π) spin resonance [54]. The mode energies obtained by fitting the tunneling spectra are in excellent agreement with the ones obtained in neutron scattering measurements [52]. In addition, most of the measured spectroscopic features are well reproduced in the calculated spectra (Fig. 9c). The symmetry of conductance features observed at positive and negative energies is obtained by taking into account the bilayer splitting of the bands, with two Van Hove singularities positioned slightly above and below the Fermi level. It clearly appears that the shoulder flanking the coherence peak is the signature of the spectral weight redistribution (hump), and hence a consequence of the collective mode excitation. The high-conductance at low bias as well as the strong energy de-

pendence of the tunneling conductance at high bias cannot be reproduced without considering additional contributions in the tunneling conductance. The fits can be considerably improved when a normal energy-dependent tunneling channel is introduced in parallel with the superconducting channel. Such an analysis is currently under progress.

1.10 Doping study of bosonic mode energy in $\text{Bi}_2\text{Sr}_2\text{Ca}_2\text{Cu}_3\text{O}_{10+\delta}$ by scanning tunneling spectroscopy (\emptyset . Fischer)

We report on a STM study of the three-layer compound $\text{Bi}_2\text{Sr}_2\text{Ca}_2\text{Cu}_3\text{O}_{10+\delta}$ (Bi-2223). We have recently shown that the energy of the collective mode, Ω , can be approximated by the difference in energy between the negative bias coherence peak and the minimum of the well-known dip structure [30]. We further showed that for a nearly-optimally doped sample, Ω decreases as Δ increases. We now have furthered these results by performing a doping dependence study of Ω . Three separate samples with different doping levels (underdoped, optimally doped, and overdoped) were investigated. The evolution of the mode energy with Δ is remarkably similar for the three samples (Fig. 10). The trend of Ω decreasing with increasing Δ clearly holds true in the underdoped regime. However the same cannot be said on the overdoped side, since Ω is seen to saturate at around 36 meV for gap sizes under 40 meV.

We suggest [30], as have others before us [54], that the bosonic mode used in the strong-coupling model to explain the dip structure in the tunneling spectra is the magnetic resonance seen by neutrons [55]. In the underdoped regime, since Ω decreases with increasing gap size, our data agree with neutron scattering experiments [56] which report a scaling of the mode energy with T_c . According to the neutron data, this scaling with T_c remains valid also in the overdoped regime (although very

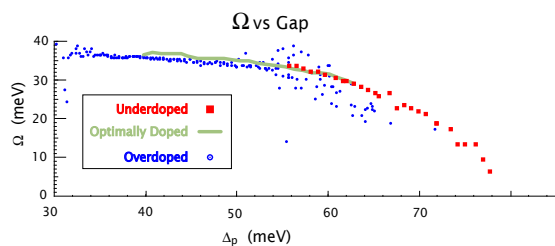


Figure 10: Ω vs Δ for three samples with different dopings, showing a clear saturation of Ω in the overdoped regime (small Δ).

few measurements were done in this regime). This is in contradiction with the evident saturation of the mode energy we observe at low doping levels by STS. ARPES measurements did not see a decrease in Ω when going towards overdoping, although from the data it is difficult to say that Ω saturates [57]. However superconductor-insulator-superconductor tunneling data suggests the contrary, that Ω scales with T_c across all dopings [58]. It should be noted that the measurements from [58] are not on the same material (Bi-2212 vs Bi-2223 in our measurements). Further inelastic neutron scattering studies are nonetheless necessary to clarify this issue.

2 Electron-phonon coupling in transition metal oxides

2.1 Many-body large polaron optical conductivity in $\text{SrTi}_{1-x}\text{Nb}_x\text{O}_3$ (*D. van der Marel*)

Insulating SrTiO_3 has a perovskite structure and manifests a metal-insulator transition at room temperature around a doping of 0.002% La or Nb per unit cell [59]. At low doping concentrations, between 0.003% and 3%, strontium titanate reveals a superconducting phase transition [60] below 0.7 K. Various optical experiments [61, 59, 62, 63, 64] show a mid-infrared band in the normal state optical conductivity of doped SrTiO_3 which is often explained by polaronic behavior. In the recently observed optical conductivity spectra of [31], shown in Fig. 11, there is a broad mid-infrared optical conductivity band starting at a photon energy of $\hbar\Omega \sim 100$ meV, which is within the range of the phonon energies of $\text{SrTi}_{1-x}\text{Nb}_x\text{O}_3$. A recent ARPES study (collaboration of the uni-

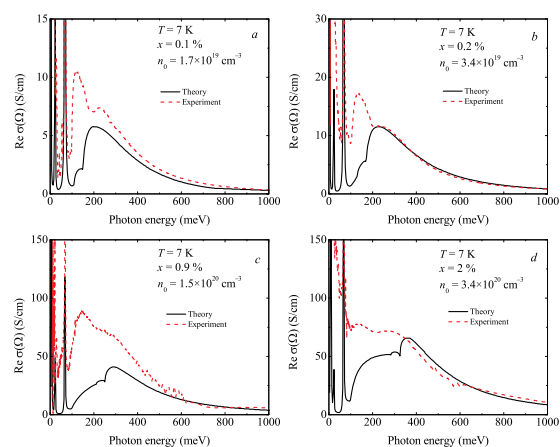


Figure 11: The many-large-polaron optical conductivity compared with the experiment at $T = 7$ K. The doping level is $x = 0.1\%$ (a), 0.2% (b), 0.9% (c) and 2% (d).

versities of Stanford and Geneva) from high-quality surfaces of lightly doped SrTiO₃ reveals the signatures of only moderate electron-phonon coupling: a dispersion anomaly associated with the low-frequency optical phonon with a $\lambda' \sim 0.3$ and an overall bandwidth renormalization suggesting an overall $\lambda' \sim 0.7$ coming from the higher frequency phonons [32].

In collaboration with J. Devreese (University of Antwerpen), the many-body large-polaron model based on the Fröhlich model is applied to electron doped SrTiO₃ [10]. This model provides a fair agreement between the theoretical large-polaron optical conductivity band and the experimental mid-infrared optical conductivity band *without any adjustment of material parameters*. In the Fröhlich model, the constant α_j , characterizing the interaction of an electron with the j -th optical vibrational mode, follows directly from the experimentally known optical phonon frequencies and oscillator strengths of SrTiO₃ [65]. The value of the effective electron-phonon coupling constant obtained in the present work corresponds to electron-phonon coupling of intermediate/weak strength. The anisotropy of the electronic effective mass of about 25 is taken into account, as well as the triple degeneracy of the Ti t_{2g} conduction bands. The large-polaron model then provides a convincing interpretation of the experimentally observed mid-infrared band of SrTi_{1-x}Nb_xO₃. Significant advances of many-polaron theory are testified by the correct prediction of the amplitude and position along the energy axis of the mid-infrared peak of SrTiO₃, without any adjustable parameters.

2.2 Analysis of the electron-phonon coupling from the tunneling spectra of RbOs₂O₆ and KOs₂O₆ (Ø. Fischer)

Tunneling conductance spectra on RbOs₂O₆ single-crystals (T_c of 5.5 K) reveal a clear signature of a superconducting gap of the order of 1 meV, which yields a $2\Delta/kT_c$ of 3, close to the s -wave BCS ratio. Strikingly, temperature dependent spectroscopy revealed that the gap remains open up to 7.4 K, 2 K above the bulk T_c . The tunneling spectra of both β -pyrochlore compounds investigated show the presence of a dip at an energy approximately 2.4 meV above that of the coherence peak. Such dips are characteristic signatures of the coupling of quasi-particles with collective mode excitations [33]. Using an inversion procedure, we extracted the so-called Eliashberg coupling

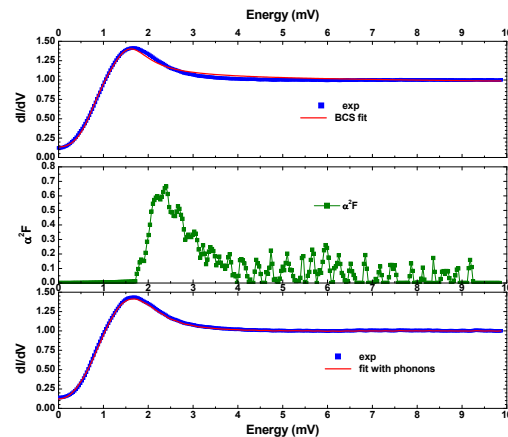


Figure 12: Spectrum and α^2F for KOs₂O₆. Top: experimental spectrum (blue dots), and BCS s -wave fit (red line). Middle: $\alpha^2F(\omega)$ extracted from the spectrum. Bottom: reconstructed spectra including the phonon contribution.

function, $\alpha^2F(\Omega)$, from our spectra for both RbOs₂O₆ and KOs₂O₆ [34]. The results for $\alpha^2F(\Omega)$ in KOs₂O₆ are shown in Fig. 12 together with the fitted and original spectra.

The Eliashberg coupling function is similar to that of RbOs₂O₆ and also exhibits a peak at ~ 2.4 mV. The observation of such a low-energy phonon mode is compatible with a rattling motion of the alkali atom [66, 67]. The energy we find is however significantly lower than the 6.4 or 5.3 meV reported from inelastic neutron scattering [67] and specific heat measurements [35] respectively. We think that this is a manifestation of a surface phonon mode which could explain the increased surface T_c for RbOs₂O₆. A first analysis showed that a simple scenario based on a softening of the bulk low-energy phonon mode cannot explain the observations for both compounds. We are therefore currently investigating the possibility of an interplay between bulk and surface phonon modes.

3 Superconducting iron chalcogenides

These recently discovered Fe-based high-temperature superconductors feature an intriguing competition between magnetic, structural and superconducting phases. Initially, superconductivity was found in single-layer RO_{1-x}F_xFeAs pnictides (R = rare-earth metal), then in oxygen free MFe₂As₂ double-layer materials (M = Ca, Sr, Ba), and later on in the FeSe chalcogenide with PbO structure ($T_c = 8$ K). When doping Fe_{1+x}Te with Se, superconductivity is found over a wide composition range. The Fe atoms are tetrahedrally coordinated by Se ions in a similar fashion as in the FeAs

planes of other pnictides. Because FeSe consists only of the “superconducting” Fe-Se layers and is thus less complex than other pnictides, it represents a good model system to study the properties of superconductivity in the pnictides. In the $\text{FeSe}_x\text{Te}_{1-x}$ series, a substitution of Se with Te leads to an increase of T_c up to 15 K ($x = 0.5$) and magnetic order changes from short range to long range by a further increase of the Te content [68].

3.1 Effect of the chemical composition on the structure and properties of superconducting iron chalcogenides (E. Giannini)

We have grown a series of crystals of $\text{Fe}_{1+x}\text{Te}_{1-y}\text{Se}_y$ with controlled Fe-excess and Se-doping ($x < 0.1$, $0 \leq y \leq 0.45$) (Fig. 13) and systematically investigated the role of the chemical composition on the structural and physical properties. The evolution of the crystallographic parameters with the actual composition was extracted from structure refinements and related to the evolution of the magnetic properties [11]. We have found that the occupation of the additional Fe site, Fe2, decreases with increasing the Se atomic fraction. The shape of the tetrahedron changes with Se doping as well, going towards a lesser anisotropy, and this change is enhanced by the reduction of excess Fe in the actual composition. The interplane Fe1-Te distance, labeled h in Fig. 13, decreases with decreasing Fe excess x .

A crossover from an antiferromagnetic (AF) to a superconducting ground state takes place at $h \simeq 1.72 \text{ \AA}$, regardless of the Se doping [11]. According to theoretical predictions based on density functional calculations [69], above such h value (and correspondingly at high/low Fe/Se contents) a double-stripe AF ordering is favored and no superconductiv-

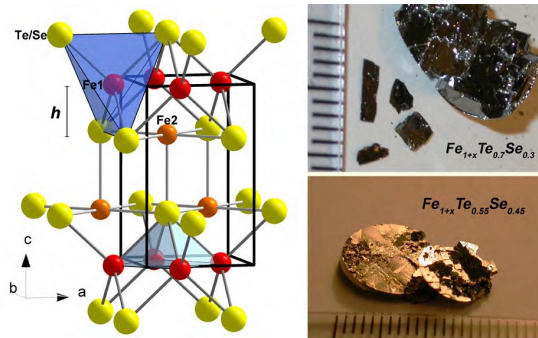


Figure 13: Crystal structure and crystals of $\text{Fe}_{1+x}\text{Te}_{1-y}\text{Se}_y$. The FeTe_4 tetrahedron and the Fe1-Te interplane distance, h , are shown.

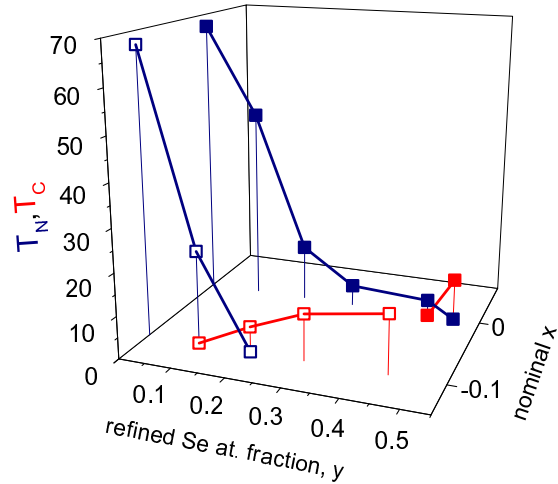


Figure 14: 3D phase diagram of $\text{Fe}_{1+x}\text{Te}_{1-y}\text{Se}_y$. x and y indicate the nominal Fe excess and Se doping, respectively.

ity occurs. Below this value, that means at low/high Fe/Se contents, a transition to a single-stripe AF ordering, rotated by 45° , takes place. This AF ordering is unstable at low temperature and superconductivity occurs. According to this scenario, superconducting pairing in Fe-chalcogenides and Fe-pnictides is mediated by the same kind of spin-fluctuations. An improved 3D phase diagram is shown in Fig. 14, in which the transition temperatures are plotted as a function of both Fe-excess and Se-doping.

3.2 Coexistence of incommensurate magnetism and superconductivity in $\text{Fe}_{1+y}\text{Se}_x\text{Te}_{1-x}$ (M. Kenzelmann)

We have grown single-crystals of $\text{Fe}_{1+y}\text{Se}_x\text{Te}_{1-x}$ ($0 \leq x \leq 0.5$) by a modified Bridgeman method similarly as reported by Sales *et al.* [68] and studied these materials through a combination of magnetic susceptibility, muon-spin rotation (μSR) and neutron diffraction. At the boundary between magnetic and superconducting phases, we observe a region of doping in which superconductivity coexists with incommensurate magnetic order. Our μSR experiments detect magnetism in the $x = 0.4, 0.25, 0.1$ and 0.0 samples below $T = 18, 30, 40$ and 70 K, respectively, consistent with neutron diffraction for the $x = 0.25$ single-crystal. Fig. 15 summarizes these results on magnetism and superconductivity in $\text{Fe}_{1+y}\text{Se}_x\text{Te}_{1-x}$. Superconductivity occurs through the bulk of the $x = 0.45$ and 0.5 crystals, but decreases continuously with decreasing x and occupies only up to 10% of the sample volume in the $x = 0.25$ and $x = 0.4$

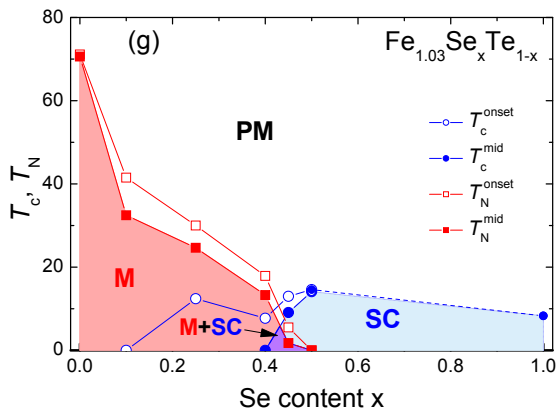


Figure 15: Phase diagram showing T_c^{onset} , T_c^{mid} , T_N^{onset} and T_N^{mid} as a function of selenium content x .

samples at $T \rightarrow 0$.

3.3 Synthesis, crystal structure and chemical stability of the superconductor FeSe_{1-x} (M. Kenzelmann)

We performed comparative studies of the superconducting FeSe_{1-x} ($x = 0.0 - 0.15$) samples synthesized by two different routes – the *low-temperature synthesis* using Se and Fe powders as the starting material and performed in sealed silica tubes at $400 - 700^\circ\text{C}$ similar to proposed by [70] and by the *high-temperature synthesis* similar to the one proposed recently by McQueen *et al.* [71] starting from Fe pieces and Se shot at temperatures up to 1075°C .

We have investigated the effect of stoichiometry on the phase purity of the obtained samples and its superconducting transition temperature. On the basis of our neutron powder diffraction data, we have revised the Fe-Se concentration phase diagram proposed by Okamoto [72]. In particular, we have found that in the Fe-Se system a stable phase exhibiting superconductivity at $T_c \sim 8$ K exists in the narrow range of selenium concentration ($\text{FeSe}_{0.974 \pm 0.005}$). As revealed by our neutron powder diffraction study, FeSe_{1-x} undergoes a second order structural phase transition at $T \sim 100$ K from a tetragonal phase (space group $P4/nmm$) to an orthorhombic (space group $Cmma$) on cooling. Fe-Se-Fe bond angles in the FeSe_4 pyramids become different in low-temperature phase, whereas the Fe-Se bond lengths are not changed at the transition.

3.4 Pressure induced static magnetic order in superconducting FeSe_{1-x} (H. Keller)

The phase diagram of the recently discovered Fe-based high-temperature superconductors

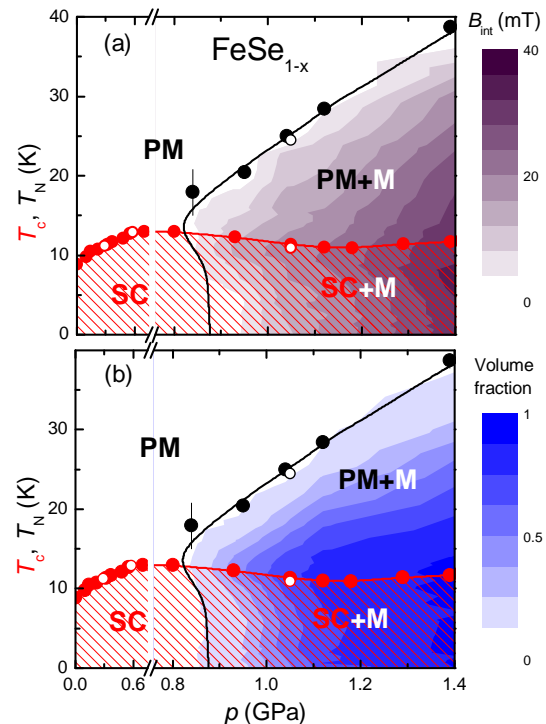


Figure 16: (a) Pressure dependence of the superconducting transition temperature T_c , the magnetic ordering temperature T_N , and the internal field B_{int} (magnetic order parameter) obtained from ac susceptibility and muon-spin rotation experiments. (b) Pressure dependence of T_N , T_c , and the magnetic volume fraction. The $T_c(p)$ and $T_N(p)$ lines are guides to the eye. The closed and the open symbols refer to the samples $\text{FeSe}_{0.94}$ and $\text{FeSe}_{0.98}$, respectively. SC, M, and PM denote the superconducting, magnetic and non-magnetic (paramagnetic) states of the sample.

(HTS) share a common feature with cuprates and heavy fermions. The parent compounds of the Fe-based HTS, such as LnOFeAs ($\text{Ln} = \text{lanthanoids}$), AFe_2As_2 ($A = \text{alkaline earth metals}$) and FeCh ($\text{Ch} = \text{chalcogenides}$) [73, 74][12] exhibit long-range static magnetic order. Upon doping or application of pressure (chemical or external), magnetism is suppressed and superconductivity emerges.

We perform a detailed study of the electronic phase diagram of FeSe_{1-x} as a function of pressure by means of μSR and ac susceptibility measurements. These techniques are direct and bulk sensitive. Furthermore, it is possible to determine the superconducting transition temperature T_c as well as the Néel temperature T_N in a region where both magnetism and superconductivity coexist. The so obtained phase diagram is presented in Fig. 16. The transition temperature T_c shows a monotonic increase up to pressures $p \simeq 0.8$ GPa. At higher pressures magnetic order coexists and competes with su-

perconductivity. Static magnetic order is established below $T_N > T_c$ and bulk superconductivity sets in below T_c . The competition of the two ground states in this pressure range is evident from the following two observations: first, T_c is weakened as a function of pressure as soon as magnetic order appears, leading to a local maximum at $p \simeq 0.8$ GPa in $T_c(p)$ (Fig. 17a); second, the internal field B_{int} (magnetic order parameter), as well as the magnetic volume fraction, decrease as a function of temperature below T_c showing that magnetism which develops at higher temperatures becomes partially (or even fully) suppressed by the onset of superconductivity (Fig. 17c, d). The superconducting volume fraction is close to 100% for all pressures (Fig. 17b), while the magnetic fraction increases continuously and reaches $\simeq 90\%$ at the highest pressure investigated $p \simeq 1.39$ GPa (Fig. 17d). In other words, both ground states coexist in the full sample volume at $p = 1.39$ GPa. The data do not provide any indication for macroscopic phase separation into superconducting and magnetic clusters (larger than a few nm in size). Actually, the data rather point to a coexistence of both or-

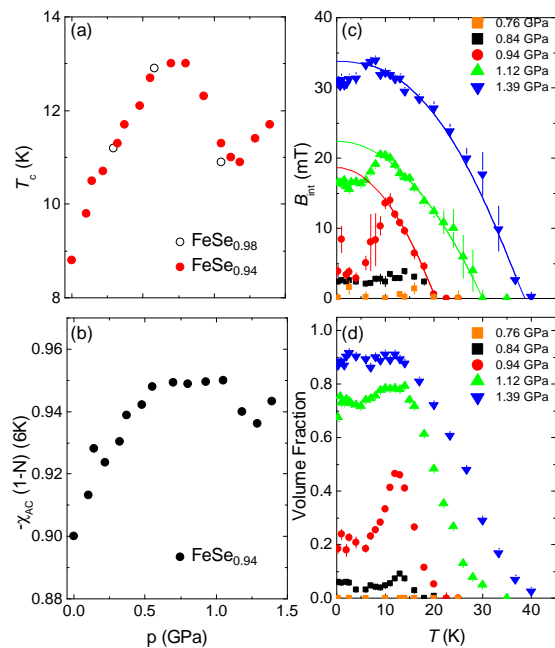


Figure 17: (a) Dependence of T_c on p of $\text{FeSe}_{0.94}$ and $\text{FeSe}_{0.98}$. (b) Pressure dependence of the normalized ac susceptibility $-\chi_{ac}(1-N)$ at $T = 6$ K. Dependence of the internal field at the muon stopping site, B_{int} , which is proportional to the magnetic order parameter (c), and the magnetic volume fraction (d), on temperature at various pressures. The solid lines in panel (b) are the fit of $B_{int}(T)$ in the region $T_c(p) \leq T \leq T_N$ to $B_{int}(T) = B_{int}(0)[1 - (T/T_N)^\alpha]^\beta$ (α and β are the power exponents).

der parameters on an *atomic* scale and seem to be stabilized by pressure, since T_c as well as T_N and the magnetic order parameter simultaneously increase with increasing pressure. This exceptional observation provides a new challenge for theories describing the mechanism of high-temperature superconductivity in the iron-based superconductors.

3.5 Resonant inelastic X-ray scattering of FeTe (D. van der Marel)

Resonant Inelastic X-ray Scattering (RIXS) spectra of $\text{Fe}_{1.087}\text{Te}$ were taken at the ADDRESS beamline of the Swiss Light Source [14]. The energy of the incident beam was tuned near the Fe L_3 edge ($2p(J = 3/2) \rightarrow 3d$ transitions) of non-superconducting $\text{Fe}_{1.087}\text{Te}$. The incident energy resolution was set to 50 meV, and the total resolution of the scattered beam (energy ω') was 73 meV. Fig. 18 displays high-resolution RIXS data in the form of a contour plot with linear interpolation between the data points. The intensity is strongest when $705 \text{ eV} < \omega$ and $\omega' < \omega$. The resonant inelastic X-ray scattering cross section at the L_3 edge of Fe rep-

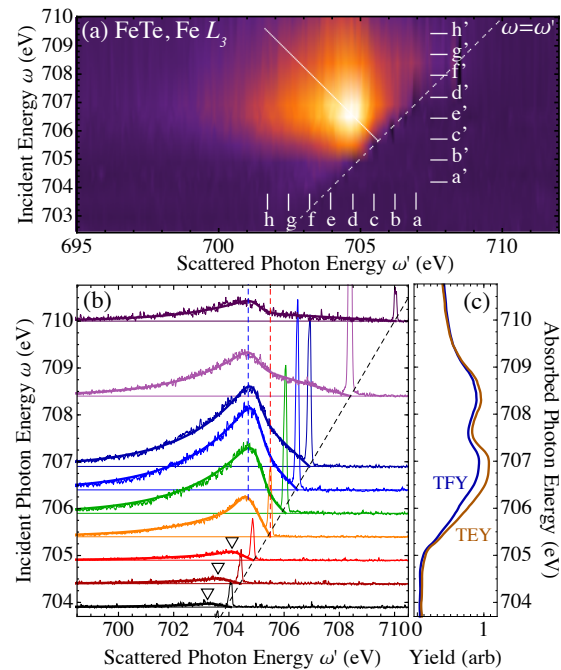


Figure 18: (a) False color plot of the RIXS data, plotted versus incident and scattered photon energies, with elastic peak subtracted and linear interpolation applied between the data points. (b) RIXS spectra in detail. The two vertical dashed lines indicate the position of the maximum (left) and a kink (right). Triangles point to the 0.9 eV feature in the Raman-dispersing, sub-threshold regime. (c) Total fluorescence yield (TFY) and total electron yield (TEY) spectra, showing the two-peak L_3 structure.

resents the response of a many-particle, itinerant electron system to the sudden generation of a localized potential, with the concomitant addition of 1 electron to the Fe $3d$ subsystem. In contrast to the sharp peaks typically seen in insulating systems at the transition metal $L3$ edge, we observe spectra which show different characteristic features. For low-energy transfer, we observe experimentally many-body effects of resonant Raman scattering from a non-interacting gas of fermions, theoretically predicted by Nozières and Abrahams [75]. Furthermore, we find that limitations to this many-body electron-only theory are realized at high Raman shift, where an exponential lineshape reveals an energy scale not present in these considerations. This regime, identified as emission, requires considerations of lattice degrees of freedom to understand the lineshape. We show that both observations are intrinsic general features of many-body physics of metals. In the fluorescence regime, we have identified an energy scale which appears to reflect material properties related to lattice vibrations.

3.6 $\text{BiOCu}_{1-y}\text{S}$ (E. Giannini)

In the search for new materials with a structure related to that of ferro-pnictides RFeAsO and similar chemical properties, we have explored As-free chemical systems in which the R is replaced by Bi. The quaternary BiOCuS is isostructural to the superconducting LaFeAsO and can be synthesized by a low-temperature (500°C) solid state reaction from Bi_2O_3 , Bi_2S_3 and Cu_2S . This compound is a diamagnetic insulator, but can be successfully doped by either partially substituting Fluorine for Oxygen, or creating vacancies on the Cu-site, or even doping both the Bi-site with lanthanides and the Cu-site with other transition metals. Single-phase $\text{BiO}_{1-x}\text{F}_x\text{CuS}$ ($x \leq 0.5$) and $\text{BiOCu}_{1-y}\text{S}$ ($y \leq 0.15$) polycrystalline samples have been

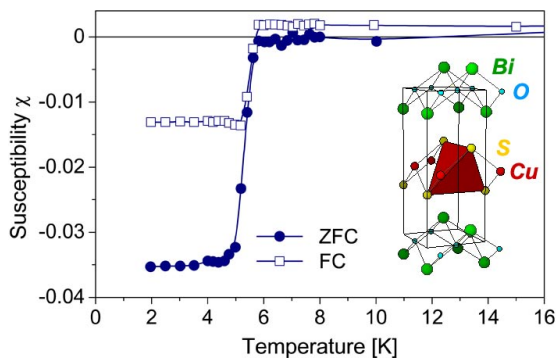


Figure 19: Superconducting transition and crystal structure of $\text{BiOCu}_{1-y}\text{S}$.

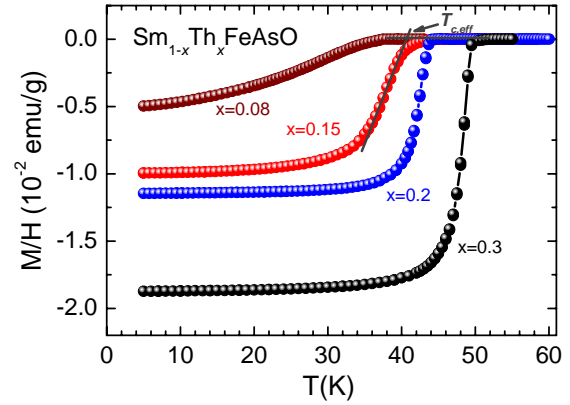


Figure 20: Temperature dependence of the magnetic susceptibility for $\text{Sm}_{1-x}\text{Th}_x\text{FeAsO}$ samples measured at 0.5 mT in zero-field-cooled (ZFC) mode. The determination of $T_{c,eff}$ is illustrated.

obtained. The latter is found to exhibit superconductivity below $T_c = 5.8$ K and nominal $y = 0.1$ (Fig. 19) [15].

4 High- T_c iron pnictides

4.1 Superconductivity above 50 K in Th-substituted SmFeAsO (J. Karpinski)

Superconducting poly- and single-crystalline samples of $\text{Sm}_{1-x}\text{Th}_x\text{FeAsO}$ with partial substitution of Sm^{3+} by Th^{4+} with a sharp diamagnetic onset at T_c up to ~ 53 K were synthesized using high-pressure technique [36]. The samples are characterized by a full diamagnetic response in low magnetic field, by a high intergrain critical current density for polycrystalline samples, and by a critical current density of the order of $8 \cdot 10^5$ A/cm² for single-crystals at 2 K in 7 T. It was found that the magnetic penetration depth anisotropy γ_λ exhibits a pronounced increase with decreasing temperature, in agreement with the already reported behavior for single-crystals of $\text{SmFeAsO}_{1-x}\text{F}_y$ (Fig. 20) [36].

4.2 Superconductivity in $\text{SmFe}(\text{As},\text{P})\text{O}$ compounds (J. Karpinski)

Polycrystalline samples and single-crystals of $\text{SmFeAs}_{1-x}\text{P}_x\text{O}$ are synthesized using high-pressure technique. Fig. 21 shows the temperature dependence of the magnetic susceptibility of $\text{SmFeAs}_{1-x}\text{P}_x\text{O}$ polycrystalline samples in a magnetic field of 10 Oe. Polycrystalline samples with $x = 0.5$ and 0.45 show bulk superconductivity with a superconducting transition at ~ 23 and 18 K, respectively. Single-crystals of P substituted SmFeAsO are also grown using NaCl/KCl as a flux. Though conditions

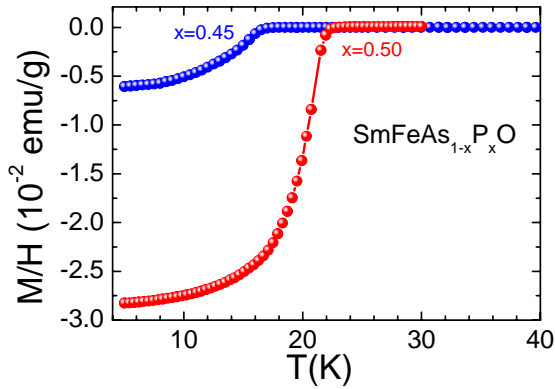


Figure 21: Temperature dependence of the magnetic susceptibility for $\text{SmFeAs}_{1-x}\text{P}_x\text{O}$ samples measured at 1.0 mT in zero-field-cooled (ZFC) mode.

of crystal growth and doping still require further optimization we have grown crystals with a size of $\sim 100 \times 100 \mu\text{m}^2$ and a refined composition $\text{SmFeAs}_{0.66}\text{P}_{0.34}\text{O}$. Fig. 22 displays the temperature dependence of the electrical resistivity (ρ) of a $\text{SmFeAs}_{0.5}\text{P}_{0.5}\text{O}$ polycrystalline sample. The resistivity exhibits metallic characteristics before the onset of the superconducting transition. The transition width is rather sharp, suggesting the homogeneous nature of the sample. Fig. 22 (right inset) shows the resistive measurements at various magnetic field strengths. The left inset of Fig. 22 shows the temperature dependence of the upper critical field calculated with 50% resistance drop criteria.

In order to increase the size and surface quality of LnFeAsO -type single-crystals, different kind

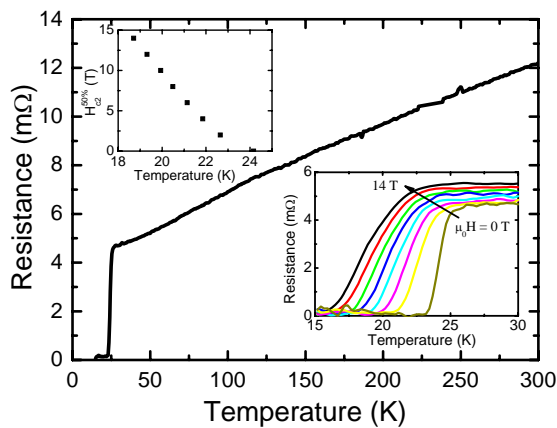


Figure 22: Temperature dependence of the electrical resistivity (ρ) of a $\text{SmFeAs}_{0.5}\text{P}_{0.5}\text{O}$ polycrystalline sample. The right inset shows the resistive measurements at various magnetic field strengths. The left inset shows the temperature dependence of the upper critical field.

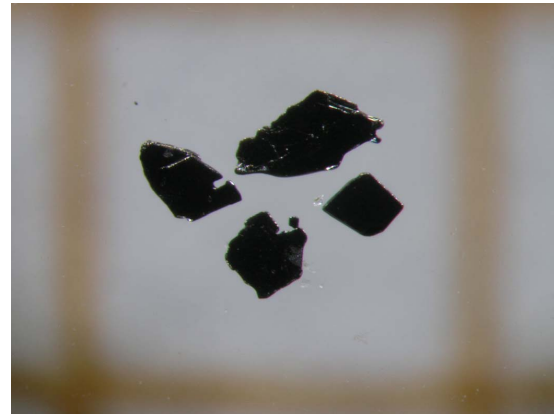


Figure 23: First single-crystals of Sm1111 grown using NaAs flux at 1380°C within 40 h (on mm scale).

of fluxes are investigated. Preliminary single-crystal growth experiments show that the NaAs flux can be a good candidate for increasing the size and X-ray quality of 1111 single-crystals. First grown single-crystals are studied on a four-circle diffractometer equipped with a CCD detector. Structure investigation confirm high structural perfection with very low mosaicity (less than 1 degree) in c direction. Further experiments are in progress. Fig. 23 shows as grown crystals.

4.3 Critical currents of $\text{SmFeAs}(\text{O},\text{F})$ crystals (B. Batlogg)

Reliable measurements perpendicular to the FeAs layers, i.e. along the crystallographic c direction, require new methods of sample prepara-

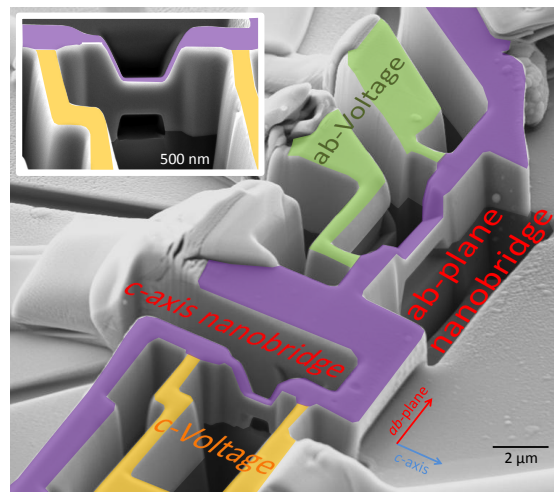


Figure 24: Two $\text{SmFeAs}_{0.7}\text{F}_{0.25}$ nano-bridges for critical current measurements along and perpendicular to the FeAs layers carved into a single-crystal. (cross-section $600 \text{ nm} \times 600 \text{ nm}$, length of narrow part $1\text{--}3 \mu\text{m}$).

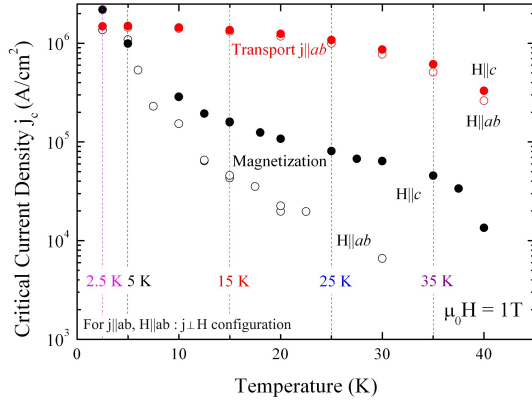


Figure 25: Temperature dependence of $j_c \parallel ab$ for $\mu_0 H = 1$ T. At low temperatures, the critical current anisotropy $j_c(H \parallel ab)/j_c(H \parallel c)$ is reduced and the values of j_c converge.

ration. We have employed a Focused Ion Beam (FIB) as a powerful tool for shaping and contacting on sub- μm dimensions. A Ga^{2+} ion beam is accelerated by 30 kV and focused onto the target, where it ablates the crystal without collateral damage. In addition, the FIB is also used to deposit μm -sized electric leads of platinum without exposing the structure to air (Fig. 24).

For applications in superconducting magnets, large critical current densities j_c are required. We find a nearly-isotropic intragrain j_c in the range of 10^6 A/cm², employing the following two methods. The most direct way to obtain the critical current density j_c is to increase the applied current through a superconducting sample until a potential drop can be observed. The second method to estimate j_c involves measurements of the magnetization loops $M(H)$ of macroscopic crystals, and j_c has been calculated using Bean's model. The results for j_c from both methods are given in Fig. 25, and each of them emphasizes different aspects.

Starting at low temperature, particularly noteworthy are: (1) j_c exceeds 10^6 A/cm², (2) j_c is essentially independent of the field and only weakly field and current orientation dependent up to 14 T, and (3) the two methods applied to different crystals from different growth runs yield very similar results. The large values of j_c reflect the highly effective pinning in this materials class and give reason to expect that j_c can be further enhanced by proper material design and treatment. Even at the present level, j_c reaches values that are generally considered a minimal requirement for technical applications.

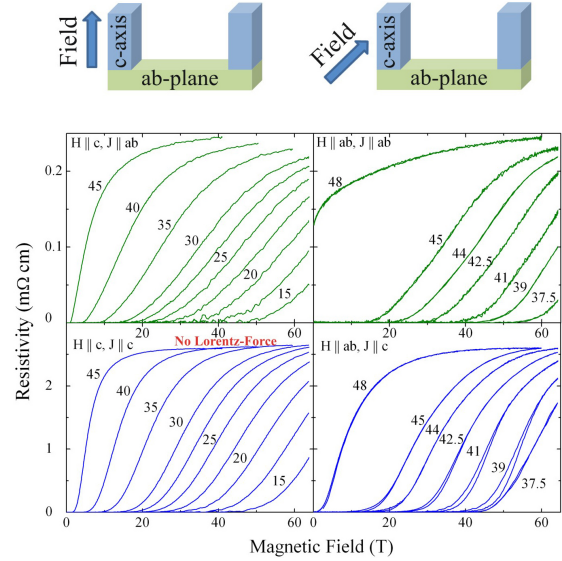


Figure 26: Magneto-resistance of $\text{SmFeAsO}_{0.7}\text{F}_{0.25}$ in pulsed fields up to 65 T at various temperatures for fields and currents along and perpendicular to the c -axis.

4.4 Magneto-resistance of $\text{SmFeAs}(\text{O},\text{F})$ crystals (B. Batlogg)

In Fig. 26, the magneto-resistance of $\text{SmFeAsO}_{0.7}\text{F}_{0.25}$ is shown for field orientations parallel and perpendicular to the FeAs-planes and for currents along both orientations. The four panels capture the main qualitative results: the over-all feature and field-scale of the resistive transition is mainly determined by the orientation of the magnetic field with respect to the crystal axes, and is essentially independent of the current direction. This is an important prerequisite for the application in superconducting wires as the supercurrent in a polycrystalline wire is always limited by the least favorably oriented crystallites.

At a given temperature, the low-dissipation region ($\rho \approx 0$) extends to higher magnetic fields when the field is parallel to ab (right panels of Fig. 26).

To identify the field scales for potential applications, we estimate the magnetic field H^* up to which dissipation-free current transport can be maintained. Given the noise floor in pulsed fields, we have adopted a conservative definition of $H^*(T)$ at $\rho(T, H^*) = 10 \mu\Omega\text{cm}$. The thus defined field scale H^* is extremely high for $H \parallel ab$, i.e. > 50 T already 10 K below T_c of 48 K, and even for $H \parallel c$, H^* extrapolates well above 50 T at temperatures below 15 K (Fig. 27). Even more relevant for technical aspects, however, is the weak dependence of H^* on the current direction and thus an addi-

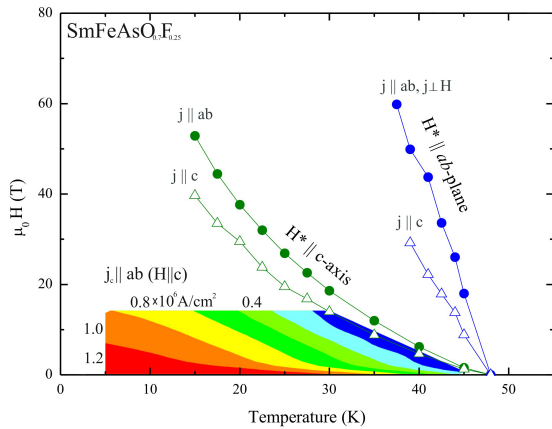


Figure 27: A color map of the critical current density $j_c \parallel ab$ ($H \parallel c$) in $SmFeAsO_{0.7}F_{0.25}$ bordered by H^* (marking the dissipation level of $10 \mu\Omega cm$) measured in pulsed fields.

tional important requirement for operation in high fields is met.

In addition to the presented highly promising intragrain transport properties, grain boundary current suppression and metallurgical issues will have to be addressed. From a microscopic physics point of view, it will be an outstanding challenge to understand how multi-band, multi-gap superconductivity with pronounced temperature dependence, e.g. of the superfluid density, will influence vortex physics and its implications for the technical critical current density.

4.5 Magnetism and superconductivity in iron based superconductors (C. Niedermayer)

The discovery of superconductivity in iron based compounds has raised the suspicion that these new materials share a similar pairing mechanism with the cuprate superconductors, as both families exhibit superconductivity following charge doping of a magnetic parent material. In this context, it is important to follow the evolution of the microscopic magnetic properties of the pnictides with doping and hence to determine whether magnetic correlations coexist with superconductivity. A detailed muon-spin rotation (μSR) study on $SmFeAsO_{1-x}F_x$ shows that static magnetism persists well into the superconducting regime (see phase diagram in Fig. 28). This analogy to the cuprates is quite surprising as the parent compounds of the two families have rather different magnetic ground states: itinerant spin-density wave for the pnictides contrasted with the Mott Hubbard insulator in the cuprates. Our findings therefore suggest that the proximity to magnetic order and associated soft mag-

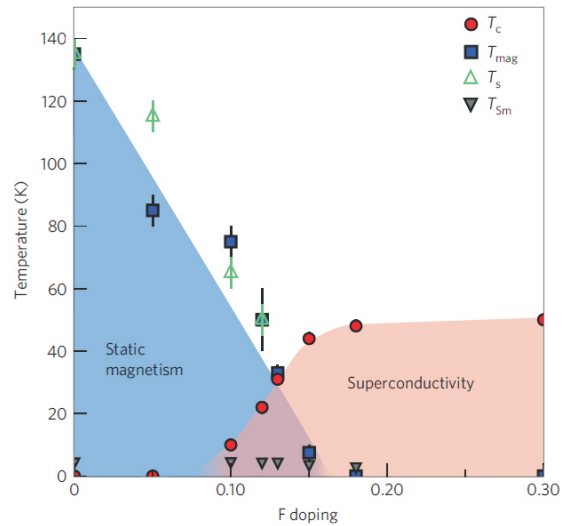


Figure 28: Phase diagram of the magnetic and superconducting properties of $SmFeAsO_{1-x}F_x$ as a function of the F substitution and thus electron doping. There is a region of coexistence between $x = 0.10$ and 0.15 and T_c reaches its maximal value just as static magnetism disappears.

netic fluctuations, rather than strong electronic correlations in the vicinity of a Mott-Hubbard transition, may be the key ingredients of high- T_c superconductors [17].

5 Oxygen-free high- T_c iron pnictides

5.1 Single-crystals of $CaFe_{2-x}Co_xAs_2$ and $EuFe_{2-x}Co_xAs_2$ (J. Karpinski)

Single-crystals of pure $CaFe_2As_2$, $EuFe_2As_2$ and Co substituted $CaFe_{2-x}Co_xAs_2$ and $EuFe_{2-x}Co_xAs_2$ were grown out of Sn flux in alumina crucibles sealed under reduced Ar pressure in quartz ampoules. Typical crystals were of plate-like shape (up to $7 \times 5 \text{ mm}^2$) with

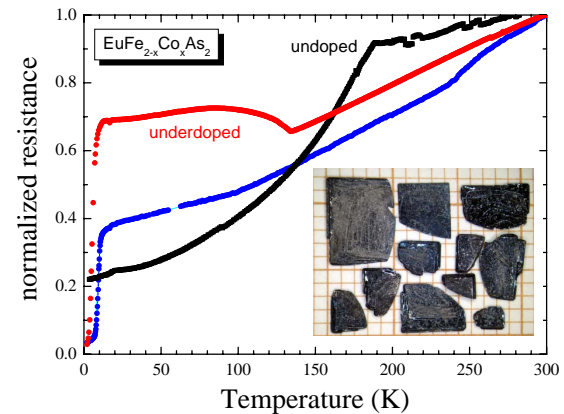


Figure 29: Temperature dependence of the resistance for $EuFe_{2-x}Co_xAs_2$ single-crystals. Inset shows single-crystals of $EuFe_2As_2$.

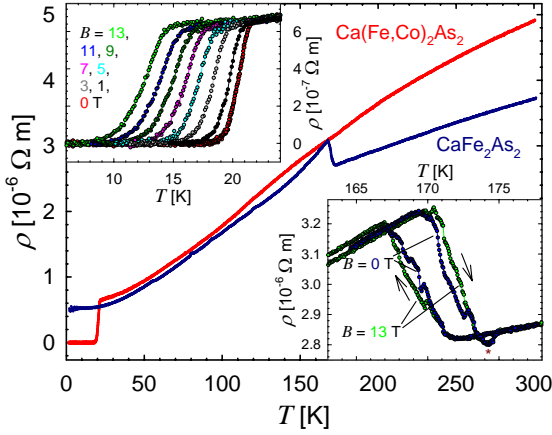


Figure 30: Temperature dependence of resistivity for $\text{CaFe}_{2-x}\text{Co}_x\text{As}_2$ single-crystals [37].

the crystallographic c -axis perpendicular to the plate (Fig. 29 inset). An interesting feature of EuFe_2As_2 is antiferromagnetic ordering of magnetic moments localized on Eu^{+2} ions ($T_N = 18$ K). This ordering is not affected by Co doping. Magnetization and resistivity data for $\text{EuFe}_{2-x}\text{Co}_x\text{As}_2$ show the suppression of the spin-density wave (SDW) state with Co substitution and finally the appearance of superconductivity (Fig. 29). The effect of Eu^{+2} magnetic ordering on superconductivity leads to the re-entrant behavior. Magnetization and resistivity measurements of $\text{CaFe}_{2-x}\text{Co}_x\text{As}_2$ single-crystals show that the SDW transition is gradually suppressed by Co doping leading to superconductivity for $x = 0.08$ (Fig. 30). Undoped CaFe_2As_2 reveals a substantial increase of the Nernst coefficient and the Seebeck coefficient in the SDW state [37].

5.2 Superconductivity in RbFe_2As_2 (J. Karpinski)

Polycrystalline samples of RbFe_2As_2 were synthesized by solid state reaction. Superconductivity was found in this compound with a $T_c = 2.6$ K [16].

5.3 Charge dynamics of the spin-density wave state in BaFe_2As_2 (L. Degiorgi)

Superconductivity in suitably doped BaFe_2As_2 compounds conclusively proves that it originates only from the iron arsenide layers, regardless of the separating sheets. It is also currently believed that the superconductivity in these systems is intimately connected with magnetic fluctuations and a spin-density wave (SDW) anomaly within the FeAs layers. This is obviously of interest, since a SDW phase may

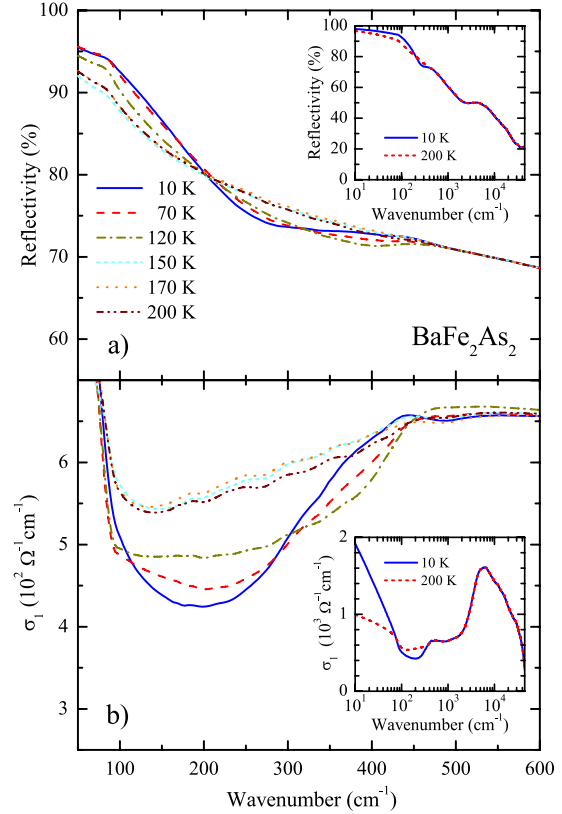


Figure 31: (a) Optical reflectivity and (b) real part $\sigma_1(\omega)$ of the optical conductivity as a function of temperature in the far-infrared spectral range. The insets in both panels show the same quantities at 10 and 200 K from the far-infrared up to the ultraviolet spectral range with logarithmic energy scale.

generally compete with other possible orderings and complicated phase diagrams are often drawn due to their interplay. It is therefore of relevance to acquire deeper insight into the SDW phase and to establish how this broken symmetry ground state affects the electronic properties of these materials.

We focused our attention on BaFe_2As_2 at temperatures both above and below T_{SDW} . Fig. 31a displays the optical reflectivity for $\omega \leq 600$ cm^{-1} . The inset shows $R(\omega)$ over the entire measured range. $R(\omega)$ of BaFe_2As_2 has an overall metallic behavior, characterized by a broad bump at about 5000 cm^{-1} and by the onset of the reflectivity plasma edge below 3000 cm^{-1} (inset Fig. 31a). The temperature dependence of $R(\omega)$ indicates a depletion of $R(\omega)$ with decreasing temperature in the energy interval between 200 and 500 cm^{-1} followed by a progressive enhancement of $R(\omega)$ below 200 cm^{-1} , so that all $R(\omega)$ spectra cross at 200 cm^{-1} . From the real part of the optical conductivity (Fig. 31b) a picture emerges in which at $T > T_{\text{SDW}}$ the free charge carrier contribution, represented by the Drude peak cen-

tered at $\omega = 0$, coexists with bound charge contributions between 50 and 700 cm^{-1} . When lowering the temperature below T_{SDW} , a pseudogap develops and a rearrangement of states takes place in such a way that excitations pile up in the spectral range around 420 cm^{-1} as well as around 50 cm^{-1} . These latter excitations merge into the high-frequency tail of the narrow Drude term. We also observe that the narrowing of the metallic contribution in $\sigma_1(\omega)$ at T_{SDW} tracks the behavior of the dc transport properties.

5.4 Two-gap behavior in the optical conductivity of $\text{BaFe}_{2-x}\text{Co}_x\text{As}_2$ (*D. van der Marel*)

We have measured temperature dependent optical data on $\text{BaFe}_{2-x}\text{Co}_x\text{As}_2$ (BCFA), with $x =$

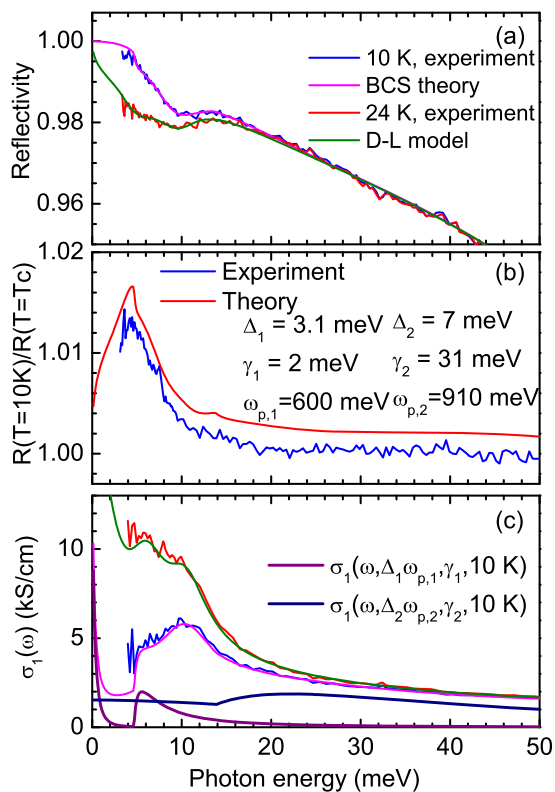


Figure 32: (a) Low-energy experimental reflectivity (blue) and reflectivity obtained from the BCS simulation (violet) at 10 K. Also shown are the reflectivity at T_c (red) and Drude-Lorentz model result (green). (b) Ratio of 10 K reflectivity to the one at T_c (24 K) for the experimental data (blue) and simulation (offset for clarity by 1.002, in red). (c) Comparison of the 10 K optical conductivity determined from experiment (blue) and simulation (violet) and the 24 K data (red) and Drude-Lorentz model (green). Note the low-frequency upturn in the simulation which arises from finite temperature broadening. We also show the two contributions to the conductivity from the BCS calculation.

0.14, between 4 meV and 6.5 eV [38]. The reflectance spectrum was measured between 4 meV and 0.75 eV, and ellipsometric measurements were made in the range 0.75 eV to 6.2 eV. The experiments were performed between 10 K and 300 K, using stabilized, high-vacuum cryostats ($\leq 10^{-9}$ mbar in the mid-infrared to ultraviolet range). The optical conductivity in the entire range reveals contributions due to interband transitions at energies as low as 10 meV. We determined the superfluid density $\rho_s \approx 2.2 \pm 0.5 \cdot 10^7 \text{ cm}^{-2}$, which places optimally doped BCFA close to the Uemura line. Our experimental data shows clear signs of a superconducting gap with $2\Delta_1 = 6.2 \pm 0.8 \text{ meV}$ (Fig. 32). In addition we found that the optical spectra are consistent with the presence of an additional band of strongly scattered carriers with a larger gap, $2\Delta_2 = 14 \pm 2 \text{ meV}$.

5.5 Two-gap superconductivity in $\text{Ba}_{1-x}\text{K}_x\text{Fe}_2\text{As}_2$: a complementary study of the magnetic penetration depth by μSR and ARPES (*E. Morenzoni*)

Much effort is devoted to the investigation of the manifestations and the mechanism of unconventional superconductivity in the iron-arsenides, since many of their features clearly set them apart from other superconductors. *Ab initio* calculations, for instance, indicate that superconductivity originates in the *d*-orbitals of the Fe ion, which normally would be expected to be pair-breaking [76]. Several disconnected Fermi-surface sheets contribute to the superconductivity, as revealed by angle-resolved photoemission spectroscopy (ARPES) [77]. Furthermore, indication for multi-gap superconductivity was obtained in measurements of the first and second critical fields H_{c1} and H_{c2} [78], the magnetic penetration depth λ [79], as well as in point-contact Andreev reflection spectroscopy experiments [80].

Within this work [20] we have studied the temperature evolution of the in-plane (λ_{ab}) and the out-of-plane (λ_c) magnetic penetration depth in a single-crystalline sample of $\text{Ba}_{1-x}\text{K}_x\text{Fe}_2\text{As}_2$ (BKFA, $T_c \simeq 32 \text{ K}$). The penetration depth anisotropy $\gamma_\lambda = \lambda_c/\lambda_{ab}$ increases with decreasing T from $\gamma_\lambda \simeq 1.1$ at $T \simeq T_c$ to $\gamma_\lambda \simeq 1.9$ at $T \simeq 1.7 \text{ K}$, just opposite to the trend found for the H_{c2} anisotropy $\gamma_{H_{c2}}$ in [81]. This resembles very much the situation in double-gap MgB_2 where both anisotropies are equal at T_c , but evolve oppositely with T . The notion of two superconducting gaps is supported by the observation of an inflection point in λ_{ab} at $\sim 7 \text{ K}$ (Fig. 33). From a fit of

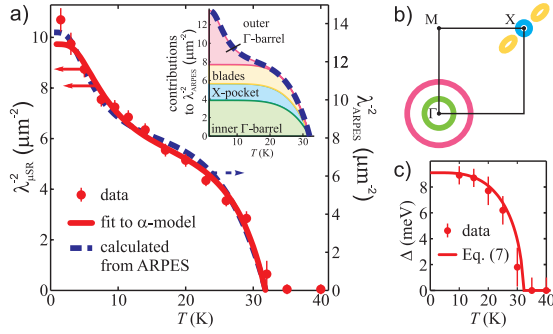


Figure 33: (a) Temperature evolution of the inverse squared in-plane magnetic penetration depth λ_{ab}^{-2} . The solid line represents the result of a fit by means of the α -model, the dashed line represents a calculation of λ_{ab}^{-2} from the electronic structure revealed by ARPES. Inset: contributions of different Fermi surface sheets to λ_{ab}^{-2} . (b) Fermi surface of BKFA. (c) Temperature dependence of the superconducting gap, extracted from ARPES spectra.

λ_{ab}^{-2} to the phenomenological α -model we obtain gap values of $\Delta_1 = 9.1$ meV and $\Delta_2 = 1.5$ meV. A comparison of $\lambda_{ab}^{-2}(T)$ measured by μSR with the one calculated from ARPES data shows a remarkable agreement between these two complementary approaches, lending further support to our conclusions and establishing ARPES as a tool to estimate λ_{ab} .

6 Influence of Mg deficiency on crystal structure and superconducting properties in MgB_2 single-crystals (J. Karpinski)

The effect of high-temperature vacuum annealing on crystal structure and superconducting properties of MgB_2 single-crystals is investigated [39]. As the annealing temperature is increased from 800 to 975°C, the average Mg content in the MgB_2 crystals systematically decreases while T_c remains essentially unchanged and the superconducting transition slightly broadens from ~ 0.55 to ~ 1.3 K (Fig. 34). The reduction of the superconducting volume fraction is noticeable already after annealing at 875°C. Samples annealed at 975°C are partially decomposed and the Mg site occupancy is decreased to 0.92 from 0.98 in as grown crystals. Annealing at 1000°C completely destroys superconductivity. First-principles calculations of the $\text{Mg}_{1-x}(\text{V}_{\text{Mg}})_x\text{B}_2$ electronic structure, within the supercell approach, show a small downshift of the Fermi level. Holes induced by the vacancies go to both σ and π bands. These small modifications are not expected to influence T_c , in agreement with observations. The significant reduction of the superconducting volume frac-

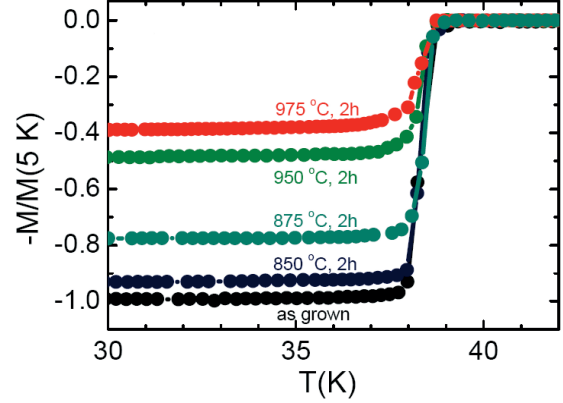


Figure 34: Diamagnetic moment in a field of 5 Oe normalized to zero field cooled magnetization value at 5 K as a function of temperature for MgB_2 as grown crystal and after being annealed under vacuum ($> 10^{-6}$ Torr) and at temperatures between 850 and 975°C. The measurements are performed upon heating from the zero-field-cooled state. The field is applied along the c -axis of the crystal.

tion without noticeable T_c reduction indicates the coexistence, within the same crystal, of superconducting and non-superconducting electronic phases, associated with regions rich and poor in Mg vacancies.

7 Collaborative efforts

Collaborative efforts are – and will continue to be – of essential importance for the success of Project 4. Highly successful examples are the numerous collaborations between all crystal growers and all experimental groups involved in this project: almost all materials mentioned above (cuprates, iron-pnictides, iron-chalcogenides, pyrochlores) have been grown in laboratories at the ETHZ, UniGE and PSI and have been studied by at least two other groups at different home-institutions. Theory groups at the ETHZ, UniFR and UniGE have strongly contributed to the modeling the results obtained with ARPES, STM and optics at PSI and UniGE, and providing theoretical feedback. Experimental groups at EPFL, UniGE and PSI have ongoing projects at PSI with experiments carried out jointly at the ADDRESS beamline, and the infrared beam-line at SLS.

MaNEP-related publications

- [1] K. Y. Yang, T. M. Rice, and F. C. Zhang, *Physical Review B* **73**, 174501 (2006).
- [2] K. Y. Yang, W. Q. Chen, T. M. Rice, and F. C. Zhang, *Physical Review B* **80**, 174505 (2009).
- [3] K. Y. Yang, H. B. Yang, P. D. Johnson, T. M. Rice, and F. C. Zhang, *Europhysics Letters* **86**, 37002 (2009).
- [4] D. Baeriswyl, D. Eichenberger, and M. Menteshshvili, *New Journal of Physics* **11**, 075010 (2009).

- [5] M. Shi, A. Bendounan, E. Razzoli, S. Rosenkranz, M. R. Norman, J. C. Campuzano, J. Chang, M. Månsson, Y. Sassa, T. Claesson, O. Tjernberg, L. Patthey, N. Momono, M. Oda, M. Ido, S. Guerrero, C. Mudry, and J. Mesot, *Europhysics Letters* **88**, 27008 (2009).
- [6] T. Claesson, M. Månsson, A. Önsten, M. Shi, Y. Sassa, S. Pailh s, J. Chang, A. Bendounan, L. Patthey, J. Mesot, T. Muro, T. Matsushita, T. Kinoshita, T. Nakamura, N. Momono, M. Oda, M. Ido, and O. Tjernberg, *Physical Review B* **80**, 094503 (2009).
- [7] U. Chatterjee, M. Shi, D. Ai, J. Zhao, A. Kanigel, S. Rosenkranz, H. Raffy, Z. Z. Li, K. Kadowaki, D. G. Hinks, Z. J. Xu, J. S. Wen, G. Gu, C. T. Lin, H. Claus, M. R. Norman, M. Randeria, and J. C. Campuzano, *Nature Physics* **6**, 99 (2010).
- [8] J. Chang, N. B. Christensen, C. Niedermayer, K. Lefmann, H. M. Rønnow, D. F. McMorrow, A. Schneidewind, P. Link, A. Hiess, M. Boehm, R. Mottl, S. Pailh s, N. Momono, M. Oda, M. Ido, and J. Mesot, *Physical Review Letters* **102**, 177006 (2009).
- [9] A. Piriou, N. Jenkins, C. Berthod, I. Maggio-Aprile, and Ø. Fischer, *submitted to Nature Physics* (2010).
- [10] J. T. Devreese, S. N. Klimin, J. L. M. van Mechelen, and D. van der Marel, *Physical Review B* **81**, 125119 (2010).
- [11] R. Viennois, E. Giannini, D. van der Marel, and R. Černý, *Journal of Solid State Chemistry* (2010), doi:10.1016/j.jssc.2010.01.024.
- [12] R. Khasanov, M. Bendele, A. Amato, P. Babkevich, A. T. Boothroyd, A. Cervellino, K. Conder, S. N. Gvasaliya, H. Keller, H.-H. Klauss, H. Luetkens, V. Pomjakushina, E. Pomjakushina, and B. Roessli, *Physical Review B* **80**, 140511(R) (2009).
- [13] E. Pomjakushina, K. Conder, V. Pomjakushina, M. Bendele, and R. Khasanov, *Physical Review B* **80**, 024517 (2009).
- [14] J. N. Hancock, R. Viennois, D. van der Marel, H. M. Rønnow, M. Guarise, P.-H. Lin, M. Gironi, M. Moretti Sala, G. Ghiringhelli, V. N. Strocov, J. Schlappa, and T. Schmitt, *submitted* (2010).
- [15] A. Ubaldini, E. Giannini, C. Senatore, and D. van der Marel, *Physica C* (2010), doi:10.1016/j.physc.2009.11.164.
- [16] Z. Bukowski, S. Weyeneth, R. Puzniak, J. Karpinski, and B. Batlogg, *Physica C* (2010), doi:10.1016/j.physc.2009.11.103.
- [17] A. J. Drew, C. Niedermayer, P. J. Baker, F. L. Pratt, S. J. Blundell, T. Lancaster, R. H. Liu, G. Wu, X. H. Chen, I. Watanabe, V. K. Malik, A. Dubroka, M. Rössle, K. W. Kim, C. Baines, and C. Bernhard, *Nature Materials* **8**, 310 (2009).
- [18] F. Pfuner, J. G. Analytis, J.-H. Chu, I. R. Fisher, and L. Degiorgi, *The European Physical Journal B* **67**, 513 (2009).
- [19] E. van Heumen, E. Muhlethaler, A. B. Kuzmenko, H. Eisaki, W. Meevasana, M. Greven, and D. van der Marel, *Physical Review B* **79**, 184512 (2009).
- [20] R. Khasanov, D. V. Evtushinsky, A. Amato, H.-H. Klauss, H. Luetkens, C. Niedermayer, B. Büchner, G. L. Sun, C. T. Lin, J. T. Park, D. S. Inosov, and V. Hinkov, *Physical Review Letters* **102**, 187005 (2009).
- [21] D. Eichenberger and D. Baeriswyl, *Physical Review B* **76**, 180504(R) (2007).
- [22] D. Eichenberger and D. Baeriswyl, *Physical Review B* **79**, 100510(R) (2009).
- [23] Y. Sassa, M. Radovic, M. Månsson, X. Cui, S. Pailh s, E. Razzoli, S. Guerrero, M. Shi, P. R. Willmott, F. M. Granozio, J. Mesot, and L. Patthey, *submitted* (2009).
- [24] T. Kondo, R. Khasanov, Y. Sassa, A. Bendounan, S. Pailh s, J. Chang, J. Mesot, H. Keller, N. D. Zhigadlo, M. Shi, Z. Bukowski, J. Karpinski, and A. Kaminski, *Physical Review B* **80**, 100505 (2009).
- [25] V. Hinkov, D. Haug, B. Fauque, P. Bourges, Y. Sidis, A. Ivanov, C. Bernhard, C. T. Lin, and B. Keimer, *Science* **319**, 597 (2008).
- [26] D. Haug, V. Hinkov, A. Suchaneck, D. S. Inosov, N. B. Christensen, C. Niedermayer, P. Bourges, Y. Sidis, J. T. Park, A. Ivanov, C. T. Lin, J. Mesot, and B. Keimer, *Physical Review Letters* **103**, 017001 (2009).
- [27] A. Piriou, E. Giannini, Y. Fasano, C. Senatore, and Ø. Fischer, *submitted to Physical Review B* (2009).
- [28] B. W. Hoogenboom, C. Berthod, M. Peter, Ø. Fischer, and A. A. Kordyuk, *Physical Review B* **67**, 224502 (2003).
- [29] G. Levy de Castro, C. Berthod, A. Piriou, E. Giannini, and Ø. Fischer, *Physical Review Letters* **101**, 267004 (2008).
- [30] N. Jenkins, Y. Fasano, C. Berthod, I. Maggio-Aprile, A. Piriou, E. Giannini, B. W. Hoogenboom, C. Hess, T. Cren, and Ø. Fischer, *Physical Review Letters* **103**, 227001 (2009).
- [31] J. L. M. van Mechelen, D. van der Marel, C. Grimaldi, A. B. Kuzmenko, N. P. Armitage, N. Reyren, H. Hagemann, and I. I. Mazin, *Physical Review Letters* **100**, 226403 (2008).
- [32] W. Meevasana, X. J. Zhou, B. Moritz, C.-C. Chen, R. H. He, S.-I. Fujimori, D. H. Lu, S.-K. Mo, R. G. Moore, F. Baumberger, T. P. Devereaux, D. van der Marel, N. Nagaosa, J. Zaanen, and Z.-X. Shen, *New Journal of Physics* **12**, 023004 (2010).
- [33] Ø. Fischer, M. Kugler, I. Maggio-Aprile, C. Berthod, and C. Renner, *Reviews of Modern Physics* **79**, 353 (2007).
- [34] C. Dubois, G. Santi, I. Cunniff, C. Berthod, N. Jenkins, A. P. Petrović, A. A. Manuel, Ø. Fischer, S. M. Kazakov, Z. Bukowski, and J. Karpinski, *Physical Review Letters* **101**, 057004 (2008).
- [35] M. Brühwiler, S. M. Kazakov, J. Karpinski, and B. Batlogg, *Physical Review B* **73**, 094518 (2006).
- [36] J. Karpinski, N. D. Zhigadlo, S. Katrych, Z. Bukowski, P. Moll, S. Weyeneth, H. Keller, R. Puzniak, M. Tortello, D. Daghero, R. Gonnelli, I. Maggio-Aprile, Y. Fasano, Ø. Fischer, K. Rogacki, and B. Batlogg, *Physica C* **469**, 370 (2009).
- [37] M. Matusiak, Z. Bukowski, and J. Karpinski, *Physical Review B* **81**, 020510(R) (2010).
- [38] E. van Heumen, Y. Huang, S. de Jong, A. B. Kuzmenko, M. S. Golden, and D. van der Marel, arXiv:0912.0636 (2009).
- [39] N. D. Zhigadlo, S. Katrych, J. Karpinski, B. Batlogg, F. Bernardini, S. Massidda, and R. Puzniak, *Physical Review B* **81**, 054520 (2010).

Other references

- [40] H.-B. Yang, J. D. Rameau, P. D. Johnson, T. Valla, A. Tsvetlik, and G. D. Gu, *Nature* **456**, 77 (2008).
- [41] Y. Kohsaka, C. Taylor, K. Fujita, A. Schmidt, C. Lupien, T. Hanaguri, M. Azuma, M. Takano, H. Eisaki, H. Takagi, S. Uchida, and J. C. Davis, *Science* **315**, 1380 (2007).

- [42] E. Illes, E. J. Nicol, and J. P. Carbotte, *Physical Review B* **79**, 100505(R) (2009).
- [43] T. Giamarchi and C. Lhuillier, *Physical Review B* **43**, 12943 (1991).
- [44] A. Paramekanti, M. Randeria, and N. Trivedi, *Physical Review B* **70**, 054504 (2004).
- [45] T. Aimi and M. Imada, *Journal of the Physical Society of Japan* **76**, 113708 (2007).
- [46] R. W. Richardson, *Journal of Mathematical Physics* **6**, 1034 (1965).
- [47] E. Demler, S. Sachdev, and Y. Zhang, *Physical Review Letters* **87**, 067202 (2001).
- [48] S. Li, Z. Yamani, H. J. Kang, K. Segawa, Y. Ando, X. Yao, H. A. Mook, and P. Dai, *Physical Review B* **77**, 014523 (2008).
- [49] D. LeBoeuf, N. Doiron-Leyraud, J. Levallois, R. Daou, J. B. Bonnemaïson, N. E. Hussey, L. Balicas, B. J. Ramshaw, R. Liang, D. A. Bonn, W. N. Hardy, S. Adachi, C. Proust, and L. Taillefer, *Nature* **450**, 533 (2007).
- [50] J. Bok and J. Bouvier, in *The Gap Symmetry and Fluctuations in High-Tc Superconductors*, J. Bok, G. Deutscher, D. Pavuna, and S. A. Wolf, eds. (Kluwer Academic Publishers, New York, 2002), vol. 371 of *NATO Science Series: B*, p. 37.
- [51] J. Mesot, N. Metoki, M. Böhm, A. Hiess, and K. Kadowaki, *Physica C* **341**, 2105 (2000).
- [52] H. F. Fong, P. Bourges, Y. Sidis, L. P. Regnault, A. Ivanov, G. D. Gu, N. Koshizuka, and B. Keimer, *Nature* **398**, 588 (1999).
- [53] H. He, Y. Sidis, P. Bourges, G. D. Gu, A. Ivanov, N. Koshizuka, B. Liang, C. T. Lin, L. P. Regnault, E. Schoenherr, and B. Keimer, *Physical Review Letters* **86**, 1610 (2001).
- [54] M. Eschrig and M. R. Norman, *Physical Review Letters* **85**, 3261 (2000).
- [55] H. F. Fong, B. Keimer, P. W. Anderson, D. Reznik, F. Doğan, and I. A. Aksay, *Physical Review Letters* **75**, 316 (1995).
- [56] Y. Sidis, S. Pailhès, B. Keimer, P. Bourges, C. Ulrich, and L. P. Regnault, *Physica Status Solidi (b)* **241**, 1204 (2004).
- [57] J. C. Campuzano, H. Ding, M. R. Norman, H. M. Fretwell, M. Randeria, A. Kaminski, J. Mesot, T. Takeuchi, T. Sato, T. Yokoya, T. Takahashi, T. Mochiku, K. Kadowaki, P. Guptasarma, D. G. Hinks, Z. Konstantinovic, Z. Z. Li, and H. Raffy, *Physical Review Letters* **83**, 3709 (1999).
- [58] J. F. Zasadzinski, L. Ozyuzer, N. Miyakawa, K. E. Gray, and C. Kendziora, *Physical Review Letters* **87**, 067005 (2001).
- [59] P. Calvani, M. Capizzi, F. Donato, S. Lupi, P. Maselli, and D. Peschiaroli, *Physical Review B* **47**, 8917 (1993).
- [60] J. F. Schooley, W. R. Hosler, and M. L. Cohen, *Physical Review Letters* **12**, 474 (1964).
- [61] F. Gervais, J.-L. Servoin, A. Baratoff, J. G. Bednorz, and G. Binnig, *Physical Review B* **47**, 8187 (1993).
- [62] D. M. Eagles, M. Georgiev, and P. C. Petrova, *Physical Review B* **54**, 22 (1996).
- [63] C. Ang, Z. Yu, Z. Jing, P. Lunkenheimer, and A. Loidl, *Physical Review B* **61**, 3922 (2000).
- [64] C. Z. Bi, J. Y. Ma, J. Yan, X. Fang, B. R. Zhao, D. Z. Yao, and X. G. Qiu, *Journal of Physics: Condensed Matter* **18**, 2553 (2006).
- [65] G. Verbist, F. M. Peeters, and J. T. Devreese, *Ferroelectrics* **130**, 27 (1992).
- [66] J. Kuneš, T. Jeong, and W. E. Pickett, *Physical Review B* **70**, 174510 (2004).
- [67] K. Sasai, K. Hirota, Y. Nagao, S. Yonezawa, and Z. Hiroi, *Journal of the Physical Society of Japan* **76**, 104603 (2007).
- [68] B. C. Sales, A. S. Sefat, M. A. McGuire, R. Y. Jin, D. Mandrus, and Y. Mozharivskiy, *Physical Review B* **79**, 094521 (2009).
- [69] C.-Y. Moon and H. Choi, arXiv:0909.2916 (2009).
- [70] F.-C. Hsu, J.-Y. Luo, K.-W. Yeh, T.-K. Chen, T.-W. Huang, P. M. Wu, Y.-C. Lee, Y.-L. Huang, Y.-Y. Chu, D.-C. Yan, and M.-K. Wu, *Proceedings of the National Academy of Science of the USA* **105**, 14262 (2008).
- [71] T. M. McQueen, Q. Huang, V. Ksenofontov, C. Felser, Q. Xu, H. Zandbergen, Y. S. Hor, J. Allred, A. J. Williams, D. Qu, J. Checkelsky, N. P. Ong, and R. J. Cava, *Physical Review B* **79**, 014522 (2009).
- [72] H. Okamoto, *Journal of Phase Equilibria* **12**, 383 (1991).
- [73] H. Luetkens, H.-H. Klauss, M. Kraken, F. J. Litterst, T. Dellmann, R. Klingeler, C. Hess, R. Khasanov, A. Amato, C. Baines, M. Kosmala, O. J. Schumann, M. Braden, J. Hamann-Borrero, N. Leps, A. Kondrat, G. Behr, J. Werner, and B. Büchner, *Nature Materials* **8**, 305 (2009).
- [74] A. Jesche, N. Caroca-Canales, H. Rosner, H. Bormann, A. Ormeci, D. Kasinathan, H.-H. Klauss, H. Luetkens, R. Khasanov, A. Amato, A. Hoser, K. Kaneko, C. Krellner, and C. Geibel, *Physical Review B* **78**, 180504(R) (2008).
- [75] P. Nozières and E. Abrahams, *Physical Review B* **10**, 3099 (1974).
- [76] C. Cao, P. J. Hirschfeld, and H.-P. Cheng, *Physical Review B* **77**, 220506(R) (2008).
- [77] D. V. Evtushinsky, D. S. Inosov, V. B. Zabolotnyy, A. Koitzsch, M. Knupfer, B. Büchner, M. S. Viazovska, G. L. Sun, V. Hinkov, A. V. Boris, C. T. Lin, B. Keimer, A. Varykhalov, A. A. Kordyuk, and S. V. Borisenko, *Physical Review B* **79**, 054517 (2009).
- [78] C. Ren, Z.-S. Wang, H.-Q. Luo, H. Yang, L. Shan, and H.-H. Wen, *Physical Review Letters* **101**, 257006 (2008).
- [79] M. Hiraishi, R. Kadono, S. Takeshita, M. Miyazaki, A. Koda, H. Okabe, and J. Akimitsu, *Journal of the Physical Society of Japan* **78**, 023710 (2009).
- [80] P. Szabó, Z. Pribulová, G. Pristáš, S. L. Bud'ko, P. C. Canfield, and P. Samuely, *Physical Review B* **79**, 012503 (2009).
- [81] H. Q. Yuan, J. Singleton, F. F. Balakirev, S. A. Baily, G. F. Chen, J. L. Luo, and N. L. Wang, *Nature* **457**, 565 (2009).

Project 5

Novel electronic phases in strongly correlated electron systems

Project leader: M. Sigrist (ETHZ)

Participating members: D. Baeriswyl (UniFR), G. Blatter (ETHZ), E. Giannini (UniGE), D. Jaccard (UniGE), M. Kenzelmann, (PSI), D. van der Marel (UniGE), M. Sigrist (ETHZ), M. Troyer (ETHZ)

Summary and highlights: Progress on various novel and unusual electronic phases in heavy fermion materials, non-centrosymmetric transition metal monosilicides, ruthenates and materials with topological electronic structure is reported here. Among the heavy fermion superconductors, the so-called Q-phase of CeCoIn₅ receives at present most attention. Neutron scattering studies explore the interplay of incommensurate spin and pair density wave order, accompanied by several theoretical studies. CeCu₂Si₂ shows strong indication for valence fluctuations induced superconductivity and is broadly investigated using a multi-probe facility. While with the newly grown crystals of CeCoGe_{3-x}Si_x so far mainly magnetic properties have been studied, here also possibility appears to analyze an exciting non-centrosymmetric superconductor. In the field of vortex matter the dynamics of the vortex lattice in the crossover from the moderate to the strong pinning regime has been analyzed. Various alloys (Mn,TM)Si have been synthesized and studied for their magnetic properties, finding that in Mn_{1-x}Co_xSi the helical magnetic order is gradually suppressed and turns into a state with spin-glass properties. A theoretical discussion of the metamagnetic transition in Sr₃Ru₂O₇ elucidates the role of a peculiar type of staggered spin-orbit coupling. The character of the pressure induced semiconductor-semimetal transition in elemental Bi has been investigated by optical measurements. Features of topological phases play a role in the studies of chiral *p*-wave superconductivity in Sr₂RuO₄, the topological insulator state of Sb-doped Bi and in anyon model systems. Moreover, optical studies show progress in characterizing the hidden order phase of URu₂Si₂.

1 Superconducting Q-phase of CeCoIn₅

The interpretation of the low-temperature high-magnetic field phase of the heavy fermion superconductor CeCoIn₅ had been believed to be a good example of a Fulde-Ferrel-Larkin-Ovchinnikov (FFLO) phase. Recent measurements of this phase – nowadays called Q-phase – suggest, however, a more complex picture [1]. The Q-phase appears as an incommensurate spin-density wave state which only exists within the superconducting phase and disappears abruptly with the vanishing of superconductivity at the upper critical field. This finding implies for theoretical reasons that the superconducting order parameter (assumed to be of $d_{x^2-y^2}$ -wave symmetry) is supplemented by a pair density wave (PDW) component, i.e. a Cooper pair amplitude with finite total momentum corresponding to the incommensurate wave vector. In this project experimental as well as theoretical work on this subject is covered.

1.1 Experimental evidence by neutron scattering

Kenzelmann's group used high-field neutron diffraction to probe the magnetic order in the Q-phase for magnetic fields along the crystal-

lographic [1 0 0] direction ($\mathbf{H} \parallel [1 0 0]$). This is a different field direction than in previous experiments reported last year (see also [1]) where $\mathbf{H} \parallel [1 -1 0]$ was taken. By measuring the properties of the magnetic order for different field directions in the basal plane, it is possible to distinguish if the field-induced spin-density wave (SDW) in CeCoIn₅ is pinned to the direction of the field, or if it is pinned to the direction of the $d_{x^2-y^2}$ line nodes. Furthermore, this experiment allows to test some of the predictions of the theories which are based essentially on concepts close to FFLO idea.

The observed spin-density wave order for $\mathbf{H} \parallel [1 0 0]$ shows an incommensurate modulation $\mathbf{Q} = (q, q, 1/2)$ and $q = 0.45(1)$, which within the experimental uncertainty is indistinguishable from the spin-density wave found for fields applied along [1 -1 0] (Fig. 1). The magnetic order is thus modulated along the lines of nodes of the $d_{x^2-y^2}$ superconducting order parameter, suggesting that it is driven by the electron nesting along the superconducting line nodes. From their results Kenzelmann *et al.* postulate that the onset of magnetic order leads to the reconstruction of the superconducting gap function and a magnetically-induced pair density wave.

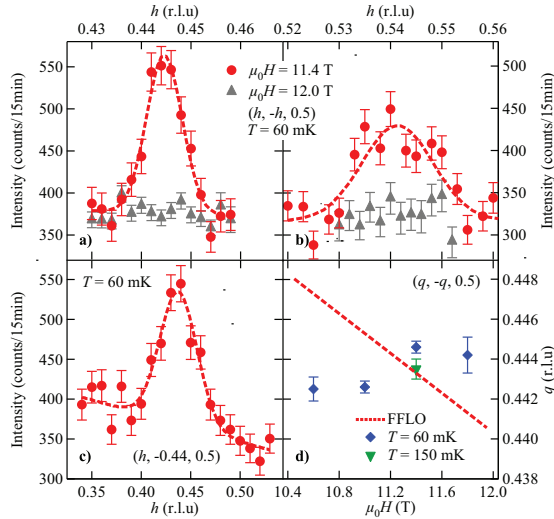


Figure 1: (a) Neutron diffraction intensity for wave-vectors $(h, -h, 0.5)$, showing the magnetic diffraction peak of the field induced magnetic order in the superconducting phase of CeCoIn_5 . (b) Intensity of the magnetic Bragg peak for wave-vectors $(h, -h, 0.5)$. (c) Tilt scan of the magnetic Bragg peak along $(h, -0.44, 0.5)$, showing that the magnetic order is long-range ordered along the flux line direction. (d) Magnetic field dependence of the incommensuration $h = q$. The solid line represents the expected field dependence of q predicted by Miyake [19].

1.2 Theoretical approaches to the Q-phase

Based on the early experimental results Agterberg, Sigrist and Tsunetsugu developed a phenomenological approach to the Q-phase which allows to identify possible symmetries of the pair density wave (PDW) [2]. The generalized Ginzburg-Landau theory, which describes, based on symmetry arguments, the coupling of the d -wave and the PDW order, still leaves a highly degenerated set of possible superconducting order parameters. Eventually, including the magnetic field as well as the coupling to the incommensurate magnetic order reduces the choice to two candidates. The resulting structure of the Ginzburg-Landau theory is compatible with the experimental finding of first and second order phase boundaries. Interestingly, the nucleation of the PDW order parameter on top of the d -wave state yields the possibility of complex vortex lattices of “split” vortices involving spatial separation of the zeros (vortex cores) of the two order parameter components. Moreover, the vortex lattice imprints its modulation on the spin-density wave order and would in this way give rise to magnetic Bragg peaks characteristic for the vortex lattice structure and observable conveniently by neutron scattering [2].

The more microscopic approach by Yanase and Sigrist starts by identifying the origin of the Q-phase as a FFLO state of the Larkin-Ovchinnikov type, i.e. a modulation of the d -wave order parameter magnitude, $\Delta_d(\mathbf{r}) = \Delta_{d0} \cos(\mathbf{Q} \cdot \mathbf{r})$ [3]. The π -phase difference of the order parameter passing through planes of zero node leads to zero-energy Andreev bound states. The accumulation of states at the Fermi energy in turn triggers an instability to an incommensurate spin-density wave order accompanied with a so-called “ π -triplet pairing” order equivalent to the PDW mentioned above (Fig. 2). From this consideration Yanase *et al.* make the prediction of the magnetic satellite peaks in addition to the known incommensurate Bragg peak. However, this has not been verified so far by neutron scattering experiments. While the theory by Miyake [19] based on the FFLO concept has been experimentally most likely ruled out, the present theory is still compatible with the present experimental status.

Both approaches have concentrated on mag-

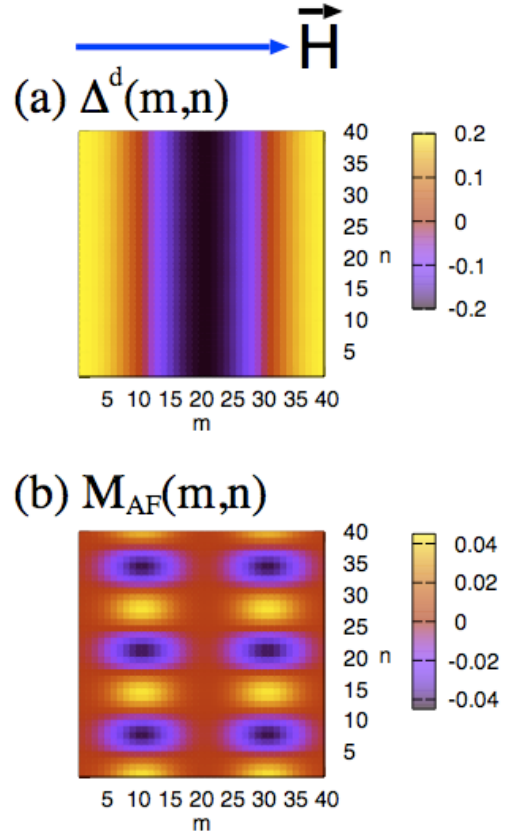


Figure 2: Results from the Bogolyubov-de Gennes approach: spatial modulation of (a) the d -wave pairing amplitude in the FFLO state with two zero nodes and (b) the z -component of the magnetic moment. The direction of the magnetic field is indicated by the arrow on the top.

netic fields along the $[1 \bar{1} 0]$ and have to be extended to other field directions in order to test their capability to reproduce the newest experimental developments.

2 CeCu_2Si_2 : new insights from magnetothermal measurements

CeCu_2Si_2 , the first identified example of a Ce-based heavy fermion (HF) superconductor, exhibits several interesting properties such as a complex H - T phase diagram at low temperature with two high-field magnetic phases called A (antiferromagnetic) and B. For a stoichiometric composition, superconductivity expels the spin-density wave (SDW) order at low magnetic field but the SDW is recovered in an over-critical magnetic field for superconductivity ("A/ S-type" CeCu_2Si_2).

Hydrostatic pressure has a pronounced influence on the antiferromagnetic (AF) and the superconducting (SC) properties of this system. The AF ordering vanishes at low pressure (~ 3.2 kbar) and the pressure dependence of T_{SC} was shown to exhibit several anomalies above 16 kbar [4]. It was observed that there exists a distinct superconducting phase in CeCu_2Si_2 under high pressure ($T_{\text{SC}} \approx 2$ K, $p \approx 4$ GPa), well beyond the superconducting phase at ambient pressure ($T_{\text{SC}} \approx 0.7$ K). While the superconducting phase at ambient pressure is believed to be due to critical spin fluctuations, the second one is suggested to be mediated by critical valence fluctuations near a second quantum critical point (QCP) [4][20]. The main motivation of the work by Jaccard and coworkers is to understand the nature and mechanism of the SC state at ambient as well as at high pressures through multiprobe measurements (resistivity, ac heat capacity, thermoelectric power, Hall and Nernst effect) in a single experimental setup. Here they are reporting some of their preliminary results of the Nernst effect at ambient pressure.

One high-purity single-crystal of CeCu_2Si_2 is used for the present study and is cut in a square shape ($600(l) \times 576(b) \times 25(w)$ μm^3). Different contacts are made in such a way so that it can be directly inserted into a pressure cell. The SC ordering temperature, determined from the onset of vanishing resistivity, is found to be 780 mK. This value is quite high compared to other reports on this system. Fig. 3 shows the Nernst signal, N , under external magnetic fields. Fig. 3a indicates the N below the SC temperature (T_{SC}) and Fig. 3b above ($T > T_{\text{SC}}$). The maximum field, applied perpendicular to the $a - b$ plane, is 8 T. At the low-

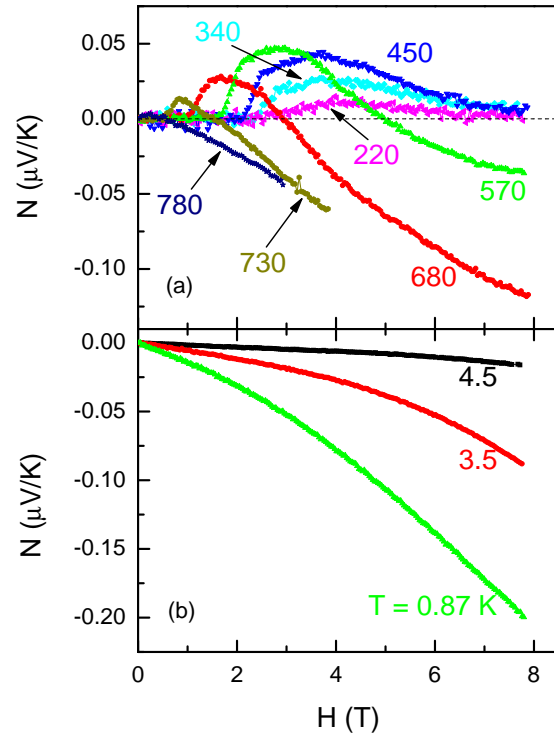


Figure 3: Nernst voltage plotted against magnetic field at different temperatures, (a) below the ordering temperature ($T < T_{\text{SC}}$) and (b) above ($T > T_{\text{SC}}$).

est temperature (220 mK) N exhibits a broad maximum at around 4 T, which is substantially above the critical field. Note that this maximum is shifted towards lower fields, but the magnitude of the maxima keeps increasing up to 570 mK. While the peak position is observed to decrease monotonically with temperature, the magnitude starts decreasing above 570 mK. The maximum ceases to exist near the T_{SC} . It is also noticed that there is a sign change starting at 570 mK, at around 5 T. The value of the fields where the sign change in the Nernst signal starts are also found to be a decreasing function of temperature. Moreover, note that, above T_{SC} , the Nernst signal is linear only up to small applied fields. Above a certain value it becomes non-linear and the non-linearity increases as one moves from 4.5 K to 0.87 K.

The H - T phase diagram is shown in Fig. 4. The open circles represent the melting curve, i.e. the field at which resistivity deviates from zero value, whereas the onset from the normal to SC states is marked by the open rectangles. The green triangles indicate the onset of the Nernst signal, which is quite close to the melting curve. The closed red circles describe the value of magnetic fields where the Nernst signal is maximum. It is interesting to note that the Nernst signal is significant only above the melting curve, i.e. above the SC state or in A-

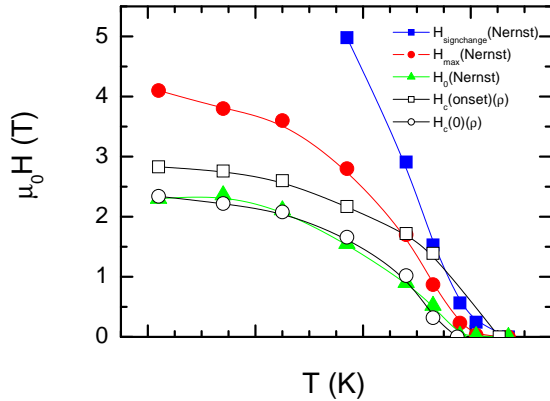


Figure 4: $H - T$ phase diagram obtained from the Fig. 3 (details see text).

phase, and this is even more obvious in Fig. 5. Figs. 5a, b and c describe the resistivity at 1, 2 and 3 T respectively and the corresponding Nernst signals at those fields. It is quite obvious that at 3 T, which is quite well inside the A-phase, the Nernst signal is non-negligible and its magnitude remains the same as for applied fields smaller than the upper critical field. This points towards the fact that the dominant contribution of the Nernst signal arises from the antiferromagnetic A-phase and not from the

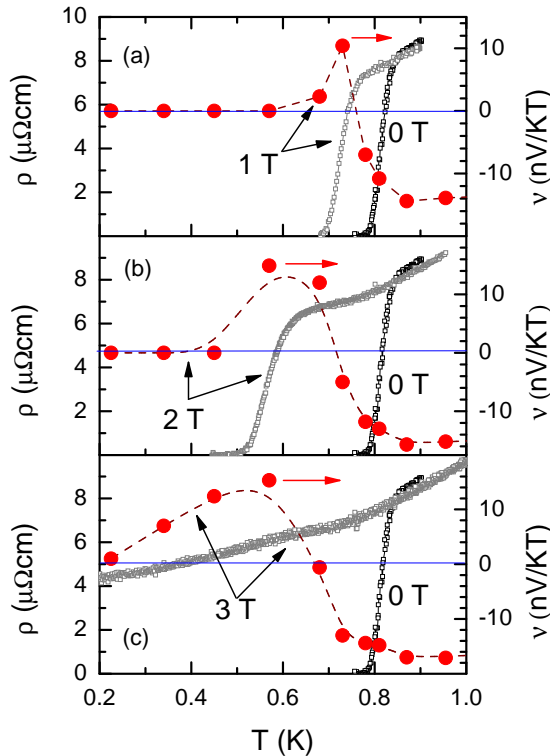


Figure 5: The Nernst coefficient and resistivity versus temperature are shown at (a) 1 T, (b) 2 T, and (c) 3 T. In all these plots, the zero-field resistivity is shown as a reference.

vortex state which is commonly found in different SC systems.

Similar investigations at high pressures are already underway.

3 Crystal growth of $\text{CeCoGe}_{3-x}\text{Si}_x$

CeCoGe_3 is a heavy fermion material showing at ambient pressure antiferromagnetic (AF) order which can be suppressed by pressure to lead to a superconducting phase, which is a recently discovered example of a non-centrosymmetric superconductor. Giannini and coworkers have studied the magnetic properties at ambient pressure for modified chemical composition. The substitution of silicon for germanium in CeCoGe_3 drives this material from the long-range AF order ($0 \leq x \leq 1$) to short-range AF order (up to $x_c = 1.2$). At such critical concentration, associated to a quantum phase transition (QPT), non-Fermi-liquid behavior is observed. This point separates the magnetic and non-magnetic regimes at $T = 0$ [21]. The understanding of the nature of the magnetic excitations in this material requires high-purity single-crystals of various compositions.

Single-crystals of the end compound CeCoGe_3 can be grown in a flux of either Sn or Bi. In order to grow Si-doped crystals, Giannini and coworkers have improved the same method by optimizing the temperature profile of the thermal treatment and the starting composition. Whereas crystals of pure CeCoGe_3 have been successfully grown up to a mm^3 size, in the presence of Si some problems have to be overcome. Si-doped crystals do not grow larger than 0.5 mm and growth dislocations appear at the surface of Si-doped crystals. Two typical crystals of pure CeCoGe_3 and $\text{CeCoGe}_{2.9}\text{Si}_{0.1}$ are shown in Fig. 6. Despite the growth terraces visible at the surface of the crystal, the composition is highly homogenous. The major problem in growing Si-doped crystal is the upper limit of Si entering the structure. Whereas highly homogeneous polycrystalline samples

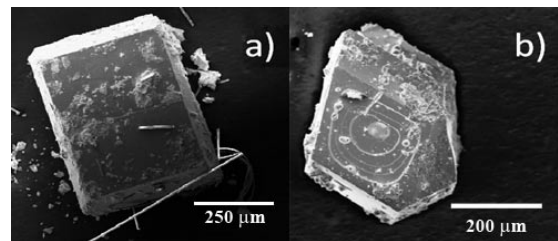


Figure 6: Crystals of (a) CeCoGe_3 , and (b) $\text{CeCoGe}_{2.9}\text{Si}_{0.1}$.

of the whole solid solution ($0 \leq x \leq 3$) can be processed, when growing crystals with nominal $x > 0.1$ secondary phases form (CoSi, elemental Ge, other Bi-alloys). This changes the melt composition and prevents the formation of crystals with the wanted stoichiometry. Further improvements of the growth technique, like changing the flux and tuning the optimum Si-rich starting composition, are in progress, in order to push the Si fraction to higher values.

4 Superconductivity and ferromagnetism in multilayers

Recent experiments on superconductor-ferromagnet (SC-FM) multilayers [5] revealed a complicated interplay between superconductivity and ferromagnetism. For instance, the onset of superconductivity was found to change qualitatively the magnetic state of the ferromagnetic layers. These findings have motivated Baeriswyl and coworkers to investigate such SC-FM multilayers theoretically. In a first step they address the question to what extent the superconducting order parameter and the free energy are affected by the relative orientation of the magnetic moments of the adjacent FM layers. The ferromagnet is modeled using Stoner-like majority/minority bands. A fixed relative angle of magnetic moments in consecutive FM layers (spiraling magnetization) is considered. The superconducting material is assumed to be described by a spin-singlet BCS state. In the multilayer, the superconducting order parameter is allowed to vary spatially. A spin-dependent potential combined with

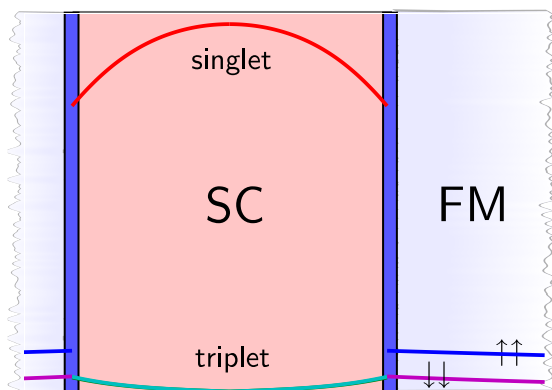


Figure 7: The spatial dependence of the anomalous amplitude for normal impact of the quasi-particle trajectory. The model parameters are typical material parameters for the multilayers used in the experiment, i.e. $T = T_c/2$, width of a single-layer 10 nm, coherence length 3.3 nm. Note the slowly decaying triplet correlations in the FM layer and the triplet correlations inside the SC layer.

Rashba spin-orbit coupling is assumed to act at the interface. The resulting spin-flip processes can generate spin-triplet pairs which may penetrate into the ferromagnet and tunnel to the next SC layer (Fig. 7). In this way two consecutive SC layers can be coupled.

5 Vortex matter: dynamic approach to strong pinning

Flux lines threading a type II superconductor exposed to a magnetic field are moved when subject to a Lorentz force, thereby generating dissipation. Electrical conduction without resistance can be reestablished by inhibiting the motion of the vortices, i.e. by pinning them by a defect-induced potential. The classification of the regimes of weak collective pinning (WCP, pinning due to joint action of many pins) and strong pinning (SP, pinning due to individual pins) can be achieved using a Labusch criterion [22] and a detailed study of the two regimes and the crossover between them in the static case was performed by Blatter *et al.* [6].

The study of the dynamics within WCP is usually restricted to a perturbative treatment of the random pinning potential at large transport currents $j > j_c$ (critical current j_c) [23]. In this project, Blatter and coworkers focus on the dynamics near the SP/WCP crossover and above in the SP regime. They determine the full force-velocity (current-voltage) relation within a generic model for the pinning of a three-dimensional, homogeneous, isotropic elastic manifold with a one-dimensional displacement field $u(\mathbf{r}, t)$ and elastic constant C . Unlike previous attempts [24], they include the full dynamics of the manifold and solve the relevant equation for a single pin at the origin (range σ , strength f_0) coupling to a specific point of the manifold; the latter then exhibits a non-trivial time evolution $y(\tau) = u(0, \tau t_0)/\sigma$, where time is measured in units of $t_0 = \eta r_0^2/\sigma$, η the viscosity, and distance in units of the width σ of the defect (a short-distance cutoff $r_0 \sim \xi$ is used). Making use of the Green's function $g(\tau) = (1 + \tau)^{-3/2}$ of the elastic problem, one obtains

$$y(\tau) = y_\infty(\tau) + \int_{-\infty}^{\tau} d\tau' \frac{f_p[y(\tau')]}{2f_{\text{Lab}}} g(\tau - \tau'), \quad (2.1)$$

where $y_\infty(\tau) = v\tau - 1$ is the position of the manifold at infinity. Here, $v = vt_0/\sigma$ is the dimensionless velocity and $f_{\text{Lab}} = 4\pi^{3/2}C\sigma r_0$ the Labusch force.

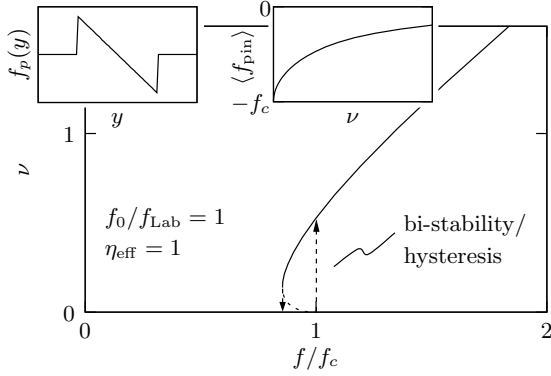


Figure 8: Exact force-velocity (current-voltage) relation $v(f)$ of a three-dimensional manifold pinned by dilute parabolic pins of strength f_0 and range σ . The insets show a sketch of the linear force $f_p(y)$ exerted by a parabolic pin and the resulting velocity-dependence of the pinning force density $\langle f_{\text{pin}} \rangle$. Note that the pinning force density decreases like $\langle f_{\text{pin}} \rangle \sim \sqrt{v}$, leading to a bi-stability in $v(f)$ for all values of η_{eff} .

For a linear force model $f_p(y) = -f_0 y$, $y \in [-1, 1]$ (Fig. 8, left inset), Eq. (2.1) can be solved exactly with the help of the Laplace transform. Note that for this potential (with sharp edges) pinning is maximally strong as the Labusch criterion $\max[f'(y)] > f_{\text{Lab}}$ is always fulfilled at $y = \pm 1$. The resulting velocity-dependence of the pinning force density $\langle f_{\text{pin}} \rangle(v)$ is found through combined time and disorder averages (Fig. 8, right inset).

Using the effective viscosity $\eta_{\text{eff}} \sim f_{\text{Lab}}/f_c \xi^3$ (critical force density f_c), the force-balance equation $f/f_c + \eta_{\text{eff}} v + \langle f_{\text{pin}} \rangle(v)/f_c = 0$ determines the force-velocity relation $v(f)$ (Fig. 8) which reveals a bi-stable region.

In order to investigate the dynamics in a moderately SP regime, Blatter and coworkers consider a piecewise linear force allowing for the tuning of the Labusch parameter f_I/f_{Lab} (f_I the initial force gradient pulling the vortex into the pin, $f_I = \infty$ in the above case). Blatter and coworkers find that close to the crossover to weak pinning a bi-stability in $v(f)$ only appears for sufficiently small viscous coefficient η_{eff} . The determination of the detailed criteria for the appearance of the bi-stability is part of ongoing work.

6 Sr₂RuO₄: chiral p -wave superconductivity

There is strong evidence that Cooper pairing has chiral p -wave character in Sr₂RuO₄, i.e. the gap function can be represented by $d(\mathbf{k}) = \Delta_0 \hat{z}(k_x \pm ik_y)$ involving a finite orbital angular momentum along the z -axis for the Cooper pairs ($L_z = \pm \hbar$). During this project period

Sigrist and collaborators addressed two effects connected with the chiral nature of the superconducting order parameter.

6.1 Chiral domains and the Josephson effect

A few years ago van Harlingen's group reported anomalous interference effects for Josephson junctions between Sr₂RuO₄ and Pb in a magnetic field [25]. These experimentalists claimed that their result is evidence for the presence of chiral domains. Domain walls intersecting the Josephson junction could lead to an order parameter phase structure along the junction which induces characteristic deviations from the standard Fraunhofer-like interference pattern. Bouhon and Sigrist analyze the basic conditions for such a kind of behavior using a Ginzburg-Landau model for domain walls and the Josephson effect [7]. They notice that the domain wall structure has to satisfy certain conditions in order to account for the observed effects. In particular, they find that the domain wall orientation as well as the degree of Fermi surface anisotropy play an important role in this context. For certain special directions domain walls undergo a symmetry breaking phase transition in their internal structure as a function of system parameters, which can be essential for the observed interference properties. Additionally they find that magnetic fields can modify domain wall states such that a hysteretic behavior is possible, in qualitative agreement with experiments, as displayed in Fig. 9. Moreover, on the same footing characteristic noise behavior can be explained.

6.2 Evolution of spontaneous flux in eutectic Ru-Sr₂RuO₄

Eutectic Ru-Sr₂RuO₄ containing μm -size Ru-metal inclusions in Sr₂RuO₄ are known for the occurrence of the so-called 3 Kelvin phase – an inhomogeneous superconducting phase above the bulk transition. Superconductivity nucleates most likely at the interface between Ru and Sr₂RuO₄. Ru-metal itself becomes superconducting at $T_{c\text{Ru}} = 0.5$ K well below the critical temperature $T_c = 1.5$ K. Kaneyasu and Sigrist study the properties of the s -wave superconducting phase in a single cylinder shaped Ru-inclusion [8]. The chiral nature of the surrounding superconductor imposes through Josephson coupling a phase winding on the s -wave order parameter of Ru: $\psi_s(r = R) \propto e^{i\theta}$ (R : cylinder radius). Immediately below $T_{c\text{Ru}}$ the external phase winding yields a flux pattern on the interface between

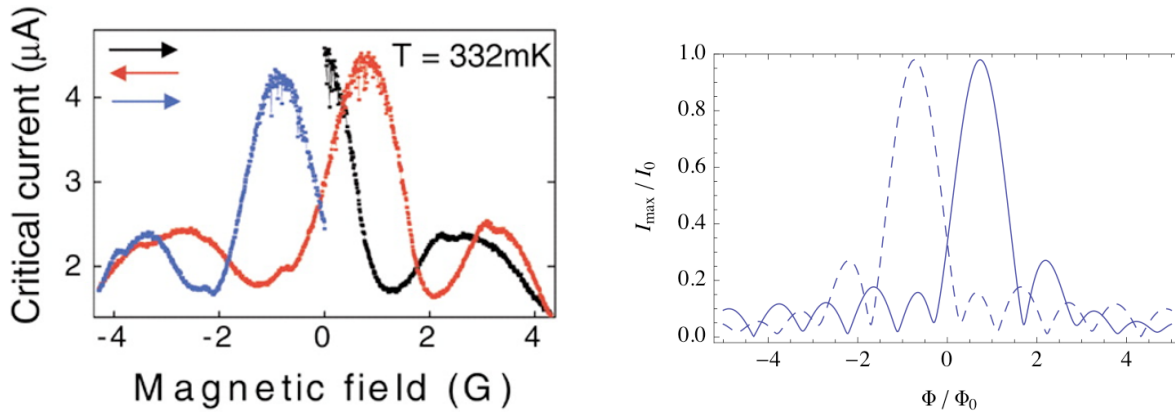


Figure 9: Left panel: experimentally observed hysteretic behavior of the field dependence of the Josephson critical current in a junction between Sr_2RuO_4 and Pb (black curve is the initial up-sweep of the magnetic field, while red and blue curves correspond to subsequent down and upsweps respectively) (from Kidwingira et al. [25]). Right panel: simulation of hysteretic behavior where the solid (dashed) line describes the critical current during a down-sweep (up-sweep) of the magnetic field.

Ru and Sr_2RuO_4 without net magnetic flux. This is an effect of phase frustration between the two superconductors. As temperature is lowered the flux pattern deforms to well-localized flux line and an extended counter flux. Eventually at low enough temperature the flux line jumps from the interface to interior of the Ru-inclusion as a ordinary vortex, while the compensating flux remains uniformly spread over the interface. While such a spontaneous flux pattern may be experimentally observable by a scanning SQUID microscope, it could also have interesting influence on quasi-particle tunneling and the Josephson effect through the interface. These latter aspects will be studied in the coming project period.

7 Spin-glass ground state in transition metal monosilicides TMSi

The helimagnetic state of MnSi is rapidly suppressed by doping with either Fe, Co or Ni. Above a given doping threshold (~ 0.2 electrons/transition metal (TM)-atom) the material enters a new magnetic ground state, never reported so far. The transition temperature of (Mn,TM)Si does not depend on the particular doping element but only on the total number of electrons in the outermost shell [9]. The transition from the helimagnetic to the new ground state is characterized by a change of sign of the Weiss temperature, indicating an antiferromagnetic interaction, and an upturn in the resistivity at low temperature. In order to elucidate the nature of such a magnetic state and the origin of the charge localization, a complete set of experimental investigations has been carried out, namely magnetic

and transport measurements, neutron diffraction, and muon-spin relaxation (μ SR) experiments. Strong indication of a spin freezing into a glass state in $Mn_{1-x}Co_xSi$ ($0.05 < x < 0.9$) is provided by the frequency-dependence of the transition temperature in ac magnetic susceptibility (Fig. 10a and b). The occurrence of a spin-glass state is confirmed by μ SR experiments. The randomly distributed potential wells introduced by the Co doping can localize itinerant electrons and create local spins. This causes a decrease of the electrical conductivity with cooling (Fig. 10c) and, below the transi-

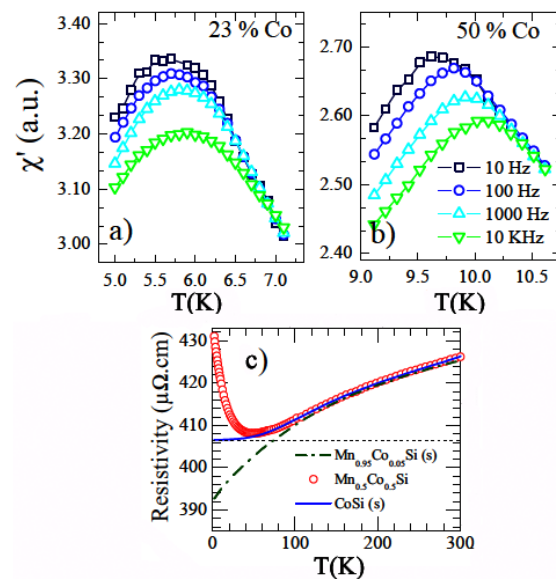


Figure 10: (a) and (b) ac susceptibility at various frequencies for the Co atomic fractions 23% and 50%, respectively. (c) Resistivity of the spin-glass $Mn_{0.5}Co_{0.5}Si$, compared to that of helimagnetic $Mn_{0.95}Co_{0.05}Si$ and pure CoSi.

tion temperature T_g , the freezing of localized spins into a spin-glass state. Differently from FeSi, the system remains a metal at low temperature. A spin-glass ground state is therefore added to the already rich phase diagram of “B20” transition metal silicides.

8 Metamagnetism in bilayer ruthenates

Ultraclean samples of the bilayer ruthenate, $\text{Sr}_3\text{Ru}_2\text{O}_7$, display a metamagnetic transition at fields between 5 and 8 T depending on the field orientation [26, 27]. It has been found that at temperatures below 1 K a new phase appears around the transition, yielding additional anomalous structures into the magnetization curve. The character of this phase, which has only been observed for fields perpendicular to the layers, has not been identified so far. One of the most popular proposals is a so-called nematic phase which results from a Pomeranchuk instability deforming the Fermi surface [28, 29]. Sigrist and collaborators address two problems in this context assuming a $d_{x^2-y^2}$ -type nematic instability for this low-temperature phase. First, Adachi and Sigrist consider a possibility to identify the phase by means of ultrasound absorption above the phase transition taking fluctuation effects into account [10]. They show that there are clear selection rules for the propagation direction and polarization of the ultrasound visible in the absorption rate and the sound velocity renormalization. As a result there is a softening for transverse modes along the $[1\ 1\ 0]$ propagation direction while no softening should be observed along $[1\ 0\ 0]$. Surprisingly the calculations show that for longitudinal modes the softening occurs in all directions. Moreover in the same study renormalization effects have been analyzed using a self-consistent renormalization scheme in order to elucidate the modifications of the phase diagram through quantum and thermal fluctuations [10].

The puzzling field anisotropy of the metamagnetic transition and the low-temperature phase cannot be simply explained by assuming an anisotropic g -tensor. Therefore Fischer and Sigrist extend the analysis of spin-orbit effects by taking specific lattice properties of $\text{Sr}_3\text{Ru}_2\text{O}_7$ into account [11]. In this layered perovskite structure the RuO_6 -octahedra are rotated around the c -axis such that a staggered inversion symmetry breaking occurs for all in-plane bonds. The resulting spin-orbit coupling leads to a Fermi surface reconstruction (FSR), if a magnetic field is applied in the

basal plane. No such effect appears for fields along the c -axis. The mechanism for a nematic instability is based on a specific form of forward scattering and occurs when the chemical potential moves through a Van Hove singularity (VHS) – this may be also the origin of the metamagnetic transition [12]. The FSR for in-plane fields removes spectral weight from the VHS such that the nematic instability is suppressed. This finding is in qualitative agreement with the experimental observation which only reports a low-temperature phase for fields along the c -axis with little in-plane components. The FSR is accompanied with an induced staggered magnetic moment of the Ruthenium sites in addition to the uniform magnetization. Therefore this study predicts the presence of a canted antiferromagnetic spin component in fields around the metamagnetic transition, which could be possibly observed in neutron scattering experiments.

9 Processing and crystal growth of topological insulators

The growth of Sb-doped Bi-crystals has been pursued by Giannini and collaborators in order to study their exciting electronic properties by tuning the Sb-content. The most attracting peculiarity of this system is the topological Dirac insulating behavior. Other materials have been predicted to exhibit a topological insulating state, and the recent activity of the Giannini group has mostly focussed on Bi-chalcogenides, predicted to be simplest 3D topological insulators [30]. In the V_2VI_3 compounds ($V = \text{As, Sb, Bi}$; $VI = \text{Se, Te}$), the physical properties can be tuned by controlling the composition in the solid solution $(\text{Sb,Bi})_2(\text{Se,Te})_3$. It is expected that in Sn-doped samples, $(\text{Bi}_{1-x}\text{Sn}_x)_2\text{Te}_3$, Sn doping can be adjusted to observe only the surface states. Single-crystals of $(\text{Bi}_{1-x}\text{Sn}_x)_2\text{Te}_3$ have been grown using a controlled cooling method, starting from stoichiometric mixtures of Bi, Te and Sn in vacuum sealed reactors. After heat-

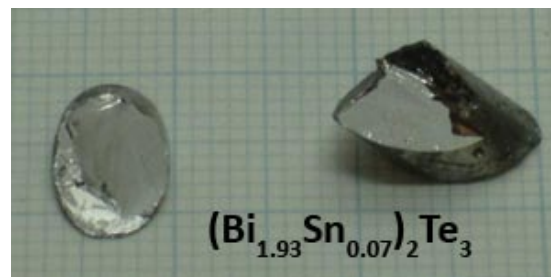


Figure 11: Crystals of $(\text{Bi}_{1-x}\text{Sn}_x)_2\text{Te}_3$.

ing, melting, and homogenizing at 700°C for 24 hours (repeated several times), the samples were heated at 850°C for 16 h and slowly cooled at 5°C/h to 400°C in a thermal gradient of $\sim 5^\circ\text{C}/\text{cm}$. Crystals grown with this method are shown in Fig. 11.

10 Pressure tuned semimetal-semiconductor transition in Bi

Since the seminal work of Wigner in 1930's, it has been believed that the large relative electron-electron interactions in low-density electron gases manifest themselves in a variety of novel phases like electronic crystals, correlated heavy electron fluids, and phase separated states. In principle elemental bismuth is a model system to investigate such physics. It is a semimetal with a small valence and conduction band overlap that results in three small electron Fermi pockets (at the L points) and a hole Fermi pocket (at the T point), massive Dirac electronic dispersions and an equal (small) number of electrons and holes [31]. A material which has been of interest for a long time with many remarkable properties [31], elemental bismuth has recently been found to be host to a variety of exotic electronic phenomena, including phase transitions at high field to a "valley-ferromagnetic" state [32], signatures of charge fractionalization in the ultraquantum high-field limit [33], and strongly coupled electron-plasmon "plasmaron" features in the optical spectra [13]. Lately, it has been claimed that $\text{Bi}_{1-x}\text{Sb}_x$ alloys are "topological insulators", with robust topologically protected surface states [34].

Among its remarkable phenomena, bismuth undergoes an interesting semimetal-semiconductor (SMSC) transition with the application of modest pressures ($\approx 20 - 25$ kbar) [35, 36]. This transition is relatively under-investigated [37, 35], but unlike more conventionally discussed Mott or Anderson-style metal-insulator transitions driven by interactions or disorder respectively, this transition is believed to be driven by a reduction of the semimetal conduction and valence bands overlap. As the overlap decreases, Fermi surfaces shrink and eventually vanish. Within a non-interacting purely band point of view this is an electronic topological transition of the "Lifshitz" variety [38]. It is unclear however which role is played by electronic correlations on the approach to the transition. Do interaction effects dominate as the charge density decreases resulting in a strongly correlated liquid state? Perhaps

the topological "Lifshitz" band transition is superseded by a phase like an electronic crystal [39, 40], excitonic insulator [41], or inhomogeneous state [42].

The application of pressure to bismuth reduces the overlap of the semimetal bands and eventually results in a semimetal-semiconductor (SMSC) transition. This transition is nominally of the "Lifshitz" Fermi surface topological variety, but there are open questions about the role of interactions at low-charge densities. Using a pressure cell with optical access developed by the group of Forró, the van der Marel group has performed an extensive study of its infrared conductivity under pressure. In contrast to the expected pure band behavior, signatures were observed of enhanced interaction effects, including strong charge-plasmon coupled (plasmaron) features [13] and plasma frequency which remains finite through the transition. Interactions appear to play a central role in driving the transition and hence it is not of the pure "Lifshitz" band variety. At first glance, the appearance of strong correlation features in the optical spectra and their role in the SMSC transition for this pressure range is surprising. Although bismuth is a low-density metal (approximately one charge per 10^5 atoms), in which one might expect strong correlation effects [39, 40], in reality the effective dimensionless Wigner-Seitz radius r_s at ambient pressure is small due to a large ϵ_∞ and small effective mass (for parabolic bands $r_s = \frac{me^2}{n^{1/3}\hbar^2 4\pi\epsilon_\infty} \approx 1.3$). Even at the highest pressure, $r_s \approx 2.3$ does not approach the regime at which a 3D Wigner crystal is believed to exist ($r_s = 62 - 100$ [40, 43]). However, there are a number of aspects of bismuth which may allow such physics to occur at even moderate values for r_s . Firstly, we should remind ourselves that typical calculations which estimate the significance of r_s are typically based on the jellium approximation, which may have only a passing relevance to real materials. In the case of bismuth, the breaking of Galilean invariance by the presence of both electrons and holes allows a pairwise interaction that is not relevant for translational invariant systems. It has been shown that there is a strong tendency for Coulomb crystallization in two components plasmas at densities where r_s is of order of unity. This is far below that necessary in one-component systems [44]. Such a tendency is reinforced in systems with a large mass asymmetry as in bismuth.

At first glance the effect of pressure is similar to the effect of temperature; the charge density decreases as the band overlap decreases. This

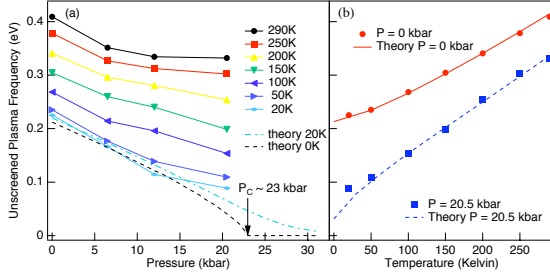


Figure 12: (a) Plasma frequency as a function of pressure at various temperatures. This quantity becomes very small in a region close to the expected critical pressure ($P_c \approx 23$ kbar) of the SMSC transition in bismuth. (b) Temperature dependence of the plasma frequency at ambient pressure and at 20.5 kbar as a function of temperature.

behavior is summarized in Fig. 12, where, as a function of pressure, the plasma frequency (ω_p) of the zero-frequency Drude component from a Drude-Lorentz fit to the reflectivity data is plotted at different temperatures. In Fig. 12, the data are compared to a theoretical calculation of the Drude spectral weight. The computation was done taking into account three different types of carriers near by the Fermi level [45]: (i) heavy holes (hh) at the T point which have a standard massive dispersion $\epsilon_k^{hh} = \hbar^2 k^2 / m_k^{hh}$; (ii) light electrons (le) and their light hole (lh) counterparts at the three-fold degenerate L point, for which the energy dispersion is $\epsilon_k = \Delta - \epsilon_g / 2 \pm \sqrt{\epsilon_g^2 / 4 + \hbar^2 |k \cdot v_F|^2}$ where ϵ_g is the direct gap between the two light bands.

Although in the whole accessible pressure range the system is liquid, it seems likely that the system is in a regime where incipient crystallization is manifesting itself. Alternatively, one may be seeing the consequence of excitonic scattering [46] or correlations [41] near the SMSC transition as is believed to be the case in $\text{TmSe}_{0.45}\text{Te}_{0.55}$ [47]. Other possibilities include the spontaneous formation of metallic inhomogeneous states such as microemulsions [42] or phase-separated electron-hole droplets [48]. Irrespective of this behavior's origin, it is shown here that correlation effects play a central role in the SMSC and need to be taken into account to describe it properly. Near the SMSC transition of bismuth, the expected "Lifshitz" transition appears to be superseded by strong correlation effects.

11 Hidden order in URu_2Si_2

Since more than two decades, the origin of the enigmatic low-temperature phase in

URu_2Si_2 [49] is still a mystery [50, 51]. At $T_{\text{HO}} = 17.5$ K, all the thermodynamical and transport measurements exhibit a clear anomaly and suggest a Fermi surface reconstruction. Therefore, this low-temperature phase is called *hidden order* and despite all the theoretical and experimental efforts, the order parameter which characterizes this phase remains unknown.

The van der Marel group has measured the detailed temperature dependence of the optical conductivity of URu_2Si_2 for electric field along the a -axis and the c -axis of the tetragonal structure. A temperature-frequency colorplot of the real part of the conductivity is displayed in Fig. 13. In addition to a pronounced anisotropy, one can see a clear partial suppression of the optical conductivity between 50 cm^{-1} and 200 cm^{-1} below 25 K, corresponding to a sharp crossover. This temperature is well above the thermodynamic phase transition at T_{HO} . Moreover, it was shown that this behavior is accompanied by a renormalization of the plasma frequency and the scattering rate. These observations imply that electronic states located within a few meV from the Fermi

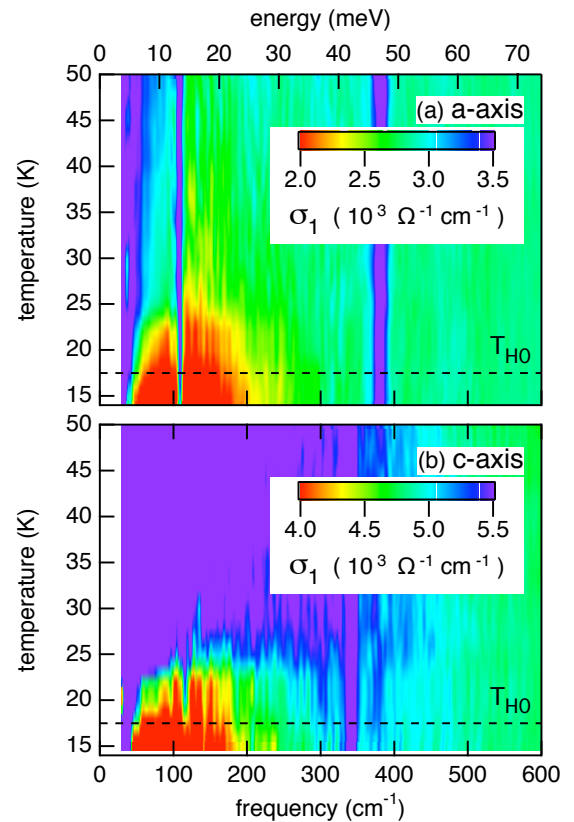


Figure 13: Temperature-frequency colorplot of the real part of the conductivity. The dash horizontal line corresponds to the known hidden-order temperature, $T_{\text{HO}} \sim 17.5$ K.

level start to slide when the temperature is decreased below 25 K.

12 Numerical simulation of complex quantum phases

The efforts by Troyer's group on the computational side of this project are focussing on the development of new schemes to treat complex strongly correlated electron systems and on the numerical simulation of complex phases in particular those with topological character.

12.1 Algorithmic developments

The main algorithmic development of the past year is the development of a diagrammatic quantum Monte Carlo (DiagMC) algorithm for the Hubbard model [14]. This algorithm samples connected Feynman diagrams instead of the partition function and works successfully in the correlated Fermi liquid regime of the Hubbard model. It will be used in the future to calculate phase diagrams and equations of state of 2D and 3D Hubbard model in the moderately correlated regime

12.2 Topological phases and anyonic models

A topological quantum liquid phase, if realized in an experiment, would pave the way towards stable, robust and decoherence-free quantum bits: it can encode information in a non-local topological property and no local source of noise can disturb this quantum bit. In this context, Troyer and coworkers have performed the following investigations. They have shown that the critical gapless ground states of these models are due to an unusual symmetry [15], and have calculated the phase diagrams of spin-1 models [15]. Similar phases have been found in related anyonic models on high-genus surfaces [16, 17]. These models allow a simple and intuitive graphical visualization of topological phases and models giving rise to such phases.

Scarola in Troyer's group has contributed significantly to a publication with experimentalists [18], who have been able to see the dispersion relation of quasi-particles and especially a roton minimum which had been first calculated by Scarola several years ago.

13 Collaborative efforts

Several subprojects involve collaborative efforts fostered by the MaNEP network. The foremost example is the study of the Q -phase which at its starting state was already based

on close interaction between the Kenzelmann group on the experimental and the Sigrist group on the theory side. During the last year both experimental and theoretical progress evolves in mutual contact. A further important case is the field of topological phases which encompasses a wide range of materials, the topological insulators, as Sb-doped Bi (Giannini, van der Marel and Morpurgo), chiral p -wave superconductors (Sigrist) and model cases (anyon models and quantum Hall systems) in the context of quantum computation (Troyer). A new collaborative project, named "Topomatter", is devoted to topological insulators and related systems, which involve mainly contributors of this project (van der Marel, Sigrist and Morpurgo). While for other subprojects there are at present no immediate collaborations between theory and experiment, there is an obvious overlap in interest due to previous studies. This is particularly true for the transition metal silicides and the non-centrosymmetric and heavy fermion superconductors, including hereby also the hidden order system URu₂Si₂.

MaNEP-related publications

- [1] M. Kenzelmann, T. Strässle, C. Niedermayer, M. Sigrist, B. Padmanabhan, M. Zolliker, A. D. Bianchi, R. Movshovich, E. D. Bauer, J. L. Sarrao, and J. D. Thompson, *Science* **321**, 1652 (2008).
- ▶ [2] D. F. Agterberg, M. Sigrist, and H. Tsunetsugu, *Physical Review Letters* **102**, 207004 (2009).
- ▶ [3] Y. Yanase and M. Sigrist, *Journal of the Physical Society of Japan* **78**, 114715 (2009).
- [4] A. T. Homes, D. Jaccard, and K. Miyake, *Physical Review B* **69**, 024508 (2004).
- ▶ [5] J. Hoppler, J. Stahn, C. Niedermayer, V. K. Malik, H. Bouyanfif, A. J. Drew, M. Rössle, A. Buzdin, G. Cristiani, H.-U. Habermeier, B. Keimer, and C. Bernhard, *Nature Materials* **8**, 315 (2009).
- [6] G. Blatter, V. B. Geshkenbein, and J. A. G. Koopmann, *Physical Review Letters* **92**, 067009 (2004).
- [7] A. Bouhon and M. Sigrist, arXiv:0909.3535 (2009).
- [8] H. Kaneyasu and M. Sigrist, arXiv:1002.4793 (2010).
- [9] J. Teyssier, R. Viennois, V. Guritanu, E. Giannini, and D. van der Marel, *Journal of Physics: Conference Series* **200**, 032076 (2010).
- [10] H. Adachi and M. Sigrist, *Physical Review B* **80**, 155123 (2009).
- ▶ [11] M. H. Fischer and M. Sigrist, *Physical Review B* **81**, 064435 (2010).
- [12] B. Binz and M. Sigrist, *Europhysics Letters* **65**, 816 (2004).
- [13] R. Tediosi, N. P. Armitage, E. Giannini, and D. van der Marel, *Physical Review Letters* **99**, 016406 (2007).
- ▶ [14] E. Kozik, K. Van Houcke, E. Gull, L. Pollet, N. Prokof'ev, B. Svistunov, and M. Troyer, arXiv:0907.0863 (2009).
- ▶ [15] C. Gils, E. Ardonne, S. Trebst, A. W. W. Ludwig, M. Troyer, and Z. Wang, *Physical Review Letters* **103**, 070401 (2009).

- [16] C. Gils, *Journal of Statistical Mechanics* p. P07019 (2009).
- [17] C. Gils, S. Trebst, A. Kitaev, A. W. W. Ludwig, M. Troyer, and Z. Wang, *Nature Physics* **5**, 834 (2009).
- [18] I. V. Kukushkin, J. H. Smet, V. W. Scarola, V. Umansky, and K. von Klitzing, *Science* **324**, 1044 (2009).
- Other references**
- [19] K. Miyake, *Journal of the Physical Society of Japan* **77**, 123703 (2008).
- [20] E. Lengyel, M. Nicklas, H. S. Jeevan, G. Sparr, C. Geibel, F. Steglich, Y. Yoshioka, and K. Miyake, *Physical Review B* **80**, 140513(R) (2009).
- [21] D. Eom, M. Ishikawa, J. Kitagawa, and N. Takeda, *Journal of the Physical Society of Japan* **67**, 2495 (1998).
- [22] R. Labusch, *Crystal Lattice Defects* **1**, 1 (1969).
- [23] G. Blatter, M. V. Feigel'man, V. B. Geshkenbein, A. I. Larkin, and V. M. Vinokur, *Reviews of Modern Physics* **66**, 1125 (1994).
- [24] T. Matsushita, E. Kusayanagi, and K. Yamafuji, *Journal of the Physical Society of Japan* **46**, 1101 (1979).
- [25] F. Kidwingira, J. D. Strand, D. J. Van Harlingen, and Y. Maeno, *Science* **314**, 1267 (2006).
- [26] S. A. Grigera, P. Gegenwart, R. A. Borzi, F. Weickert, A. J. Schofield, R. S. Perry, T. Tayama, T. Sakakibara, Y. Maeno, A. G. Green, and A. P. Mackenzie, *Science* **306**, 1154 (2004).
- [27] R. A. Borzi, S. A. Grigera, J. Farrell, R. S. Perry, S. J. S. Lister, S. L. Lee, D. A. Tennant, Y. Maeno, and A. P. Mackenzie, *Science* **315**, 214 (2007).
- [28] H. Y. Kee and Y. B. Kim, *Physical Review B* **71**, 184402 (2005).
- [29] H. Yamase, V. Oganesyan, and W. Metzner, *Physical Review B* **72**, 035114 (2005).
- [30] H. J. Zhang, C. X. Liu, X.-L. Qi, X. Dai, Z. Fang, and S. C. Zhang, *Nature Physics* **5**, 438 (2009).
- [31] V. S. Édel'man, *Advances In Physics* **25**, 555 (1976).
- [32] L. Li, J. G. Checkelsky, Y. S. Hor, C. Uher, A. F. Hebard, R. J. Cava, and N. P. Ong, *Science* **321**, 547 (2008).
- [33] K. Behnia, L. Balicas, and Y. Kopelevich, *Science* **317**, 1729 (2007).
- [34] D. Hsieh, D. Qian, L. Wray, Y. Xia, Y. S. Hor, R. J. Cava, and M. Z. Hasan, *Nature* **452**, 970 (2008).
- [35] D. Balla and N. B. Brandt, *Journal of Experimental and Theoretical Physics* **20**, 1111 (1965).
- [36] M. Dressel and G. Grüner, *Electrodynamics of Solids: Optical Properties of Electrons in Matter* (Cambridge University Press, Cambridge, 2002).
- [37] W. Kraak, R. Herrmann, and H. Haupt, *Physica Status Solidi (b)* **109**, 785 (1982).
- [38] I. M. Lifshitz, *Journal of Experimental and Theoretical Physics* **11**, 1130 (1960).
- [39] E. Wigner, *Physical Review* **46**, 1002 (1934).
- [40] D. M. Ceperley and B. J. Alder, *Physical Review Letters* **45**, 566 (1980).
- [41] B. I. Halperin and T. M. Rice, *Reviews of Modern Physics* **40**, 755 (1968).
- [42] B. Spivak, S. V. Kravchenko, S. A. Kivelson, and X. P. A. Gao, arXiv:0905.0414 (2009).
- [43] G. Ortiz, M. Harris, and P. Ballone, *Physical Review Letters* **82**, 5317 (1999).
- [44] M. Bonitz, V. S. Filinov, V. E. Fortov, P. R. Levashov, and H. Fehske, *Physical Review Letters* **95**, 235006 (2005).
- [45] G. E. Smith, G. A. Baraff, and J. M. Rowell, *Physical Review* **135**, A1118 (1964).
- [46] F. X. Bronold, H. Fehske, and G. Röpke, *Journal of the Physical Society of Japan* **76** (Suppl. A), 27 (2007).
- [47] P. Wachter, B. Bucher, and J. Malar, *Physical Review B* **69**, 094502 (2004).
- [48] C. D. Jeffries and L. V. Keldysh, eds., *Electron-hole droplets in semiconductors* (Nauka, Moscow, 1988).
- [49] T. T. M. Palstra, A. A. Menovsky, J. van den Berg, A. J. Dirkmaat, P. H. Kes, G. J. Nieuwenhuys, and J. A. Mydosh, *Physical Review Letters* **55**, 2727 (1985).
- [50] S. Elgazzar, J. Ruzs, M. Amft, P. M. Oppeneer, and J. A. Mydosh, *Nature Materials* **8**, 337 (2009).
- [51] K. Haule and G. Kotliar, *Nature Physics* **5**, 796 (2009).

Project **6****Magnetism and competing interactions in bulk materials**

Project leaders: F. Mila (EPFL), A. Zheludev (PSI and ETHZ)

Participating members: T. Giamarchi (UniGE), J. Mesot (PSI and ETHZ), F. Mila (EPFL), H.-R. Ott (ETHZ), H. Rønnow (EPFL), U. Staub (PSI), M. Troyer (ETHZ), A. Zheludev (PSI and ETHZ)

Introduction: The aim of this project is to apply a variety of complementary techniques to address some of the most intriguing problems in the modern field of quantum magnetism. The focus this year was on specific structural features: low-dimensionality, geometric frustration, quenched disorder and magnetoelectric coupling. Their effect on “classical” systems is well understood, but the challenge is to see what happens in “quantum” magnets, i.e. spin-systems where quantum fluctuations play a significant role. What we discovered is the emergence of several qualitatively new and previously inaccessible quantum magnetic phases.

Summary and highlights

One part of the research effort involves a search for new prototype materials, synthesis and sample characterization. Magnetic properties of the newly discovered and several previously known compounds are then investigated using neutron scattering, resonant magnetic X-ray scattering, NMR spectroscopy and bulk methods. At the same time, a theoretical and numerical effort aims to explain the results and provide directions for further experiments.

For spin-ladders, we focus on exotic magnetic excitations beyond the simplistic single-mode approximation. In particular, neutron scattering experiments provide unique insight on the breakdown of the single-particle picture at field-induced quantum phase transitions in two metalloorganic materials. In one case, $(\text{C}_5\text{H}_{12}\text{N})_2\text{CuBr}_4$, the effect is due to the extreme one-dimensionality of magnetic interactions. Here theory (DMRG calculations) is very successful in making quantitative predictions for comparison with experiments. In another material, $\text{Sul-Cu}_2\text{Cl}_4$, the quasi-particle breakdown is found to result from strong geometric frustration. Theoretical studies provide a comprehensive picture of magnetization plateaus in such frustrated ladders.

The effect of structural (chemical) disorder is studied in two other ladder materials. In one case, $\text{Bi}(\text{Cu}_{1-x}\text{Zn}_x)_2\text{PO}_6$, the disorder directly involves the magnetic ions. Here NMR experiments for the first time detect a “freezing” of finite-size spin clusters formed around the spin-liquid-destroying $S = 0$ defects. When the disorder affects only the magnitude of magnetic interactions, $\text{IPA-Cu}(\text{Cl}_{1-x}\text{Br}_x)_3$, the spin-liquid state is found to persist. Nevertheless, at high magnetic fields we obtain the first direct evidence for a new quantum “Bose glass” phase.

The effect of extreme geometric frustration is also studied in two dimensions. In the Sutherland-Shastry frustrated dimer network $\text{SrCu}_2(\text{BO}_3)_2$ a new quantum phase is found at high pressure. Neutron scattering experiments on two prototypical Kagome lattice systems find tantalizing evidence of a two-dimensional spin-liquid phase. As in the one-dimensional case of spin-ladders, rather remarkable properties are predicted to emerge in frustrated 2D systems in the presence of disorder. Results obtained in numerical studies of this problem are directly relevant to experiments on the above-mentioned Sutherland-Shastry and Kagome lattice materials.

1 Magnetic excitations and quantum phase transitions in spin-ladders

Arguably the simplest geometrical realization of a model where triplet excitations delocalize and become dispersive is the spin-ladder. We investigate several realizations of this model – from $\text{Sr}_{14}\text{Cu}_{24}\text{O}_{41}$, whose copper-oxygen configuration is related to the high- T_c cuprates with similar energy scales of sev-

eral hundred meV; to piperidinium copper bromide $(\text{C}_5\text{H}_{12}\text{N})_2\text{CuBr}_4$ (pipCuBr₄), whose 1000 times lower energy scale allows studies all the way to saturation in an external magnetic field; and to $\text{Cu}_2\text{Cl}_4\text{-Sul}$, where a geometric frustration of rung interactions gives rise to a qualitatively new chiral high-field phase.

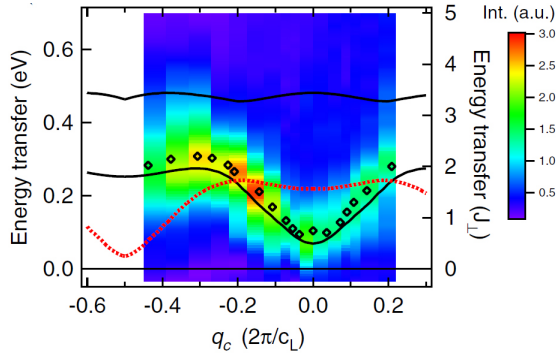


Figure 1: RIXS intensity after subtraction of the elastic signal and calculated one- (red dashed line) and two-tripion (black full lines) dispersion curves.

1.1 X-ray study of magnons in $\text{Sr}_{14}\text{Cu}_{24}\text{O}_{41}$ (H. Rønnow)

Exploiting world best resolution of the new resonant inelastic X-ray scattering (RIXS) beamline ADDRESS at Swiss Light Source (SLS) at PSI, we identified two-triplet excitations in $\text{Sr}_{14}\text{Cu}_{24}\text{O}_{41}$ (Fig. 1) [1]. This important step towards a quantitative understanding of the RIXS cross-section for magnetic excitations establishes an exciting alternative to neutron scattering. It can be performed on sub-millimeter crystals. A new MaNEP joint collaboration has been launched to pursue excitations in other low-dimensional quantum magnets.

1.2 Magnon fractionalization in spin-ladders (H. Rønnow)

In pipCuBr_4 , tuning the magnetic field into the Luttinger liquid phase, the magnons fractionalize into spinons displaying both commensurate and incommensurate continua (Fig. 2) [2]. Several other studies, including low-temperature susceptibility, thermal transport [3] etc. were also performed. More details can be found also in the theoretical contribution by the Giamarchi group below in paragraph 1.4.

1.3 Dynamics of a chiral magnon condensate (A. Zheludev)

The metalloorganic material $\text{Sul-Cu}_2\text{Cl}_4$ is composed of very weakly interacting 4-leg $S = \frac{1}{2}$ “spin-tubes”. The ground state is a spin-singlet, protected by a gap of $\Delta \sim 0.5$ meV. Due to a strong frustration of rung interactions, the minimum of one-dimensional dispersion is at an incommensurate position $q_{\parallel} = 0.48\pi$. The most exciting observation is that applying a magnetic field beyond $H_c \sim$

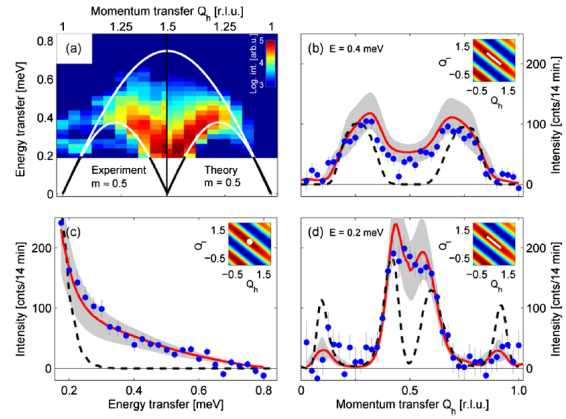


Figure 2: Excitation spectrum in the Luttinger liquid phase ($T_N < T = 250$ mK $< T_{LL}$) at $B = 10.1$ T ($m = 0.5$) compared to theoretical calculations.

3.75 T produces an incommensurate helimagnetically ordered chiral phase [17]. This transition breaks the complete $O(2) = SO(2) \times Z_2$

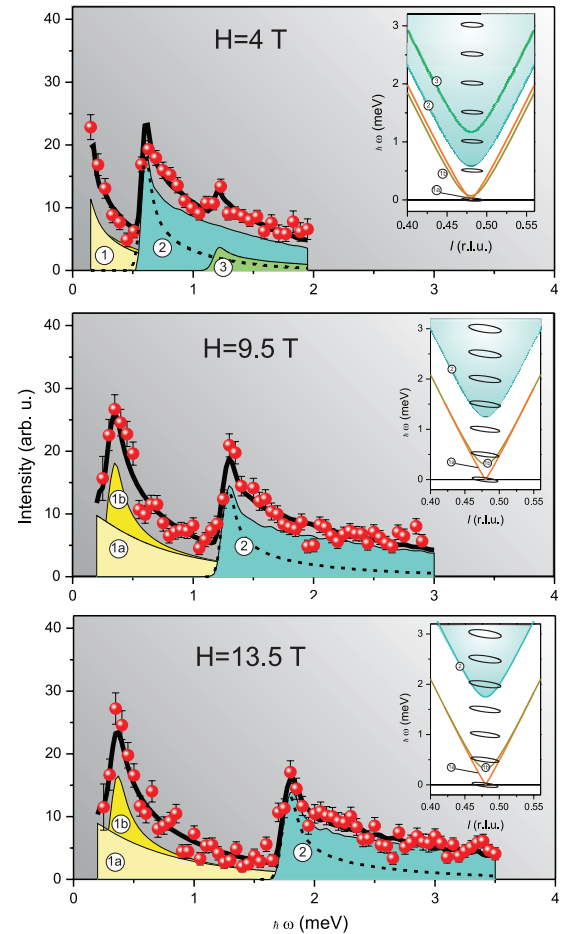


Figure 3: Neutron spectra measured in $\text{Sul-Cu}_2\text{Cl}_4$ at the 1D AF zone-center $(0.5, 0, 0.48)$ in various applied magnetic fields above the critical field, $H > H_c$. Shaded areas are partial contributions of separate excitation branches.

point symmetry group and was argued to belong to one of the chiral universality classes. The new study employs inelastic neutron scattering to investigate the spin dynamics in this novel helimagnetic phase. The results are discussed in detail in [4]. As illustrated in Fig. 3, the spectrum measured at $H > H_c$ at the magnetic zone center is qualitatively different from that in conventional magnetic Bose-Einstein condensate (BEC). An understanding of this behavior was drawn from a field-theoretical analysis. It turns out that there are actually *two* low-energy modes. One is indeed gapless, though it is not directly visible in the neutron data due to resolution effects. The second corresponds to the observed gap excitation. The magnitude of the gap scales with the square of the ordered helimagnetic moment, in excellent quantitative agreement with experiment.

1.4 Dynamical correlation functions from DMRG calculations (T. Giamarchi)

On the theory side, we explore the dynamics of spin- $\frac{1}{2}$ ladders using time dependent density

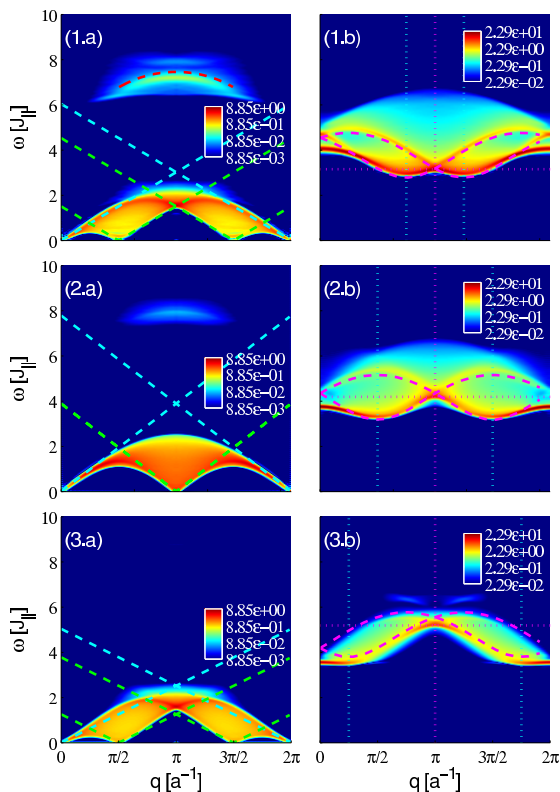


Figure 4: Example of the $S_z S_z$ dynamical structure factor computed by the DMRG technique, for various values of the external magnetic field (top to bottom). The left are the symmetric excitations whose low-energy part can be described by a Luttinger liquid theory. The right are the antisymmetric excitations, that are specific to the ladder.

matrix renormalization group (DMRG). This method allows us to compute the time and space dependent correlations that are Fourier transformed to obtain the spectral functions, directly comparable with neutron experiments. Our method gives an excellent energy and momentum resolution (at the moment, even better than the existing neutron experiments). An example of the spectrum computed by the DMRG method is shown in Fig. 4.

We compare our results with measurements on the compound $\text{CuBr}_4(\text{C}_5\text{H}_{12}\text{N})_2$ which is a unique realization of weakly coupled spin- $\frac{1}{2}$ ladders with small inter-spin couplings. All the high-energy excitations can now be characterized.

1.5 Frustration-induced plateaus (F. Mila)

A parallel theoretical effort is aimed at understanding the magnetization process of frustrated spin-ladders [5]. In the strong-rung limit, we have used degenerate perturbation theory to prove that frustration leads to magnetization plateaus at fractional values of the magnetization for all spins S and to determine the critical ratios of parallel to diagonal inter-rung couplings for the appearance of these plateaus. A typical example ($S = 1$) is depicted in Fig. 5. To confirm these results and to investigate the properties of these ladders away from the strong-coupling limit, we have performed extensive DMRG calculations up to $S = 2$. For intermediate inter-rung couplings, several surprises have appeared, including the development of magnetization jumps and, in some cases, the appearance of one or more phase transitions inside a given plateau.

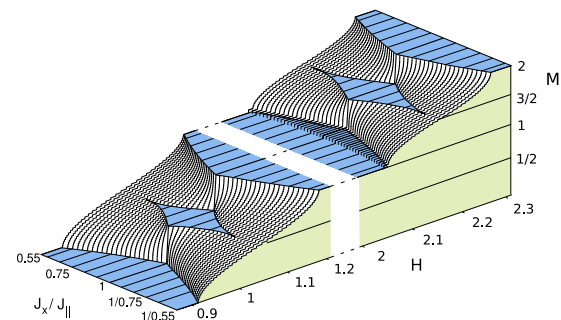


Figure 5: Magnetization of the frustrated spin-1 ladder in the strong-rung limit as a function of the ratio of the leg to cross coupling.

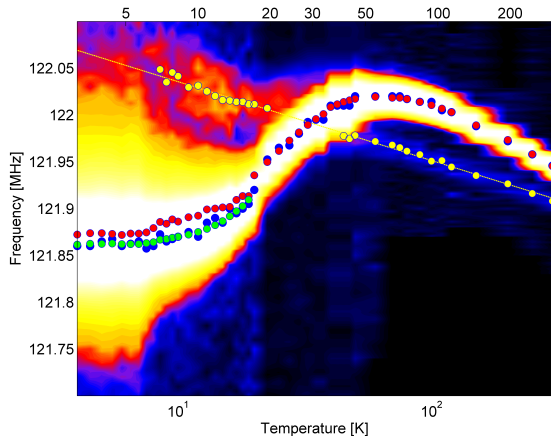


Figure 6: ^{31}P NMR line positions and widths vs temperature for $\text{Bi}(\text{Cu}_{1-x}\text{Zn}_x)_2\text{PO}_6$ with $x = 0.01$. Red, blue and green dots are Gaussian fits to the main line, yellow dots mark the maximum of the impurity signal.

2 Quenched disorder in spin-ladders

2.1 Spin-ladder with site dilution (*H.-R. Ott and J. Mesot*)

With the present project we aim at the identification of generic magnetic features of a 2-leg spin-ladder system with a low concentration of non-magnetic defects using $\text{Bi}(\text{Cu}_{1-x}\text{Zn}_x)_2\text{PO}_6$ as the model system [6]. For $x = 0$, the $\chi(T)$ data reveal the expected features of a low-dimensional dimerized spin $S = \frac{1}{2}$ arrangement. The temperature induced shift of the magnetic resonance signal reflects the generic magnetization of the spin-system. For $x = 0.01$, evidence for impurity-induced local magnetization is obtained again from $\chi(T)$ data at low temperatures and from NMR spectra. In addition to the main NMR line, which broadens considerably in the low- T regime, we observe an impurity-induced peak which exhibits a logarithmic temperature dependence. This peak shifts from the low-frequency side of the main line at high temperatures to the high-frequency region in the NMR spectra at low temperatures (Fig. 6). Preliminary quantum Monte Carlo (QMC) calculations using reasonable values for the exchange interactions along and perpendicular to the ladder legs confirm the generic character of these features.

Data of the NMR spin-lattice relaxation rate $T_1^{-1}(T)$ are obtained for $x = 0, 0.01$ and 0.05 . Above 25 K, $T_1^{-1}(T)$ is approximately the same for all three Zn concentrations and the exponential temperature dependence reflects a spin gap Δ in the dimer excitation spectrum with $\Delta/k_B \simeq 55$ K, which does not change

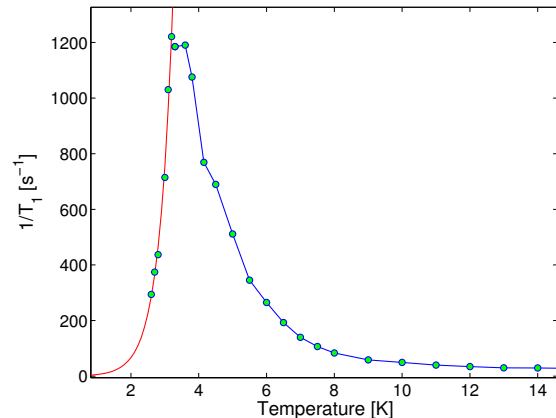


Figure 7: Low-temperature spin-lattice relaxation rate $T_1^{-1}(T)$ for $\text{Bi}(\text{Cu}_{1-x}\text{Zn}_x)_2\text{PO}_6$ with $x = 0.05$. The blue line is a guide to the eye; the red line emphasizes the exponential decrease of $T_1^{-1}(T)$.

visibly with increasing x and persists up to temperatures above 200 K. This is compatible with the assumption that the spin-ladder system is thermally quite isolated from the crystal lattice. Distinct differences are, however, observed at low temperatures. The exponential decrease of the relaxation rate is interrupted at low temperatures and $T_1^{-1}(T)$ passes through an x -dependent minimum at $T_{\min}(x)$. For $x = 0$ and 0.01 , the relaxation rate increases slightly below T_{\min} and smoothly reaches an x -dependent saturation value. For $x = 0.05$, a considerable enhancement of the relaxation rate indicates substantial magnetic fluctuations in the spin-system. Before saturation is reached, $T_1^{-1}(T)$ exhibits a rather narrow maximum with a sharp reduction of the relaxation at lower temperatures. This feature, displayed in Fig. 7, clearly indicates a transition in the spin-system, most likely a freezing of the impurity-induced local magnetization clouds.

2.2 Observation of a magnetic Bose glass (*A. Zheludev*)

The metalloorganic compound IPA-CuCl_3 is one of the most thoroughly studied spin-ladder materials, and is a beautiful realization of BEC of magnons that occurs at $H_c \sim 10$ T [18]. The present study [7] addresses a very fundamental question: how will BEC of magnons be affected by the introduction of quenched disorder?

Our experiments are performed on single-crystals of $\text{IPA-Cu}(\text{Cl}_{1-x}\text{Br}_x)_3$. Br-doping does not affect the magnetic Cu^{2+} sites, but randomizes the strength of antiferromagnetic (AF) leg and rung interactions in the spin-ladders. For the magnons, such a bond strength varia-

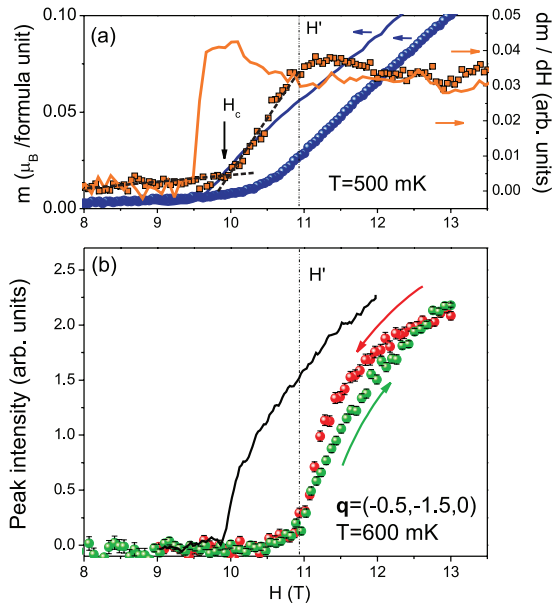


Figure 8: The uniform magnetization (a, circles), differential susceptibility (a, squares) and magnetic Bragg intensity (b) measured in IPA-Cu(Cl_{0.95}Br_{0.05})₃. The solid curves correspond to the undoped material.

tion is equivalent to a random potential. Most data are collected on a $x = 0.05$ sample. In zero field the magnetic properties and excitation spectrum are very similar to those in the undoped compound, and typical of a spin gap system. However, in high magnetic fields, *two* consecutive transitions are observed (Fig. 8). Beyond the first transition at $H_c = 10$ T the spin-liquid is destroyed. Uniform magnetization becomes non-zero and magnetic susceptibility dM/dH shows a roughly linear increase. However, long-range AF order is not observed until $H' = 11$ T, where half-integer magnetic Bragg reflections are detected, and dM/dH is a constant. The intermediate phase between H_c and H' is absent in the undoped material, where the two fields coincide. All evidence, including a history-dependent magnetic correlation length, suggests that the new phase is the thought-after Bose glass [19]. As expected, it has a non-zero compressibility (magnetic sus-

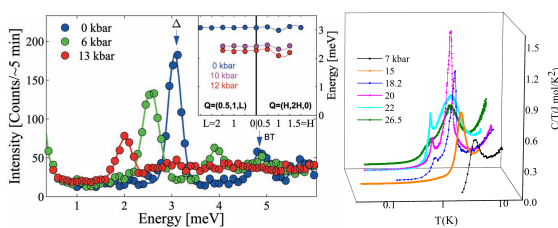


Figure 9: Neutron spectra (left) and specific heat (right) from SrCu₂(BO₃)₂.

ceptibility), but lacks at true Bose condensate (AF order). To improve our experimental understanding of this phenomenon, we are currently investigating the possibility of doping several new spin-ladder and chain compounds [8].

3 Two-dimensional frustrated spin-systems

3.1 The 2D antiferromagnet (*H. Rønnow and F. Mila*)

SrCu₂(BO₃)₂ (SCBO) is the only known realization of the highly frustrated Shastry-Sutherland antiferromagnetic spin- $\frac{1}{2}$ model. We discovered that the 3 meV singlet-triplet gap softens with applied pressure (Fig. 9). The 2-triplet bound state (BT) softens faster. When it catches up with the 1-triplet, the system enters a new quantum phase. We further measured ac specific heat up to 30 kbar [9]. As the broad peak in specific heat C_p shifts to lower temperature (consistent with the decreasing gap), it sharpens dramatically into almost a divergence at 20 kbar. Simultaneously, a new lower temperature peak appears. The analysis to identify the nature of this intermediate phase is ongoing.

Motivated by the possibility of controlled impurity-doping of SrCu₂(BO₃)₂, we have investigated the properties of the model with non-magnetic impurities [10]. We have shown that, in this geometry of orthogonal dimers, non-magnetic impurities generate bound states below the spin gap. These bound states and their symmetry properties have been determined by exact diagonalization of small clusters and successfully interpreted within a simple effective model describing a spinon submitted to an attractive extended potential. We have also calculated the Raman spectrum in a simple geometry and shown that Raman spectroscopy is an ideal technique to probe these bound states.

3.2 Spin- $\frac{1}{2}$ Kagome antiferromagnets (*H. Rønnow*)

Despite intense theoretical focus, there exist to date only two prominent candidates for physical realization of the $S = \frac{1}{2}$ Kagome model: Herbertsmithite ZnCu₃(OH)₆Cl₂, and Volborthite Cu₃V₂O₇(OH)₂·2H₂O.

Herbertsmithite reveals scale free fluctuations with Q -dependence corresponding to nearest neighbor correlations (Fig. 10) [11]. The momentum, energy and temperature dependence is confirmed by polarized neutron scattering

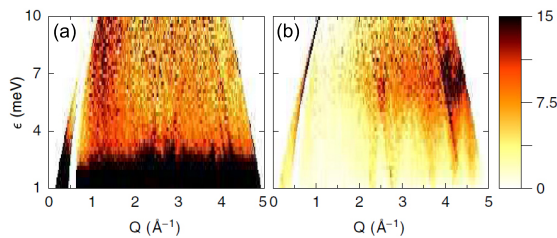


Figure 10: Excitation spectra of Herbertsmithite. Fitting time-of-flight data at 5 temperatures pixel-by-pixel, allowed separating into (a) constant and (b) Bose statistics components. Phonon contributions follow Bose statistics. A rod of energy independent scattering occur around 1.2 \AA^{-1} in the constant part.

measurements. Indications are that this feature is indeed the footprint of a quantum spin-liquid (and if so of which type).

The spectrum in Volborthite (Fig. 11) [12] is markedly different from that of Herbertsmithite, with a flat band around 5 meV and two rods in energy at Q 's corresponding to theoretically proposed ordering patterns. The energy integrated magnetic scattering recorded using polarization analysis reveals the superposition of a broad liquid like structure factor with sharper peaks suggesting semi-classical short range order below 5 K. Likely a combination of a structural distortion and Dzyaloshinskii-Moriya (DM) interaction drives Volborthite towards this situation.

3.3 Non-magnetic impurities and Dzyaloshinskii-Moriya interactions in the Kagome antiferromagnet (F. Mila)

Motivated by recent nuclear magnetic resonance experiments on Herbertsmithite, $\text{ZnCu}_3(\text{OH})_6\text{Cl}_2$, we have performed an exact diagonalization study of the combined effects of non-magnetic impurities and Dzyaloshinskii-Moriya (DM) interactions in the $S = \frac{1}{2}$ Kagome antiferromagnet [13]. The local response to an applied field has revealed that the response of the dimers next to the impurities remains typical of that of frozen dimers, which are known to be present around each impurity for $D = 0$, up to large values of the DM interaction, in fact far beyond the critical value that stabilizes the $q = 0$ order in the clean system. This has led to a consistent interpretation of the two-peak structure of the oxygen NMR line of Herbertsmithite in terms of oxygen sites near or further away from a vacancy.

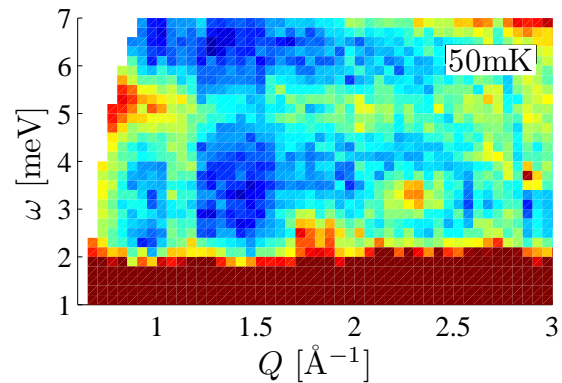


Figure 11: $S(Q, \omega)$ at 50 mK in Volborthite.

3.4 Quantum Monte Carlo and other algorithms in application to exotic frustrated lattices (M. Troyer)

In order to explore more esoteric interaction geometries, we use quantum Monte Carlo (QMC) to map out the peculiar phase diagram of bosons on a star lattice [14]. Additional simulations on the so-called compass model in two dimensions reveal how thermal fluctuations lead to a canting of magnetic order at elevated temperatures [15]. Seeking numerical methods beyond QMC, we have explored new two-dimensional generalizations of the DMRG method [20], and compared it to benchmark results on non-frustrated and frustrated spin-systems [16]. With additional improvements the novel algorithm might be very useful for strongly correlated systems in two dimensions.

4 Magnetoelectric effects (U. Staub)

In systems with strong magnetoelectric interactions, a multiferroic order parameter based on the coupling of magnetic moments and electric polarization could be produced by considering the toroidal moment (also called anapole moment), which in its simplest form is $\mathbf{\Omega} = \mathbf{S}_i \times \mathbf{R}_i$, with \mathbf{S}_i the spin and \mathbf{R}_i the electric dipole moment at the same place. The observation of toroidal moments on the atomic level on a given site i is more challenging.

An ideal candidate for a fundamental study of these strange magnetoelectric multipoles is GaFeO_3 , a magnetoelectric material with a ferromagnetic transition at 230 K. The material is piezoelectric and crystallizes in the polar space group $Pc2_1n$. We have performed resonant X-ray diffraction experiments at the K edge and the $L_{2,3}$ edges of Fe. We could show that these experiments at space group forbidden reflections are sensitive to magnetoelectric multipoles of rank zero (magnetoelectric monopole)

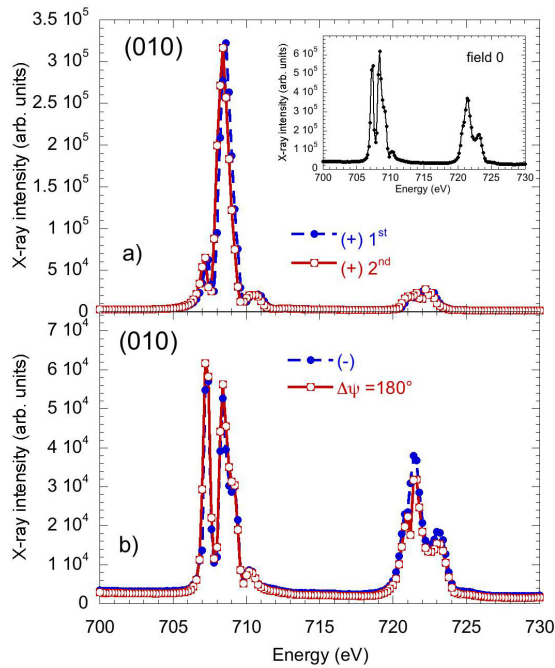


Figure 12: Magnetic field dependence of the (0 1 0) reflection at $T = 100$ K and σ primary polarization. Intensities in panel (a) have (+) polarity, in panel (b) have (-) polarity or are collected in (+) polarity but the azimuthal angle (ψ) differs by 180° from the angle used in the other three sets of data. Open circles in panel (a) are obtained following recovery of the magnetic state from (-) in panel (b). Inset to panel (a) is data collected prior to the imposition of a magnetic field on the sample.

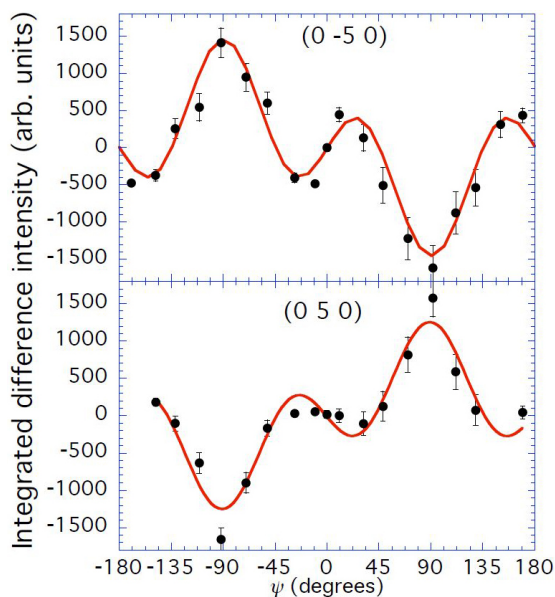


Figure 13: Azimuthal angle (ψ) dependences of the difference X-ray intensity for a magnetization sign change for the Friedel pair of $k = \pm 5$ in GaFeO_3 . The fit is based on a model of magnetoelectric multipole moments with an orbital contribution.

and two magnetoelectric quadrupole of the open Fe valence shell. The energy scan of the (0 1 0) reflection containing the magnetoelectric signal is shown in Fig. 12 for experiments at the $L_{2,3}$ edges [21]. Fig. 13 shows the magnetization difference signal as a function of rotation around the Bragg wave vector taken at the pre-edge of K absorption line of the (0 k 0) Friedel pair reflections. The main difference in the intensities between the two Friedel pair reflections are the change in sign, which occurs over the whole range of the azimuthal scan. This sign change is directly linked to the change of sign of a magnetic parity odd multipole (magnetoelectric).

5 Collaborative efforts

By design, the project is structured to maximize collaboration between theorists and experimentalists. For example, neutron scattering experiments that are employed in many of the above-mentioned studies directly measure spin-spin correlation functions. The very same characteristics are computed numerically for a direct comparison. On the one hand, we try to take maximum advantage of the various experimental techniques available in different groups. In this context, a truly breakthrough development is our use of synchrotron X-rays to probe magnetic properties.

MaNEP-related publications

- ▶ [1] J. Schlappa, T. Schmitt, F. Vernay, V. N. Strocov, V. Ilakovac, B. Thielemann, H. M. Rønnow, S. Vanishri, A. Piazzalunga, X. Wang, L. Braicovich, G. Ghiringhelli, C. Marin, J. Mesot, B. Delley, and L. Patthey, *Physical Review Letters* **103**, 047401 (2009).
- ▶ [2] B. Thielemann, C. Rüegg, H. M. Rønnow, A. M. Läuchli, J.-S. Caux, B. Normand, D. Biner, K. W. Krämer, H.-U. Güdel, J. Stahn, K. Habicht, K. Kiefer, M. Boehm, D. F. McMorrow, and J. Mesot, *Physical Review Letters* **102**, 107204 (2009).
- ▶ [3] A. V. Sologubenko, T. Lorenz, J. A. Mydosh, B. Thielemann, H. M. Rønnow, C. Rüegg, and K. W. Krämer, *Physical Review B* **80**, 220411 (2009).
- ▶ [4] A. Zheludev, V. O. Garlea, A. Tselvik, L.-P. Regnault, K. Habicht, K. Kiefer, and B. Roessli, *Physical Review B* **80**, 214413 (2009).
- ▶ [5] F. Michaud, T. Coletta, S. R. Manmana, J.-D. Picon, and F. Mila, *Physical Review B* **81**, 014407 (2010).
- [6] T. Shiroka, F. Casola, S. Wang, K. Conder, E. Pomjakushina, J. Mesot, and H.-R. Ott, *submitted* (2010).
- ▶ [7] T. Hong, A. Zheludev, H. Manaka, and L.-P. Regnault, *Physical Review B* **81**, 060410(R) (2010).
- [8] T. Hong, R. Custelcean, B. C. Sales, B. Roessli, D. K. Singh, and A. Zheludev, *Physical Review B* **80**, 132404 (2009).
- [9] H. Rønnow, *submitted* (2010).
- [10] S. Capponi, D. Poilblanc, and F. Mila, *Physical Review B* **80**, 094407 (2009).

- ▶ [11] M. A. de Vries, J. R. Stewart, P. P. Deen, J. O. Piatek, G. J. Nilsen, H. M. Rønnow, and A. Harrison, *Physical Review Letters* **103**, 237201 (2009).
- ▶ [12] G. J. Nilsen, F. C. Coomer, M. A. de Vries, J. R. Stewart, P. P. Deen, A. Harrison, and H. M. Rønnow, arXiv:1001.2462 (2010).
- ▶ [13] I. Rousochatzakis, S. R. Manmana, A. M. Läuchli, B. Normand, and F. Mila, *Physical Review B* **79**, 214415 (2009).
- [14] S. V. Isakov, K. Sengupta, and Y. B. Kim, *Physical Review B* **80**, 214503 (2009).
- [15] V. W. Scarola, K. B. Whaley, and M. Troyer, *Physical Review B* **79**, 085113 (2009).
- ▶ [16] B. Bauer, G. Vidal, and M. Troyer, *Journal of Statistical Mechanics* p. P09006 (2009).

Other references

- [17] V. O. Garlea, A. Zheludev, K. Habicht, M. Meissner, B. Grenier, L.-P. Regnault, and E. Ressouche, *Physical Review B* **79**, 060404(R) (2009).
- [18] V. O. Garlea, A. Zheludev, T. Masuda, H. Manaka, L.-P. Regnault, E. Ressouche, B. Grenier, J.-H. Chung, Y. Qiu, K. Habicht, K. Kiefer, and M. Boehm, *Physical Review Letters* **98**, 167202 (2007).
- [19] T. Giamarchi and H. J. Schulz, *Physical Review B* **37**, 325 (1988).
- [20] J. Jordan, R. Orús, G. Vidal, F. Verstraete, and J. I. Cirac, *Physical Review Letters* **101**, 250602 (2008).
- [21] U. Staub, V. Scagnoli, Y. Bodenthin, M. García-Fernández, R. Wetter, A. M. Mulders, H. Grimmer, and M. Horisberger, *Journal of Synchrotron Radiation* **15**, 469 (2008).

Project **7****Electronic materials with reduced dimensionality**

Project leader: L. Forró (EPFL)

Participating members: Ph. Aebi (UniFR), L. Degiorgi (ETHZ), Ø. Fischer (UniGE), L. Forró (EPFL), T. Giamarchi (UniGE), M. Gioni (EPFL)

Summary and highlights: The program of the project is to study various electronic instabilities in low-dimensional materials and their competition in stabilizing the ground state of the system. The most focused part of the project is devoted to the transition metal dichalcogenides where excitonic, charge density wave (CDW), superconductivity instabilities and Mott-localization form a very rich phase diagram. The highlight is the finding the fingerprints of an excitonic condensate in $1T$ -TiSe₂ and the stabilization of superconductivity by pressure in the region of the phase diagram where the excitonic order parameter shows strong fluctuations. In another dichalcogenide, $1T$ -TaS₂, the suppression of the long range commensurate order of CDW favors the appearance of superconductivity. Further highlight is the in-depth STM spectroscopic characterization of the Chevrel phases.

1 Study of the excitonic insulator: the case of TiSe₂ (Ph. Aebi)

In the early 1960s, a new insulating phase was predicted to possibly exist at low temperature in solids having small energy gaps. Jérôme *et al.* [16] published an extended study of this phase developing a BCS-like theory of its ground state. However, at that time an experimental realization of this phase was missing.

The excitonic insulator phase may occur in a semi-metallic or semiconducting system exhibiting a small (negative respectively positive) gap. Indeed, for a low carrier density, the Coulomb interaction is weakly screened, allowing therefore bound states of holes and electrons, called excitons, to build up in the system. If the binding energy E_B of such pairs is larger than the gap E_G , the energy to create an exciton becomes negative, so that the ground state of the normal phase becomes unstable with respect to the spontaneous formation of excitons. According to Jérôme *et al.* [16], at low temperature, these excitons may condense into a macroscopic coherent state in a manner similar to Cooper pairs in conventional BCS superconductors. Kohn [17] argued that exciton condensation may lead to the formation of charge density waves (CDW) of purely electronic origin (neglecting any lattice distortion), characterized by an order parameter.

$1T$ -TiSe₂ is a layered transition-metal dichalcogenide exhibiting a commensurate ($2 \times 2 \times 2$) CDW [18] accompanied by a periodic lattice distortion below the transition temperature of $T_c \cong 200$ K. The origin of its CDW phase was

controversial for a long time. Different scenarios have been proposed, the best candidates being a band Jahn-Teller effect [19] and the excitonic insulator phase [20, 21]. An angle-resolved photoemission spectroscopy (ARPES) study, evidencing directly the CDW, gave recently much support to the latter by comparison between experiment and theory [1]. Photoemission intensity maps were generated with the spectral function calculated in the framework of the excitonic insulator phase model, which has been adapted to TiSe₂ and renamed the exciton condensate phase model [2].

In order to get a better understanding of how this exotic phase appears and grows up, we studied its temperature dependence both theoretically and experimentally. Our goal was in particular to extract from ARPES measurement the behavior of the order parameter as a function of temperature, $\Delta(T)$. From that perspective, we have first investigated the renormalized band structure of TiSe₂ in the exciton condensate phase model. It is found that the influence of the order parameter is the most visible at the border of the Brillouin zone (L point). By choosing a specific form for $\Delta(T)$ (in the present case a BCS-like behavior), we can calculate the corresponding temperature dependent spectral function at L and look for a spectral feature characteristic of $\Delta(T)$ [3]. The calculated spectra are shown in Fig. 1a. We see that the backfolded valence band v_1 , which lies in the occupied states, is the most distinctive signature of the temperature dependence of $\Delta(T)$.

Armed with this knowledge, we performed

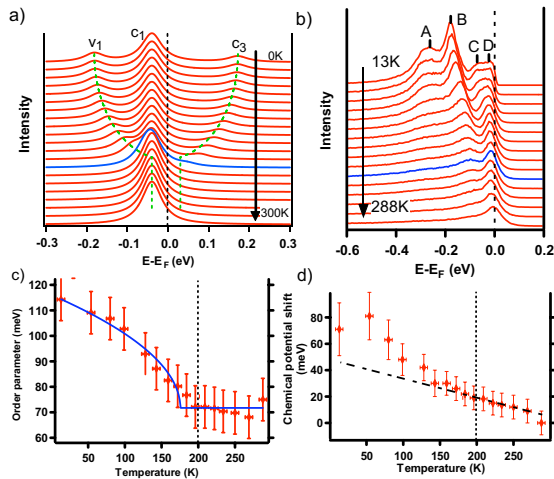


Figure 1: (a) Calculated spectral function of the exciton condensate phase at L , as a function of temperature. (b) Photoemission spectra of TiSe_2 measured at L , as a function of temperature. (c) Order parameter $\Delta(T)$ extracted from the photoemission measurements shown in (b). (d) Chemical potential shift extracted from the photoemission measurements shown in (b).

temperature dependent ARPES measurements on TiSe_2 , focusing on the situation at L [4]. The spectra are shown in Fig. 1b. Peak B in the experiment is identified with the backfolded valence band v_1 (peak A is a second backfolded valence band which is, for simplicity, not considered in our model) and peaks C and D are contributions from the conduction band c_1 . From the position of the peak B (backfolded valence band) as a function of temperature, we derived the order parameter $\Delta(T)$ of the exciton condensate phase, shown in Fig. 1c. Below the critical temperature of $T_c \simeq 200$ K, it exhibits a clear increase, reminiscent of a BCS-like exciton condensation. However, in this study, we also find a non-zero order parameter above T_c , which we interpret as the signature of a strong electron-hole fluctuation regime (above T_c). Finally, we also evidence a chemical potential shift (Fig. 1d), mainly caused by the spectral weight transfer occurring in the exciton condensate phase among the original and the backfolded bands.

2 Superconductivity through disorder in the Mott-insulator $1T\text{-TaS}_2$ (M. Griioni)

One of the most intriguing phenomena in the solid state is the occurrence of electronic instabilities towards broken symmetry states. When two or more instabilities are simultaneously at work, complex phase diagrams and unusual physical properties are found, and new states of matter may eventually emerge.

Broken-symmetry phases are especially prominent in the 2D transition metal dichalcogenides (TMDs), which exhibit a variety of charge density waves (CDW) transitions and, in few cases, superconductivity (SC). CDW and SC tend to gap parts of the same Fermi surface, and are generally considered to be competing.

In a collaboration with the MaNEP groups of Forró and Rønnow, we have studied the TMD $1T\text{-TaS}_2$, which exhibits a unique sequence of CDW and Mott-phases, as a result of the interplay of electron-phonon and Coulomb interactions. Sipos *et al.* [5] have shown that the application of external pressure suppresses the Mott-transition, and that for $p > 2.5$ GPa SC coexists with a CDW below ~ 5 K. We have now found that SC can also be induced in TaS_2 at ambient pressure by a small amount of disorder. ARPES data show that SC emerges from a normal state where strongly damped quasi-particles (QP) bear the spectral signatures of the underlying CDW and of the incipient Mott-transition.

It is known that tiny amounts of disorder – induced, e.g., by irradiation or non-stoichiometry – suppress the metal-insulator transition in TaS_2 by destroying the long-range coherence of the CDW. Our single-crystal sample, prepared by H. Berger with a stoichiometry $\text{Ta}_{0.985}\text{S}_2$ (herewith $d\text{-TaS}_2$), contains a small amount of disorder. Unlike pristine TaS_2 , the in-plane electrical resistivity of $d\text{-TaS}_2$ bears no signature of the Mott-transition at ~ 180 K, and at 2.1 K it exhibits a sharp drop. The occurrence of SC is unambiguously proven by the magnetic susceptibility, which indicates that small SC regions start to form below 2.9 K, but do not percolate through the whole sample.

ARPES spectra measured at 70 K in the Mott-phase of TaS_2 and in the “normal” phase of $d\text{-TaS}_2$ are shown in Fig. 2. They were symmetrized around E_F to remove the Fermi cut-off. Thanks to electron-hole symmetry the symmetrized spectra are proportional to the spectral function $A(k_F, E)$, since for the Fermi function $f(E, T) = (1 - f(-E, T))$. The line shape of TaS_2 is that expected for a Mott-insulator, where the spectral weight is piled up in the Hubbard subbands, separated by a correlation gap, or possibly a deep pseudogap. The picture of $d\text{-TaS}_2$ is qualitatively different. $A(k_F, E)$ exhibits a weak coherent QP peak at E_F . Spectral weight is removed from E_F and placed in the broad incoherent sidebands. Clearly $d\text{-TaS}_2$ is on the verge of opening a gap. The broad, intense, sidebands show that the QPs are strongly renormalized both by electron-phonon and Coulomb interactions.

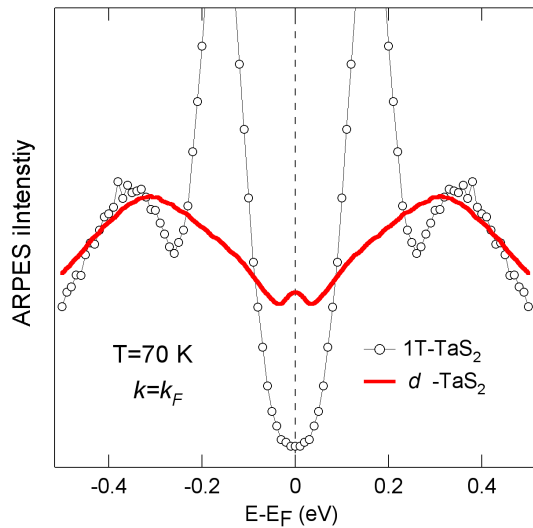


Figure 2: ARPES spectra of pristine $1T\text{-TaS}_2$ and $d\text{-TaS}_2$, measured at $k = k_F$ and 70 K, and symmetrized around E_F .

These data show that SC can emerge even in the presence of domains of a strong CDW, when the Mott-instability is suppressed in TaS_2 . The ARPES line shape in the normal state indicates that the coherent weight of the quasiparticles is considerably reduced by the interactions, and that the system remains quite close to a metal-insulator instability. Future experiments will aim at establishing a quantitative relation between the superconducting fraction and the amount of disorder.

3 Superconductivity in $1T\text{-TiSe}_2$ (L. Forró)

We report on the superconductivity in pure $1T\text{-TiSe}_2$, studied around sub-Kelvin temperatures, as a function of pressure up to 10 GPa, with the superconducting dome appearing around the critical pressure related to the CDW meltdown (Fig. 3) [6]. The doping-induced disorder is not present in our system, therefore impurity effects may not be held responsible for the closing of the superconducting dome [22]. The results of the present study strongly suggest that the CDW fluctuations are tightly linked with superconductivity in $1T\text{-TiSe}_2$. The parallels with several families of materials where the superconducting dome has been discovered in the vicinity of purely electronic ordered phase, dressing the quantum critical point, strengthen the viewpoint of excitonic superconductivity in $1T\text{-TiSe}_2$. On the other hand, the continuous development of the soft phonon mode in the vicinity of the CDW transition, both in Cu-intercalated and pure and pressurized material [22], suggests that the lat-

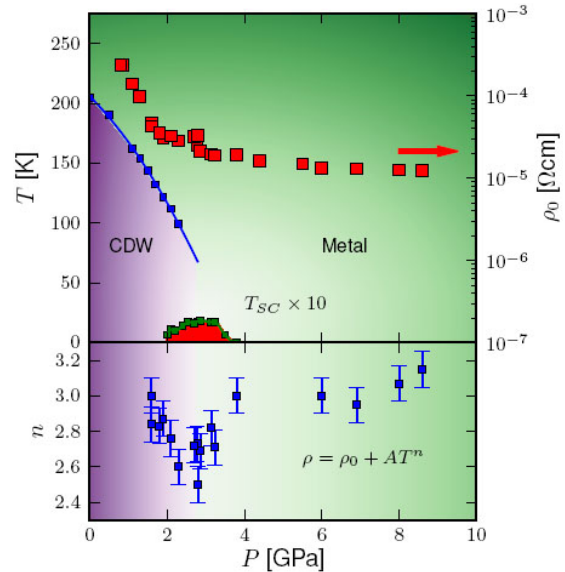


Figure 3: Pressure-temperature phase diagram of $1T\text{-TiSe}_2$. On the left axis we see the evolution of the CDW transition temperature and the superconductivity transition temperature ($\times 10$) with pressure. The superconducting dome is constrained to the pressure ranges of 2–4 GPa. On the right axis we see the strong pressure dependence of the residual resistivity over the entire investigated pressure range (note the logarithmic scale). The lower part of the diagram shows the pressure dependence of the thermal exponent n of the resistivity.

tice deformation may not be regarded as a secondary effect that simply follows the electronic ordering. The soft phonon mode, generally regarded as unfavorable for superconductivity within the weak-coupling BCS single-phonon exchange picture, has been identified as helpful in several instances for higher values of the electron-phonon coupling. This marks an alternative route for searching for the origin of the superconducting dome in $1T\text{-TiSe}_2$.

The new phase diagram of pristine $1T\text{-TiSe}_2$ under pressure complements and puts in a new light recently reported superconductivity in Cu-intercalated $1T\text{-TiSe}_2$ [6]. The absence of dopants in our case implies that the closure of the superconducting dome is unrelated to impurity-induced scattering. Given the similarities between the intercalated and the pressurized system, analogous reasoning may be extended for Cu-intercalated system. On the other hand we also point out the qualitative differences in electronic states that develop along P and x axis, marked by opposing signs of the Hall coefficient in the normal state, different maximum superconducting transition temperatures T_{SC}^{\max} (1.8 K versus 4.15 K for pressure and intercalation, respectively) and diverse magnetic properties in

the superconducting state. These dissimilarities leave open the question whether two separate superconducting domes develop in this phase diagram, corresponding to two distinct critical points. The alternative perspective of a critical line in the $T = 0$ plane of the phase diagram, covered by the “superconducting tunnel”, is a challenging topic for future studies.

4 Magnon dispersion and extended magnetic interactions in $\text{Sr}_2\text{CuO}_2\text{Cl}_2$ (M. Grioni)

$\text{Sr}_2\text{CuO}_2\text{Cl}_2$ (SCOC) is an insulating single-layer parent compound of the high- T_c superconducting (SC) materials, isostructural to the high-temperature tetragonal phase of La_2CuO_4 (LCO), with La replaced by Sr, and the apical Oxygen ions of the CuO_6 octahedra replaced by Cl. SCOC exhibits antiferromagnetic (AF) order below $T_N = 256$ K, with a reduced Cu moment of $0.34 \mu_B$. For its structure and properties, SCOC can be considered as an almost ideal realization of an ($S = \frac{1}{2}$) 2D square-lattice Heisenberg AF. The superexchange energy has been estimated to be $J = 0.13$ eV. So far the spin-wave dispersion could be measured by inelastic neutron scattering (INS) only close to $Q = 0$, due to the large J and the small volume of available crystals.

In collaboration with the MaNEP groups of Rønnow and van der Marel, and with collaborators in Milan, we set out to study magnetic excitations in SCOC by resonant inelastic X-ray scattering (RIXS). RIXS is the X-ray counterpart of resonant optical Raman spectroscopy but, since the X-ray photon carries a momentum comparable to the size of the Brillouin zone (BZ), it is not limited to $Q = 0$ excitations. The large spin-orbit energy (~ 20 eV) of the Cu $2p$ hole enables the observation of $\Delta S \neq 0$ single-magnon excitations by RIXS at the Cu L -edge (930 eV) [23]. Data were measured at the ADDRESS end station of the Swiss Light Source, which provides unsurpassed energy and momentum resolution for soft X-ray RIXS.

The Q -dependence of the magnon energy extracted from the RIXS data is summarized in Fig. 4. It is consistent with the small- Q results from INS, but reveals for the first time the full dispersion up to the boundary of the BZ. A striking 60 meV difference is observed between the magnon energies at $(\pi, 0)$ and $(\pi/2, \pi/2)$. This can be compared with the ~ 20 meV dispersion observed in LCO [24]. The energy at $(\pi, 0)$ is similar in the two compounds, but the $(\pi/2, \pi/2)$ value is higher in LCO (292 meV) than in SCOC (250 meV).

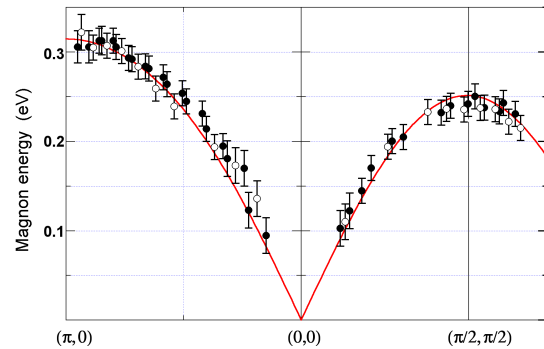


Figure 4: Magnon energies extracted from the RIXS data. The red line is a Hubbard model fit yielding $J = 142$ meV, and a ring exchange term $J_c = 89$ meV.

For the simple ($S = \frac{1}{2}$) 2D Heisenberg model with nearest-neighbor (NN) exchange, linear spin-wave theory predicts a constant magnon energy $\hbar\omega = 2Z_c J$ along the AF zone boundary, where $Z_c = 1.18$ is a uniform renormalization factor. A larger energy at $(\pi, 0)$ is expected in an extended model which includes second- and third-nearest-neighbor as well as 4-spin ring exchange interactions, described by additional exchange parameters J' , J'' and J_c . The dispersion of Fig. 4 is therefore direct evidence of magnetic interactions, beyond nearest-neighbor spins. A good fit to the data (red line) is obtained with $J = 142$ meV, $J' = J'' = 4$ meV, and $J_c = 89$ meV. These values can be compared with $J = 146$ meV, $J' = J'' = 3$ meV and $J_c = 61$ meV for LCO at $T = 10$ K [24]. The largest difference is found in the ring exchange term, which is 50% larger in SCOC. These results strongly suggest that long-range magnetic interactions are generally important in the parent compounds of the high- T_c cuprate superconductors. They also confirm that RIXS is a valuable probe of magnetic interactions, quite complementary to the more traditional INS. In the cuprates, in particular, its lower energy resolution is compensated by the easy access to energies of order J , and by the small sample volume it requires.

5 Raman scattering evidence for a cascade-like evolution of the charge density wave collective amplitude mode in rare-earth tri-tellurides (L. Degiorgi)

A family of layered compounds which have attracted a lot of attention recently are the rare-earth (R) tri-tellurides $R\text{Te}_3$. They host an *unidirectional*, incommensurate CDW already well above room temperature for all R elements lighter than Dy, while in the heavy rare-earth tri-tellurides (i.e. $R = \text{Tm}, \text{Er}, \text{Ho}, \text{Dy}$) the

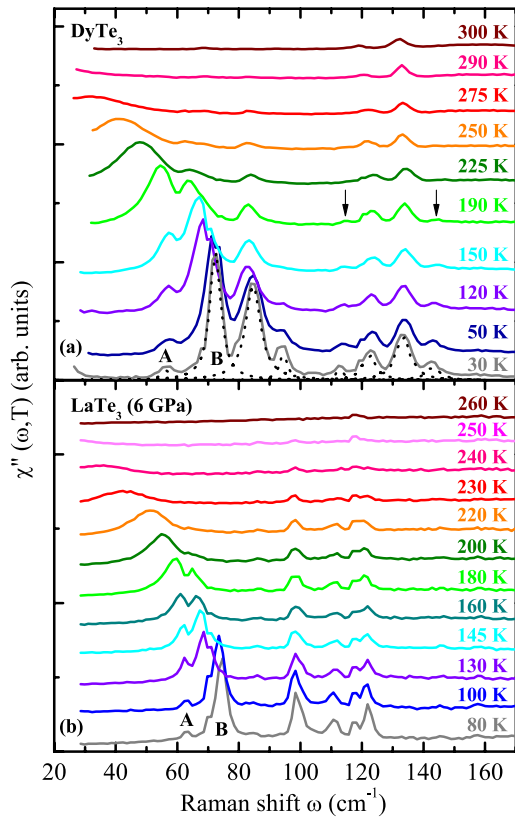


Figure 5: Temperature dependence of the Raman scattering spectra of DyTe_3 at ambient pressure (a) and of LaTe_3 at 6 GPa (b). The spectra have been shifted for clarity. In panel (a) the oscillators employed for the data fits are shown for the measurement at 30 K (dotted lines) and the arrows mark the weak features at 113 and 143 cm^{-1} . The labels A and B denote the weak mode at $\sim 60 \text{ cm}^{-1}$ and the sharp one at $\sim 70 \text{ cm}^{-1}$ at low temperatures, respectively.

corresponding transition temperature, T_{CDW1} , lies below $\sim 300 \text{ K}$ and decreases with increasing R mass. In the latter systems, a further transition to a *bidirectional* CDW state occurs at T_{CDW2} , ranging from 180 K for TmTe_3 to 50 K for DyTe_3 . The drastic change in transition temperatures with the size of the R ion or externally applied pressure on a given material is accompanied by a similarly large change in the properties of the CDW itself. In particular, the CDW gap of $R\text{Te}_3$ progressively collapses when the lattice constant is reduced, which, in turn, induces a transfer of spectral weight into the metallic component of the excitation spectrum, the latter resulting from the fact that the Fermi surface in these materials is only partially gapped by the formation of the CDW. The response of this residual metallic component completely screens all optically active modes (including the collective CDW phase excitation) and makes their observation by infrared absorption methods impossible. This is why

we turned to Raman scattering in our recent study of these materials.

We have new Raman scattering investigations as a function of temperature on DyTe_3 at ambient pressure ($T_{\text{CDW1}} = 307 \text{ K}$, $T_{\text{CDW2}} = 49 \text{ K}$) and on LaTe_3 at 6 GPa, with a lattice constant between that of DyTe_3 and HoTe_3 , and $T_{\text{CDW1}} \sim 260 \text{ K}$. Typical spectra are shown in Fig. 5. The covered spectral range extends from 5 to 200 cm^{-1} , thus giving access to the energy region in which the collective modes are expected to appear. Raman scattering experiments as a function of temperature on DyTe_3 and on LaTe_3 at 6 GPa provide a clear-cut evidence for the emergence of the respective collective CDW amplitude excitations. The temperature dependence of the A and B modes behaves as an order parameter. In the unidirectional CDW phase, we discover that the amplitude mode develops as a succession of two mean-field, BCS-like transitions with different critical temperatures, which we associate with the presence of two adjacent Te planes in the structure [7, 8, 9, 10].

6 Scanning tunneling spectroscopy studies of cluster compounds (\emptyset . Fischer)

The metal-insulator transition in $M_2\text{Mo}_6\text{Se}_6$ quasi-1D systems has been investigated by means of transport and X-ray measurements and confronted with local density approximation (LDA) calculations of the band structure. The transport data are entirely compatible with the theoretical picture of a dynamic charge density wave, with a quantum critical point separating this phase from the superconducting one. Scanning tunneling spectroscopy (STS) measurements on the quasi-3D materials reveal pseudogapped core spectra for both PbMo_6S_8 and SnMo_6S_8 , probably related to the strongly anisotropic Fermi surfaces and strong interband scattering. STS vortex mapping reveal a transition from a quasi-ordered to a disordered glassy phase at high field.

6.1 Dynamic density waves and quantum criticality in quasi-one-dimensional molybdenum selenides

The nature of the metal-insulator transition in $M_2\text{Mo}_6\text{Se}_6$ ($M = \text{Na}, \text{K}, \text{Rb}, \text{Cs}$) has remained mysterious since its discovery in the early 1980s. These materials are quasi-one-dimensional (Q1D) metals at room temperature, but their electrical resistivity passes through a broad minimum upon cooling before diverging at low temperature. The position of the minimum (considered to be the transition)

shifts progressively to higher temperature as the mass of M increases. Revised band structure calculations performed in Stuttgart reveal a single-Q1D Mo d band at the Fermi level, leading to a remarkably simple Fermi surface consisting of two lightly-warped plates at $k_F \sim \pm\pi/2c$ (where c is the chain axis lattice parameter). Such a highly-nested Fermi surface is immediately suggestive of a Peierls transition; however low-temperature X-ray diffraction experiments at the European Synchrotron Radiation Facility in Grenoble have indicated the absence of a structural phase transition throughout the $M_2\text{Mo}_6\text{Se}_6$ family.

Fortunately, this apparent impasse may be circumnavigated: X-ray measurements have a relatively long timescale (several minutes) and are hence insensitive to high-frequency fluctuations. LDA calculations for the electron-phonon coupling reveal a very shallow phonon potential, implying that any Peierls transition in $M_2\text{Mo}_6\text{Se}_6$ is likely to be dynamic rather than static and hence explaining the absence of any structural modulation at low temperature. This interpretation is reinforced by recent ARPES experiments carried out at the Elettra synchrotron in Trieste, Italy. In addition to confirming the calculated band structure, a temperature-dependent pseudogap was observed to open upon cooling in $\text{K}_2\text{Mo}_6\text{Se}_6$. This behavior is entirely compatible with both our transport data and the theoretical picture of a dynamic charge density wave. Further ARPES experiments are planned to confirm

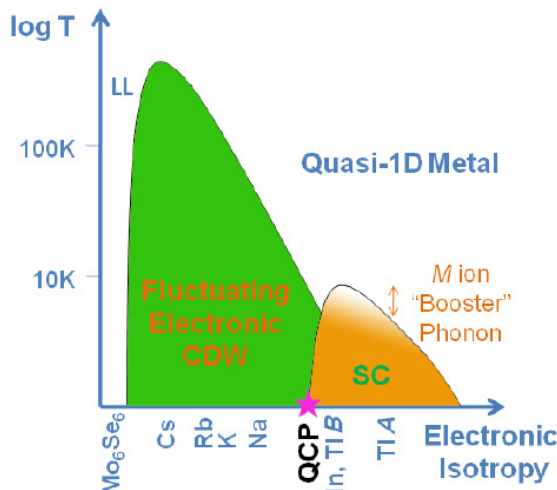


Figure 6: Phase diagram for Q1D $M_2\text{Mo}_6\text{Se}_6$. Upon increasing the isotropy, the system passes from a Luttinger liquid (LL) to a Q1D superconductor (SC) via a fluctuating or dynamic charge density wave (CDW). The x -axis (electronic isotropy) may be tuned by chemical doping, hydrostatic pressure or uniaxial stress along the $(\text{Mo}_6\text{Se}_6)_\infty$ chains.

that a pseudogap is universally present in insulating molybdenum selenides, as well as investigating the scaling of the gap magnitude with transition temperature.

Following our previous work on the superconducting molybdenum selenides ($M = \text{Tl}, \text{In}$) [11], we may now assemble the entire phase diagram for $M_2\text{Mo}_6\text{Se}_6$ (Fig. 6). We postulate that a Quantum Critical Point (QCP) – in this case representing a critical warping of the Fermi surface plates – separates the dynamic density wave and superconducting phases. Above this QCP, fluctuations of the density wave order parameter may result in superconductivity developing from a pseudogapped ground state, in a situation analogous to the high- T_c cuprates.

6.2 Vortex core spectroscopy and the link to Fermi surface anisotropy in Chevrel phase superconductors

Previously, we have obtained conclusive spectroscopic and thermodynamic evidence for multi-band superconductivity in the Chevrel phases SnMo_6S_8 and PbMo_6S_8 [12]. Upon extending our measurements to the mixed state of these materials, we reveal further exotic behavior. Fig. 7 displays a spectroscopic trace through a vortex core in SnMo_6S_8 : an anomalous non-state-conserving pseudogap is present within the vortex cores. This pseudogap is distinct from that seen in the cuprates, since there is no competing magnetism in

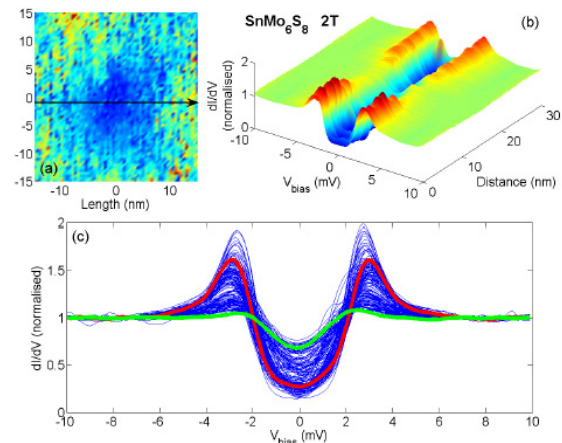


Figure 7: Vortex core spectroscopy in SnMo_6S_8 at 2 T. (a) Fast contrast map to pinpoint an individual vortex, followed by (b) 30 nm spectroscopic scan through the center of the core (trace depicted by arrow in (a)). (c) Superposition of spectra from the trace. A typical spectrum from the superconducting matrix outside the core is shown in red, while a spectrum from the center of the core is highlighted in green.

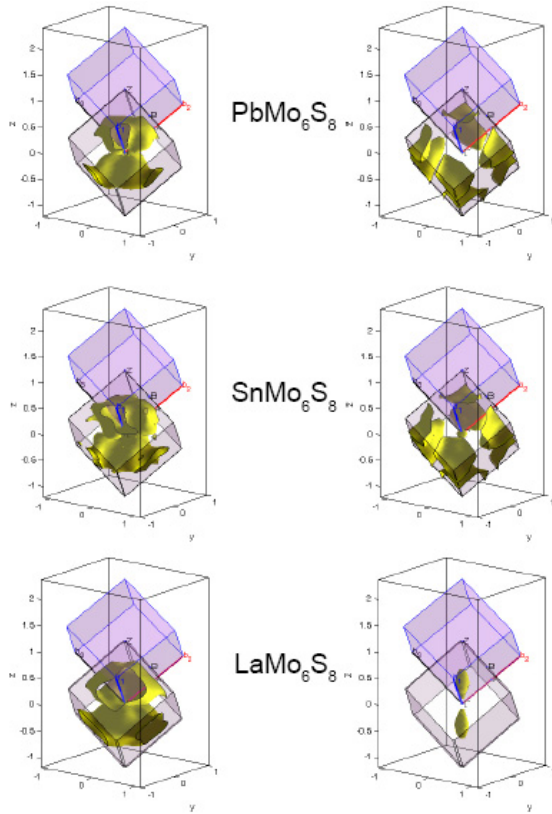


Figure 8: Calculated Fermi surfaces in PbMo_6S_8 , SnMo_6S_8 and LaMo_6S_8 . All Fermi surfaces are centered on the Γ point and displayed within the first Brillouin zone. The calculated Sommerfeld constant γ scales linearly with the critical temperature T_c in each compound, illustrating that the electronic density of states is the primary factor influencing the superconducting transition in Chevrel phases.

Chevrel phases and no normal-state gap above the superconducting transition. Even more extreme behavior is seen in PbMo_6S_8 , where the vortex core spectra are barely distinguishable from superconducting spectra outside the cores (except for a very slight suppression of the coherence peaks). Despite imaging at temperatures well below the quantum limit, no discrete core states may be observed in either material. The upper critical field H_{c2} of PbMo_6S_8 is nearly double that of SnMo_6S_8 , suggesting that the depth of the pseudogap may scale with H_{c2} .

The precise origin of this pseudogap remains mysterious. However, clues for its existence may be found in the strongly anisotropic Fermi surfaces intrinsic to the Chevrel phases. Fig. 8 displays calculated Fermi surfaces for several members of the Chevrel family: the minority contributor to the density of states (right panel) clearly has a highly anisotropic distribution in momentum space. During our STM experiments, tunneling occurs parallel to the

(001) axis and preferentially probes the quasi-isotropic majority band. Upon applying a magnetic field parallel to (001), although the supercurrent surrounding the vortex core is naturally carried by both bands, it is not implausible to suggest that superconductivity may survive in the minority band due to its anisotropic nature. In the case of strong interband scattering, this minority band may induce pairing (though not phase coherence) within the vortex cores observed in the majority band, thus leading to the observed pseudogap.

Further experiments to clarify the nature of this pseudogap and investigate the role of interband scattering in Chevrel phase superconductors are planned. In particular, evaluating the influence of two-band superconductivity on H_{c2} in these compounds may lead to important breakthroughs in understanding the pnictides, which also exhibit a multi-band order parameter and high values of H_{c2} .

6.3 Real-space vortex imaging and glassy topology in extreme type-II superconductors

Scanning tunneling spectroscopy (STS) is an unrivalled tool for vortex imaging in superconductors, since it is the only technique which permits real-space mapping in high magnetic fields. In order to probe the vortex ground state, we have performed sub-Kelvin STS on the Chevrel phase SnMo_6S_8 in fields up to 9 T. The maps obtained (Fig. 9) display a transition from a quasi-ordered low-field state – which we identify as a Bragg glass – to a disordered glassy phase at 9 T.

Complementary studies reveal a peak effect in the bulk magnetization at much higher temperatures. The lack of correlation between the observed peak effect and the vortex glass formation implies that these two phenomena are unrelated. Heat capacity measurements in a magnetic field display a small lambda anomaly just below the superconducting transition, indicative of a metastable vortex melting transition. Together, our spectroscopic and thermodynamic data combine to support a kinetic glass model for vortex glass formation [13]. Given that the upper critical field of SnMo_6S_8 is around 40 T, the majority of $(H - T)$ phase space appears to be occupied by a vortex glass in this material: an unprecedented result which is largely due to its small coherence length and hence increased susceptibility to fluctuations.

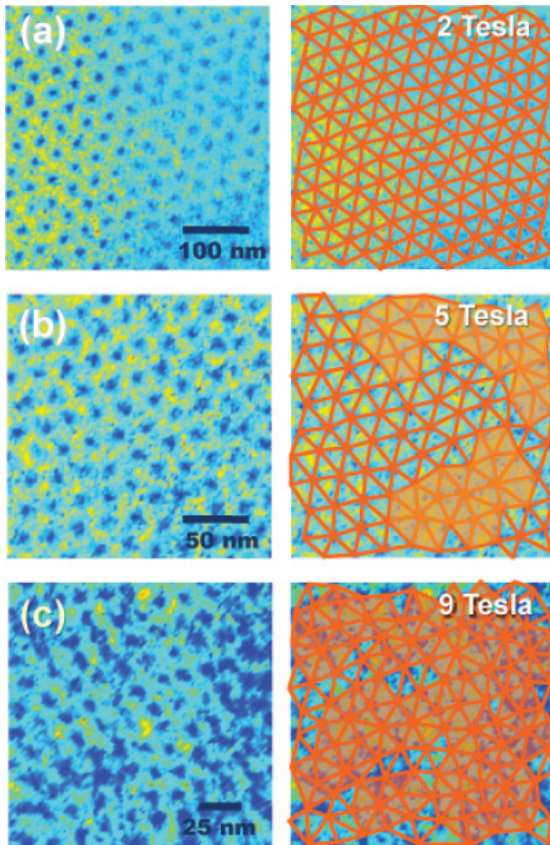


Figure 9: Vortex structure in SnMo_6S_8 at 400 mK imaged by STS at (a) 2, (b) 5 and (c) 9 T. Right panels: corresponding Delaunay triangulations with nearest-neighbors linked by orange lines and topological defects highlighted with orange triangles.

7 Transport and orbital currents in low-dimensional systems (T. Giamarchi)

We computed the Hall effect in quasi-1D conductors in a geometry with the field along the chains. We determined the effects of impurities in an orbital current phase of a two-leg ladder.

7.1 Hall effect in Bechgaard salts

Measuring the Hall coefficient R_H in organic conductors is exceedingly delicate, and the experimental data available so far is sparse. In $(\text{TMTSF})_2\text{PF}_6$ – the compound in which organic superconductivity was first observed under pressure in 1980 [25] – measurements of $R_H(T)$ were reported for two different orientations of the magnetic field with respect to the crystalline axes. In one case [26] the field was along the least conducting axis c and the current along the most conducting axis a (geometry I). $R_H(T)$ was found to increase with T at temperatures well above the ordering temperature ~ 20 K. In another case [27], the field was along a and the current along c (geome-

try II). There $R_H(T)$ was found to be essentially T -independent at high temperature. Classically the Hall effect is a remarkably robust property, insensitive to scattering effects and anisotropies, which admits a simple interpretation in terms of the carrier charge and carrier density. When the Hall coefficient varies with temperature, this is generally attributed either to strong-correlation effects, or to a phase transition in which the charge and/or density of the carriers changes. A first calculation for geometry I, including strong correlations – but not dissipation – led to a temperature-independent R_H consistent with the classical result, despite the fact that both longitudinal and transverse conductivities showed Luttinger liquid power-law temperature dependencies [28]. We have previously found [14] that the temperature dependence of $R_H(T)$ in geometry I can be ascribed to the interaction-induced dissipation along the a axis that was neglected in [28]. We have pursued this investigation by studying the role of dissipation in geometry II, in the case where the umklapp scattering responsible for dissipation is an irrelevant perturbation. Thanks to a scaling analysis we find that both transverse and longitudinal conductivities are again temperature-dependent power laws in this case, but that the exponents exactly cancel, so that R_H becomes T -independent, unlike in geometry I, consistently with experiment. The more difficult case where the umklapp scattering is a relevant perturbation remains to be investigated.

7.2 Orbital currents in ladder systems

We continue our analysis of three-band ladders. As we showed in the previous report such ladders, contrarily to a single-band ladder, can exhibit a massless phase with orbital currents, with relatively simple and microscopically reasonable interactions. In these works we explore the consequences of such orbital currents and in particular we explore the possibility to detect such orbital currents without having to perform a polarized neutron scattering experiment. We examine in particular the effect of impurities in such a phase [15]. We find that impurities lead to distinct signatures, that can be explored both by STM experiments or by NMR. For example we show in Fig. 10 the oscillatory part of the local density of states (LDOS), induced by the presence of an impurity located either on a Cu or an O atom.

We also examine the effects induced by the coupling of charge flow with spin degree of freedom. This is a specific type of spin-orbit

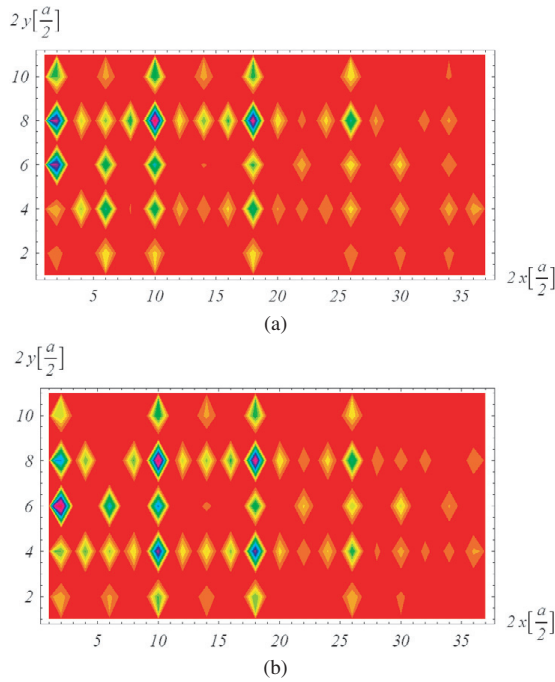


Figure 10: Example of the alternating part of the LDOS around an impurity. The impurity sits in the cell at the left of the left boundary of each panel (hence is not shown). Interference patterns around (a) a strongly asymmetric impurity (Zn substitution of a Cu atom for example) and (b) a weakly asymmetric one (for example on-rung or apical O).

coupling, which can be caused by the orbital current pattern (OCP) flowing within the ladder. The problem is treated in a renormalization group framework, generalized to the case when interactions in the spin-sector are anisotropic. We show that, despite the smallness of the induced magnetic field, because of the spin-rotation $SU(2)$ symmetry breaking, a pseudo-gap can emerge in the spin-sector. This gives rise to observable effects in NMR or neutron scattering experiments, but also may increase the conductivity along the ladder (paper submitted to *Physical Review B*).

8 Collaborative efforts

The most intense collaboration is devoted to the study of the transition metal dichalcogenide family. Beyond regular email and telephone exchanges, a half day meeting was organized in Lausanne with the participation of the Aebi group, Hans Beck, Marco Grioni, Helmuth Berger, a guest scientist Eduard Tutiš (University of Zagreb) and the project leader. The strategy of improving sample quality, the relevant doping/intercalation scenarios and the future common experiments were discussed. The theoretical models of the ex-

citonic mechanism of superconductivity were also raised.

The collaboration with other MaNEP projects are related to graphene and pnictide superconductors.

MaNEP-related publications

- [1] H. Cercellier, C. Monney, F. Clerc, C. Battaglia, L. Despont, M. G. Garnier, H. Beck, P. Aebi, L. Patthey, H. Berger, and L. Forró, *Physical Review Letters* **99**, 146403 (2007).
 - [2] C. Monney, H. Cercellier, F. Clerc, C. Battaglia, E. F. Schwier, C. Didiot, M. G. Garnier, H. Beck, P. Aebi, H. Berger, L. Forró, and L. Patthey, *Physical Review B* **79**, 045116 (2009).
 - ▶ [3] C. Monney, H. Cercellier, C. Battaglia, E. F. Schwier, C. Didiot, M. G. Garnier, H. Beck, and P. Aebi, *Physica B* **404**, 3172 (2009).
 - ▶ [4] C. Monney, E. F. Schwier, C. Battaglia, M. G. Garnier, N. Mariotti, C. Didiot, H. Beck, P. Aebi, H. Cercellier, J. Marcus, H. Berger, and A. N. Titov, arXiv:0911.0327 (2009).
 - [5] B. Sipoš, A. F. Kusmartseva, A. Akrap, H. Berger, L. Forró, and E. Tutiš, *Nature Materials* **7**, 960 (2008).
 - ▶ [6] A. F. Kusmartseva, B. Sipoš, H. Berger, L. Forró, and E. Tutiš, *Physical Review Letters* **103**, 236401 (2009).
 - ▶ [7] M. Lavagnini, H.-M. Eiter, L. Tassini, B. Muschler, R. Hackl, R. Monnier, J.-H. Chu, I. R. Fisher, and L. Degiorgi, arXiv:0909.1289 (2009).
 - ▶ [8] F. Pfüner, J. G. Analytis, J.-H. Chu, I. R. Fisher, and L. Degiorgi, *The European Physical Journal B* **67**, 513 (2009).
 - ▶ [9] A. Sacchetti, C. L. Condron, S. N. Gvasaliya, F. Pfüner, M. Lavagnini, M. Baldini, M. F. Toney, M. Merlini, M. Hanfland, J. Mesot, J.-H. Chu, I. R. Fisher, P. Postorino, and L. Degiorgi, *Physical Review B* **79**, 201101(R) (2009).
 - ▶ [10] M. Lavagnini, A. Sacchetti, C. Marini, M. Valentini, R. Sopracase, A. Perucchi, P. Postorino, S. Lupi, J.-H. Chu, I. R. Fisher, and L. Degiorgi, *Physical Review B* **79**, 075117 (2009).
 - [11] A. P. Petrović, R. Lortz, G. Santi, M. Decroux, H. Monnard, L. Boeri, O. Andersen, J. Kortus, D. Salloum, P. Gougeon, M. Potel, and Ø. Fischer, *submitted to Physical Review B* (2010).
 - [12] A. P. Petrović, R. Lortz, G. Santi, C. Berthod, C. Dubois, M. Decroux, A. Demuer, A. B. Antunes, A. Paré, D. Salloum, P. Gougeon, M. Potel, and Ø. Fischer, *submitted to Physical Review Letters* (2010).
 - ▶ [13] A. P. Petrović, Y. Fasano, R. Lortz, C. Senatore, A. Demuer, A. B. Antunes, A. Paré, D. Salloum, P. Gougeon, M. Potel, and Ø. Fischer, *Physical Review Letters* **103**, 257001 (2009).
 - [14] G. León, C. Berthod, T. Giamarchi, and A. J. Millis, *Physical Review B* **78**, 085105 (2008).
 - ▶ [15] P. Chudzinski, M. Gabay, and T. Giamarchi, *New Journal of Physics* **11**, 055059 (2009).
- ### Other references
- [16] D. Jérôme, T. M. Rice, and W. Kohn, *Physical Review* **158**, 462 (1967).
 - [17] W. Kohn, *Physical Review Letters* **19**, 439 (1967).
 - [18] F. J. Di Salvo, D. E. Moncton, and J. V. Waszczak, *Physical Review B* **14**, 4321 (1976).

- [19] H. P. Hughes, *Journal of Physics C* **10**, L319 (1977).
- [20] J. A. Wilson and S. Mahajan, *Communications on Physics* **2**, 23 (1977).
- [21] J. A. Wilson, *Physica Status Solidi (b)* **86**, 11 (1978).
- [22] E. Morosan, H. W. Zandbergen, B. S. Dennis, J. W. G. Bos, Y. Onose, T. Klimczuk, A. P. Ramirez, N. P. Ong, and R. J. Cava, *Nature Physics* **2**, 544 (2006).
- [23] F. M. F. De Groot, P. Kuiper, and G. A. Sawatzky, *Physical Review B* **57**, 14584 (1998).
- [24] R. Coldea, S. M. Heyden, G. Aeppli, T. G. Perring, C. D. Frost, T. E. Mason, S.-W. Cheong, and Z. Fisk, *Physical Review Letters* **86**, 5377 (2001).
- [25] D. Jérôme, A. Mazaud, M. Ribault, and K. J. Bechgaard, *Journal de Physique (Paris) Lettres* **41**, L95 (1980).
- [26] J. Moser, J. R. Cooper, D. Jérôme, B. Alavi, S. E. Brown, and K. Bechgaard, *Physical Review Letters* **84**, 2674 (2000).
- [27] G. Mihály, I. Kézsmárki, F. Zámorszky, and L. Forró, *Physical Review Letters* **84**, 2670 (2000).
- [28] A. Lopatin, A. Georges, and T. Giamarchi, *Physical Review B* **63**, 075109 (2001).

Project 8

Cold atomic gases as novel quantum simulators for condensed matter

Project leader: T. Giamarchi (UniGE)

Participating members: G. Blatter (ETHZ), T. Esslinger (ETHZ), T. Giamarchi (UniGE), V. Gritsev (UniFR), M. Troyer (ETHZ)

Introduction: The project focusses on issues common to cold atomic gases and condensed matter physics. Indeed cold atomic systems offer unique possibilities to realize model systems with an unprecedented level of control and tunability, allowing to test many issues pertinent to the field of strong correlations, and thus directly centered on the interest of the MaNEP community.

The project revolves mainly around three axes. i) The exploration both theoretical and experimental of the various model systems, such as the Hubbard model, that can be realized by cold atomic gases. ii) The issues of probes and thermometry that are mandatory if one wants to be able to investigate the physics of the strongly correlated quantum systems that can be realized in the cold atomic gases. iii) The out of equilibrium dynamical situations and the novel phases that can be realized in the cold atomic gases and that have not yet their counterpart in condensed matter but can potentially open new fields of investigation, or prompt for new materials in the later.

Summary and highlights

During this year several progress have been made in using the cold atoms as quantum simulators for fermionic and bosonic systems. For bosons, experiments have been validated against very precise numerical calculations. For fermions an excellent agreement has been obtained between theory and experiments on measurements of the double occupation, allowing for a very precise determination of the temperature and entropy in the fermionic Hubbard model. Other systems relevant for condensed matter have been explored, such as disordered and quasi-periodic interacting bosons, showing localization and Bose glass phases, and photons in microcavities, allowing for Mott to superfluid transitions. Several

out of equilibrium phenomena have been analyzed both theoretically and experimentally such as the doublon decay in the Hubbard model. For out of equilibrium physics a general class of systems for which the time evolution can be obtained exactly has been found. Novel phases, offered by the versatility of the cold atomic gases have been explored, in particular the ones that one can obtain in dipolar gases which allow for long range interactions between the atoms. For Bose-Bose mixture the possibility to realize a novel universality class of one-dimensional systems, a ferromagnetic liquid, has been investigated. Last but not least, several analytical and numerical techniques were developed in the context of this project, many of which are directly relevant to other MaNEP projects.

1 Model systems

Experimental progress in the field of atomic quantum gases has led to a fundamentally new approach to examining open questions in quantum many-body physics. The realization of quantum degenerate and strongly interacting Fermi gases, as well as the successful implementation of optically induced lattice potentials [32] allow the study of a centerpiece of quantum condensed matter, the Fermi-Hubbard model, using ultracold atoms [33]. Recent experiments [34, 35] have reported important progress in efforts to access phases of the low-temperature Fermi-Hubbard model with repulsive interactions. Using improved

cooling methods, experiments are now reaching out to explore spin ordered phases. However, the lack of a quantitative determination of temperature and entropy in the lattice has, so far, remained a key obstacle in the approach to quantum magnetism.

1.1 Fermions in optical lattices

a) *Hubbard model* Previous methods to determine the temperature of fermions in the lattice were used in extreme regimes of the Hubbard model. These include the non-interacting or zero-tunneling [34] regimes. The non-

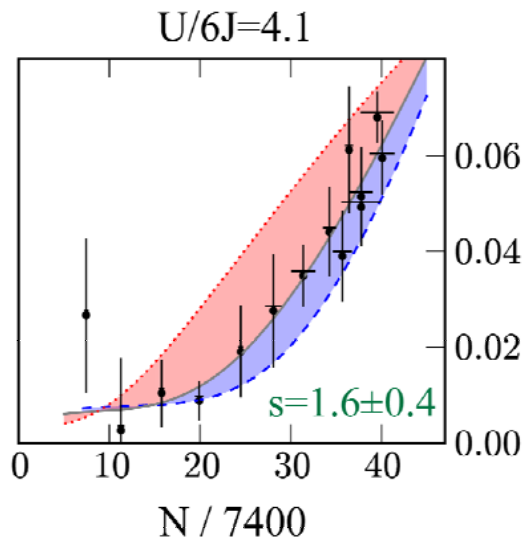


Figure 1: Comparison between the experimental results, and the theoretical calculations for the double occupancy in the Hubbard model, as a function of the total number of atoms N . The agreement is excellent and allows for an accurate determination of the entropy of the system, and hence the temperature.

trivial intermediate regime encompasses rich physics. Here quantitative agreement between theory and experiment should be attainable as long as the current parameters are numerically tractable. It is therefore desirable to develop a reliable method to calibrate experimental results and locate them in parameter space. The essential element here is an accurate, measurable, and sensitive experimental observable allowing a determination of the temperature in the lattice.

In a collaborative work from the groups of T. Esslinger, M. Troyer and the group in Ecole Polytechnique (Paris) a combined experimental and theoretical study of entropy and temperature in the metallic and Mott-insulating regimes of two-component fermions in an optical lattice was reported [1]. Accurately measuring the double occupancy of the system gives direct access to thermal excitations. The crossover from the regime of thermal creation of double occupancies to the regime of thermal depletion was analyzed. The variability of the double occupancy with respect to temperature allows the entropy of the system to be inferred directly from two complementary *ab initio* theoretical methods. An example is shown in Fig. 1. By determining all other quantities entering the analysis separately and with methods that are independent of the double occupancy measurement, the versatility and sensitivity of the double occupancy in quantifying the state of the system was demonstrated. The reliabil-

ity of the entropy determination has been substantiated by a comprehensive analysis of all systematic errors. In the center of the Mott-insulating cloud they have obtained an entropy per atom as low as $0.77k_B$ which is about twice as large as the entropy at the Néel transition. The corresponding temperature depends on the atom number and, for small fillings, reaches values on the order of the tunneling energy. In addition, the group of M. Troyer proposed [2] a probe to measure the “core compressibility” to check for the existence of incompressible phases in trapped fermionic atoms in optical lattices.

To go beyond the Mott regime, and observe, e.g., doped phases, and determine whether a two-dimensional Hubbard model could be superconducting, would be difficult due to the presence of the trap that imposes inhomogeneous phases. An alternative method was proposed, in the group of T. Giamarchi, based on a canonical transformation between the attractive and repulsive Hubbard model [3].

b) *One-dimensional fermions* One-dimensional fermions exhibit also quite interesting features. In particular, in experiments with confined ultracold gases, the 1D interaction parameters are precisely known and can be tuned using Feshbach resonances or by varying the harmonic transverse confinement strength. Such a 1D experimental system has been already realized for potassium. For spin-polarized fermions, only scattering in odd partial wave channels is present, and, at low energies, p -wave scattering is the strongest. However the effective range of scattering needs to be taken into account. The group of V. Gritsev studied this issue and provided an exact solution that accounts for both scattering volume and effective range [4]. They found several new effects, such as the inversion of particle- and hole-like spectra for low momenta, or roton-like minima in the excitation spectrum. They also calculated density profiles and breathing mode frequencies in the harmonic trap. They developed an asymptotic Bethe ansatz (BA) solution which is justified at sufficiently small densities, when only two-particle collisions are important.

1.2 Bosons and photons

a) *Photons and cavities* The recent experimental success in engineering strong interactions between photons and atoms in high-quality micro-cavities has triggered an immense interest in quantum condensed and coherent light-matter systems. One of the

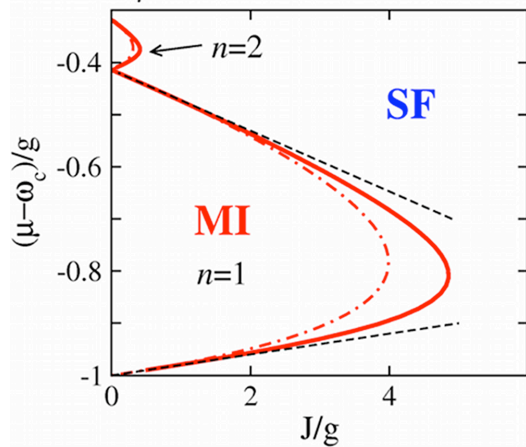


Figure 2: Phase diagram for a hypercubic lattice in $D = 2$, with the polariton chemical potential $(\mu - \omega_c)/g$ (shifted by cavity frequency ω_c) versus photon hopping J/g , displaying a Mott-insulating (MI) and superfluid (SF) phase. Two Mott-lobes for $n = 1, 2$ polaritons at zero detuning are shown for first-order perturbation theory (dashed), mean-field RPA (dot-dashed) and quantum fluctuations (solid).

most exciting questions in this emerging field is whether one can realize a Mott-insulator-superfluid transition of strongly correlated polaritons. The so-called Jaynes-Cummings-Hubbard model (JCHM) [36] has been introduced to describe such a quantum phase transition of light in an array of coupled quantum electrodynamics (QED) cavities, each containing a single photonic mode interacting with a two-level system (qubit), e.g. using an atom. The competition between strong atom-photon coupling g , giving rise to an effective photon repulsion (localization), and the photon hopping J between cavities (delocalization) leads to a quantum phase diagram featuring Mott-lobes reminiscent of those of ultracold atoms in optical lattices as described by the seminal Bose-Hubbard model (BHM) [37]. The group of G. Blatter used a diagrammatic linked-cluster expansion to obtain simple, analytic formulas for the phase diagram as well as elementary excitations in the Mott-phase for arbitrary temperatures, detuning parameters and lattice geometries. They find two new modes and discuss dispersion relations, spectral weights, and effective masses within strong-coupling random phase approximation (RPA) [5]. The effects of quantum fluctuations on the phase boundary are studied beyond RPA (Fig. 2).

b) *Bosons* In the case of bosons, combined diagrammatic techniques and quantum Monte Carlo simulation have been used in the group of M. Troyer to test a variant of Beliaev's diagrammatic methods for calculating proper-

ties of bosonic gases. They obtained a set of relations that accurately describes the properties of interacting 2D and 3D Bose gases away from the critical region [6]. In addition, in [7], the Troyer group has quantitatively compared experiments on interacting bosonic systems with quantum Monte Carlo numerical simulations. This allows to validate the experiments as quantum simulator for such systems and to get the limits of such an approach. The experiments can then be carried out in a reliable way in regions that the numerics cannot reach (dynamics for example).

1.3 Disordered systems

Cold atomic systems offer very controlled realization of disordered interacting systems. Quite recently one-dimensional systems have been realized and Anderson localization has been observed. For strongly interacting particles, one-dimensional systems with quasi-periodic lattices have been realized and the questions of the existence of a Bose glass in such systems has been investigated.

For true disorder the phase diagram of disordered bosons was investigated by the group of M. Troyer [8, 9]. They could settle a long-standing open question of whether there can be a direct transition between a superfluid and a Mott-insulating phase in disordered bosonic systems. They have proven theorems that show the absence of such a direct transition, and that there always has to be an insulating gapless phase bordering the superfluid phase. The group of T. Giamarchi focussed on the issue of the comparison between the effects of true disorder and the one that was realized by biperiodic lattices. Indeed such a system is in fact quasi-periodic, and it is thus important to know how much the properties of such systems resemble or not, for interacting particles, the ones of a true disorder. The phase diagram was shown to be very similar [10]. However important differences appear when one examines the response of the two systems to a shaking of the optical lattice. This method, which is similar albeit not identical to an optical conductivity experiment, has been a very useful probe for systems in optical lattices. The absorption of energy coming from such a shaking was computed for both systems [11]. Surprisingly, a perturbative treatment in both cases, weak and strong disorders, gives a good description at all frequencies, as is shown in Fig. 3.

This result is unexpected since for other quantities, like the conductivity in one-dimensional

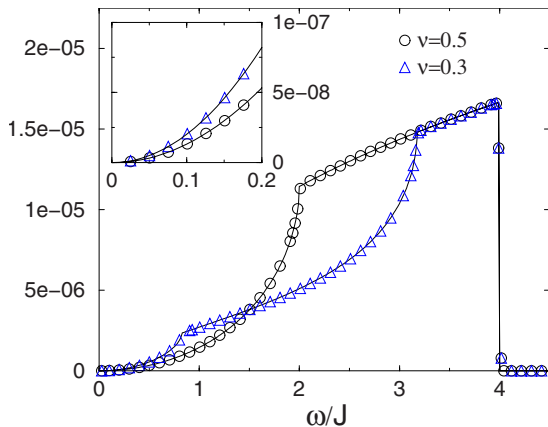


Figure 3: Energy absorbed in a shaking of the optical lattice for a one-dimensional disordered system. The agreement between the analytical calculation (lines) and a numerical solution (dots) is remarkable at all energies. The insert shows a blowup of the low-energy part where the absorption is quadratic at low frequencies. Quasi-periodic systems can be studied in a similar way, and show a quite different absorption spectrum.

systems, perturbation theory is only applicable at high frequencies. The infrared-absorption rate in the thermodynamic limit is found to be quadratic in frequency. Quasi-periodic and truly disordered systems show some marked differences in the absorption.

2 Probes, thermometry and out of equilibrium physics

Understanding the far-from-equilibrium dynamics of strongly correlated systems is a highly challenging task. Even the identification of the basic processes involved and the associated time scales is non-trivial when the system cannot be described by weakly interacting excitations or quasi-particles. Dynamics may couple states with widely different energies making the description in terms of a restricted set of low-energy states impossible.

2.1 Density ripples

The group of V. Gritsev investigated theoretically the evolution of the two-point density correlation function of a low-dimensional ultracold Bose gas after release from a tight transverse confinement. In the course of expansion thermal and quantum fluctuations present in the trapped systems transform into density fluctuations. For the case of free ballistic expansion relevant to current experiments, simple analytical relations between the spectrum of density ripples and the correlation functions of the original confined sys-

tems were derived for weakly and strongly interacting one-dimensional (1D) Bose gases and two-dimensional (2D) Bose gases below the Berezinskii-Kosterlitz-Thouless (BKT) transition. For weakly interacting 1D Bose gases, they obtained an explicit analytical expression for the spectrum of density ripples which can be used for thermometry. For 2D Bose gases below the BKT transition, for sufficiently long expansion times, the spectrum of the density ripples has a self-similar shape controlled only by the exponent of the first-order correlation function. This exponent can be extracted by analyzing the evolution of the spectrum of density ripples as a function of the expansion time [12].

2.2 Out of equilibrium physics in low-dimensional systems

While numerous approximate and exact solutions exist for systems in equilibrium, examples of non-equilibrium dynamics of many-body systems, which allow reliable theoretical analysis, are few and far between. Recently the group of V. Gritsev found a broad class of time-dependent interacting systems subject to external linear and parabolic potentials, for which the many-body Schrödinger equation can be solved using a scaling transformation. They demonstrated that scaling solutions exist for both local and non-local interactions and derive appropriate self-consistency equations and applied this approach to several specific experimentally relevant examples of interacting bosons in one and two dimensions. An example is shown in Fig. 4.

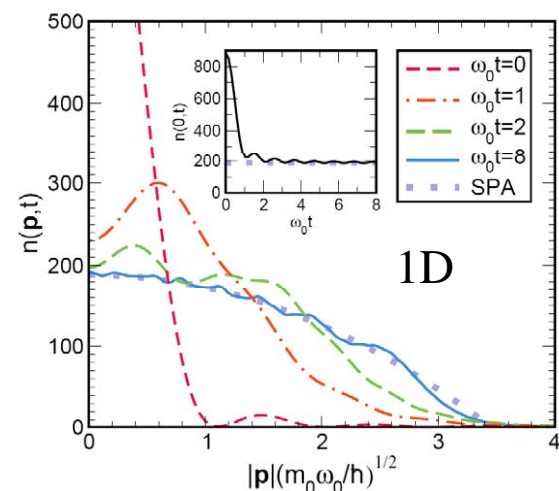


Figure 4: Plot of the momentum distribution for an out of equilibrium 1D system, at different times t . Because of a dynamical symmetry the momentum distribution converges towards a universal distribution.

As an intriguing result they found that weakly and strongly interacting Bose gases expanding from a parabolic trap can exhibit very similar dynamics [13].

The Gritsev group also studied the time evolution of antiferromagnetic order in the Heisenberg chain after a sudden change of the anisotropy parameter, using various numerical and analytical methods [14]. The study is based on numerical simulations using matrix product state method for infinite system sizes (iMPS). As a generic result they found that the order parameter, which can show oscillatory or non-oscillatory dynamics, decays exponentially except for the effectively non-interacting case of the XX limit. For weakly ordered initial states they also found evidence for an algebraic correction to the exponential law. These results were compared to approximative analytical approaches including an effective description by the XZ-model as well as by mean-field, Luttinger liquid and sine-Gordon theories. This reveals which aspects of non-equilibrium dynamics can as in equilibrium be described by low-energy theories and which are the novel phenomena specific to quantum quench dynamics. The relevance of the energetically high part of the spectrum is illustrated by means of a full numerical diagonalization of the Hamiltonian [15].

Finally, motivation for studying out of equilibrium physics comes not only from the basic interests in many-body dynamics but also from possible applications of ultracold atoms such as quantum information processing and interferometric sensing. The group of V. Gritsev theoretically analyzed the decoherence dynamics of Ramsey interference fringes in one-dimensional quasi-condensates which are considered for possible applications in atomic clocks and quantum enhanced metrology. They showed that Ramsey interferometer is also a powerful tool for studying many-body dynamics of low-dimensional quantum systems. The time evolution of the full distribution function of fringe contrast provides unique signatures of the many-body decoherence mechanism and shows that decoherence of Ramsey fringes is strongly affected by the multimode character of 1D systems. The idea of using the full distribution functions to characterize equilibrium many-body states of ultracold atoms has been discussed in [38] and applied in experiments [39]. However there has been so far no application of this approach to non-equilibrium dynamics. The paper [16] is the first proposal to study non-equilibrium dynamics of ultracold atoms with quantum noise.

2.3 Doublon decay in the Fermi-Hubbard model

The group of T. Esslinger took advantage of the realization of the repulsive Fermi-Hubbard model with ultracold atom systems [33, 34, 35] to investigate the relaxation of dynamically generated double occupancy (DGDO) in a fermionic Mott-insulator due to modulation of the optical lattice [17].

In the experiment, they have studied the time evolution of doubly occupied lattice sites (doublons) in the repulsive Fermi-Hubbard model. This model describes fermionic particles hopping on a lattice with tunneling J and on-site repulsion U and is realized by a two-component Fermi gas in an optical lattice. The observation of elastic decay of artificially created doublons into single-particles has been reported [34]. The resulting lifetime is found to increase exponentially with the ratio $U/6J$ (i.e. the lifetime becomes longer as the interactions become stronger). The argument is that a doublon, having an excess energy U , decays in a scattering process involving several single-fermions. Since each of these scattering partners can only absorb an average energy of $6J$, the number of virtual states involved in the simultaneous many-body process is $U/6J$. Hence the decay is exponentially suppressed for increasing $U/6J$. Due to the negligible coupling to an external environment, a direct comparison of experiment and theory was possible. The experimental data is in fair agreement with diagrammatic calculations where the strongly correlated nature of the underlying state is crucial in obtaining the correct value of the scaling exponent [18]. The interpretation of these results shows the importance of high-order scattering processes in bridging the energy gap between low- and high-energy excitations and how they can lead to exponentially slow thermalization.

A theoretical analysis was also worked out in the group of G. Blatter [19, 20]. Using a slave-spin technique at half-filling, they obtained two effective mean-field Hamiltonians describing the (renormalized) hopping of free fermions and a transverse Ising model describing the spin degrees of freedom, described the transition to the insulator, and determined the excitation spectrum. The latter involves coherent fermionic quasi-particle excitations around zero energy (for $U < U_c$) and incoherent (preformed) Hubbard bands around $\max(U, U_c)/2$ deriving from the gapped (Δ) spin degrees of freedom. The double-occupancy signal draws weight from both types, with the one at Δ vanishing at the transition (and thereby allowing to identify the Mott-phase) and the broad peak

at $\max(U, U_c)$ (excitations between Hubbard bands) surviving the transition (and saturating at large $U \gg U_c$). They concluded that a characterization of the localized phase requires a quantitative analysis of the DGDO signal. A calculation of the heat transport through the interface between (bosonic) superfluid and insulating layers in a wedding cake structure was also performed [21].

3 Novel Phases

3.1 Ferromagnetic liquids

Cold atomic systems allow the possibility to realize novel phases, hard to obtain in a condensed matter situation. Motivated by the possibility of experiments in Bose-Bose mixtures the group of T. Giamarchi analyzed the case of a one-dimensional two-component Bose system. These two components can be referred to as “spin”. Contrarily to the case of fermions, such a Bose system has predominantly ferromagnetic interactions. As a result the ground state is totally polarized. Excitations that consist in adding one spin-down particle thus cannot be described by the canonical Luttinger liquid description of one-dimensional systems, and the question of the nature and correlation of such excitations is thus an important open theoretical question. It was shown for a continuum model [22] that such a system has a novel behavior, named “ferromagnetic liquid”, quite different from the standard Luttinger liquid and also from a simple localized ferromagnet, where the charge degrees of freedom would play no role. Such systems are thus examples of “non-Luttinger liquids” in one dimension, and have strong connections with the question of a mobile impurity in a Luttinger liquid and with Caldeira-Leggett problems.

In order to further explore the properties of this novel universality class, the group of T. Giamarchi solved, in the strong coupling limit, the two-component Bose-Hubbard model [23, 24]. This model can be mapped onto a $t - J$ model in a way similar albeit not identical to the fermionic case. All the correlations could be computed, confirming the universal behavior at threshold of the structure factor. The spectral function is shown in Fig. 5.

In the presence of the lattice, the proximity to half filling leads to new effects on the correlation functions that could be computed. In addition, an exactly solvable model (Gaudin-Yang) was analyzed using a combination of exact techniques (Bethe ansatz) and effective field theory [25]. This allowed to obtain for all interactions the behavior close to thresh-

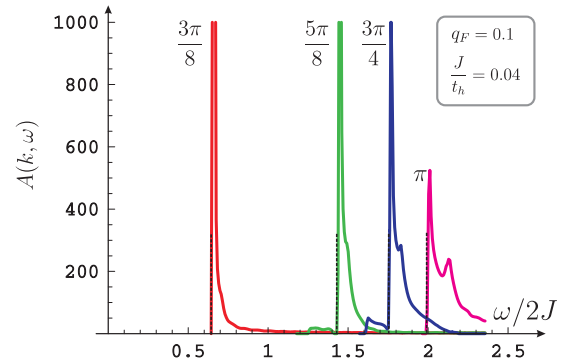


Figure 5: Spectral function for the two-component Bose-Hubbard model as a function of the frequency ω for various values of the momentum k . The spectral function shows a threshold with a universal powerlaw divergence. This defined a novel universality class, a “ferromagnetic liquid”, for a one-dimensional system that is neither a Luttinger liquid, nor a simple localized ferromagnet, since the interplay between the charge and “spin” degrees of freedom conspire to give such a behavior.

old, fully confirming the proposed universality class, and also to derive the low-energy effective Hamiltonian of this universality class, replacing the canonical Luttinger liquid one. Experiments on mobile impurities in cold atom systems have started [40], and comparison and further experiments should shed further light on this problem.

3.2 Dipolar phases

Competing structures and effects of commensuration appear in numerous physical systems, e.g. krypton on graphite or flux quanta in structured superconductors. A new realization of this physics is accomplished by assembling cold dipolar molecules in a two-dimensional optical trap and stabilizing them with the help of a perpendicular electric field [41]. Several aspects of this problem were investigated.

The group of M. Troyer calculated the phase diagram of such dipolar gases on triangular optical lattices and showed the existence of a supersolid phase: a phase with coexisting superfluid and solid order. They showed that, once the temperature of these molecular gases becomes comparable to what can nowadays be achieved for atomic gases, such a supersolid can be realized using dipolar gases in optical lattices [26]. Experiments, if they can be performed at lower temperatures than presently available, should allow to test such predictions.

Adding a square optical lattice provides an effective substrate potential which competes against the triangular lattice arrangement fa-

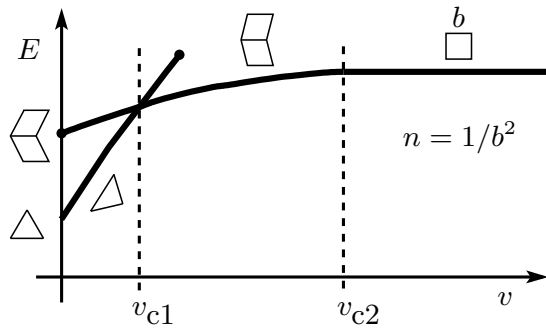


Figure 6: The four phases, floating triangular at $v = 0$, distorted and rotated triangular at $0 < v < v_{c1} \approx 0.045$ (orientationally locked), period-doubled at $v_{c1} < v < v_{c2} \approx 0.20$ (asymmetrically fully locked), and square for $v > v_{c2}$ (symmetrically fully locked), are separated by smooth or sharp transitions: the ordered triangular and square lattices smoothly transform into the distorted triangular and the period-double phases, respectively, whereas the transition at v_{c1} is a sharp one.

vored by the long-range repulsive dipolar interaction. The system exhibits an interesting phase diagram with an interplay between commensuration effects and quantum/classical floating or melting transitions; the group of G. Blatter searched for the minimal energy states in the absence of (quantum/classical) fluctuations and analyzed particle densities n close to commensurate filling $n = 1/b^2$ (b the period of the optical lattice) and different ratios v between the substrate potential V_0 and the interparticle interaction D/b^3 (D the dipolar coupling constant), see Fig. 6.

For weak substrate potentials, the substrate-induced deformation of the particle lattice [42] can be studied using perturbation theory combined with a continuum approximation and the resulting distorted phase is characterized by a non-trivial rotation angle. In the opposite case, at strong substrate potentials, the particles are locked in a square-lattice configuration. Reducing the substrate potential, the square lattice becomes unstable towards a shear mode at the Brillouin zone edge. The new lattice features a period-doubling resulting in an orthorhombic unit cell with a basis; the atoms arrange in a zigzag structure along one direction with symmetry $p2mg$. Such a phase has been predicted to show up in the vortex state of a two-dimensional superconductor with square pinning array [43]. First steps to understand the situation away from commensurate filling are underway.

4 Collaborative efforts

As is obvious when reading the above research there are already strong collaborative efforts between the theory groups and the experimental group of T. Esslinger. There are of course also many interactions with other experimental and theory groups in the field.

Within the other groups of MaNEP there are collaborative efforts in two directions. i) The nature of the themes treated in this project (strongly correlated systems, Hubbard model, phases in dipolar systems, etc.) have direct bearing on several other problems and projects of MaNEP; these points are obvious and will not be detailed again. ii) Some of the techniques that have been developed in the context of the cold atom projects can be directly used in other projects as well. Let us mention some of the specific developments.

The group of M. Troyer developed several algorithms. The main algorithmic development of the past year was the development of a diagrammatic quantum Monte Carlo (DiagMC) algorithm for the Hubbard model [27]. This algorithm samples connected Feynman diagrams instead of the partition function, and works successfully in the correlated Fermi liquid regime of the Hubbard model. It will be used in the future to calculate phase diagrams and equations of state of 2D and 3D fermionic gases. The contractor-renormalization group (CORE) method was extended to models with constraints that could not be treated with the standard CORE method [28]. Methods to improve on systems with broad ensemble distributions, such as close to a first order phase transition, were developed [29]. Finally, in [30], they proposed a new method of distinguishing between several proposed variational wave functions for the ground state of a quantum system, by considering the probability of error as a new measure instead of the overlap. A pedagogical article [31] on how to reliably calculate errors in Monte Carlo simulations was also written.

The group of T. Giamarchi developed methods (described in Project 6) to deal, via dynamical density matrix renormalization group, with the time dependence of correlation functions in real time. Such methods are of course directly useful for the cold atom context. Similarly, to solve the ferromagnetic liquid problem, it was necessary to compute correlation functions of string operators, and a method to write such correlations as a Fredholm determinant was found [24]. Such methods are directly applicable for situations where string operators are important such as spin-chains and ladders.

MaNEP-related publications

- ▶ [1] R. Jördens, L. Tarruell, D. Greif, T. Uehlinger, N. Strohmaier, H. Moritz, T. Esslinger, L. De Leo, C. Kollath, A. Georges, V. Scarola, L. Pollet, E. Burovski, E. Kozik, and M. Troyer, arXiv:0912.3790 (2009).
- [2] V. W. Scarola, L. Pollet, J. Oitmaa, and M. Troyer, *Physical Review Letters* **102**, 135302 (2009).
- [3] A. F. Ho, M. A. Cazalilla, and T. Giamarchi, *Physical Review A* **79**, 033620 (2009).
- ▶ [4] A. Imambekov, A. A. Lukyanov, L. I. Glazman, and V. Gritsev, *Physical Review Letters* **104**, 040402 (2010).
- ▶ [5] S. Schmidt and G. Blatter, *Physical Review Letters* **103**, 086403 (2009).
- ▶ [6] B. Capogrosso-Sansone, S. Giorgini, S. Pilati, L. Pollet, N. Prokof'ev, B. Svistunov, and M. Troyer, arXiv:0911.5383 (2009).
- ▶ [7] S. Trotzky, L. Pollet, F. Gerbier, U. Schnorrberger, I. Bloch, N. V. Prokof'ev, B. Svistunov, and M. Troyer, arXiv:0905.4882 (2009).
- ▶ [8] L. Pollet, N. V. Prokof'ev, B. V. Svistunov, and M. Troyer, *Physical Review Letters* **103**, 140402 (2009).
- [9] V. Gurarie, L. Pollet, N. V. Prokof'ev, B. V. Svistunov, and M. Troyer, *Physical Review B* **80**, 214519 (2009).
- [10] G. Roux, T. Barthel, I. P. McCulloch, C. Kollath, U. Schollwöck, and T. Giamarchi, *Physical Review A* **78**, 023628 (2008).
- [11] G. Orso, A. Iucci, M. A. Cazalilla, and T. Giamarchi, *Physical Review A* **80**, 033625 (2009).
- ▶ [12] A. Imambekov, I. E. Mazets, D. S. Petrov, V. Gritsev, S. Manz, S. Hofferberth, T. Schumm, E. Demler, and J. Schmiedmayer, *Physical Review A* **80**, 033604 (2009).
- [13] V. Gritsev, P. Barmettler, and E. Demler, arXiv:0912.2744 (2009).
- [14] V. Gritsev, T. Rostunov, and E. Demler, arXiv:0904.3221 (2009).
- ▶ [15] P. Barmettler, M. Punk, V. Gritsev, E. Demler, and E. Altman, *Physical Review Letters* **102**, 130603 (2009).
- [16] T. Kitagawa, S. Pielawa, A. Imambekov, J. Schmiedmayer, V. Gritsev, and E. Demler, arXiv:0912.4643 (2009).
- [17] C. Kollath, A. Iucci, I. P. McCulloch, and T. Giamarchi, *Physical Review A* **74**, 041604 (2006).
- ▶ [18] N. Strohmaier, D. Greif, R. Jördens, L. Tarruell, H. Moritz, T. Esslinger, R. Sensarma, D. Pekker, E. Altman, and E. Demler, arXiv:0905.2963 (2009).
- ▶ [19] S. D. Huber and A. Rüegg, *Physical Review Letters* **102**, 065301 (2009).
- [20] F. Hassler and S. D. Huber, *Physical Review A* **79**, 021607(R) (2009).
- [21] S. D. Huber and G. Blatter, *Physical Review B* **79**, 174504 (2009).
- [22] M. B. Zvonarev, V. V. Cheianov, and T. Giamarchi, *Physical Review Letters* **99**, 240404 (2007).
- ▶ [23] M. B. Zvonarev, V. V. Cheianov, and T. Giamarchi, *Physical Review Letters* **103**, 110401 (2009).
- [24] M. B. Zvonarev, V. V. Cheianov, and T. Giamarchi, *Journal of Statistical Mechanics* p. P07035 (2009).
- [25] M. B. Zvonarev, V. V. Cheianov, and T. Giamarchi, *Physical Review B* **80**, 201102(R) (2009).
- ▶ [26] L. Pollet, J. D. Picon, H. P. Büchler, and M. Troyer, arXiv:0906.2126 (2009).
- ▶ [27] E. Kozik, K. Van Houcke, E. Gull, L. Pollet, N. Prokof'ev, B. Svistunov, and M. Troyer, arXiv:0907.0863 (2009).
- [28] A. F. Albuquerque, H. G. Katzgraber, and M. Troyer, *Physical Review E* **79**, 046712 (2009).
- [29] B. Bauer, E. Gull, S. Trebst, M. Troyer, and D. A. Huse, *Journal of Statistical Mechanics* p. P01020 (2010).
- [30] B. Bauer, M. Troyer, V. W. Scarola, and K. B. Whaley, *Physical Review B* **81**, 085118 (2010).
- [31] V. Ambegaokar and M. Troyer, *American Journal of Physics* **78**, 150 (2010).

Other references

- [32] M. Greiner, O. Mandel, T. Esslinger, T. W. Hänsch, and I. Bloch, *Nature* **415**, 39 (2002).
- [33] M. Köhl, H. Moritz, T. Stöferle, K. Günter, and T. Esslinger, *Physical Review Letters* **94**, 080403 (2005).
- [34] R. Jördens, N. Strohmaier, K. Günter, H. Moritz, and T. Esslinger, *Nature* **455**, 204 (2008).
- [35] U. Schneider, L. Hackermüller, S. Will, T. Best, I. Bloch, T. A. Costi, R. W. Helmes, D. Rasch, and A. Rosch, *Science* **322**, 1520 (2008).
- [36] A. D. Greentree, C. Tahan, J. H. Cole, and L. C. L. Hollenberg, *Nature Physics* **2**, 856 (2006).
- [37] M. P. A. Fisher, P. B. Weichman, G. Grinstein, and D. S. Fisher, *Physical Review B* **40**, 546 (1989).
- [38] V. Gritsev, E. Altman, E. Demler, and A. Polkovnikov, *Nature Physics* **2**, 705 (2006).
- [39] S. Hofferberth, I. Lesanovsky, T. Schumm, A. Imambekov, V. Gritsev, E. Demler, and J. Schmiedmayer, *Nature Physics* **4**, 489 (2008).
- [40] S. Palzer, C. Zipkes, C. Sias, and M. Köhl, *Physical Review Letters* **103**, 150601 (2009).
- [41] H. P. Büchler, E. Demler, M. Lukin, A. Micheli, N. Prokof'ev, G. Pupillo, and P. Zoller, *Physical Review Letters* **98**, 060404 (2007).
- [42] J. P. McTague and A. D. Novaco, *Physical Review B* **19**, 5299 (1979).
- [43] V. Zhuravlev and T. Maniv, *Physical Review B* **68**, 174507 (2003).



Techniques and know-how

Responsibles: Enrico Giannini (UniGE), Patrycja Paruch (UniGE), Andreas Schilling (UniZH), Ivan Maggio-Aprile (UniGE), Christof Niedermayer (PSI), Philipp Aebi (UniFR), Urs Staub (PSI), Leonardo Degiorgi (ETHZ), Matthias Troyer (ETHZ)

Summary: During Phase II of MaNEP, two specific projects were dedicated to stimulate the search for new materials and the growth of single-crystals of high quality. This effort brought together materials scientists from various MaNEP institutions and created a common concern for the importance of the search for new materials and the elaboration of high-quality crystals. In the third phase, we chose to put experimentalists, materials scientists and theoreticians together in each of the 8 projects focused each on a specific topic. In order to compensate for the loss of contacts between materials specialists, we decided to appoint a special person to stimulate contacts between the materials people. In order to extend this idea, we created the 9 Techniques and know-how topics which each represent a technique watch of the technical domains important in MaNEP. Some activities have started and several are planned for the coming year.

1 Crystal growth and bulk materials processing

Responsible: Enrico Giannini (UniGE)

The third phase of MaNEP has started under the sign of an exciting novelty in solid state physics: the discovery of superconductivity in Fe-based pnictides and chalcogenides in 2008. This discovery has stimulated a prompt reaction of the crystal growers within MaNEP. In a very short time, state-of-the-art crystalline samples of numerous new compounds have been grown in the MaNEP laboratories, thus contributing to dozens of outstanding publications and affirming the Swiss research at the forefront in this field.

Single-crystals of quaternary ferro-pnictides ("1111") are grown at the ETHZ by the group of J. Karpinski, by using a flux growth technique under high pressure in a cubic-anvil high-pressure furnace. The crystals of $LnFeAsO_{1-x}F_x$ ($Ln = La, Pr, Nd, Sm, Gd$) grown by this technique exhibit a high structural and chemical purity, and a unique size for this kind of compounds ($> 200 \mu m$). Single-crystals of ternary superconducting pnictides (of the so called "122" type), have been grown as well by the same group, by using a flux growth technique. Sizeable crystals of $Ba_{1-x}Rb_xFe_2As_2$, $CaFe_{2-x}Co_xAs_2$ and $EuFe_{2-x}Co_xAs_2$ are successfully used for the investigation of the effect of doping on the spin-density wave transition. Various MaNEP groups, at ETHZ, UniZH, and UniGE, are closely collaborating on this topic.

The third family of Fe-based superconductors is that of binary chalcogenides $FeCh$ ($Ch = S,$

Se, Te), called "11" whose structural simplicity offers the best tool for investigating the nature of superconductivity and magnetism in these class of compounds. Single-crystals of Fe-based chalcogenides are grown at PSI (K. Conder and E. Pomjakushina) and at UniGE (E. Giannini), by either the Bridgeman method or floating zone melting. A complete set of experimental investigations, including transport and magnetic measurements, muon-spin rotation, X-ray and neutron diffraction, STM, ARPES and optical spectroscopy is carried out at PSI and UniGE, as well as at ETHZ and EPFL. Four MaNEP institutions and ten MaNEP members are actively involved in this research. More than twenty publications have resulted in 2009 based on crystals of Fe-based superconductors grown within MaNEP.

Complex oxides with peculiar ladder- or chain-like structures are grown by the Traveling Solvent Floating Zone (TSFZ) method using image furnaces. High-quality centimeter size single-crystals of $Bi(Cu_{1-x}Zn_x)_2PO_6$ ($x = 0\%, 1\%, 5\%$) have been grown and fully characterized at PSI. A series of spin ladder compounds $Sr_{14-x}Ca_xCu_{24}O_{41}$ ($x \leq 12.2$) have been grown at PSI under oxygen pressures up to 15 bar, and Bi- and Ca- co-doped crystals of the same compound have been grown at UniGE. Various materials exhibiting low-dimensionality in the electronic and magnetic properties are grown at EPFL (H. Berger). Crystals of $BaVS_3$ and various oxo-halogenides (i.e. $Cu_2Te_2O_5Br_2$) are grown by chemical vapor transport in 2-zone furnaces and make the object of extensive studies of the EPFL group as well as of external collaborations.

A substantial amount of work is devoted to novel materials for technological applications. Crystals of mixed valence $\text{CaMn}_{0.98}\text{Nb}_{0.02}\text{O}_3$, a promising material for thermoelectric applications, have been grown at Empa (A. Weidenkaff) by a TSFZ method in an image furnace. Thanks to an innovative microwave-hydrothermal equipment, the group of G. Patzke at the Institute of Inorganic Chemistry (UniZH) has established a new access to nano-scale zinc copper gallates. These spinel systems are difficult to synthesize in nano-structured form and they are promising for the construction of nano-catalysts.

The Single-Crystal Catalog of MaNEP has been updated with the Year 9 new crystals (see p. 123).

New Facilities

A new cubic anvil high-pressure apparatus (Rockland Research Corp.) has been installed at ETHZ (J. Karpinski). Thanks to this equipment, the increasing demand of materials to be grown under extreme conditions (e.g. quaternary pnictides and MgB_2) can be complied with.

The TSFZ growth in a mirror furnace has emerged as a versatile and efficient technique, particularly suitable for growing crystals of non-congruent melting oxides. A new mirror furnace for TSFZ has been installed at Empa (A. Weidenkaff), that expands the facilities already existing at PSI and UniGE. The TSFZ apparatus at PSI has been upgraded to work at a pressure of 15 bar, and further upgrade is in progress to achieve 30–40 bar of oxygen pressure.

A state-of-the-art microwave-hydrothermal system (MARS5 microwave reactor from CEM Corporation) is operated at UniZH (G. Patzke). With this equipment, it is possible to access nano-scale oxides, starting from readily available precursor materials, on a hour time-scale. Such a microwave-assisted oxide synthesis is suitable for a large scale production of nano-materials that are difficult to produce with classical techniques.

2 Thin film growth and characterization

Responsible: Patrycja Paruch (UniGE)

Regarding the thin films techniques and know-how section, we have begun compiling information for a database of the different thin films and the corresponding deposition techniques that are implemented by the groups in MaNEP. This database should be available for users by

April-May, and include an internally-available bulletin board where students can post questions about troubleshooting a growth chamber/deposition process. In addition, we plan to participate in the upcoming MaNEP winter school, together with the other techniques and know-how sections, either via short presentations of the different available processes, or by providing notes for the students outlining the thin film deposition methods used in MaNEP.

3 Electronic transport, high-pressure and thermodynamic techniques

Responsible: Andreas Schilling (UniZH)

A number of groups within the MaNEP network share a specialized know-how on measurements of electronic transport properties, thermodynamic quantities and physical properties under high pressure. L. Forró (EPFL): resistivity and ESR under hydrostatic pressure; D. Jaccard (UniGE): resistivity, ac calorimetry and Seebeck coefficient under pressure; H. Keller (UniZH): high-pressure SQUID magnetization; A. Schilling (UniZH): ac and continuous-heating calorimetry, magneto-caloric effect; H.-R. Ott (ETHZ): heat capacity with relaxation techniques, NMR in the milliKelvin range under hydrostatic pressure; L. Degiorgi (ETHZ): optical spectroscopy under pressure; U. Zimmermann (PSI): μSR investigations under pressure; and Th. Strässle (PSI): neutron-scattering experiments under pressure. While several of these groups already have a long tradition in informal collaborations, we plan to establish a workshop for PhD students and other interested researchers that primarily focuses on the practical experimental challenges of these techniques, rather than on the particular underlying scientific questions.

4 Scanning local probes techniques

Responsible: Ivan Maggio-Aprile (UniGE)

Many groups in MaNEP share the common interest of investigating characterizing or manipulating materials at the nanometer scale with local probes. The first goal of this technical know-how network consists in collecting all information about the available equipments used by the different teams in MaNEP. This task is currently under progress. On the basis of the collected information, we will set up a database which will be accessible by all interested users through the MaNEP website. The general interests and needs of researchers using local

probes techniques will be evaluated in order to organize a one-day user meeting on a specific theme. A participation in the 2011 MaNEP winter school is also considered.

5 Neutron scattering and muon spin resonance

Responsible: Christof Niedermayer (PSI)

Neutron scattering developments

The new thermal triple axis instrument EIGER is being constructed to expand the energy range and open new measurement possibilities at the SINQ neutron source at PSI. It consists of a focused in-pile section with a direct view of the thermal neutron source, a primary spectrometer optimized for high flux and low background. For the commissioning phase (end of 2010/beginning of 2011) and the initial tests and experiments a standard secondary spectrometer with a single-detector will be used. A multiplexing secondary spectrometer allowing significantly increased solid angle coverage from small samples without sacrificing momentum-resolution is planned for the future.

Muon spin spectroscopy (μ SR) developments

Among the μ SR user community a rising demand to perform μ SR studies under high-magnetic fields is clearly noticeable. To cope with this increasing demand, a proposal for new μ SR high-field instrument has been submitted to the PSI research commission (FOKO) and approved in June 2009. The spectrometer will consist of a very compact superconducting 10 T magnet with a very high field homogeneity (few ppm) and a very small field drift (< 1 ppm/h). A cryogen free horizontal dilution refrigerator will extend the temperature range into the mK regime. Novel research areas in condensed matter physics and chemistry will become possible with the commissioning of the high-field μ SR instrument in 2011.

Conclusion

In order to promote these new experimental tools and to identify possible areas within research program of MaNEP, which could profit from applying the new techniques, it is planned to organize a workshop in early 2011.

6 Electron spectroscopies

Responsible: Philipp Aebi (UniFR)

During the project period several developments have taken place. At the new ADDRESS beam-line of the Swiss Light Source the end-station for the soft X-ray ARPES experiment in the energy range 300–1600 eV has been delivered and extensive commissioning has started. The photon energy range of this beam-line will allow for so-called high-energy ARPES around 1 keV in order to render it more bulk sensitive. The first pilot experiments are envisioned in March 2010 and full user operation from June 2010 on.

Another planned new beam-line, the PEARL beam-line is well underway. PEARL stands for PhotoEmission and Atomic Resolution Laboratory and will be specialized for photoelectron diffraction experiments combined with STM/AFM on nano-structured surfaces of novel materials. The financing is settled, a new beamline scientist has been appointed, the front-end for the beam line has been ordered and the decision on the optics to be used has been taken. The perspective is that user operation can start end of 2011.

There is also good news from the ARPES laboratory at EPFL (M. Grioni). An instrumental up-grade has been organized and implemented with a new electron analyzer (SPECS), docking capabilities for a pulsed laser deposition system and a surface-science preparation chamber.

Last but not least, an international workshop on ARPES and strong correlations (CORPES09) has been organized by members of MaNEP and the PSI. MaNEP has also sponsored this workshop. More details on this conference can be found in chapter 4.1.4, p. 134.

7 X-ray elastic and inelastic scattering

Responsible: Urs Staub (PSI)

For the technique of X-ray elastic and inelastic scattering, there is, early November 2010, a planned short one day workshop to be held at the Swiss Light Source (SLS) at PSI (organized by M. Grioni and U. Staub), to gather and update interested groups within MaNEP. The workshop is focused on resonant X-ray techniques. The main purpose is twofold. First, it is to present tutorials for groups interested getting used to the often highly complex resonant X-ray techniques available at the SLS. This is in particular focused on level of understanding of students and postdocs. Secondly, it is to bolster

collaborations within MaNEP and to help getting collaborations going, bridging the gap between university based techniques with those of large facilities. For that purpose, the experimental possibilities at the light source will be presented. This is combined with contributions of results presented by groups using already resonant X-ray techniques within MaNEP. The program will also contain a key lecture of an expert outside the network, to explain a single topic in more detail. The program will be round up by an open discussion on what new techniques will be available and the possibilities of possible improvements and of possible collaborations.

8 Infrared spectroscopy

Responsible: Leonardo Degiorgi (ETHZ)

Optical spectroscopic methods are known to be powerful experimental tools in order to address the complete excitation spectrum of a large variety of novel materials, which are of relevance in the ongoing solid state physics research. There is a broad know-how on optics within the Swiss scientific community, particularly as far as the infrared (IR) spectroscopy is concerned. Three research groups at UniGE (D. van der Marel), UniFR (C. Bernhard) and ETHZ (L. Degiorgi) exploit a wealth of optical techniques, like reflectivity and transmission measurements, broadband ellipsometry, time domain THz and Kerr-effect spectroscopy, as well as IR-microscopy. These methods allow covering a rather broad energy interval from the THz up to the ultraviolet, which is the prerequisite for having access to all energy scales, relevant to the nowadays modern problems in condensed matter. Moreover, ellipsometry and time domain THz spectroscopy allow to measure simultaneously amplitude and phase reflection/transmission, which in turn provide the real and imaginary part of the optical constant. It is also worthwhile to emphasize the combination of those spectroscopies with externally tunable variables like temperature, magnetic and electric field, and also pressure. Needless to say that complex phase diagrams can be addressed with our experimental setups. There is furthermore an ongoing effort to coordinate and exploit all available synergies and know-how among the three Swiss groups, in order to optimize the employment of this large variety of spectroscopic tools. In this respect, a relevant role is played by the infrared (IR) beam-line at the Swiss Light Source (SLS). Following the initiative of the Zurich group, a team at the SLS built a facility that

collects IR radiation from a bending magnet. The beamline passed first tests. Further developments were necessary to improve the performance, in particular several noise reduction steps were taken to fully exploit the advantages of the synchrotron radiation (SR) source in the far-IR energy range. Also in the future, special efforts from the IR-community will be dedicated in order to boost possible improvements and equipment-developments of the IR-beamline at SLS. The successful experiments conducted during 2009 involved the participation of several groups of investigators from Switzerland and abroad; this will continue in 2010 as well. The IR micro-spectrometer coupled to the SR source is moreover in regular user operation at the SLS. This analytical tool opens-up new perspectives in fields like condensed and soft matter physics, chemistry and life science, to name just a few. The pressure dependent IR response of samples can be measured using the small spot offered by the SR source. Moreover, temperature dependent optical reflection and transmission as well as chemical mapping at the diffraction limit are possible. In addition to the new nearby SLS facility, the three Swiss groups have very good connections to other synchrotron facilities at ANKA-Karlsruhe, Brookhaven and ELETTRA-Trieste. In summary, top-quality instrumentations will allow broad-band collaborations going well beyond the IR-community and involving other groups within the MaNEP program. In the spirit of MaNEP Phase III, we wish to strengthen the contacts within the IR-community in Switzerland by organizing regular meetings and workshops, allowing a productive exchange of know-how and results among the PhD students and postdocs. The 9th conference on low energy electrodynamics of solids (LEES) will take place in July 2010 in Switzerland. Experts on optical spectroscopy from all over the world will gather at this meeting. The know-how on optical spectroscopy in Switzerland is involved through MaNEP scientists acting as a conference chair, as local organizers and as program committee members.

9 Theoretical and numerical methods

Responsible: Matthias Troyer (ETHZ)

In the technology platform on computational and theoretical methods there has been the start of two activities in this first year of MaNEP Phase III. On the educational side we are organizing a tutorial on simulations of strongly correlated systems, to be held at ETHZ in September 2010. For this the majority

of funding comes from CECAM and the ESF network Intelibiomat.

The main activity was the start of the MAQUIS project (Modern Algorithms for QUantum Interactions Systems) on petaflop-scale implementation of modern simulation algorithms such as quantum Monte Carlo, the density matrix renormalization group method, exact diagonalization, series expansion and new tensor network algorithm. For this project, a

collaboration between T. Giamarchi, F. Mila and M. Troyer, we have obtained funding of 1'200'000 Swiss Francs from the Swiss High Performance and Productivity Computing (HP2C) initiative. With these funds we are in the process of hiring three to four software engineers to develop faster implementation of the above mentioned algorithms for future computing platforms. These codes will then be used for scientific projects within MaNEP.

Material	Growth technique	Furnace	Conductor	Insulator	Magnetic	MaNEP Institution	Responsible
Various elemental metals	Bridgman, Zone melting	RF Induction, Electronic bombardment	yes			UnGe	Giannini (022.3796076, enrico.giannini@unige.ch)
Bi(1-x)SbX	Zone melting	Mirror image furnace	yes	yes (depending on x)		UnGe	Giannini (022.3796076, enrico.giannini@unige.ch)
Bi2Se3	self flux, TSFZ	1-zone furnace, Mirror image furnace	yes	yes (depending on doping)		UnGe	Giannini (022.3796076, enrico.giannini@unige.ch)
FeTe(1-x)Sex	self flux, TSFZ	1-zone vertical furnace, Mirror image furnace	yes, superc. Tc<13K			UnGe	Giannini (022.3796076, enrico.giannini@unige.ch)
BiIn	self flux	1-zone vertical furnace	yes/no		some	UnGe	Giannini (022.3796076, enrico.giannini@unige.ch)
TMSi, (TM)=Transition Metal; Co, Fe, Mn, ...)	Czochralski, TSFZ	RF Induction, Mirror image furnace	yes/no		some	UnGe	Giannini (022.3796076, enrico.giannini@unige.ch)
(TM, TM')S, solid solutions	Czochralski	RF Induction	yes/no			UnGe	Giannini (022.3796076, enrico.giannini@unige.ch)
CeCoGe3	flux growth	1-zone vertical furnace	yes, superc. Tc=39K			UnGe	Giannini (022.3796076, enrico.giannini@unige.ch)
MgB2	Mg-flux under HP	cubic anvil hot press	no	yes		UnGe	Giannini (022.3796076, enrico.giannini@unige.ch)
Sr14Cu24O41	TSFZ	Mirror image furnace	no	yes		UnGe	Giannini (022.3796076, enrico.giannini@unige.ch)
(Sr,M1,M2)74Cu24O41-x (M1, M2 = Ca, Bi, Y...)	TSFZ	Mirror image furnace	no	yes		UnGe	Giannini (022.3796076, enrico.giannini@unige.ch)
Bi2Sr2Ca2Cu3O10	TSFZ	Mirror image furnace	Yes, superc. Tc=110 K			UnGe	Giannini (022.3796076, enrico.giannini@unige.ch)
Bi2-xPb-xSr2Ca2Cu3O10+d	TSFZ	Mirror image furnace	Yes, superc. Tc=110 K			UnGe	Giannini (022.3796076, enrico.giannini@unige.ch)
Bi2Sr2Ca2O8	TSFZ	Mirror image furnace	Yes, superc. Tc=91 K			UnGe	Giannini (022.3796076, enrico.giannini@unige.ch)
Bi2-xPb-xSr2Ca2O8	TSFZ	Mirror image furnace	Yes, superc. Tc=83 K			UnGe	Giannini (022.3796076, enrico.giannini@unige.ch)
Bi2-xPb-xSr2Ca2O8	TSFZ, self flux	Mirror image furnace, 3-zone vertical	Yes, superc. Tc=83 K			UnGe	Giannini (022.3796076, enrico.giannini@unige.ch)
Bi2Sr2CuO6	TSFZ	Mirror image furnace	Yes, superc. Tc=80 K			UnGe	Giannini (022.3796076, enrico.giannini@unige.ch)
REBa2Cu3O7	self flux	3-zone furnace, Top seeded growth	Yes, superc. Tc=80 K			UnGe	Giannini (022.3796076, enrico.giannini@unige.ch)
PbMo6S8	solid state synthesis		Yes, superc. Tc=15K			UnGe	Fischer (022.3796270, Oystein.Fischer@unige.ch)
SnMo6S8	solid state synthesis		Yes, superc. Tc=14K			UnGe	Fischer (022.3796270, Oystein.Fischer@unige.ch)
Sr(1-x)PbxMo6S8	solid state synthesis		Yes, superc. Tc=14K			UnGe	Fischer (022.3796270, Oystein.Fischer@unige.ch)
LaMo6S8	solid state synthesis		Yes, superc. Tc=7K			UnGe	Fischer (022.3796270, Oystein.Fischer@unige.ch)
Mo6S8	solid state synthesis		Yes, superc. Tc=6K			UnGe	Fischer (022.3796270, Oystein.Fischer@unige.ch)
Mo6S8	solid state synthesis		Yes, superc. Tc=1K			UnGe	Fischer (022.3796270, Oystein.Fischer@unige.ch)
Mo6S8B2	solid state synthesis		Yes, superc. Tc=13.5K			UnGe	Fischer (022.3796270, Oystein.Fischer@unige.ch)
InMo6S8	solid state synthesis		Yes			UnGe	Fischer (022.3796270, Oystein.Fischer@unige.ch)
Ti2Mo6S6e6	solid state synthesis		Yes, superc. Tc=4.2K			UnGe	Fischer (022.3796270, Oystein.Fischer@unige.ch)
In2Mo6S6e6	solid state synthesis		Yes, superc. Tc=2.9K			UnGe	Fischer (022.3796270, Oystein.Fischer@unige.ch)
Ni2Mo6S6e6	solid state synthesis		Yes, superc. Tc=2.9K			UnGe	Fischer (022.3796270, Oystein.Fischer@unige.ch)
K2Mo6S6e6	solid state synthesis		No	Metal-insulator		UnGe	Fischer (022.3796270, Oystein.Fischer@unige.ch)
Rb2Mo6S6e6	solid state synthesis		No	Metal-insulator		UnGe	Fischer (022.3796270, Oystein.Fischer@unige.ch)
Cs2Mo6S6e6	solid state synthesis		No	Metal-insulator		UnGe	Fischer (022.3796270, Oystein.Fischer@unige.ch)
Mo6Se6	solid state synthesis		No			UnGe	Fischer (022.3796270, Oystein.Fischer@unige.ch)
CsMo12S14	solid state synthesis		Yes, superc. Tc=7K			UnGe	Fischer (022.3796270, Oystein.Fischer@unige.ch)
Rb2Mo6S9	solid state synthesis		Yes, superc. Tc=5K			UnGe	Fischer (022.3796270, Oystein.Fischer@unige.ch)
Ba2Mo6S9	solid state synthesis		Yes, superc. Tc=4-10K			UnGe	Fischer (022.3796270, Oystein.Fischer@unige.ch)
Rb2(M1)6(n-9)S(6n+13) (n = 1-4)	flux growth, under HP	cubic anvil hot press	Yes, superc. Tc=20 - 55K			ETHZ	Karpinski (044.6332254, karpinski@phys.ethz.ch)
LnFeAsO(1-x)FxF2 (Ln=La, Pr, Nd, Sm, Gd)	flux growth		Yes, superc. Tc=20K			ETHZ	Karpinski (044.6332254, karpinski@phys.ethz.ch)
CaFe(2-x)CoxAs2	flux growth		Yes, superc. Tc=20K			ETHZ	Karpinski (044.6332254, karpinski@phys.ethz.ch)
EuFe(2-x)CoxAs2	flux growth		Yes, superc. Tc=20K			ETHZ	Karpinski (044.6332254, karpinski@phys.ethz.ch)
Ba1-xRbxFe2As2	flux growth		Yes, superc. Tc=23K	yes		ETHZ	Karpinski (044.6332254, karpinski@phys.ethz.ch)
AkGa1-xN	flux growth		Yes, superc. Tc=23K			ETHZ	Karpinski (044.6332254, karpinski@phys.ethz.ch)
MgB2	Mg-flux under HP	high-pressure furnace	yes, superc. Tc=39K			ETHZ	Karpinski (044.6332254, karpinski@phys.ethz.ch)
Mg(1-x)AlxB2	Mg-flux under HP	cubic anvil hot press	yes, superc. Tc=39K			ETHZ	Karpinski (044.6332254, karpinski@phys.ethz.ch)
MgB2-xCxB2	Mg-flux under HP	cubic anvil hot press	yes			ETHZ	Karpinski (044.6332254, karpinski@phys.ethz.ch)
Mg(1-x)MnxB2	Mg-flux under HP	cubic anvil hot press	yes			ETHZ	Karpinski (044.6332254, karpinski@phys.ethz.ch)
Mn(1-x)FexB2	Mg-flux under HP	cubic anvil hot press	yes			ETHZ	Karpinski (044.6332254, karpinski@phys.ethz.ch)
KOx2O6	arapoude method	resistive furnace	yes, superc. Tc=9.6K			ETHZ	Karpinski (044.6332254, karpinski@phys.ethz.ch)
Na2Ox2O6.5	HP	cubic anvil hot press	no			ETHZ	Karpinski (044.6332254, karpinski@phys.ethz.ch)
YBaCu4O8	HP	high O2 pressure	yes, superc. Tc=80K			ETHZ	Karpinski (044.6332254, karpinski@phys.ethz.ch)
Ca(2-x)NaxCuO2C2	HP	cubic anvil hot press	yes, superc. Tc=80K			ETHZ	Karpinski (044.6332254, karpinski@phys.ethz.ch)
YBa(2-x)SrxCu4O8	HP	high O2 pressure	yes, superc. Tc=13-25K			ETHZ	Karpinski (044.6332254, karpinski@phys.ethz.ch)
CaMn0.98Nb0.02O3	HP	Mirror image furnace	yes, superc. Tc=80K			ETHZ	Karpinski (044.6332254, karpinski@phys.ethz.ch)
FeTe(1-x)Sex	self flux	1-zone vertical furnace	yes, superc. Tc=80K			ETHZ	Karpinski (044.6332254, karpinski@phys.ethz.ch)
Bi(Cu(1-x)Zn(x))2P2O6 (x=0 - 0.05)	high pressure TSFZ	Mirror image furnace	yes, superc. Tc=13K	yes		ETHZ	Weidenkaff (044.8234131, Anke.Weidenkaff@empa.ch)
Sr(14-x)Ca(x)Cu24O41 (x up to 12.2)	high pressure TSFZ	Mirror image furnace	yes, superc. Tc=13K			ETHZ	Weidenkaff (044.8234131, Anke.Weidenkaff@empa.ch)
YMoO3	TSFZ	Mirror image furnace	yes, superc. Tc=19K			ETHZ	Conder (kazmierz.conder@psi.ch)
DyMoO3	TSFZ	Mirror image furnace	yes, superc. Tc=19K			ETHZ	Conder (kazmierz.conder@psi.ch)
LaCoO3	TSFZ	Mirror image furnace	stacked-triangular AF			ETHZ	Pomjakushina (ekaterina.pomjakushina@psi.ch)
La(1-x)SrxCoO3	TSFZ	Mirror image furnace	AF Th=40K, ferroelectric T<19K			ETHZ	Kazmierz Conder/Ekaterina Pomjakushina
SrCu2(BO3)2	TSFZ	Mirror image furnace	magnetic and spin state transitions			ETHZ	Kazmierz Conder/Ekaterina Pomjakushina
EUNi2S(1-x)Gex)2	TSFZ	Mirror image furnace	magnetic and spin state transitions			ETHZ	Kazmierz Conder/Ekaterina Pomjakushina
			2D spin system			ETHZ	Kazmierz Conder/Ekaterina Pomjakushina
			valence transition in Eu-PSI			ETHZ	Kazmierz Conder/Ekaterina Pomjakushina

Material	Growth technique	Furnace	Conductor	Insulator	Magnetic	MaNEP Institution	Responsible
LaFeO3	TSFZ	Mirror image furnace		magneto-optical Faraday effect	PSI	Kazimierz Conder/Ekaterina Pomjakushina	
La(1-x)SrxFeO3	TSFZ	Mirror image furnace		magneto-optical Faraday effect	PSI	Kazimierz Conder/Ekaterina Pomjakushina	
ErFeO3	TSFZ	Mirror image furnace		magneto-optical Faraday effect	PSI	Kazimierz Conder/Ekaterina Pomjakushina	
YFeO3	TSFZ	Mirror image furnace		magneto-optical Faraday effect	PSI	Kazimierz Conder/Ekaterina Pomjakushina	
TbBaCo2O(5+x)	TSFZ	Mirror image furnace		magnetic, metal-insulator, spin state transitions	PSI	Kazimierz Conder/Ekaterina Pomjakushina	
LuFe2O4	TSFZ	Mirror image furnace		ferroelectric, charge frustrated system	PSI	Kazimierz Conder/Ekaterina Pomjakushina	
NaxCoO2 (x=0.7, 0.75, 1)	TSFZ	Mirror image furnace		FM, AFM, MI transitions	PSI	Kazimierz Conder/Ekaterina Pomjakushina	
NdBaCo2O(5+x)	TSFZ	Mirror image furnace	superconductor	magnetic, metal-insulator, spin state transitions	PSI	Kazimierz Conder/Ekaterina Pomjakushina	
La2CuO4	TSFZ	Mirror image furnace		AFM	PSI	Kazimierz Conder/Ekaterina Pomjakushina	
Nd1/3Srx/23FeO3	TSFZ	Mirror image furnace	metal below 1K	AFM, charge disproportionation	PSI	Kazimierz Conder/Ekaterina Pomjakushina	
CaV03	TSFZ	Mirror image furnace	superconductor	charge ordering, orbital ordering	PSI	Kazimierz Conder/Ekaterina Pomjakushina	
SnBaMn2O6	TSFZ	Mirror image furnace	superconductor	magnetic, metal-insulator, spin state transitions	PSI	Kazimierz Conder/Ekaterina Pomjakushina	
YBaZrCuO(6-x), x=0-1, 16O-18O	solid state synthesis		superconductor		PSI	Kazimierz Conder/Ekaterina Pomjakushina	
LnBaCo2O(6-x), x=0-1, 16O-18O	solid state synthesis		superconductor		PSI	Kazimierz Conder/Ekaterina Pomjakushina	
Ln(2-x)SrxCuO4, 16O-18O	solid state synthesis		superconductor		PSI	Kazimierz Conder/Ekaterina Pomjakushina	
Ca3Cu(3-x)NiX(PO4)4	arc melting		superconductor		PSI	Kazimierz Conder/Ekaterina Pomjakushina	
NdNi2B2C	solid state synthesis		superconductor	quantum spin trimer	PSI	Kazimierz Conder/Ekaterina Pomjakushina	
(La(1-x)Prx)1-yCavMnO3, 16O-18O	Flux grown	1-zone furnace with temp.gradient	Yes	AF, FM	EPFL	Kazimierz Conder/Ekaterina Pomjakushina	
Bi1.6Pb0.4S2CaCu2O8 Pr, Y doped	Flux grown	1-zone furnace with temp.gradient	Yes		EPFL	Berger (021 693 4484, helmuth.berger@epfl.ch)	
Bi,Pb-2212	Flux grown	1-zone furnace with temp.gradient	Yes		EPFL	Berger (021 693 4484, helmuth.berger@epfl.ch)	
Bi-2212	Flux grown	1-zone furnace with temp.gradient	Yes		EPFL	Berger (021 693 4484, helmuth.berger@epfl.ch)	
Bi2S2CaCu2O8	Flux grown	1-zone furnace with temp.gradient	Yes		EPFL	Berger (021 693 4484, helmuth.berger@epfl.ch)	
Bi2S2CaCu2O8 Ni, Co doped	Flux grown	1-zone furnace with temp.gradient	Yes		EPFL	Berger (021 693 4484, helmuth.berger@epfl.ch)	
Bi-2212	Flux grown	1-zone furnace with temp.gradient	Yes		EPFL	Berger (021 693 4484, helmuth.berger@epfl.ch)	
Fe3O4	CVT	2-zone furnace	Yes	ferromagnetic, Tc 123K	EPFL	Berger (021 693 4484, helmuth.berger@epfl.ch)	
CoS2	CVT	2-zone furnace	Yes	ferromagnetic, Tc 12K	EPFL	Berger (021 693 4484, helmuth.berger@epfl.ch)	
BaVS3	Flux grown	1-zone furnace with temp.gradient	No	Insulator	EPFL	Berger (021 693 4484, helmuth.berger@epfl.ch)	
LiCu2O2	Flux grown	1-zone furnace with temp.gradient	No		EPFL	Berger (021 693 4484, helmuth.berger@epfl.ch)	
NbSe2	CVT	2-zone furnace	Yes Tc 7.2K		EPFL	Berger (021 693 4484, helmuth.berger@epfl.ch)	
CuTeO6	CVT and flux grown	1-zone furnace with temp.gradient	No		EPFL	Berger (021 693 4484, helmuth.berger@epfl.ch)	
Na0.75CoO2	Flux grown	2-zone furnace	Yes		EPFL	Berger (021 693 4484, helmuth.berger@epfl.ch)	
CuSb2O5	CVT	2-zone furnace	No		EPFL	Berger (021 693 4484, helmuth.berger@epfl.ch)	
CdCl2S4	CVT	2-zone furnace	Tc	ferromagnetic	EPFL	Berger (021 693 4484, helmuth.berger@epfl.ch)	
CdCl2Se4	CVT	2-zone furnace	Tc	ferromagnetic	EPFL	Berger (021 693 4484, helmuth.berger@epfl.ch)	
C-60	Sublimation	10-zone furnace	No	Insulator	EPFL	Berger (021 693 4484, helmuth.berger@epfl.ch)	
NbTe2	CVT	2-zone furnace	Yes	ferromagnetic Tc= 86K	EPFL	Berger (021 693 4484, helmuth.berger@epfl.ch)	
TiTe2	CVT	2-zone furnace	Yes	ferromagnetic Tc=130K	EPFL	Berger (021 693 4484, helmuth.berger@epfl.ch)	
alpha TeVO4	CVT	2-zone furnace	Yes		EPFL	Berger (021 693 4484, helmuth.berger@epfl.ch)	
beta TeVO4	CVT	2-zone furnace	No	magnetic properties	EPFL	Berger (021 693 4484, helmuth.berger@epfl.ch)	
ZrO	CVT	2-zone furnace	No		EPFL	Berger (021 693 4484, helmuth.berger@epfl.ch)	
Ni5(SrO3)4Cl2	CVT	2-zone furnace	No	magnetic properties	EPFL	Berger (021 693 4484, helmuth.berger@epfl.ch)	
Ni5(SrO3)4Br2	CVT	2-zone furnace	No	magnetic properties	EPFL	Berger (021 693 4484, helmuth.berger@epfl.ch)	
Cu2Te2O5Cl2	CTV	2-zone furnace	No	magnetic properties	EPFL	Berger (021 693 4484, helmuth.berger@epfl.ch)	
Cu2Te2O5Br2	CTV	2-zone furnace	No	magnetic properties	EPFL	Berger (021 693 4484, helmuth.berger@epfl.ch)	
Co6(TeO3)2(TeO6)Cl2	CVT	2-zone furnace	No	magnetic properties	EPFL	Berger (021 693 4484, helmuth.berger@epfl.ch)	
Co6(TeO3)2(TeO6)Br2	CVT	2-zone furnace	No	antiferromagnetic	EPFL	Berger (021 693 4484, helmuth.berger@epfl.ch)	
CdRe2O7	CVT	2-zone furnace	Yes Tc= 1k		EPFL	Berger (021 693 4484, helmuth.berger@epfl.ch)	
Co2TeO3Cl2	CVT	2-zone furnace	No	magnetic properties	EPFL	Berger (021 693 4484, helmuth.berger@epfl.ch)	
Co2TeO3Br2	CVT	2-zone furnace	No	magnetic properties	EPFL	Berger (021 693 4484, helmuth.berger@epfl.ch)	
Ni5(TeO3)4Cl2	CVT	2-zone furnace	No	magnetic properties	EPFL	Berger (021 693 4484, helmuth.berger@epfl.ch)	
Ni5(TeO3)4Br2	CVT	2-zone furnace	No	magnetic properties	EPFL	Berger (021 693 4484, helmuth.berger@epfl.ch)	
Ni5(TeO3)4I2	CVT	2-zone furnace	No	magnetic properties	EPFL	Berger (021 693 4484, helmuth.berger@epfl.ch)	
Ni5(TeO3)4Br2-xClx	CVT	2-zone furnace	No	magnetic properties	EPFL	Berger (021 693 4484, helmuth.berger@epfl.ch)	
CuW04	Flux grown and CVT	2-zone furnace	No		EPFL	Berger (021 693 4484, helmuth.berger@epfl.ch)	
CoTe4O12B6	CVT	2-zone furnace	No	Insulator	EPFL	Berger (021 693 4484, helmuth.berger@epfl.ch)	
CuSbTeO3Cl2	CTV	2-zone furnace	No		EPFL	Berger (021 693 4484, helmuth.berger@epfl.ch)	
Cu3(SrO3)4Cl2	CTV	2-zone furnace	No		EPFL	Berger (021 693 4484, helmuth.berger@epfl.ch)	
CuTe2O5	CVT	2-zone furnace	No		EPFL	Berger (021 693 4484, helmuth.berger@epfl.ch)	
CuSe2O5	CVT	2-zone furnace	No		EPFL	Berger (021 693 4484, helmuth.berger@epfl.ch)	
Pentacene	CTV	2-zone furnace	No	Insulator	EPFL	Berger (021 693 4484, helmuth.berger@epfl.ch)	
Rubrene	CTV	2-zone furnace	No	Insulator	EPFL	Berger (021 693 4484, helmuth.berger@epfl.ch)	

Material	Growth technique	Furnace	Conductor	Insulator	Magnetic	MaNEP Institution	Responsible
Coronene	CTV	2-zone lumace	No	Insulator		EPFL	Berger (021.693.4484, helmuth.berger@epfl.ch)
Tetracene	CTV	2-zone lumace	No	Insulator		EPFL	Berger (021.693.4484, helmuth.berger@epfl.ch)
Anthracene	CTV	2-zone lumace	No	Insulator		EPFL	Berger (021.693.4484, helmuth.berger@epfl.ch)
TCNQ	CTV	2-zone lumace	No	Insulator		EPFL	Berger (021.693.4484, helmuth.berger@epfl.ch)
TTF-TCNQ	CTV	2-zone lumace	No	Organic Conductor		EPFL	Berger (021.693.4484, helmuth.berger@epfl.ch)
Perylene	CTV	2-zone lumace	No	Insulator		EPFL	Berger (021.693.4484, helmuth.berger@epfl.ch)
TCNQ-Perylene complexe	CTV	2-zone lumace	No	p-type semiconductor		EPFL	Berger (021.693.4484, helmuth.berger@epfl.ch)
Copper Phthalocyanine	CTV	2-zone lumace	No	Insulator	magnetic properties	EPFL	Berger (021.693.4484, helmuth.berger@epfl.ch)
FeTeZnSBr	CTV	2-zone lumace	No	Insulator	magnetic properties	EPFL	Berger (021.693.4484, helmuth.berger@epfl.ch)
Na _{0.7} CoO ₂	Flux grown	1-zone lumace with temp.gradient			magnetic properties	EPFL	Berger (021.693.4484, helmuth.berger@epfl.ch)
Ca ₃ Co ₂ O ₆	Flux grown	1-zone lumace with temp.gradient			magnetic properties	EPFL	Berger (021.693.4484, helmuth.berger@epfl.ch)
Ca ₃ Co ₄ O ₉	Flux grown	1-zone lumace with temp.gradient			magnetic properties	EPFL	Berger (021.693.4484, helmuth.berger@epfl.ch)
In ₂ VO ₅	CTV	2-zone lumace			magnetic properties	EPFL	Berger (021.693.4484, helmuth.berger@epfl.ch)
Co ₄ Te ₂ O ₁₁ Cl ₄	CTV	2-zone lumace	No			EPFL	Berger (021.693.4484, helmuth.berger@epfl.ch)
Co ₂ (TeO ₃) ₂ X ₂ (X = Cl, Br)	CTV	2-zone lumace	No	Insulator	magnetic properties	EPFL	Berger (021.693.4484, helmuth.berger@epfl.ch)
Co ₂ (SeO ₃) ₂ X ₂ (X = Cl, Br)	CTV	2-zone lumace	No	Insulator	magnetic properties	EPFL	Berger (021.693.4484, helmuth.berger@epfl.ch)
NiSeO ₃	CTV	2-zone lumace	No	Insulator	magnetic properties	EPFL	Berger (021.693.4484, helmuth.berger@epfl.ch)
ZrS ₃	CTV	2-zone lumace	No	Semiconductor	magnetic properties	EPFL	Berger (021.693.4484, helmuth.berger@epfl.ch)
ZrS ₆	CTV	2-zone lumace	No	Semiconductor		EPFL	Berger (021.693.4484, helmuth.berger@epfl.ch)
ZrTe ₃	CTV	2-zone lumace	No	Semiconductor		EPFL	Berger (021.693.4484, helmuth.berger@epfl.ch)
HfS ₃	CTV	2-zone lumace	No	Semiconductor		EPFL	Berger (021.693.4484, helmuth.berger@epfl.ch)
HfTe ₃	CTV	2-zone lumace	No	Semiconductor		EPFL	Berger (021.693.4484, helmuth.berger@epfl.ch)
TiOBr	CTV	2-zone lumace	No	Insulator	magnetic properties	EPFL	Berger (021.693.4484, helmuth.berger@epfl.ch)
Pd ₃ (PS) ₄ 2	CTV	2-zone lumace	No	Semiconductor	diamagnetic	EPFL	Berger (021.693.4484, helmuth.berger@epfl.ch)
MnP-S ₃	CTV	2-zone lumace	No	Semiconductor	magnetic properties	EPFL	Berger (021.693.4484, helmuth.berger@epfl.ch)
MnP-Se ₃	CTV	2-zone lumace	No	Semiconductor	magnetic properties	EPFL	Berger (021.693.4484, helmuth.berger@epfl.ch)
NiPS ₃	CTV	2-zone lumace	No	Semiconductor	magnetic properties	EPFL	Berger (021.693.4484, helmuth.berger@epfl.ch)
NiPS ₆	CTV	2-zone lumace	No	Semiconductor	magnetic properties	EPFL	Berger (021.693.4484, helmuth.berger@epfl.ch)
FeP-S ₃	CTV	2-zone lumace	No	Semiconductor	magnetic properties	EPFL	Berger (021.693.4484, helmuth.berger@epfl.ch)
FeP-S ₆	CTV	2-zone lumace	No	Semiconductor	magnetic properties	EPFL	Berger (021.693.4484, helmuth.berger@epfl.ch)
Ni ₃ TeO ₆	Flux grown	1-zone lumace with temp.gradient			magnetic properties	EPFL	Berger (021.693.4484, helmuth.berger@epfl.ch)
Co ₃ TeO ₆	Flux grown	1-zone lumace with temp.gradient			magnetic properties	EPFL	Berger (021.693.4484, helmuth.berger@epfl.ch)
Cu ₂ CoTeO ₆	Flux grown	1-zone lumace with temp.gradient			magnetic properties	EPFL	Berger (021.693.4484, helmuth.berger@epfl.ch)
LiCu ₂ O ₂	Flux grown	1-zone lumace with temp.gradient	No	Semiconductor	magnetic properties	EPFL	Berger (021.693.4484, helmuth.berger@epfl.ch)

3 Knowledge and technology transfer

The key objective during this period was to initiate several new collaborative projects with industry as well as to continue our most successful collaborations. Another key challenge in this period was the elaboration of the Geneva Creativity Center in collaboration with HES-SO in Geneva and industry organizations in Geneva with an important participation in the event organized by the *Office de Promotion des Industries et des Technologies* of Geneva, "Acte Industries", on May 26, 2009. Another important challenge was the organization of a joint NCCR event at ITU Telecom World 2009. Further outreach events of a smaller scale took place and new contracts were signed with industrial partners. Matthias Kuhn, MaNEP technology transfer manager, left at the end of October 2009.

3.1 Contacts

Oerlikon

An non-disclosure agreement (NDA) was signed with Oerlikon in April 2009 in relation to an expression of interest from the Oerlikon affiliate in the US. The goal was to initiate discussions about the synthesis by physical vapor deposition (PVD) of ferroelectric perovskite materials.

Freescale Semiconductors

As a follow up from the teleconference which took place in November 2008 in the European Freescale headquarters with company executives, a white paper was written for Freescale in relation to the piezopinich technology. Freescale is interested in evaluating this ground breaking technology developed by Prof. Christoph Renner (MaNEP, UniGE), Dr Steve Arscott (CNRS, IEMN, Lille) and Dr Alistair Rowe (Ecole Polytechnique, Palaiseau) to replace one of its pressure sensors, the MPX 12. Freescale is the market leader for automotive sensors and integrated circuits. This request suggests that the commercial potential of this technology may be interesting.

Marketing of the piezopinich technology

Marketing efforts continued to promote the piezopinich technology mentioned above. This technology, which is co-owned by three institutions, has many applications. The University

of Geneva is particularly interested in commercializing the technology in the field of atomic force microscopy. To this end, several companies were contacted. Participating in the Tech-Connect conference in June 2009 in Houston helped make contacts and understand the market players better. Companies such as Veeco, Nanosurf and Mikromash were contacted and a follow up is taking place in order to establish a development plan with them. Another company active in technology development, TTP¹, expressed an interest in this technology.

Lord

On May 29, 2009, MaNEP welcomed Lord in its premises for a first exchange of presentations and ideas. Lord is a multinational company in the field of aerospace. It recently set its European headquarters in Geneva. Five senior representatives of Lord coming from various European locations were present. Representatives of the Geneva HES-SO were also invited in order to provide a fuller picture of what Geneva has to offer in the fields of interest to Lord. The visit was appreciated by all parties and several follow up elements took place, among them, first discussions between Lord and MaNEP with respect to magneto-rheologic fluids, a strategic field for Lord. Another element of follow up was the invitation sent to Lord by HES-SO to visit their facilities.

¹www.ttp.com



Figure 1: Welcome desk at the joint NCCR conference at ITU Telecom World 2009.

3.2 Conferences and exhibitions

Joint NCCR Conference at ITU Telecom World 2009

This project was initiated in 2007 during a meeting between the KTT managers of the NCCRs Quantum Photonics, MICS and MaNEP. All three NCCRs have the same KTT mission and all three are involved in research fields related to telecommunications. It was thus decided to set up a joint KTT event at ITU Telecom World 2009, an exhibition which gathers many industry representatives from all over the world. The event took place on October 8, 2009 in the form of conferences revolving around cryptography and quantum telecommunications. It gathered about 100 guests of whom 50 percent stemmed from the private sector (Fig 1). It was concluded by a performance by the artistic company Exos, featuring superconducting levitation, followed by a networking cocktail. The public appreciated the speeches (Fig. 2), the organization of the conference and was very impressed by the combination of arts and science with the levitation show. The networking which followed during the cocktail was valuable with a large at-



Figure 2: Audience at the joint NCCR conference at ITU Telecom World 2009.


Matthias Kuhn

De: guichet-prme@etat.ge.ch
Envoyé: mercredi 30 septembre 2009 14:33
À: Matthias Kuhn
Objet: Newsletter septembre 2009 - Service de la promotion économique de Genève

Newsletter septembre 2009

**Service de la promotion économique
de Genève**

www.whygeneva.ch



ITU TELECOM WORLD 2009

Show Case de la plateforme Alp ICT: Innovation génératrice de développements technologiques à applications multiples
Mercredi 7 octobre, dès 16h00, Genève Palexpo
Comment prennent forme les innovations qui engendrent un progrès important des technologies utilisées? De quelle manière s'élargit leur champ d'application et quels sont les moyens qui permettent d'encourager aujourd'hui le transfert des innovations dans de nouveaux domaines d'application? Telles sont les questions que cette conférence et la table ronde qui suivra se proposent d'explorer. En présentant sept projets innovants issus des cantons qui composent la plateforme de promotion Alp ICT, la conférence souhaite valoriser les innovations réalisées et leur transfert vers de nouveaux champs d'application.
[Informations complémentaires et inscriptions](#)

Trois pôles de recherche nationaux réputés s'associent pour créer un événement exceptionnel au salon Telecom World 2009
Jeudi 8 octobre 2009, de 16h00 à 18h00
Intitulé "A Quantum Leap for Telecommunications Today and Tomorrow", cette conférence présentera l'état de l'art dans la cryptographie et les télécommunications quantiques. Elle présentera aussi la vision des chercheurs à la pointe du sujet, notamment avec le projet SwissQuantum. La soirée se terminera pour un cocktail de réseautage pendant lequel aura lieu une performance artistique unique au monde, faisant appel à la lévitation supraconductrice.
Contact et renseignements : swissquantum@idquantique.com ou sur http://inform.epfl.ch/index.php?form=SWISS_QUANTUM

Figure 3: Advertisement for the joint NCCR event at ITU Telecom World 2009 in the e-Newsletter of the Geneva Economic Promotion Agency.

tendance and representatives from companies such as Nokia, Freescale, STMicroelectronics and Swisscom.

The e-Newsletter of the Geneva Economic Promotion Agency published an announcement regarding this event (Fig 3). This e-Newsletter reaches more than 4000 executives in the Geneva region. This certainly contributed to the good attendance at this event.

SWM 2009 supplier exhibition

Like every second year, 2009 hosted its Swiss Workshop on Materials with Novel Electronic Properties (SWM 2009) in Les Diablerets, Switzerland. This highly regarded conference has regularly been holding a supplier exhibition. This year four companies participated, Pfeiffer Vacuum, Teco René Koch, Ryf AG and Imina Technologies, enjoying visits and discussions with the research community.

MaNEP technology promotion at the BioInnovation Day 2009

In June 2009, Prof. Christoph Renner presented its piezopinch technology at the BioInnovation Day conference in Geneva (Fig 4). BioInnovation Day is a partnering meeting aimed at presenting the latest University technologies



Figure 4: BioInnovation Day 2009: Prof. Christoph Renner presenting the piezopinchn technology.

from western Switzerland to the private sector. The latter comprises companies, consultants and venture capitalists from the Lake Geneva Region and beyond. It also allows excellent networking between the parties. C. Renner presented a way to perform high-speed, high-efficiency bio-assays with the piezopinchn technology.

3.3 Projects

ABB

Our collaboration with the company ABB has the goal to prepare for the use of thin superconducting films in future fault current limiters. In this project we are currently focusing on YBCO coated conductors since these are expected to become much cheaper than the thin films grown on sapphire which we studied in the first phase of this collaboration. The first studies have shown that the performance of such ribbons for current limiting is considerably lower than what is found for YBCO grown epitaxially on sapphire substrates. This situation calls for detailed thermal and electrical characterization of the complex coated conductors in order to get an understanding of how the current limiting performance of the coated conductors can be improved. We report in more detail on these efforts under Project 3, in chapter 2, in this report.

AGIE Charmilles

The search for wear and corrosion resistant materials is one of the most important tasks for the tool machine industry. Electrical discharge machining (EDM) is a well developed technology (mostly by Swiss and Japanese manufacturers) that is used to cut and shape a wide variety

of conducting materials. The *economic stimulus package* project “Cut-and-coat process by wire-EDM” with AGIE Charmilles aims at producing surface and sub-surface alloys by combining wire-EDM machining and new electrode materials. The produced surface alloys will improve mechanical properties such as wear and friction behavior, and also increase the corrosion resistance of the machined parts. Test workpieces will be produced and tested under real conditions. The results will be displayed to trigger interest among potential customers of the technology. We report in detail separately to the SNSF on this project

Asulab SA (a member of Swatch Group)

Hydrogen fuel cells play a key role in future energy scenarios. Mass markets such as H₂ powered vehicles and H₂ production units for residential areas require H₂ detectors and sensors on a very large scale. The devices must be cheap, sensitive and selective, and allow to detect H₂ and to monitor H₂-O₂ combustion processes. The CTI project, entitled “Hydrogen detectors and sensors for PEM fuel cell combustion systems”, together with Asulab SA, aims at developing tailored sensing devices that are cheaper and more selective than those currently available, by using thin films and novel materials undergoing H₂-induced metal-insulator transitions. More details on this work can be found in chapter 2, on Project 3.

Bruker Biospin

The longstanding collaboration with Bruker BioSpin AG has led to several remarkable results this year. Detailed reports on this are given in chapter 2, on Project 3. This collaboration received an additionally boost through the *economic stimulus package* which finances the specific project: “Developments of MgB₂ wires with high critical current densities for economical NMR magnets at 4.2 and at 20K”. This project aims at developing the use of MgB₂ for intermediate field superconducting magnets. Separate reports on this sub-project will be sent to SNSF.

Nirva Industries SA

The goal of the project “Electrochemical sensors with higher resolution”, in the frame of the *economic stimulus package* of the SNF with Nirva Industries SA, is to develop high resolution electrochemical sensors by implement-

ing optimized surface structures in the sensing electrodes. There is a strong demand for these sensors, for example to measure trace amounts of oxygen (< 1 ppb) in dissolved form, in the beverage, pharmaceutical and power industries. Scientifically, the key issue to improve the sensitivity is to find the way to generate a higher current for a given gas concentration. New materials and/or fine-tuning of the cathode surface morphology can contribute to this end. The increased signal-to-noise ratio will be further enhanced by transposing STM current measuring electronics to the sensing devices. We report in detail separately to the SNSF on this project.

Sécheron SA

MaNEP has been actively involved in synthesis and characterization projects with Sécheron SA. The synthesis project is completed and had been dealt with through a contract of its own including detailed intellectual property terms. For the other numerous characterization tasks performed by MaNEP, it was agreed with Sécheron to set up a general service agreement (GSA) covering all such present and future mandates. This GSA, which provides appropriate protection to the University of Geneva has been agreed by both parties and is being signed.

SwissNeutronics

The collaboration with SwissNeutronics was reinforced by the project on "Neutron optical devices for small samples" financed through the *economic stimulus package*. This additional project started in October 2009 and includes three tasks: 1) multichannel focusing guides; 2) adaptive focusing optics; 3) reflectometer concept for tiny samples. Progress has been made on all three tasks and the present status on this specific project is reported separately to the SNSF.

Vacheron Constantin

The CTI project, entitled "Technology for marking watch components at the microscopic scale" together with Vacheron Constantin, uses a STM-inspired experimental setup to print microscopic marks on the surface of metallic parts. The printing mechanism is based on the transfer of nanopowder material dispersed in a

liquid dielectric at the surface of the substrate. The chemical composition of the marks can be tailored to provide a chemical fingerprint for traceability purposes. The main goals of this CTI project are 1) to further develop the technology to achieve microscopic marks of metallurgical quality compatible with fine watchmaking, and 2) to develop the peripheral systems required for marking watch parts at the industrial scale. More details on this work can be found in chapter 2, on Project 3.

3.4 Creativity center

The positive evolution of MaNEP and the efforts to transform MaNEP in Geneva into a stable institution has led to the idea to reinforce and transform the whole of physics at the University of Geneva (see chapter 6 on structural aspects). Here we focus on one aspect of this effort, the Geneva Creativity Center (GCC), which aims at a reinforced collaboration between the Physics section of the University, the engineering school in Geneva (Hepia, a part of HES-SO in Geneva) and industry around applied research and development projects. The idea was proposed by MaNEP at the inauguration of the Physiscope in October 2008 and during winter 2008/2009 a taskforce from MaNEP and the Physics section was set up to elaborate the concept. This concept was presented at the meeting "Actes Industries" organized by the *Office de Promotion des Industries et des Technologies* (OPI) of Geneva with 130 participants on May 26, 2009. Following this meeting a "Comité de pilotage" *ad hoc* was set up composed of Rolf Gobet, director OPI, Yves Leuzinger, director Hepia, Didier Raboud, director of communication UniGE and Øystein Fischer, director MaNEP. Nicolas Aune, secretary-general of the *Union Industrielle Genevoise* (UIG) did later also join this group. After several meetings, including several discussions with the minister in charge of the Geneva department of public education, Charles Beer, a founding document was elaborated. Based on this we are presently employing the first collaborators of GCC whose job is to elaborate the detailed program for GCC. The plan is to start officially operation before the end of 2010. The center is planned to be a Forum where scientists, engineers and industry can meet to elaborate new ideas for technology transfer.

4 Education, training and advancement of women

4.1 Education and training

4.1.1 Doctoral School

PhD students: statistics for 2009

During 2009 eight PhD students finished their studies and presented with success their thesis in DPMC at UniGE. On the other hand, nine young students – two women and seven men – started their work and joined the program in the same period. Among them, two applied through the recruitment procedure of the MaNEP doctoral school, while the others used different means. Thus the total number of PhD students is stable at twenty. An international call for applications to the program was made in December 2009. As much as 199 individuals responded, and these applications are currently under investigation.

Teaching activities

The basic course entitled *Applications of the Many-Body Formalism in Condensed-Matter Physics*, which started in the 2008 autumn semester, continued in the 2009 spring and autumn semesters. This course was regularly followed by 7 to 13 PhD students. Among other subjects, two experimental techniques were first presented from the point-of-view of the experiment, and then studied theoretically. Prof. Didier Jaccard (UniGE) introduced the measurement of the electrical resistivity, which in spite of its apparent simplicity and widespread use in condensed-matter research, raises difficult experimental and theoretical questions. Dr Sigrun Köster from Prof. Christoph Renner's group (UniGE) uncovered the secrets behind the technique of scanning tunneling microscopy/spectroscopy (STM/STS). Both techniques are among the core experimental methods used in the MaNEP research activities. The course was positively evaluated by the students, and will be given

again, starting from the 2010 spring semester.

Collaboration with the 3^{ème} Cycle

The 3^{ème} *Cycle de la Physique en Suisse Romande* under the control of the *Conférence Universitaire de Suisse Occidentale* (CUSO) provides an important part of the post-graduate training offered to our students, in the form of high-level short courses given by internationally renowned speakers. The 3^{ème} *Cycle* also used to provide a longer course with content and target similar to the basic course of our program. As requested by the CUSO, the 3^{ème} *Cycle de la Physique* will be transformed into a doctoral program. We have taken this opportunity to unite our efforts for the doctoral training with those of the 3^{ème} *Cycle* and of the EPFL. During 2009 we have taken part in the preparation of the future CUSO doctoral program for physics, which should start in 2011. In addition to continuing with the organization of high-quality short courses as in the past, the new structure should provide a common platform for distributing information and making it easily available to the students. In this way the courses of the MaNEP doctoral program will become accessible to all students registered at the 3^{ème} *Cycle*, and our basic course could thus complement or replace the basic course of the 3^{ème} *Cycle de la Physique*. Conversely, our students will benefit from an extended and more transparent offer, as well as additional services ("PhD days", contacts to industries, etc.) which are planned in the future CUSO doctoral program for physics.

4.1.2 PhysiScope Genève

Summary

The PhysiScope team can look back at a great vintage 2009. Attendance is steadily increas-

ing, with school children from as far as Denmark and a number of VIP visitors enjoying the shows. Several special events were organized, including a day with an active NASA astronaut and a one week workshop gathering fellow European physics shows. The PhysiScope took also part in the celebration of the 450 years of the University of Geneva throughout the year 2009.

One year on



The PhysiScope is a public laboratory-theater operated jointly by MaNEP and the Physics Section of the University of Geneva. This endeavor strives to contribute to invert the steady reduction in science students observed worldwide, via a participative and entertaining discovery of physics¹.

Following its inauguration in 2008, the PhysiScope has measured up to expectations, with a successful first year of exploitation. Attendance is steadily increasing, with over 1700 visitors last year, some traveling all the way from Denmark. Each show lasts for about 75 minutes for an average group size of 15, granting each visitor a personal experience of physics. We did also perform for a number of VIPs, including C. Kleiber, the former Swiss State Secretary for Science, M. Gago, Minister for Science, Technology and Higher Education of Portugal, the Geneva Rotary Club and a delegation of directors of Leiden University, Netherlands. 2009 concluded with a rewarding excursion in November to the *Palais de la Découverte* in Paris, an excellent source of inspiration for new shows for the entire team.

Maintaining high standards and a constant renewal are paramount to the long term durability of the PhysiScope. Hence, developing new content to convey the fascination of science in an attractive manner deserves special attention. New shows dealing with waves and light, magnetism and energy have been prepared. We also commissioned a small astronomy observatory (see section 4.1.2), opening a window on the sky in the center of town.

The PhysiScope relies on a team of 9 assistants who develop the content and take turns presenting the shows as part of their regular teaching duties. With attendance peaking at four shows per day during several weeks

¹C. Renner, *Hands-on inspiration for science*, Nature Materials 8, 245 (2009).



Figure 1: Fascinating superconducting levitation (Photo @CERN).

in January-March, May-June and October, this makes for a busy schedule.

Adriana Bonito Aleman, MaNEP's communication officer, joined the PhysiScope executive team to take care of all special events. In 2009, the University of Geneva celebrated its 450 years of existence. The PhysiScope did participate in several events organized on that occasion, including a 16 days *open doors* in November-December 2009. The PhysiScope also took part in a number of annual events across Geneva, such as the *Girl's day*, the *Nuit de l'UNIGE*, the *Journée des collégiens* and the *Cité des Métiers et de la Formation*, all destined to advertise science to the general public. Two very successful exhibition shows were set up in two large regional shopping malls.

Collaboration with other outreach initiatives are invaluable opportunities to reach a broader audience. One example is *TSR découvertes* with whom we interact regularly. We have also started to greet much younger visitors than our 12–19 year old target audience. Enthusiastic children from the *Centres Aérés*, a Geneva summer camp, and from an original project *Dessine-moi un physicien* (Fig. 1) lead by the CERN communication team were offered a close encounter with the magic of physics.

The PhysiScope turns to space

2009 was the *International Year of Astronomy* celebrating 400 years of scientific astronomical observations pioneered by Galileo Galilei in 1609. On that occasion, the PhysiScope established a small observatory (Fig. 2) on the roof of Science II with the support of the H. Dudley Wright Foundation. It consists in a 2.5 m diameter dome housing two telescopes; a 350 mm diameter Schmidt-Cassegrain telescope on an equatorial mount, and a *Coronado* personal solar telescope (Fig. 3). The Schmidt-Cassegrain telescope enables the observation of the Moon,



Figure 2: *The PhysiScope observatory on the roof of Science II in the heart of Geneva.*

Planets and even some fainter object from deeper space. The observation of the faintest objects is improved by the use of a CCD camera. The personal solar telescope, operating in the H-Alpha wavelength, enables an unprecedented live view of sunspots and spectacular solar flares. Despite its urban location and associated atmospheric and light pollution, the observatory is a unique tool to initiate the visitors to astronomy and even perform some scientific experiments. Daytime and nighttime sessions take place on a regular basis and by special appointment.

On September 29, 2009 the PhysiScope had the privilege to welcome an active NASA astronaut, Donald Pettit, to share his space travel experience and debate about the impact of the manned space program on our society. This event was part of a one week visit to Switzerland organized in collaboration with Daria Lopez-Alegria (Space Bridges) and EPFL, with the financial support of the Mark Birkigt Foundation, MaNEP and the University of Geneva. Highlights of his visit were a brainstorming session with students and postdocs on designing general physics experiments and a late afternoon public conference. On that occasion, Dr D. Pettit took a very interested audience on an entertaining tour of the *Saturday Morning Science* show he devised during his 2003 stay aboard the International Space Station featuring numerous surprising microgravity experiments. The day concluded with a friendly net-



Figure 3: *J.-G. Bosch demonstrating the personal solar telescope to a young visitor.*

working aperitif sponsored by the rectorate of the University of Geneva.

EuroPhysicsFun

Since 2008, the PhysiScope is a member of EuroPhysicsFun (EPF), a cooperative project between European physics shows whose goal is to form a community of science shows. The PhysiScope, with the support of the Mark Birkigt Foundation, did host and organize the 2009 edition of the annual EPF meeting "Show Physics 2009". From March 31st to April 4th 2009, about 50 scientists from across Europe enjoyed a stimulating and diverse program ranging from how to stage a show to the most efficient way of interacting with the media. The workshop concluded with a one day fair at a major Geneva shopping mall (Balaxert), where each participating show was offered a stand to present its favorite physics experiment. It was a great popular success. In September 2009, the PhysiScope took over the presidency of EuroPhysicsFun in the person of Olivier Gaumer, the PhysiScope's scientific collaborator.

Acknowledgements

The PhysiScope is grateful to the foundations H. Dudley Wright, Mark Birkigt and E. Boninchi for their continued and generous support. We further acknowledge support from the University of Geneva, the Faculty of Science and the Geneva department of public education.

The PhysiScope team 2009/2010

Executive committee: Christoph Renner (president), Øystein Fischer, Martin Pohl, Jean-Gabriel Bosch, Olivier Gaumer, Adriana Bonito Aleman.

Assistants and students: Gauthier Alexandre, Umberto Cannella, Noé Curtz, Fanny Dufour, Lidia Favre-Quattropani, Stefano Gariglio, Florian Glass, Stefano Henin, Olivier Landry,



Figure 4: SWM 2009 participants.

Dook van Mechelen, Benjamin Sacépé.

Teachers: Ruxandra Achimescu, Arnault Barriot, Denis Boehm and Bernard Gisin.

4.1.3 SWM 2009: Swiss Workshop on MaNEP in Les Diablerets

The eighth edition of the Swiss Workshops on Materials with Novel Electronic Properties organized since 1996, took place at the Eurotel in Les Diablerets on August 26–28, 2009. This meeting, corresponding to the fifth MaNEP conference, gathered over 194 registered MaNEP members and scientists from abroad, of those 69 PhD students from the different MaNEP partner institutes (Fig. 4). The program was organized around 9 invited speakers spread over 9 sessions addressing all the main topics of interest to the MaNEP community, including superconductivity (HTS and pnictides), low dimensions and interfaces, multiferroics, cold atoms, materials, novel experimental techniques and applications. 28 contributed talks were selected by scientific merit and for their representativeness of MaNEP's research activities. Two poster sessions offered ample opportunities for further discussions and debates around 97 poster that remained posted for the entire duration of the meeting. Like in previous editions, there was also the possibility to discuss equipment and hardware with four exhibitors distributing technical components in Switzerland. We thank Pfeiffer Vacuum, Teco René Koch, Ryf AG and Imina Technologies for their support. Finally, many thanks to Marie Bagnoud, Ginger Laughlin, Matthias Kuhn, Greg Manfrini and Ivan Maggio-Aprile for their efficient help with the organization of the meeting. The next edition is already planned for June 29 to July 1, 2011.

4.1.4 CORPES09

Coming from 19 nations, 143 experts in the field of photoemission met at Zurich for the CORPES09, the third international workshop on strong correlations and angle-resolved photoemission spectroscopy, organized by the Paul Scherrer Institut (PSI) in Villigen and sponsored by MaNEP. CORPES09 is an interdisciplinary workshop situated at crossroads between angle-resolved photoemission spectroscopy (ARPES) measurements and many-body theories of strongly correlated electron systems. It was an excellent opportunity for PhD students and postdocs to be in contact with the specialists and the newest developments in the field. In 2011, CORPES11 will take place at the ALS, in Berkeley (USA).

4.1.5 Topical meeting and “Martin Peter Colloquium”

This year, on June 19, 2009, we had one topical meeting focused on the subject of *Spectroscopic properties and quantum materials* at the University of Geneva. About 50 scientists attended this meeting, with scientific contributions from researchers at EPFL, PSI, UniFR and UniGE. The meeting ended with the Martin Peter Colloquium given by Professor Z. X. Shen (Stanford University). 70 participants attended his colloquium on “Extraordinary advances on photoemission experiments”. This was a perfect conclusion of this interesting one day meeting.

4.1.6 MaNEP Winter School 2011

The next MaNEP Winter School will be held in Saas-Fee from January 9 to 14, 2011. The chairman of this edition is Prof. Bertram Batlogg, ETHZ and the program committee will soon be created.

4.2 Advancement of women

4.2.1 Summer internships

For the 2009 internships, MaNEP received four female students within the program of Advancement of Women and one male student within the program of exchange student. All the internships lasted one month, except for one candidate, for whom the internship was extended over two months. All the stages were very fruitful both for the women and the hosting group. For instance in the process of selection of a future PhD, these stages give a unique opportunity to evaluate a candidate in real working conditions. Therefore it has been decided to renew these programs for 2010, with the hope of an increased participation.

4.2.2 New developments

We mentioned last year a survey that we were preparing together with the Equality Office of the University of Geneva and that we intended to send to all the women researchers in MaNEP. Due to the strong implication of the Equality Office in the events around the 450th anniversary of the University of Geneva, the preparation of the survey was postpone. It is however almost ready and will be sent to the women researchers of MaNEP before the summer 2010.

5 Communication

Year 9 was marked by a change in personnel. Anne Rougemont, MaNEP Communication Officer, left in April 2009 and her successor, Adriana Bonito Aleman, took over from her in July 2009. This year was also characterized by a variety of communication activities created in order to reach a wide range of target audiences. While public outreach activities remain of major importance, we are thinking about ways and means of creating opportunities to reach decision-makers and key stakeholders and to inform them of MaNEP's activities and future actions. Particular attention was paid to the industry for which a special public relations event was organized. We also strengthened our links with academic partners, especially with MaNEP's host institution, the University of Geneva, by creating joint events and actively participating in its public outreach actions organized to celebrate its 450th anniversary.

5.1 Networking

MaNEP's stakeholder's analysis is completed and we are working on obtaining an effective management tool which will be absolutely essential to continue our work with targeted audiences. The implementation of the new data base system FileMaker Pro will be ready for use in 2010. This tool is crucial in our daily activities and particularly for strategic public relations and networking. It is therefore indispensable for MaNEP's activities in the Phase III and to prepare for the long-term planning of the network.

5.2 Two creative and innovative projects

In 2011, we will be celebrating the 100th anniversary of the discovery of superconductivity. It will be a real opportunity to reach out to the general public on one hand, but also the key stakeholders on the other hand by creating very special events. We already initiated two innovative projects which will be part of the festivities programm.

Art-Science

In its efforts to communicate science to the general public MaNEP has commissioned an artist to create a sculpture depicting the magic of our research and to convey the futuristic potential it has. The world of science has met with the world of arts in order to make physics ac-

cessible to everyone. The Swiss sculptor Etienne Krähenbühl, known for his work involving surprising and unusual materials, is creating an artwork based on superconductivity. The work between the artist and scientists is progressing under the watchful eye of a filmmaker who is making a documentary on this unprecedented encounter (Fig. 1). The sculpture will be exhibited at the Geneva School of Physics where MaNEP has its headquarters. The artwork should be inaugurated in 2011 to celebrate the 100th anniversary of the discovery of superconductivity.

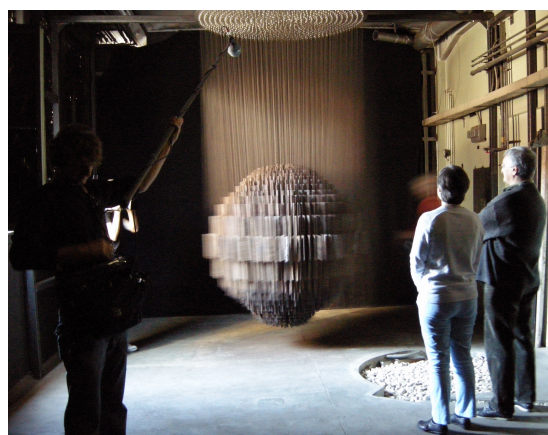


Figure 1: MaNEP physicist Dr Lidia Favre-Quattropani and MaNEP engineer Jean-Gabriel Bosch, at Etienne Krähenbühl's workshop, discovering "Bing Bang", one of his astonishing sculptures.



Figure 2: ITU Telecom World 2009: spectacular levitation, the head of a statue which was part of the Exos artistic show.

Levitation with Exos

Another creative outreach initiative is MaNEP's partnership with the artistic company Exos which is staging superconductivity. A real artistic performance featuring superconducting levitation is being prepared and will be presented to the general public and key stakeholders. A small group from the public has already discovered a sample of this surprising show during the conference "A Quantum Leap for Telecommunications - Today and Tomorrow", on October 8, 2009. This public relation event was organized for industry by three National Centres of Competence in Research MICS, Quantum Photonics and MaNEP within the framework of ITU Telecom World 2009. More information about this event can be found in the KTT chapter (p. 128). The show featured levitating objects as well as a dancer carried on by flying items in a thick cloud of nitrogen: an astonishing performance (Figs. 2 and 3).



Figure 3: Exos show at ITU Telecom World 2009: a dancer performing on a "grimoire" (book of spells) in levitation.

A sample of this performance was also shown at the "Christmas Party" of the Physics Section of the University of Geneva. The audience was essentially packed with scientists who particularly enjoyed the show. We are now working on a project for the public that should be delivered in 2011 as a world premier.

5.3 University of Geneva's 450th anniversary

The jubilee year of MaNEP's home institution, the University of Geneva, comprised many events. MaNEP was an enthusiastic contributor for many of them with the aim of promoting science to the general public as well as to young audience.

MaNEP took part in *Le Savoir au Centre*, two very successful exhibitions held at two large shopping malls, from March 23 to April 4 at Balexert in Geneva, and from April 27 to May 9, 2009 at Chavannes Centre in the canton of Vaud. A stand with many activities, including MaNEP's demonstrating devices, gathered a lot of visitors, particularly families.

Our NCCR participated in the *Nuit de l'UNIGE* on June 13 on a sunny Saturday afternoon and evening which encouraged the general public to come and play with us. The group of Prof. Klaus Yvon operated an hydrogen fuel cell to supply a neighbored music stage with electricity. MaNEP researchers together with the PhysiScope team presented physical curiosities on an interactive stand near Sciences II (Fig. 4) associated with demonstrations at the PhysiScope, Sun observations at the PhysiScope observatory and presentation of our Mix&Remix exhibition on superconductivity. During the evening, a dancing night was organized with a video-jockey featuring images provided by the three Geneva NCCRs.

The umbrella campaign exhibition created by the Swiss National Foundation (SNF) was particularly appreciated by many visitors who were able to discover it during the *Nuit de l'UNIGE* at the *Centre Médical Universitaire* (CMU) (Fig. 5). MaNEP was also involved in the umbrella campaign by distributing promotional material.

During the 16 days open doors in November–December 2009, high school students of the canton of Geneva were invited to come and discover the activities of the different faculties and centers of research. MaNEP opened its doors and gave demonstrations of various experiments in the PhysiScope.

Also in collaboration with the University of



Figure 4: Young visitor enjoying MaNEP demo during the Nuit de l'UNIGE.

Geneva, but outside the anniversary celebrations, MaNEP seized this invaluable opportunity to be present with the PhysiScope at the *Cité des métiers et de la Formation* on November 24–29, at Geneva Palexpo. This event offered a large panorama of training in the Geneva region. Our researchers and scientists demonstrated fun experiments and displays linked to modern physics. It was a great occasion to reach out to a young audience.



Figure 5: People visiting the SNF Umbrella campaign exposition at the CMU in Geneva.

5.4 MaNEP in media

MaNEP has appeared in the general and specialized media, with articles in newspapers as well as on the Internet. The Conference at ITU Telecom World 2009 had significant coverage in the media. The Purvege project, which consists of new ozone sensors, has also raised media attention, which reported this new process using ozone to decontaminate fruits and vegetables and thus prolong their shelf life. Moreover, MaNEP collaborated with the Internet site www.swissuniversity.ch which published a presentation of our NCCR. MaNEP has also been present in “Horizons”, the SNF magazine, in an article about NCCRs¹. It underlined how the collaboration between researchers as well as with industry is important and MaNEP was mentioned as an example of success. There was an article about the PhysiScope in the prestigious review *Nature Materials*². It was the subject of a three-page feature in the “Commentary” section and the editorial entitled “Lessons in science education”. The article was commissioned by the magazine’s editors and written by the PhysiScope’s director Prof. Christoph Renner. This highlights that this MaNEP initiative for popularizing physics is unique and progressively building a strong reputation, even on an international level. Another article about MaNEP has been published in the Public Service Review: European Union (issue 19, spring 2010) distributed primarily within departments, directorates and agencies of governments of the European Union member states and as well as to European Union institutions and industries.

5.5 Several other outreach activities in Year 9

MaNEP’s experts are continually and with ever increasing frequency solicited to communicate science to the public. MaNEP’s deputy director Prof. Christoph Renner and Prof. Jan Lacki delivered a conference entitled “Peut-on voir les atomes ? De la lunette de Galilée au microscope à effet tunnel” at the *Musée d’Histoire des Sciences* in Geneva in October 2009. Prof. Patrycja Paruch and Prof. Jan Lacki also gave a conference at the *Musée d’Histoire des Sciences*, in November, entitled “La physique et la vie – Un nouveau microscope pour un nouveau

¹Urs Hafner and Ori Schipper, *Appréhender le futur ensemble*, Horizons 82, 6 (2009).

²C. Renner, *Hands-on inspiration for science*, Nature Materials 8, 245 (2009).

partenariat”.

Another successful science-city event was the science talk organized on November 8, at the ETHZ with Rolf Hiltl, gastro-entrepreneur, and Prof. Tilman Esslinger, quantum physicist, where they looked at links between basic research and cooking.

5.6 Website and e-Newsletter

MaNEP’s web site has been translated into French this year, the language of the home in-

stitution. This give an important new tool for MaNEP Phase III, which first addressed regional key stakeholders, but also the general public and MaNEP scientific network. The site is of course regularly updated with all the latest news. During Year 9, we proposed three issues of MaNEP’s e-Newsletter, all sent to more than 300 people working within the MaNEP network. We received a great deal of input from our industrial partners, in particular in the January 2010 issue. This is of course very promising.

6 Structural aspects

The plan outlined in the Proposal is being implemented as put forward. The Laboratory of Crystallography has been transferred and integrated in MaNEP as of January 1, 2010. The University of Geneva has also fulfilled the increased budget for 2009. The plan for 2010 is in the process of implementation. The two professor positions (successors Yvon and Fischer) have been taken into account in the plan for the physics section and are presently being discussed at the Faculty and University level.

The MaNEP director has also been invited by the University to elaborate a plan for a new center of physics in Geneva. This would comprise the future structure which would take over from MaNEP in Geneva. This new center, which would include at this stage the whole of physical sciences, is largely inspired

by MaNEP activities and organization. During Year 9, all this has been discussed at the highest level in the Canton of Geneva and decisions about how to proceed with this project are expected during 2010.

At the moment, the big question is how to support the nation wide MaNEP network after 2013. Here we expect support from the SNSF to find a practical solution. This solution must take into account the real cantonal and confederal structure of Switzerland in order to find ways to maintain the best networks coming out of the NCCR scheme. On the MaNEP side we shall do our best to try to find a practical solution. The meeting of the scientific committee on April 14, 2010 shall focus on this question.

7 Management

7.1 Activities

The beginning of Phase III on 1 July 2009 saw the establishment of a new scientific and administrative structure. The MaNEP management has been very busy implementing the administration and accounting. As initially planned, MaNEP has adapted to the appointments and departures in its field in the Swiss institutions. The result is that we have included 15 new, young scientists as full members of MaNEP. We have also appointed 13 further associate members. Since the beginning of the third phase we have added one new full member to the MaNEP Forum: Professor Andrey Zheludev, director of the Laboratory for neutron scattering at PSI. He has also replaced Professor Joël Mesot as co-project leader of Project 6, as Prof. Mesot was appointed Director of PSI last year.

The **Forum** has 43 full members and 17 associate members. Prof. A. Zheludev was added at the very beginning of Phase III. The new Forum met in a reduced form during the SWM 2009 meeting at les Diablerets in August 26-28, 2009 and it was officially convened on Wednesday January 27, 2010 during the Internal Workshops in Neuchâtel.

The **Scientific Committee** is composed of the director, two deputy directors, the project leaders plus two additional members appointed by the director. The composition is as follows: Prof. Leonardo Degiorgi (ETHZ), Prof. Øystein Fischer (UniGE), Director, Prof. László Forró (EPFL), Prof. Thierry Giamarchi (UniGE), Prof. Dirk van der Marel (UniGE), Deputy Director, Prof. Frédéric Mila (EPFL), Prof. Alberto Morpurgo (UniGE), Prof. Christoph Renner (UniGE), Deputy Director, Prof. Manfred Sigrist (ETHZ), Prof. Jean-Marc Triscone (UniGE), Dr. Urs Staub (PSI), Prof. Andrey Zheludev (PSI).

The committee met on December 15, 2009 and will meet again on April 14, 2010. This meeting will be devoted to discussing the future

of MaNEP after 2013. In particular we plan to discuss what the MaNEP community can do to maintain and develop the scientific network. The scientific committee also served as a program committee for MaNEP at the upcoming conference of the Swiss Physical Society on June 21-22, 2010, in Basel. This meeting took place on March 22, 2010.

The **Internal Evaluation Board** will be established during 2010 and will evaluate the MaNEP scientific output.

The **Advisory Board** is composed of eminent scientists from outside Switzerland and will meet during the winter of 2010-2011 to evaluate and discuss the scientific progress and the future of MaNEP.

The **Management Committee** meets regularly once a month to discuss and monitor the evolution of all daily activities of MaNEP: events, meetings, newsletters, accounting, KTT, education, doctoral school, advancement of women, communication, etc.

There were several changes of staff at MaNEP this year. We hired the successor to Anne Rougemont as the new communication officer of MaNEP: Adriana Bonito Aleman. The executive assistant, Sophie Griessen left at the end of 2009 and she has now been replaced by Elizabeth Gueniat. Finally, Matthias Kuhn, the KTT officer left at the end of October 2009. His replacement will be decided in relation to the new Geneva Creativity Center.

The MaNEP management also oversaw the organization of several meetings during the year:

- The **Review Panel** met at PSI on May 14-15, 2009. The meeting was organized by the Swiss National Science Foundation in collaboration with Ms Pamela Knupp of PSI, and the management team of MaNEP.
- The **Swiss Workshop on Materials with Novel Electronic Properties (SWM 2009)**, basic research and applications, took place

at les Diablerets August 26-28, 2009. There were 194 participants, 69 of which were PhD students. The meeting was fully organized by the MaNEP management.

- The MaNEP **Internal Workshops** took place in Neuchâtel from Tuesday 26 January until Friday 29 January, 2010. These workshops are the basis for the scientific reports of MaNEP.

7.2 Experiences, recommendations to the SNSF

As anticipated, NIRA 2.0 is a wonderfully complex and exciting tool for those who are not concerned with keeping the cost of administration low. By creating links between the different inputs and calculating everything in a manner that cannot be easily controlled

by the user it represents a fabulous administrative labyrinth with no real exit between the progress report and the financial report. Therefore we have to reinforce our administrative staff with a specialist devoted entirely to NIRA 2.0.

8 Reactions to the recommendations of the Review Panel

We are grateful to the Review Panel for its detailed and thorough evaluation of our proposal for the third phase and the progress report for year 8. Several key questions for the future are raised in the Review Panel report and we shall address these questions below.

Transferred funds, collaborations and KTT

We thank the Review Panel and the SNSF for supporting and allowing the transfer of funds from Phase II to Phase III. We are following the recommendations to use this amount largely for collaborations and for technology transfer. In fact, half of the transferred amount has already been used to stimulate further collaborations (see comment under section 2.1.2 Status of integration, p. 8). Another important part will be used to stimulate technology transfer.

We would also like to comment here on the question concerning future KTT activities and the question of who will take over these activities when the senior people who have been pushing these projects retire. We are perfectly aware of this situation and the importance to maintain and stimulate further applied projects in collaboration with industry. Concerning the high-power applications of superconductivity, developed by Prof. R. Flükiger, we explained in our last report the strategy to find a person especially selected to take over this activity. We have now identified this person, a young scientist, who will be appointed to a stable position. Once his appointment secured, it is planned that he shall take over the activities of Flükiger's group before the end of 2010. This means that he shall also take over a good part of the laboratories used by Flükiger. Concerning other KTT activities, we have a remarkable scientist with both research and industry experience, Dr. Jorge Cors. He plays already a key role in several industrial collaborations and shall continue to work on such applied projects. Thus, at least two younger generation scientists shall continue to lead the efforts presently in place. The question whether or not the University of Geneva will be able to appoint a full professor to further stimulate the KTT activities will also depend on the future plans presently being elaborated for the

physics in Geneva. One aspect of these plans, The Geneva Creativity Center, presently under elaboration, will become a new vector in this technology transfer effort.

The future of the MaNEP network, and the role of SNSF in the search for a solution for the future of NCCR networks

The Review Panel raises a very important question concerning the future of MaNEP's network. We decided to go into a large network mode in Phase III. This choice was explained last year and is related to the combination of our wish to add new excellent young members and the complex transformation of MaNEP Geneva, planned at the end of Phase III. However, the question which is raised by the Review Panel has its full importance for the period after Phase III. Do MaNEP researchers want to continue with a broad research network or do they want to make a more restricted network of excellence where only the very best groups participate?

This question will be discussed within MaNEP in the near future, thus it is too early to give a definitive answer at this point. However, this question is at the moment very hypothetical since there is no real funding scheme in Switzerland for any of the two possibilities. Thus, an answer to the question of the Review Panel must pass by the establishment of a new funding source and for that a close collaboration between SNSF, the Federal Department of Home Affairs and the researchers is certainly necessary. We are pleased to note that the Review Panel recommends that the SNSF should try to find solutions for the future of the NCCR networks. The MaNEP director and his colleagues in MaNEP are eager to work with the SNSF to achieve such solutions.

Concerning MaNEP's efforts in this direction, we have used the first 9 months of Phase III to

install the new structure, and to prepare for the integration of MaNEP Geneva into the University. We shall now start to address the question related to the MaNEP network. To initiate this work we have dedicated the meeting of the Scientific Committee on April 14, 2010 precisely

to a discussion of the future of the MaNEP network. Questions, as the one which has been raised by the Review Panel, will be addressed and a scheme of how to work with the authorities to solve the problem will be analyzed.

9.3 Publications over the last period

The following lists cover the period from April 1st, 2008 to March 31st, 2009:

1. Scientific articles in journals with peer review
2. Scientific articles in journals without peer review
3. Publications from lists 1 and 2 involving several groups

The first two lists are sorted by the name of the group leaders. The most important publications are outlined by a red mark.

9.3.1 Scientific articles in journals with peer review

Group of Ph. Aebi

- ▶ C. MONNEY, H. CERCELLIER, C. BATTAGLIA, E. F. SCHWIER, C. DIDOT, M. G. GARNIER, H. BECK, AND P. AEBI

Temperature dependence of the excitonic insulator phase model in 1T-TiSe₂

Physica B **404**, 3172 (2009).

Group(s): Aebi / Project(s): 7

- C. BATTAGLIA, G. ONIDA, K. GAÁL-NAGY, AND P. AEBI

Structure and stability of the Si(331)-(12×1) surface reconstruction investigated with first-principles density functional theory

Physical Review B **80**, 214102 (2009).

Group(s): Aebi / Project(s): 7

- C. MONNEY, H. CERCELLIER, F. CLERC, C. BATTAGLIA, E. F. SCHWIER, C. DIDOT, M. G. GARNIER, H. BECK, P. AEBI, H. BERGER, L. FORRÓ, AND L. PATHEY

Spontaneous exciton condensation in 1T-TiSe₂: BCS-like approach

Physical Review B **79**, 045116 (2009).

Group(s): Aebi, Forró / Project(s): 7

- M. HOESCH, X. CUI, K. SHIMADA, C. BATTAGLIA, S.-I. FUJIMORI, AND H. BERGER

Splitting in the Fermi surface of ZrTe₃: A surface charge density wave system

Physical Review B **80**, 075423 (2009).

Group(s): Aebi, Forró / Project(s): 7

Group of D. Baeriswyl

- D. BAERISWYL, D. EICHENBERGER, AND M. MENTESHASHVILI

Variational ground states of the two-dimensional Hubbard model

New Journal of Physics **11**, 075010 (2009).

Group(s): Baeriswyl / Project(s): 4

- ▶ D. EICHENBERGER AND D. BAERISWYL
- Electron doping and superconductivity in the two-dimensional Hubbard model*

Physical Review B **79**, 100510(R) (2009).

Group(s): Baeriswyl / Project(s): 4

- L. TINCANI, R. M. NOACK, AND D. BAERISWYL

Critical properties of the band-insulator-to-Mott-insulator transition in the strong-coupling limit of the ionic Hubbard model

Physical Review B **79**, 165109 (2009).

Group(s): Baeriswyl / Project(s): 5

Group of B. Batlogg

- ▶ M. P. WALSER, W. L. KALB, T. MATHIS, T. J. BRENNER, AND B. BATLOGG

Stable complementary inverters with organic field-effect transistors on Cytop fluoropolymer gate dielectric

Applied Physics Letters **94**, 053303 (2009).

Group(s): Batlogg / Project(s): 4

- ▶ J. KARPINSKI, N. D. ZHIGADLO, S. KATRYCH, Z. BUKOWSKI, P. MOLL, S. WEYENETH, H. KELLER, R. PUZNIAK, M. TORTELLO, D. DAGHERO, R. GONNELLI, I. MAGGIO-APRILE, Y. FASANO, Ø. FISCHER, K. RO-GACKI, AND B. BATLOGG

Single crystals of $\text{LnFeAsO}_{1-x}\text{F}_x$ ($\text{Ln} = \text{La, Pr, Nd, Sm, Gd}$) and $\text{Ba}_{1-x}\text{Rb}_x\text{Fe}_2\text{As}_2$: Growth, structure and superconducting properties

Physica C **469**, 370 (2009).

Group(s): Batlogg, Fischer, Karpinski, Keller / Project(s): 4

A. BELOUSOV, S. KATRYCH, J. JUN, J. ZHANG, D. GÜNTHER, R. SOBOLEWSKI, J. KARPINSKI, AND B. BATLOGG

Bulk single-crystal growth of ternary $\text{Al}_x\text{Ga}_{1-x}\text{N}$ from solution in gallium under high pressure

Journal of Crystal Growth **311**, 3971 (2009).

Group(s): Batlogg, Karpinski / Project(s): 4

- ▶ Z. BUKOWSKI, S. WEYENETH, R. PUZNIAK, P. MOLL, S. KATRYCH, N. D. ZHIGADLO, J. KARPINSKI, H. KELLER, AND B. BATLOGG

Superconductivity at 23 K and low anisotropy in Rb-substituted BaFe_2As_2 single crystals

Physical Review B **79**, 104521 (2009).

Group(s): Batlogg, Karpinski, Keller / Project(s): 4

Group of Ch. Bernhard

N. OJHA, V. K. MALIK, C. BERNHARD, AND G. D. VARMA

Enhanced superconducting properties of Eu_2O_3 -doped MgB_2

Physica C **469**, 846 (2009).

Group(s): Bernhard / Project(s): 4

- ▶ J. CHALOUPKA, C. BERNHARD, AND D. MUNZAR

Microscopic gauge-invariant theory of the c-axis infrared response of the bilayer cuprate superconductors and the origin of superconductivity-induced absorption bands

Physical Review B **79**, 184513 (2009).

Group(s): Bernhard / Project(s): 4

- ▶ S. S. A. SEO, M. J. HAN, G. W. J. HASSINK, W. S. CHOI, S. J. MOON, J. S. KIM, T. SUSAKI,

Y. S. LEE, J. YU, C. BERNHARD, H. Y. HWANG, G. RIJNDERS, D. H. A. BLANK, B. KEIMER, AND T. W. NOH

Two-dimensional confinement of $3d^1$ electrons in $\text{LaTiO}_3/\text{LaAlO}_3$ multilayers

Physical Review Letters **104**, 036401 (2010).

Group(s): Bernhard / Project(s): 1

N. OJHA, V. K. MALIK, R. SINGLA, C. BERNHARD, AND G. D. VARMA

The effect of citric and oxalic acid doping on the superconducting properties of MgB_2

Superconductor Science & Technology **22**, 125014 (2009).

Group(s): Bernhard / Project(s): 4

- ▶ A. DUBROKA, M. RÖSSLE, K. W. KIM, V. K. MALIK, L. SCHULZ, S. THIEL, C. W. SCHNEIDER, J. MANNHART, G. HERRANZ, O. COPIE, M. BIBES, A. BARTHÉLÉMY, AND C. BERNHARD

Dynamical Response and confinement of the electrons at the $\text{LaAlO}_3/\text{SrTiO}_3$ interface

to be published in Physical Review Letters (2010).

Group(s): Bernhard / Project(s): 1

- ▶ J. HOPPLER, J. STAHN, C. NIEDERMAYER, V. K. MALIK, H. BOUYANFIE, A. J. DREW, M. RÖSSLE, A. BUZDIN, G. CRISTIANI, H.-U. HABERMEIER, B. KEIMER, AND C. BERNHARD

Giant superconductivity-induced modulation of the ferromagnetic magnetization in a cuprate-manganite superlattice

Nature Materials **8**, 315 (2009).

Group(s): Bernhard, Niedermayer / Project(s): 1

- ▶ A. J. DREW, C. NIEDERMAYER, P. J. BAKER, F. L. PRATT, S. J. BLUNDELL, T. LANCASTER, R. H. LIU, G. WU, X. H. CHEN, I. WATANABE, V. K. MALIK, A. DUBROKA, M. RÖSSLE, K. W. KIM, C. BAINES, AND C. BERNHARD

Coexistence of static magnetism and superconductivity in $\text{SmFeAsO}_{1-x}\text{F}_x$ as revealed by muon spin rotation

Nature Materials **8**, 310 (2009).

Group(s): Bernhard, Niedermayer / Project(s): 4

C. BERNHARD, A. J. DREW, L. SCHULZ, V. K. MALIK, M. RÖSSLE, C. NIEDERMAYER, T. WOLF, G. D. VARMA, G. MU, H.-H. WEN, G. WU, AND X. H. CHEN

Muon spin rotation study of magnetism and superconductivity in $\text{BaFe}_{2-x}\text{Co}_x\text{As}_2$ and $\text{Pr}_{1-x}\text{Sr}_x\text{FeAsO}$

New Journal of Physics **11**, 055050 (2009).

Group(s): Bernhard, Niedermayer / Project(s): 4

J. STAHN, C. NIEDERMAYER, J. HOPPLER, AND

C. BERNHARD
PNR studies of proximity and coupling effects in $\text{YBa}_2\text{Cu}_3\text{O}_7/\text{La}_{2/3}\text{Ca}_{1/3}\text{MnO}_3$ superlattices
 Neutron News **20**, 13 (2009).
 Group(s): Bernhard, Niedermayer / Project(s): 1

Group of G. Blatter

F. HASSLER AND S. D. HUBER
Coherent pumping of a Mott insulator: Fermi golden rule versus Rabi oscillations
 Physical Review A **79**, 021607(R) (2009).
 Group(s): Blatter / Project(s): 8

A. U. THOMANN, V. B. GESHKENBEIN, AND G. BLATTER
Quantum instability in a dc SQUID with strongly asymmetric dynamical parameters
 Physical Review B **79**, 184515 (2009).
 Group(s): Blatter / Project(s): 5

S. D. HUBER AND G. BLATTER
Mesoscopic aspects of strongly interacting cold atoms
 Physical Review B **79**, 174504 (2009).
 Group(s): Blatter / Project(s): 8

► S. SCHMIDT AND G. BLATTER
Strong Coupling Theory for the Jaynes-Cummings-Hubbard Model
 Physical Review Letters **103**, 086403 (2009).
 Group(s): Blatter / Project(s): 8

► S. D. HUBER AND A. RÜEGG
Dynamically Generated Double Occupancy as a Probe of Cold Atom Systems
 Physical Review Letters **102**, 065301 (2009).
 Group(s): Blatter / Project(s): 8

Group of M. Büttiker

M. MOSKALETS AND M. BÜTTIKER
Heat production and current noise for single- and double-cavity quantum capacitors
 Physical Review B **80**, 081302 (2009).
 Group(s): Büttiker / Project(s): 2

► J. SPLETTSTOESSER, M. MOSKALETS, AND M. BÜTTIKER
Two-Particle Nonlocal Aharonov-Bohm Effect from Two Single-Particle Emitters
 Physical Review Letters **103**, 076804 (2009).
 Group(s): Büttiker / Project(s): 2

► S. E. NIGG AND M. BÜTTIKER
Universal Detector Efficiency of a Mesoscopic Capacitor
 Physical Review Letters **102**, 236801 (2009).
 Group(s): Büttiker / Project(s): 2

► P. SAMUELSSON, I. NEDER, AND M. BÜTTIKER
Reduced and Projected Two-Particle Entanglement at Finite Temperatures
 Physical Review Letters **102**, 106804 (2009).
 Group(s): Büttiker / Project(s): 2

Group of M. Decroux

► L. ANTOGNAZZA, M. THERASSE, M. DECROUX, F. ROY, B. DUTOIT, M. ABPLANALP, AND Ø. FISCHER
Comparison between the behavior of HTS thin film grown on sapphire and coated conductors for fault current limiter applications
 IEEE Transactions on Applied Superconductivity **19**, 1960 (2009).
 Group(s): Abplanalp, Decroux, Fischer / Project(s): 3

F. ROY, M. THERASSE, B. DUTOIT, F. SIROIS, L. ANTOGNAZZA, AND M. DECROUX
Numerical studies of the quench propagation in coated conductors for fault current limiters
 IEEE Transactions on Applied Superconductivity **19**, 2496 (2009).
 Group(s): Decroux / Project(s): 3

F. ROY, S. PÉREZ, M. THERASSE, B. DUTOIT, F. SIROIS, M. DECROUX, AND L. ANTOGNAZZA
Quench propagation in coated conductors for fault current limiters
 Physica C **469**, 1462 (2009).
 Group(s): Decroux / Project(s): 3

N. CURTZ, E. KOLLER, H. ZBINDEN, M. DECROUX, L. ANTOGNAZZA, Ø. FISCHER, AND N. GISIN
Patterning of ultrathin YBCO nanowires using a new focused-ion-beam process
 Superconductor Science & Technology **23**, 045015 (2010).
 Group(s): Decroux, Fischer / Project(s): 3

Group of L. Degiorgi

F. PFUNER, L. DEGIORGI, T. I. BATURINA, V. M. VINOKUR, AND M. R. BAKLANOV
Optical properties of TiN thin films close to the superconductor-insulator transition
 New Journal of Physics **11**, 113017 (2009).
 Group(s): Degiorgi / Project(s): 7

F. PFUNER, L. DEGIORGI, J.-H. CHU, N. RU, K. Y. SHIN, AND I. R. FISHER
Optical properties of the charge-density-wave rare-earth tri-telluride compounds: A view on PrTe_3

Physica B **404**, 533 (2009).

Group(s): Degiorgi / Project(s): 7

- ▶ M. LAVAGNINI, A. SACCHETTI, C. MARINI, M. VALENTINI, R. SOPRACASE, A. PERUCCHI, P. POSTORINO, S. LUPI, J.-H. CHU, I. R. FISHER, AND L. DEGIORGI

Pressure dependence of the single particle excitation in the charge-density-wave CeTe₃ system

Physical Review B **79**, 075117 (2009).

Group(s): Degiorgi / Project(s): 7

- ▶ F. PFUNER, J. G. ANALYTIS, J.-H. CHU, I. R. FISHER, AND L. DEGIORGI

Charge dynamics of the spin-density-wave state in BaFe₂As₂

The European Physical Journal B **67**, 513 (2009).

Group(s): Degiorgi / Project(s): 7

F. PFUNER, L. DEGIORGI, H. BERGER, AND L. FORRÓ

Infrared investigation of the phonon spectrum in the frustrated spin cluster compound FeTe₂O₅Cl

Journal of Physics: Condensed Matter **21**, 375401 (2009).

Group(s): Degiorgi, Forró / Project(s): 6, 7

- ▶ A. SACCHETTI, C. L. CONDRON, S. N. GVASALIYA, F. PFUNER, M. LAVAGNINI, M. BALDINI, M. F. TONEY, M. MERLINI, M. HANFLAND, J. MESOT, J.-H. CHU, I. R. FISHER, P. POSTORINO, AND L. DEGIORGI

Pressure-induced quenching of the charge-density-wave state in rare-earth tritellurides observed by x-ray diffraction

Physical Review B **79**, 201101(R) (2009).

Group(s): Degiorgi, Mesot / Project(s): 7

Group of Ø. Fischer

- ▶ L. ANTOGNAZZA, M. THERASSE, M. DECROUX, F. ROY, B. DUTOIT, M. ABPLANALP, AND Ø. FISCHER

Comparison between the behavior of HTS thin film grown on sapphire and coated conductors for fault current limiter applications

IEEE Transactions on Applied Superconductivity **19**, 1960 (2009).

Group(s): Abplanalp, Decroux, Fischer / Project(s): 3

- ▶ J. KARPINSKI, N. D. ZHIGADLO, S. KATRYCH, Z. BUKOWSKI, P. MOLL, S. WEYENETH, H. KELLER, R. PUZNIAK, M. TORTELLO, D. DAGHERO, R. GONNELLI, I. MAGGIO-APRILE, Y. FASANO, Ø. FISCHER, K. ROGACKI, AND B. BATLOGG

Single crystals of LnFeAsO_{1-x}F_x (Ln = La, Pr, Nd, Sm, Gd) and Ba_{1-x}Rb_xFe₂As₂: Growth, structure and superconducting properties

Physica C **469**, 370 (2009).

Group(s): Batlogg, Fischer, Karpinski, Keller / Project(s): 4

N. CURTZ, E. KOLLER, H. ZBINDEN, M. DECROUX, L. ANTOGNAZZA, Ø. FISCHER, AND N. GISIN

Patterning of ultrathin YBCO nanowires using a new focused-ion-beam process

Superconductor Science & Technology **23**, 045015 (2010).

Group(s): Decroux, Fischer / Project(s): 3

- ▶ A. P. PETROVIĆ, Y. FASANO, R. LORTZ, C. SENATORE, A. DEMUER, A. B. ANTUNES, A. PARÉ, D. SALLOUM, P. GOUGEON, M. POTTEL, AND Ø. FISCHER

Real-Space Vortex Glass Imaging and the Vortex Phase Diagram of SnMo₆S₈

Physical Review Letters **103**, 257001 (2009).

Group(s): Fischer, Flükiger / Project(s): 7

- ▶ N. JENKINS, Y. FASANO, C. BERTHOD, I. MAGGIO-APRILE, A. PIRIOU, E. GIANNINI, B. W. HOOGENBOOM, C. HESS, T. CREN, AND Ø. FISCHER

Imaging the Essential Role of Spin Fluctuations in High-T_c Superconductivity

Physical Review Letters **103**, 227001 (2009).

Group(s): Fischer, Giamarchi, Giannini / Project(s): 4

- ▶ B. M. WOJEK, E. MORENZONI, D. G. ESHCHENKO, A. SUTER, T. PROKSCHA, E. KOLLER, E. TREBOUX, O. FISCHER, AND H. KELLER

Magnetism and superconductivity in cuprate heterostructures studied by low energy μ SR

Physica B **404**, 720 (2009).

Group(s): Fischer, Keller, Morenzoni / Project(s): 1, 4

P. S. HÄFLIGER, R. KHASANOV, R. LORTZ, A. PETROVIĆ, K. TOGANO, C. BAINES, B. GRANALI, AND H. KELLER

Muon-Spin Rotation Study of the Ternary Noncentrosymmetric Superconductors Li₂Pd_xPt_{3-x}B

Journal of Superconductivity and Novel Magnetism **22**, 337 (2009).

Group(s): Keller, Fischer / Project(s): 4

Group of R. Flükiger

- ▶ A. P. PETROVIĆ, Y. FASANO, R. LORTZ, C. SENATORE, A. DEMUER, A. B. ANTUNES, A. PARÉ, D. SALLOUM, P. GOUGEON, M. POTTEL, AND Ø. FISCHER

- Real-Space Vortex Glass Imaging and the Vortex Phase Diagram of SnMo_6S_8*
Physical Review Letters **103**, 257001 (2009).
Group(s): Fischer, Flükiger / Project(s): 7
- C. SCHEUERLEIN, M. DI MICHIEL, AND F. BUTA
Synchrotron Radiation Techniques for the Characterization of Nb_3Sn Superconductors
IEEE Transactions on Applied Superconductivity **19**, 2653 (2009).
Group(s): Flükiger / Project(s): 3
- T. BOUTBOUL, L. OBERLI, A. DEN OUDEN, D. PEDRINI, B. SEEBER, AND G. VOLPINI
Heat Treatment Optimization Studies on PIT Nb_3Sn Strand for the NED Project
IEEE Transactions on Applied Superconductivity **19**, 2564 (2009).
Group(s): Flükiger / Project(s): 3
- J. LU, K. HAN, R. P. WALSH, I. DIXON, A. FERRERA, AND B. SEEBER
Characterization of High J_c Nb_3Sn Strands for the Series-Connected Hybrid Magnet
IEEE Transactions on Applied Superconductivity **19**, 2615 (2009).
Group(s): Flükiger / Project(s): 6
- N. N. MARTOVETSKY, D. R. HATFIELD, J. R. MILLER, C. Y. GUNG, J. S. SCHULTZ, N. CHEGGOUR, L. F. GOODRICH, P. BRUZZONE, B. STEPANOV, R. WESCHE, AND B. SEEBER
Test Results of the First US ITER TF Conductor in SULTAN
IEEE Transactions on Applied Superconductivity **19**, 1478 (2009).
Group(s): Flükiger / Project(s): 3
- L. THILLY, C. SCHEUERLEIN, U. STUHR, B. BORDINI, AND B. SEEBER
Residual Strain in a Nb_3Sn Strand Mounted on a Barrel for Critical Current Measurements
IEEE Transactions on Applied Superconductivity **19**, 2645 (2009).
Group(s): Flükiger / Project(s): 3
- R. FLÜKIGER, M. S. A. HOSSAIN, AND C. SENATORE
Strong enhancement of J_c and B_{irr} in binary in situ MgB_2 wires after cold high pressure densification
Superconductor Science & Technology **22**, 085002 (2009).
Group(s): Flükiger / Project(s): 3
- M. S. A. HOSSAIN, C. SENATORE, R. FLÜKIGER, M. A. RINDFLEISCH, M. J. TOMSIC, J. H. KIM, AND S. X. DOU
The enhanced J_c and B_{irr} of in situ MgB_2 wires and tapes alloyed with $\text{C}_4\text{H}_6\text{O}_5$ (malic acid) after cold high pressure densification
Superconductor Science & Technology **22**, 095004 (2009).
Group(s): Flükiger / Project(s): 3
- C. SENATORE AND R. FLÜKIGER
Correlation between superconducting transition width and relaxation rates in various industrial Y123-coated conductors
Superconductor Science & Technology **22**, 095016 (2009).
Group(s): Flükiger / Project(s): 3
- S. R. GHORBANI, X. L. WANG, M. S. A. HOSSAIN, S. X. DOU, AND S. I. LEE
Coexistence of the δI and δT_c flux pinning mechanisms in nano-Si-doped MgB_2
Superconductor Science & Technology **23**, 025019 (2010).
Group(s): Flükiger / Project(s): 3
- A. UBALDINI, E. GIANNINI, C. SENATORE, AND D. VAN DER MAREL
 BiOCuS : A new superconducting compound with oxypnictide-related structure
Physica C (2010), doi:10.1016/j.physc.2009.11.164.
Group(s): Flükiger, Giannini, van der Marel / Project(s): 4
- Group of L. Forró**
- C. MONNEY, H. CERCELLIER, F. CLERC, C. BATTAGLIA, E. F. SCHWIER, C. DIDIOT, M. G. GARNIER, H. BECK, P. AEBI, H. BERGER, L. FORRÓ, AND L. PATTHEY
Spontaneous exciton condensation in $1T\text{-TiSe}_2$: BCS-like approach
Physical Review B **79**, 045116 (2009).
Group(s): Aebi, Forró / Project(s): 7
- M. HOESCH, X. CUI, K. SHIMADA, C. BATTAGLIA, S.-I. FUJIMORI, AND H. BERGER
Splitting in the Fermi surface of ZrTe_3 : A surface charge density wave system
Physical Review B **80**, 075423 (2009).
Group(s): Aebi, Forró / Project(s): 7
- F. PFUNER, L. DEGIORGI, H. BERGER, AND L. FORRÓ
Infrared investigation of the phonon spectrum in the frustrated spin cluster compound $\text{FeTe}_2\text{O}_5\text{Cl}$
Journal of Physics: Condensed Matter **21**, 375401 (2009).
Group(s): Degiorgi, Forró / Project(s): 6,7

- D. ZHANG, M. JOHNSON, H. BERGER, R. K. KREMER, D. WULFERDING, AND P. LEMMENS
Separation of the Oxide and Halide Part in the Oxohalide $Fe_3Te_3O_{10}Cl$ Due to High Lewis Acidity of the Cations
Inorganic Chemistry **48**, 6599 (2009).
Group(s): Forró / Project(s): 6
- L. GASPAROV, A. RUSH, T. PEKAREK, N. PATEL, AND H. BERGER
Raman studies of doped magnetite above and below the Verwey transition
Journal of Applied Physics **105**, 07E109 (2009).
Group(s): Forró / Project(s): 6
- R. FLEURIER, S. BHATTACHARYYA, M. L. SABOUNGI, N. RAIMBOUX, P. SIMON, J. KLIVAVA, A. MAGREZ, T. FEHER, L. FORRÓ, AND J. P. SALVETAT
Increase in the Curie temperature and magnetic anisotropy in FePd/Pt-iron oxide core-shell nanoparticles
Journal of Applied Physics **106**, 073903 (2009).
Group(s): Forró / Project(s): 6
- I. ŽIVKOVIĆ, K. PRŠA, O. ZAHARKO, AND H. BERGER
 Ni_3TeO_6 -a collinear antiferromagnet with ferromagnetic honeycomb planes
Journal of Physics: Condensed Matter **22**, 056002 (2010).
Group(s): Forró / Project(s): 6
- J. L. HER, Y. H. MATSUDA, K. SUGA, K. KINDO, S. TAKEYAMA, H. BERGER, AND H. D. YANG
High-field magnetization of a two-dimensional spin frustration system, $Ni_5(TeO_3)_4X_2$ ($X = Br, Cl$)
Journal of Physics: Condensed Matter **21**, 436005 (2009).
Group(s): Forró / Project(s): 6
- L. ĆIRIĆ, A. SIENKIEWICZ, B. NÁFRÁDI, M. MIONIĆ, A. MAGREZ, AND L. FORRÓ
Towards electron spin resonance of mechanically exfoliated graphene
Physica Status Solidi (b) **246**, 2558 (2009).
Group(s): Forró / Project(s): 2
- K.-Y. CHOI, D. WULFERDING, H. BERGER, AND P. LEMMENS
Interplay of electronic correlations and lattice instabilities in $BaVS_3$
Physical Review B **80**, 245108 (2009).
Group(s): Forró / Project(s): 7
- C. P. SUN, C. C. LIN, J. L. HER, C. J. HO, S. TARAN, H. BERGER, B. K. CHAUDHURI, AND H. D. YANG
Field-dependent dielectric and magnetic properties in multiferroic $CdCr_2S_4$
Physical Review B **79**, 214116 (2009).
Group(s): Forró / Project(s): 6
- L. V. GASPAROV, A. RUSH, G. GÜENTHERODT, AND H. BERGER
Electronic Raman scattering in magnetite: Spin versus charge gap
Physical Review B **79**, 144303 (2009).
Group(s): Forró / Project(s): 6
- M. PRESTER, I. ŽIVKOVIĆ, O. ZAHARKO, D. PAJIĆ, P. TREGENNA-PIGGOTT, AND H. BERGER
Ferromagnetism in $Co_7(TeO_3)_4Br_6$: A byproduct of complex antiferromagnetic order and single-ion anisotropy
Physical Review B **79**, 144433 (2009).
Group(s): Forró / Project(s): 6
- K. L. NAGY, B. NÁFRÁDI, N. D. KUSHCH, E. B. YAGUBSKII, E. HERDTWECK, T. FEHÉR, L. F. KISS, L. FORRÓ, AND A. JÁNOSSY
Multifrequency ESR in $ET_2MnCu[N(CN)_2]_4$: A radical cation salt with quasi-two-dimensional magnetic layers in a three-dimensional polymeric structure
Physical Review B **80**, 104407 (2009).
Group(s): Forró / Project(s): 7
- A. PALLINGER, B. SAS, G. KRIZA, K. VAD, L. FORRÓ, H. BERGER, F. PORTIER, AND F. I. B. WILLIAMS
Metastability of two-dimensional vortex glass in $Bi_2Sr_2CaCu_2O_{8+\delta}$
Physical Review B **80**, 024206 (2009).
Group(s): Forró / Project(s): 7
- ▶ A. F. KUSMARTSEVA, B. SIPOS, H. BERGER, L. FORRÓ, AND E. TUTIŠ
Pressure Induced Superconductivity in Pristine $1T-TiSe_2$
Physical Review Letters **103**, 236401 (2009).
Group(s): Forró / Project(s): 7
- ▶ M. PREGELJ, O. ZAHARKO, A. ZORKO, Z. KUTNJAK, P. JEGLIČ, P. J. BROWN, M. JAGODIČ, Z. JAGLIČIĆ, H. BERGER, AND D. ARČON
Spin Amplitude Modulation Driven Magnetolectric Coupling in the New Multiferroic $FeTe_2O_5Br$
Physical Review Letters **103**, 147202 (2009).
Group(s): Forró / Project(s): 6
- ▶ S. V. BORISENKO, A. A. KORDYUK, V. B. ZABOLOTNYI, D. S. INOSOV, D. EVTUSHINSKY, B. BÜCHNER, A. N. YARESKO,

A. VARYKHALOV, R. FOLLATH, W. EBERHARDT, L. PATTHEY, AND H. BERGER

Two Energy Gaps and Fermi-Surface "Arcs" in NbSe₂

Physical Review Letters **102**, 166402 (2009).

Group(s): Forró / Project(s): 7

G. GHIRINGHELLI, A. PIAZZALUNGA, X. WANG, A. BENDOUNAN, H. BERGER, F. BOTTEGONI, N. CHRISTENSEN, C. DALLERA, M. GRIONI, J.-C. GRIVEL, M. MORETTI SALA, L. PATTHEY, J. SCHLAPPA, T. SCHMITT, V. STROCOV, AND L. BRAICOVICH

Crystal field and low-energy excitations measured by high resolution RIXS at the L₃ edge of Cu, Ni and Mn

The European Physical Journal – Special Topics **169**, 199 (2009).

Group(s): Forró, Grioni / Project(s): 7

B. SIPOS, M. DUCHAMP, A. MAGREZ, L. FORRÓ, N. BARIŠIĆ, A. KIS, J. W. SEO, F. BIERI, F. KRUMEICH, R. NESPER, AND G. R. PATZKE

Mechanical and electronic properties of vanadium oxide nanotubes

Journal of Applied Physics **105**, 074317 (2009).

Group(s): Forró, Patzke / Project(s): 7, 3

Group of T. Giamarchi

- ▶ N. JENKINS, Y. FASANO, C. BERTHOD, I. MAGGIO-APRILE, A. PIRIOU, E. GIANNINI, B. W. HOOGENBOOM, C. HESS, T. CREN, AND Ø. FISCHER

Imaging the Essential Role of Spin Fluctuations in High-T_c Superconductivity

Physical Review Letters **103**, 227001 (2009).

Group(s): Fischer, Giamarchi, Giannini / Project(s): 4

- ▶ T. JARLBORG

Mechanisms for higher T_c in copper oxide superconductors: Ideas from band calculations

Applied Physics Letters **94**, 212503 (2009).

Group(s): Giamarchi / Project(s): 4

- ▶ T. JARLBORG

Q-dependence of spin excitations in high-T_c cuprates from spin-phonon coupling

Journal of Physics: Condensed Matter **21**, 142202 (2009).

Group(s): Giamarchi / Project(s): 4

M. B. ZVONAREV, V. V. CHEIANOV, AND T. GIAMARCHI

The time-dependent correlation function of the Jordan-Wigner operator as a Fredholm determinant

Journal of Statistical Mechanics p. P07035 (2009).

Group(s): Giamarchi / Project(s): 8

- ▶ T. JARLBORG

Properties of high-T_c Copper Oxides from Band Models of Spin-Phonon Coupling

Journal of Superconductivity and Novel Magnetism **22**, 247 (2009).

Group(s): Giamarchi / Project(s): 4

- ▶ P. CHUDZINSKI, M. GABAY, AND T. GIAMARCHI

Influence of non-magnetic impurities on hole-doped two-leg Cu-O Hubbard ladders

New Journal of Physics **11**, 055059 (2009).

Group(s): Giamarchi / Project(s): 7

G. ORSO, A. IUCCI, M. A. CAZALILLA, AND T. GIAMARCHI

Lattice modulation spectroscopy of strongly interacting bosons in disordered and quasiperiodic optical lattices

Physical Review A **80**, 033625 (2009).

Group(s): Giamarchi / Project(s): 8

A. F. HO, M. A. CAZALILLA, AND T. GIAMARCHI

Quantum simulation of the Hubbard model: The attractive route

Physical Review A **79**, 033620 (2009).

Group(s): Giamarchi / Project(s): 8

- ▶ A. M. LOBOS, A. IUCCI, M. MÜLLER, AND T. GIAMARCHI

Dissipation-driven phase transitions in superconducting wires

Physical Review B **80**, 214515 (2009).

Group(s): Giamarchi / Project(s): 2

L. BENFATTO, C. CASTELLANI, AND T. GIAMARCHI

Broadening of the Beresinskii-Kosterlitz-Thouless superconducting transition by inhomogeneity and finite-size effects

Physical Review B **80**, 214506 (2009).

Group(s): Giamarchi / Project(s): 1

M. B. ZVONAREV, V. V. CHEIANOV, AND T. GIAMARCHI

Edge exponent in the dynamic spin structure factor of the Yang-Gaudin model

Physical Review B **80**, 201102(R) (2009).

Group(s): Giamarchi / Project(s): 8

V. LECOMTE, S. E. BARNES, J.-P. ECKMANN, AND T. GIAMARCHI

Depinning of domain walls with an internal degree of freedom

Physical Review B **80**, 054413 (2009).

Group(s): Giamarchi / Project(s): 1

A. B. KOLTON, A. ROSSO, T. GIAMARCHI,
AND W. KRAUTH

Creep dynamics of elastic manifolds via exact transition pathways

Physical Review B **79**, 184207 (2009).

Group(s): Giamarchi / Project(s): 1

► T. JARLBORG

Spin-phonon coupling and q -dependence of spin excitations and high- T_C superconductivity from band models

Physical Review B **79**, 094530 (2009).

Group(s): Giamarchi / Project(s): 4

► M. B. ZVONAREV, V. V. CHEIANOV, AND
T. GIAMARCHI

Dynamical Properties of the One-Dimensional Spin-1/2 Bose-Hubbard Model near a Mott-Insulator to Ferromagnetic-Liquid Transition

Physical Review Letters **103**, 110401 (2009).

Group(s): Giamarchi / Project(s): 8

► T. JARLBORG

Supercell Band Calculations and Correlation for High- T_C Copper Oxide Superconductors

Advances in Condensed Matter Physics **2010**, 912067 (2009).

Group(s): Giamarchi / Project(s): 4

Group of E. Giannini

► N. JENKINS, Y. FASANO, C. BERTHOD,
I. MAGGIO-APRILE, A. PIRIOU, E. GIANNINI,
B. W. HOOGENBOOM, C. HESS, T. CREN, AND
Ø. FISCHER

Imaging the Essential Role of Spin Fluctuations in High- T_c Superconductivity

Physical Review Letters **103**, 227001 (2009).

Group(s): Fischer, Giamarchi, Giannini / Project(s): 4

A. UBALDINI, E. GIANNINI, C. SENATORE,
AND D. VAN DER MAREL

BiOCuS: A new superconducting compound with oxypnictide-related structure

Physica C (2010),
doi:10.1016/j.physc.2009.11.164.

Group(s): Flükiger, Giannini, van der Marel / Project(s): 4

S. WEYENETH, T. SCHNEIDER, AND E. GIANNINI

Evidence for Kosterlitz-Thouless and three-dimensional XY critical behavior in $Bi_2Sr_2CaCu_2O_{8+\delta}$

Physical Review B **79**, 214504 (2009).

Group(s): Giannini / Project(s): 4

M. WEIGAND, M. EISTERER, E. GIANNINI,
AND H. W. WEBER

Mixed state properties of $Bi_2Sr_2Ca_2Cu_3O_{10+\delta}$ single crystals before and after neutron irradiation

Physical Review B **81**, 014516 (2010).

Group(s): Giannini / Project(s): 4

R. VIENNOIS, E. GIANNINI, J. TEYSSIER,
J. ELIA, J. DEISENHOFER, AND D. VAN DER
MAREL

Two-dimensional orbital ordering in d^1 Mott insulator Sr_2VO_4

Journal of Physics: Conference Series **200**, 012219 (2010).

Group(s): Giannini, van der Marel / Project(s): 4

J. TEYSSIER, R. VIENNOIS, V. GURITANU,
E. GIANNINI, AND D. VAN DER MAREL

Kondo effect and quantum critical point in $Mn_{(1-x)}Co_xSi$

Journal of Physics: Conference Series **200**, 032076 (2010).

Group(s): Giannini, van der Marel / Project(s): 5

R. VIENNOIS, E. GIANNINI, D. VAN DER
MAREL, AND R. ČERNÝ

Effect of Fe excess on Structural, Magnetic and Superconducting Properties of Single-Crystalline $Fe_{1+x}Te_{1-y}Se_y$

Journal of Solid State Chemistry (2010),
doi:10.1016/j.jssc.2010.01.024.

Group(s): Giannini, van der Marel / Project(s): 4

R. VIENNOIS, E. GIANNINI, D. VAN DER
MAREL, AND R. ČERNÝ

Phase diagram of single-crystalline tetragonal iron chalcogenides

Physica C (2010),
doi:10.1016/j.physc.2009.11.126.

Group(s): Giannini, van der Marel / Project(s): 4

I. PALLECCHI, G. LAMURA, M. TROPEANO,
M. PUTTI, R. VIENNOIS, E. GIANNINI, AND
D. VAN DER MAREL

Seebeck effect in $Fe_{1+x}Te_{1-y}Se_y$ single crystals

Physical Review B **80**, 214511 (2009).

Group(s): Giannini, van der Marel / Project(s): 4

Group of M. Gioni

G. GHIRINGHELLI, A. PIAZZALUNGA,
X. WANG, A. BENDOUNAN, H. BERGER,
F. BOTTEGONI, N. CHRISTENSEN,
C. DALLERA, M. GRIONI, J.-C. GRIVEL,
M. MORETTI SALA, L. PATTHEY,
J. SCHLAPPA, T. SCHMITT, V. STROCOV,
AND L. BRAICOVICH

Crystal field and low-energy excitations measured by high resolution RIXS at the L_3 edge of Cu, Ni and Mn

The European Physical Journal – Special Topics **169**, 199 (2009).

Group(s): Forró, Grioni / Project(s): 7

H. BENTMANN, F. FORSTER, G. BIHLMAYER, E. V. CHULKOV, L. MORESCHINI, M. GRIONI, AND F. REINERT

Origin and manipulation of the Rashba splitting in surface alloys

Europhysics Letters **87**, 37003 (2009).

Group(s): Grioni / Project(s): 7

E. FRANTZESKAKIS, S. PONS, AND M. GRIONI
Giant spin-orbit splitting in a surface alloy grown on a Si substrate: BiAg₂/Ag/Si(111)

Physica B **404**, 419 (2009).

Group(s): Grioni / Project(s): 7

L. MORESCHINI, A. BENDOUNAN, I. GIERZ, C. R. AST, H. MIRHOSSEINI, H. HÖCHST, K. KERN, J. HENK, A. ERNST, S. OStanIN, F. REINERT, AND M. GRIONI

Assessing the atomic contribution to the Rashba spin-orbit splitting in surface alloys: Sb/Ag(111)

Physical Review B **79**, 075424 (2009).

Group(s): Grioni / Project(s): 7

- ▶ L. MORESCHINI, A. BENDOUNAN, H. BENTMANN, M. ASSIG, K. KERN, F. REINERT, J. HENK, C. R. AST, AND M. GRIONI

Influence of the substrate on the spin-orbit splitting in surface alloys on (111) noble-metal surfaces

Physical Review B **80**, 035438 (2009).

Group(s): Grioni / Project(s): 7

- ▶ I. GIERZ, T. SUZUKI, E. FRANTZESKAKIS, S. PONS, S. OStanIN, A. ERNST, J. HENK, M. GRIONI, K. KERN, AND C. R. AST

Silicon Surface with Giant Spin Splitting

Physical Review Letters **103**, 046803 (2009).

Group(s): Grioni / Project(s): 7

E. FRANTZESKAKIS, L. MORESCHINI, M. C. FALUB, M. GRIONI, S. PONS, C. R. AST, D. PACILÉ, AND M. PAPAGNO

New Mechanism for Spin-Orbit Splitting of Conduction States in Surface Alloys

e-Journal of Surface Science and Nanotechnology **7**, 264 (2009).

Group(s): Grioni / Project(s): 7

M. MEDARDE, C. DALLERA, M. GRIONI, B. DELLEY, F. VERNAY, J. MESOT, M. SIKORA, J. A. ALONSO, AND M. J. MARTÍNEZ-LOPE

Charge disproportionation in RNiO₃ perovskites (R = rare earth) from high-resolution x-ray absorption spectroscopy

Physical Review B **80**, 245105 (2009).

Group(s): Grioni, Mesot / Project(s): 7

Group of V. Gritsev

- ▶ A. IMAMBEKOV, I. E. MAZETS, D. S. PETROV, V. GRITSEV, S. MANZ, S. HOFFERBERTH, T. SCHUMM, E. DEMLER, AND J. SCHMIED-MAYER

Density ripples in expanding low-dimensional gases as a probe of correlations

Physical Review A **80**, 033604 (2009).

Group(s): Gritsev / Project(s): 8

- ▶ P. BARMETTLER, M. PUNK, V. GRITSEV, E. DEMLER, AND E. ALTMAN

Relaxation of Antiferromagnetic Order in Spin-1/2 Chains Following a Quantum Quench

Physical Review Letters **102**, 130603 (2009).

Group(s): Gritsev / Project(s): 8

- ▶ A. IMAMBEKOV, A. A. LUKYANOV, L. I. GLAZMAN, AND V. GRITSEV

Exact Solution for 1D Spin-Polarized Fermions with Resonant Interactions

Physical Review Letters **104**, 040402 (2010).

Group(s): Gritsev / Project(s): 8

Group of D. Jaccard

- ▶ N. REYREN, S. GARIGLIO, A. D. CAVIGLIA, D. JACCARD, T. SCHNEIDER, AND J.-M. TRISCONI

Anisotropy of the superconducting transport properties of the LaAlO₃/SrTiO₃ interface

Applied Physics Letters **94**, 112506 (2009).

Group(s): Jaccard, Triscone (JM) / Project(s): 1

Group of J. Karpinski

- ▶ J. KARPINSKI, N. D. ZHIGADLO, S. KATRYCH, Z. BUKOWSKI, P. MOLL, S. WEYENETH, H. KELLER, R. PUZNIAK, M. TORTELLO, D. DAGHERO, R. GONNELLI, I. MAGGIO-APRILE, Y. FASANO, Ø. FISCHER, K. RO-GACKI, AND B. BATLOGG

Single crystals of LnFeAsO_{1-x}F_x (Ln = La, Pr, Nd, Sm, Gd) and Ba_{1-x}Rb_xFe₂As₂: Growth, structure and superconducting properties

Physica C **469**, 370 (2009).

Group(s): Batlogg, Fischer, Karpinski, Keller / Project(s): 4

A. BELOUSOV, S. KATRYCH, J. JUN, J. ZHANG, D. GÜNTHER, R. SOBOLEWSKI, J. KARPINSKI,

AND B. BATLOGG

Bulk single-crystal growth of ternary $Al_xGa_{1-x}N$ from solution in gallium under high pressure

Journal of Crystal Growth **311**, 3971 (2009).

Group(s): Batlogg, Karpinski / Project(s): 4

- Z. BUKOWSKI, S. WEYENETH, R. PUZNIAK, P. MOLL, S. KATRYCH, N. D. ZHIGADLO, J. KARPINSKI, H. KELLER, AND B. BATLOGG
Superconductivity at 23 K and low anisotropy in Rb-substituted $BaFe_2As_2$ single crystals

Physical Review B **79**, 104521 (2009).

Group(s): Batlogg, Karpinski, Keller / Project(s): 4

L. Y. VINNIKOV, T. M. ARTEMOVA, I. S. VESHCHUNOV, N. D. ZHIGADLO, J. KARPINSKI, P. POPOVICH, D. L. SUN, C. LIN, AND A. V. BORIS

Vortex Structure in Superconducting Iron Pnictide Single Crystals

Journal of Experimental and Theoretical Physics Letters **90**, 299 (2009).

Group(s): Karpinski / Project(s): 4

T. MERTELJ, V. V. KABANOV, C. GADERMAIER, N. D. ZHIGADLO, S. KATRYCH, Z. BUKOWSKI, J. KARPINSKI, AND D. MIHAILOVIC

Photoinduced Quasiparticle Relaxation Dynamics in Near-optimally Doped $SmFeAsO_{0.8}F_{0.2}$ Single Crystals

Journal of Superconductivity and Novel Magnetism **22**, 575 (2009).

Group(s): Karpinski / Project(s): 4

D. DAGHERO, M. TORTELLO, R. S. GONNELLI, V. A. STEPANOV, N. D. ZHIGADLO, AND J. KARPINSKI

Possible Multigap Superconductivity in $SmFeAsO_{0.8}F_{0.2}$: A Point-contact Andreev-reflection Spectroscopy Study

Journal of Superconductivity and Novel Magnetism **22**, 543 (2009).

Group(s): Karpinski / Project(s): 4

R. S. GONNELLI, D. DAGHERO, M. TORTELLO, G. A. UMMARINO, V. A. STEPANOV, R. K. KREMER, J. S. KIM, N. D. ZHIGADLO, AND J. KARPINSKI

Point-contact Andreev-reflection spectroscopy in $ReFeAsO_{1-x}F_x$ ($Re = La, Sm$): Possible evidence for two nodeless gaps

Physica C **469**, 512 (2009).

Group(s): Karpinski / Project(s): 4

Y. J. JO, J. JAROSZYNSKI, A. YAMAMOTO, A. GUREVICH, S. C. RIGGS, G. S. BOEBINGER, D. LARBALESTIER, H. H. WEN,

N. D. ZHIGADLO, S. KATRYCH, Z. BUKOWSKI, J. KARPINSKI, R. H. LIU, H. CHEN, X. H. CHEN, AND L. BALICAS

High-field phase-diagram of Fe arsenide superconductors

Physica C **469**, 566 (2009).

Group(s): Karpinski / Project(s): 4

Z. BUKOWSKI, S. WEYENETH, R. PUZNIAK, J. KARPINSKI, AND B. BATLOGG

Bulk Superconductivity at 2.6 K in Undoped $RbFe_2As_2$

Physica C (2010), doi:10.1016/j.physc.2009.11.103.

Group(s): Karpinski / Project(s): 4

M. MATUSIAK, T. PLACKOWSKI, Z. BUKOWSKI, N. D. ZHIGADLO, AND J. KARPINSKI

Evidence of spin-density-wave order in $RFeAsO_{1-x}F_x$ from measurements of thermoelectric power

Physical Review B **79**, 212502 (2009).

Group(s): Karpinski / Project(s): 4

D. DAGHERO, M. TORTELLO, R. S. GONNELLI, V. A. STEPANOV, N. D. ZHIGADLO, AND J. KARPINSKI

Evidence for two-gap nodeless superconductivity in $SmFeAsO_{1-x}F_x$ from point-contact Andreev-reflection spectroscopy

Physical Review B **80**, 060502 (2009).

Group(s): Karpinski / Project(s): 4

M. CALAMIOTOU, A. GANTIS, E. SIRANIDI, D. LAMPAKIS, J. KARPINSKI, AND E. LIAROKAPIS

Pressure-induced lattice instabilities and superconductivity in $YBa_2Cu_4O_8$ and optimally doped $YBa_2Cu_3O_{7-\delta}$

Physical Review B **80**, 214517 (2009).

Group(s): Karpinski / Project(s): 4

N. D. ZHIGADLO, S. KATRYCH, J. KARPINSKI, B. BATLOGG, F. BERNARDINI, S. MASSIDDA, AND R. PUZNIAK

Influence of Mg deficiency on crystal structure and superconducting properties in MgB_2 single crystals

Physical Review B **81**, 054520 (2010).

Group(s): Karpinski / Project(s): 4

M. MATUSIAK, Z. BUKOWSKI, AND J. KARPINSKI

Nernst effect in single crystals of the pnictide superconductor $CaFe_{1.92}Co_{0.08}As_2$ and parent compound $CaFe_2As_2$

Physical Review B **81**, 020510(R) (2010).

Group(s): Karpinski / Project(s): 4

- ▶ V. MOSHCHALOV, M. MENGHINI, T. NISHIO, Q. H. CHEN, A. V. SILHANEK, V. H. DAO, L. F. CHIBOTARU, N. D. ZHIGADLO, AND J. KARPINSKI
Type-1.5 Superconductivity
Physical Review Letters **102**, 117001 (2009).
Group(s): Karpinski / Project(s): 4
- ▶ T. KONDO, R. KHASANOV, Y. SASSA, A. BENDOUNAN, S. PAILHES, J. CHANG, J. MESOT, H. KELLER, N. D. ZHIGADLO, M. SHI, Z. BUKOWSKI, J. KARPINSKI, AND A. KAMINSKI
Anomalous asymmetry in the Fermi surface of the high-temperature superconductor $YBa_2Cu_4O_8$ revealed by angle-resolved photoemission spectroscopy
Physical Review B **80**, 100505 (2009).
Group(s): Karpinski, Keller, Mesot / Project(s): 4
- M. LE TACON, T. R. FORREST, C. RÜEGG, A. BOSAK, A. C. WALTERS, R. MITTAL, H. M. RØNNOW, N. D. ZHIGADLO, S. KATRYCH, J. KARPINSKI, J. P. HILL, M. KRISCH, AND D. F. MCMORROW
Inelastic x-ray scattering study of superconducting $SmFeAsO_{1-x}F_y$ single crystals: Evidence for strong momentum-dependent doping-induced renormalizations of optical phonons
Physical Review B **80**, 220504 (2009).
Group(s): Karpinski, Rønnow / Project(s): 4, 6
- Group of H. Keller**
- ▶ J. KARPINSKI, N. D. ZHIGADLO, S. KATRYCH, Z. BUKOWSKI, P. MOLL, S. WEYENETH, H. KELLER, R. PUZNIAK, M. TORTELLO, D. DAGHERO, R. GONNELLI, I. MAGGIO-APRILE, Y. FASANO, Ø. FISCHER, K. RO-GACKI, AND B. BATLOGG
Single crystals of $LnFeAsO_{1-x}F_x$ ($Ln = La, Pr, Nd, Sm, Gd$) and $Ba_{1-x}Rb_xFe_2As_2$: Growth, structure and superconducting properties
Physica C **469**, 370 (2009).
Group(s): Batlogg, Fischer, Karpinski, Keller / Project(s): 4
- ▶ Z. BUKOWSKI, S. WEYENETH, R. PUZNIAK, P. MOLL, S. KATRYCH, N. D. ZHIGADLO, J. KARPINSKI, H. KELLER, AND B. BATLOGG
Superconductivity at 23 K and low anisotropy in Rb-substituted $BaFe_2As_2$ single crystals
Physical Review B **79**, 104521 (2009).
Group(s): Batlogg, Karpinski, Keller / Project(s): 4
- ▶ B. M. WOJEK, E. MORENZONI, D. G. ESHCHENKO, A. SUTER, T. PROKSCHA, E. KOLLER, E. TREBOUX, O. FISCHER, AND H. KELLER
Magnetism and superconductivity in cuprate heterostructures studied by low energy μ SR
Physica B **404**, 720 (2009).
Group(s): Fischer, Keller, Morenzoni / Project(s): 1, 4
- ▶ T. KONDO, R. KHASANOV, Y. SASSA, A. BENDOUNAN, S. PAILHES, J. CHANG, J. MESOT, H. KELLER, N. D. ZHIGADLO, M. SHI, Z. BUKOWSKI, J. KARPINSKI, AND A. KAMINSKI
Anomalous asymmetry in the Fermi surface of the high-temperature superconductor $YBa_2Cu_4O_8$ revealed by angle-resolved photoemission spectroscopy
Physical Review B **80**, 100505 (2009).
Group(s): Karpinski, Keller, Mesot / Project(s): 4
- ▶ A. MAISURADZE, R. KHASANOV, A. SHENGE-LAYA, AND H. KELLER
Comparison of different methods for analyzing μ SR line shapes in the vortex state of type-II superconductors
Journal of Physics: Condensed Matter **21**, 075701 (2009).
Group(s): Keller / Project(s): 4
- ▶ A. BUSSMANN-HOLDER AND H. KELLER
Evidence for Polaron Formation in High-Temperature Superconducting Cuprates: Experiments and Theory
Journal of Superconductivity and Novel Magnetism **22**, 123 (2009).
Group(s): Keller / Project(s): 4
- S. STRÄSSLE, R. KHASANOV, T. KONDO, D. O. G. HERON, A. KAMINSKI, H. KELLER, S. L. LEE, AND T. TAKEUCHI
Superfluid Density and Angular Dependence of the Energy Gap in Optimally Doped $(BiPb)_2(SrLa)_2CuO_{6+\delta}$
Journal of Superconductivity and Novel Magnetism **22**, 189 (2009).
Group(s): Keller / Project(s): 4
- ▶ A. BUSSMANN-HOLDER, A. SIMON, H. KELLER, AND A. R. BISHOP
Superconductivity in Fe and As Based Compounds: A Bridge Between MgB_2 and Cuprates
Journal of Superconductivity and Novel Magnetism **23**, 365 (2010).
Group(s): Keller / Project(s): 4
- ▶ A. MAISURADZE, A. SHENGE-LAYA, B. I. KOCHELAEV, E. POMJAKUSHINA, K. CONDER, H. KELLER, AND K. A. MÜLLER
Probing the Yb^{3+} spin relaxation in $Y_{0.98}Yb_{0.02}Ba_2Cu_3O_x$ by electron paramagnetic resonance
Physical Review B **79**, 054519 (2009).

Group(s): Keller / Project(s): 4

- ▶ R. KHASANOV, T. KONDO, S. STRÄSSLE, D. O. G. HERON, A. KAMINSKI, H. KELLER, S. L. LEE, AND T. TAKEUCHI
Zero-field superfluid density in a d-wave superconductor evaluated from muon-spin-rotation experiments in the vortex state

Physical Review B **79**, 180507(R) (2009).

Group(s): Keller / Project(s): 4

- ▶ F. LA MATTINA, J. G. BEDNORZ, S. F. ALVARADO, A. SHENGELAYA, K. A. MÜLLER, AND H. KELLER
Controlled oxygen vacancies and space correlation with Cr³⁺ in SrTiO₃

Physical Review B **80**, 075122 (2009).

Group(s): Keller / Project(s): 4

- ▶ H. KELLER AND A. BUSSMANN-HOLDER
Local Electron-Lattice Interactions in High-Temperature Cuprate Superconductors

Advances in Condensed Matter Physics **2010**, 393526 (2009).

Group(s): Keller / Project(s): 4

- P. S. HÄFLIGER, R. KHASANOV, R. LORTZ, A. PETROVIĆ, K. TOGANO, C. BAINES, B. GRANELL, AND H. KELLER
Muon-Spin Rotation Study of the Ternary Noncentrosymmetric Superconductors Li₂Pd_xPt_{3-x}B

Journal of Superconductivity and Novel Magnetism **22**, 337 (2009).

Group(s): Keller, Fischer / Project(s): 4

- ▶ R. KHASANOV, M. BENDELE, A. AMATO, P. BABKEVICH, A. T. BOOTHROYD, A. CERVELLINO, K. CONDER, S. N. GVASALIYA, H. KELLER, H.-H. KLAUSS, H. LUETKENS, V. POMJAKUSHIN, E. POMJAKUSHINA, AND B. ROESSLI
Coexistence of incommensurate magnetism and superconductivity in Fe_{1+y}Se_xTe_{1-x}

Physical Review B **80**, 140511(R) (2009).

Group(s): Keller, Kenzelmann / Project(s): 4, 5

Group of M. Kenzelmann

- ▶ R. KHASANOV, M. BENDELE, A. AMATO, P. BABKEVICH, A. T. BOOTHROYD, A. CERVELLINO, K. CONDER, S. N. GVASALIYA, H. KELLER, H.-H. KLAUSS, H. LUETKENS, V. POMJAKUSHIN, E. POMJAKUSHINA, AND B. ROESSLI
Coexistence of incommensurate magnetism and superconductivity in Fe_{1+y}Se_xTe_{1-x}

Physical Review B **80**, 140511(R) (2009).

Group(s): Keller, Kenzelmann / Project(s): 4, 5

M. SCHNEIDER, J. STAHN, AND P. BÖNI

Focusing of cold neutrons: Performance of a laterally graded and parabolically bent multilayer

Nuclear Instruments and Methods in Physics Research A **610**, 530 (2009).

Group(s): Kenzelmann / Project(s): 3

E. POMJAKUSHINA, K. CONDER, V. POMJAKUSHIN, M. BENDELE, AND R. KHASANOV
Synthesis, crystal structure, and chemical stability of the superconductor FeSe_{1-x}

Physical Review B **80**, 024517 (2009).

Group(s): Kenzelmann / Project(s): 4, 5

C. SCHANZER, P. BÖNI, AND M. SCHNEIDER
High Performance Supermirrors on Metallic Substrates

to be published in Journal of Physics: Conference Series (2010).

Group(s): Kenzelmann / Project(s): 3

Group of D. van de Marel

A. UBALDINI, E. GIANNINI, C. SENATORE, AND D. VAN DER MAREL

BiOCuS: A new superconducting compound with oxyaptnictide-related structure

Physica C (2010), doi:10.1016/j.physc.2009.11.164.

Group(s): Flükiger, Giannini, van der Marel / Project(s): 4

R. VIENNOIS, E. GIANNINI, J. TEYSSIER, J. ELIA, J. DEISENHOFER, AND D. VAN DER MAREL

Two-dimensional orbital ordering in d¹ Mott insulator Sr₂VO₄

Journal of Physics: Conference Series **200**, 012219 (2010).

Group(s): Giannini, van der Marel / Project(s): 4

J. TEYSSIER, R. VIENNOIS, V. GURITANU, E. GIANNINI, AND D. VAN DER MAREL

Kondo effect and quantum critical point in Mn_(1-x)Co_xSi

Journal of Physics: Conference Series **200**, 032076 (2010).

Group(s): Giannini, van der Marel / Project(s): 5

R. VIENNOIS, E. GIANNINI, D. VAN DER MAREL, AND R. ČERNÝ

Effect of Fe excess on Structural, Magnetic and Superconducting Properties of Single-Crystalline Fe_{1+x}Te_{1-y}Se_y

Journal of Solid State Chemistry (2010), doi:10.1016/j.jssc.2010.01.024.

Group(s): Giannini, van der Marel / Project(s): 4

R. VIENNOIS, E. GIANNINI, D. VAN DER MAREL, AND R. ČERNÝ

- Phase diagram of single-crystalline tetragonal iron chalcogenides*
 Physica C (2010), doi:10.1016/j.physc.2009.11.126.
 Group(s): Giannini, van der Marel / Project(s): 4
- I. PALLECCHI, G. LAMURA, M. TROPEANO, M. PUTTI, R. VIENNOIS, E. GIANNINI, AND D. VAN DER MAREL
Seebeck effect in $Fe_{1+x}Te_{1-y}Se_y$ single crystals
 Physical Review B **80**, 214511 (2009).
 Group(s): Giannini, van der Marel / Project(s): 4
- H. J. A. MOLEGRAAF, J. HOFFMAN, C. A. F. VAZ, S. GARIGLIO, D. VAN DER MAREL, C. H. AHN, AND J. M. TRISCONI
Magnetoelectric Effects in Complex Oxides with Competing Ground States
 Advanced Materials **21**, 3470 (2009).
 Group(s): Triscone (JM), van der Marel / Project(s): 1
- E. VAN HEUMEN, A. B. KUZMENKO, AND D. VAN DER MAREL
Optics clues to pairing glues in high T_c cuprates
 Journal of Physics: Conference Series **150**, 052278 (2009).
 Group(s): van der Marel / Project(s): 4
- W. MEEVASANA, X. J. ZHOU, B. MORITZ, C.-C. CHEN, R. H. HE, S.-I. FUJIMORI, D. H. LU, S.-K. MO, R. G. MOORE, F. BAUMBERGER, T. P. DEVEREAUX, D. VAN DER MAREL, N. NAGAOSA, J. ZAAANEN, AND Z.-X. SHEN
Strong energy-momentum dispersion of phonon-dressed carriers in the lightly doped band insulator $SrTiO_3$
 New Journal of Physics **12**, 023004 (2010).
 Group(s): van der Marel / Project(s): 4
- J. N. HANCOCK, G. CHABOT-COUTURE, AND M. GREVEN
Lattice coupling and Franck-Condon effects in K-edge resonant inelastic x-ray scattering
 New Journal of Physics **12**, 033001 (2010).
 Group(s): van der Marel / Project(s): 5
- E. VAN HEUMEN, W. MEEVASANA, A. B. KUZMENKO, H. EISAKI, AND D. VAN DER MAREL
Doping-dependent optical properties of $Bi2201$
 New Journal of Physics **11**, 055067 (2009).
 Group(s): van der Marel / Project(s): 4
- ▶ A. B. KUZMENKO, E. VAN HEUMEN, D. VAN DER MAREL, P. LERCH, P. BLAKE, K. S. NOVOSELOV, AND A. K. GEIM
Infrared spectroscopy of electronic bands in bilayer graphene
 Physical Review B **79**, 115441 (2009).
 Group(s): van der Marel / Project(s): 2
- ▶ A. B. KUZMENKO, I. CRASSEE, D. VAN DER MAREL, P. BLAKE, AND K. S. NOVOSELOV
Determination of the gate-tunable band gap and tight-binding parameters in bilayer graphene using infrared spectroscopy
 Physical Review B **80**, 165406 (2009).
 Group(s): van der Marel / Project(s): 2
- E. VAN HEUMEN, E. MUHLEHALER, A. B. KUZMENKO, H. EISAKI, W. MEEVASANA, M. GREVEN, AND D. VAN DER MAREL
Optical determination of the relation between the electron-boson coupling function and the critical temperature in high- T_c cuprates
 Physical Review B **79**, 184512 (2009).
 Group(s): van der Marel / Project(s): 4
- ▶ R. TEDIOSI, F. CARBONE, A. B. KUZMENKO, J. TEYSSIER, D. VAN DER MAREL, AND J. A. MYDOSH
Evidence for strongly coupled charge-density-wave ordering in three-dimensional $R_5Ir_4Si_{10}$ compounds from optical measurements
 Physical Review B **80**, 035107 (2009).
 Group(s): van der Marel / Project(s): 5
- ▶ A. B. KUZMENKO, L. BENFATTO, E. CAPPELLUTI, I. CRASSEE, D. VAN DER MAREL, P. BLAKE, K. S. NOVOSELOV, AND A. K. GEIM
Gate Tunable Infrared Phonon Anomalies in Bilayer Graphene
 Physical Review Letters **103**, 116804 (2009).
 Group(s): van der Marel / Project(s): 2
- J. T. DEVREESE, S. N. KLIMIN, J. L. M. VAN MECHELEN, AND D. VAN DER MAREL
Many-body large polaron optical conductivity in $SrTi_{1-x}Nb_xO_3$
 Physical Review B **81**, 125119 (2010).
 Group(s): van der Marel / Project(s): 4
- Group of J. Mesot**
- ▶ A. SACCHETTI, C. L. CONDRON, S. N. GVASALIYA, F. PFUNER, M. LAVAGNINI, M. BALDINI, M. F. TONEY, M. MERLINI, M. HANFLAND, J. MESOT, J.-H. CHU, I. R. FISHER, P. POSTORINO, AND L. DEGIORGI
Pressure-induced quenching of the charge-density-wave state in rare-earth tritellurides observed by x-ray diffraction
 Physical Review B **79**, 201101(R) (2009).
 Group(s): Degiorgi, Mesot / Project(s): 7
- M. MEDARDE, C. DALLERA, M. GRIONI, B. DELLEY, F. VERNAY, J. MESOT, M. SIKORA,

J. A. ALONSO, AND M. J. MARTÍNEZ-LOPE
Charge disproportionation in RNiO₃ perovskites (R = rare earth) from high-resolution x-ray absorption spectroscopy

Physical Review B **80**, 245105 (2009).

Group(s): Grioni, Mesot / Project(s): 7

- ▶ T. KONDO, R. KHASANOV, Y. SASSA, A. BENDOUNAN, S. PAILHES, J. CHANG, J. MESOT, H. KELLER, N. D. ZHIGADLO, M. SHI, Z. BUKOWSKI, J. KARPINSKI, AND A. KAMINSKI

Anomalous asymmetry in the Fermi surface of the high-temperature superconductor YBa₂Cu₄O₈ revealed by angle-resolved photoemission spectroscopy

Physical Review B **80**, 100505 (2009).

Group(s): Karpinski, Keller, Mesot / Project(s): 4

- ▶ M. SHI, A. BENDOUNAN, E. RAZZOLI, S. ROSENKRANZ, M. R. NORMAN, J. C. CAMPUZANO, J. CHANG, M. MÅNSSON, Y. SASSA, T. CLAESSION, O. TJERNBERG, L. PATTHEY, N. MOMONO, M. ODA, M. IDO, S. GUERRERO, C. MUDRY, AND J. MESOT

Spectroscopic evidence for preformed Cooper pairs in the pseudogap phase of cuprates

Europhysics Letters **88**, 27008 (2009).

Group(s): Mesot / Project(s): 4

- ▶ U. CHATTERJEE, M. SHI, D. AI, J. ZHAO, A. KANIGEL, S. ROSENKRANZ, H. RAFFY, Z. Z. LI, K. KADOWAKI, D. G. HINKS, Z. J. XU, J. S. WEN, G. GU, C. T. LIN, H. CLAUS, M. R. NORMAN, M. RANDEIRA, AND J. C. CAMPUZANO

Observation of a d-wave nodal liquid in highly underdoped Bi₂Sr₂CaCu₂O_{8-δ}

Nature Physics **6**, 99 (2010).

Group(s): Mesot / Project(s): 4

T. CLAESSION, M. MÅNSSON, A. ÖNSTEN, M. SHI, Y. SASSA, S. PAILHÉS, J. CHANG, A. BENDOUNAN, L. PATTHEY, J. MESOT, T. MURO, T. MATSUSHITA, T. KINOSHITA, T. NAKAMURA, N. MOMONO, M. ODA, M. IDO, AND O. TJERNBERG

Electronic structure of La_{1.48}Nd_{0.4}Sr_{0.12}CuO₄ probed by high- and low-energy angle-resolved photoelectron spectroscopy

Physical Review B **80**, 094503 (2009).

Group(s): Mesot / Project(s): 4

- ▶ D. HAUG, V. HINKOV, A. SUCHANECK, D. S. INOSOV, N. B. CHRISTENSEN, C. NIEDERMAYER, P. BOURGES, Y. SIDIS, J. T. PARK, A. IVANOV, C. T. LIN, J. MESOT, AND B. KEIMER

Magnetic-Field-Enhanced Incommensurate Magnetic Order in the Underdoped High-Temperature Superconductor YBa₂Cu₃O_{6.45}

Physical Review Letters **103**, 017001 (2009).

Group(s): Mesot, Niedermayer / Project(s): 4

- ▶ J. CHANG, N. B. CHRISTENSEN, C. NIEDERMAYER, K. LEFMANN, H. M. RØNNOW, D. F. MCMORROW, A. SCHNEIDEWIND, P. LINK, A. HIESS, M. BOEHM, R. MOTTI, S. PAILHÉS, N. MOMONO, M. ODA, M. IDO, AND J. MESOT

Magnetic-Field-Induced Soft-Mode Quantum Phase Transition in the High-Temperature Superconductor La_{1.855}Sr_{0.145}CuO₄: An Inelastic Neutron-Scattering Study

Physical Review Letters **102**, 177006 (2009).

Group(s): Mesot, Niedermayer, Rønnow / Project(s): 4, 6

- ▶ J. SCHLAPPA, T. SCHMITT, F. VERNAY, V. N. STROCOV, V. ILAKOVAC, B. THIELEMANN, H. M. RØNNOW, S. VANISHRI, A. PIAZZALUNGA, X. WANG, L. BRAICOVICH, G. GHIRINGHELLI, C. MARIN, J. MESOT, B. DELLEY, AND L. PATTHEY

Collective Magnetic Excitations in the Spin Ladder Sr₁₄Cu₂₄O₄₁ Measured Using High-Resolution Resonant Inelastic X-Ray Scattering

Physical Review Letters **103**, 047401 (2009).

Group(s): Mesot, Rønnow / Project(s): 6

- ▶ B. THIELEMANN, C. RÜEGG, H. M. RØNNOW, A. M. LÄUCHLI, J.-S. CAUX, B. NORMAND, D. BINER, K. W. KRÄMER, H.-U. GÜDEL, J. STAHN, K. HABICHT, K. KIEFER, M. BOEHM, D. F. MCMORROW, AND J. MESOT

Direct Observation of Magnon Fractionalization in the Quantum Spin Ladder

Physical Review Letters **102**, 107204 (2009).

Group(s): Mesot, Rønnow / Project(s): 6

Group of F. Mila

V. LANTE, I. ROUSOCHATZAKIS, K. PENC, O. WALDMANN, AND F. MILA

Spin-Peierls instabilities of antiferromagnetic rings in a magnetic field

Physical Review B **79**, 180412(R) (2009).

Group(s): Mila / Project(s): 6

- ▶ I. ROUSOCHATZAKIS, S. R. MANMANA, A. M. LÄUCHLI, B. NORMAND, AND F. MILA

Dzyaloshinskii-Moriya anisotropy and non-magnetic impurities in the $s = \frac{1}{2}$ kagome system ZnCu₃(OH)₆Cl₂

Physical Review B **79**, 214415 (2009).

Group(s): Mila / Project(s): 6

- S. CAPPONI, D. POILBLANC, AND F. MILA
Theory of the Raman spectra of the Shastry-Sutherland antiferromagnet $\text{SrCu}_2(\text{BO}_3)_2$ doped with nonmagnetic impurities
Physical Review B **80**, 094407 (2009).
Group(s): Mila / Project(s): 6
- F. MICHAUD, T. COLETTA, S. R. MANMANA, J.-D. PICON, AND F. MILA
Frustration-induced plateaus in $S \geq \frac{1}{2}$ Heisenberg spin ladders
Physical Review B **81**, 014407 (2010).
Group(s): Mila / Project(s): 6
- N. LAFLORENCIE AND F. MILA
Theory of the Field-Induced BEC in the Frustrated Spin- $\frac{1}{2}$ Dimer Compound $\text{BaCuSi}_2\text{O}_6$
Physical Review Letters **102**, 060602 (2009).
Group(s): Mila / Project(s): 6
- Group of E. Morenzoni**
- B. M. WOJEK, E. MORENZONI, D. G. ESHCHENKO, A. SUTER, T. PROKSCHA, E. KOLLER, E. TREBOUX, O. FISCHER, AND H. KELLER
Magnetism and superconductivity in cuprate heterostructures studied by low energy μSR
Physica B **404**, 720 (2009).
Group(s): Fischer, Keller, Morenzoni / Project(s): 1, 4
- E. MORENZONI
A (closer) look below surfaces and at heterostructures with polarized muons
Physica B **404**, 577 (2009).
Group(s): Morenzoni / Project(s): 1
- D. G. ESHCHENKO, V. G. STORCHAK, E. MORENZONI, T. PROKSCHA, A. SUTER, X. LIU, AND J. K. FURDYNA
Low energy μSR studies of semiconductor interfaces
Physica B **404**, 873 (2009).
Group(s): Morenzoni / Project(s): 1
- V. G. STORCHAK, O. E. PARFENOV, J. H. BREWER, P. L. RUSSO, S. L. STUBBS, R. L. LICHTI, D. G. ESHCHENKO, E. MORENZONI, S. P. COTTRELL, J. S. LORD, T. G. AMINOV, V. P. ZLOMANOV, A. A. VINOKUROV, R. L. KALLAHER, AND S. VON MOLNÁR
Electron localization into magnetic polaron in EuS
Physica B **404**, 896 (2009).
Group(s): Morenzoni / Project(s): 1
- V. G. STORCHAK, O. E. PARFENOV, J. H. BREWER, P. L. RUSSO, S. L. STUBBS, R. L. LICHTI, D. G. ESHCHENKO, E. MORENZONI, V. P. ZLOMANOV, A. A. VINOKUROV, AND V. G. BAMBUIROV
Novel muonium centers—magnetic polarons—in magnetic semiconductors
Physica B **404**, 899 (2009).
Group(s): Morenzoni / Project(s): 1
- D. G. ESHCHENKO, V. G. STORCHAK, E. MORENZONI, AND D. ANDREICA
High-pressure muon spin rotation studies of magnetic semiconductors: EuS
Physica B **404**, 903 (2009).
Group(s): Morenzoni / Project(s): 1
- V. G. STORCHAK, J. H. BREWER, D. J. ARSENEAU, S. L. STUBBS, O. E. PARFENOV, D. G. ESHCHENKO, E. MORENZONI, AND T. G. AMINOV
Magnetic polaron bound to the positive muon in SmS: Exchange-driven formation of a mixed-valence state
Physical Review B **79**, 193205 (2009).
Group(s): Morenzoni / Project(s): 1
- M. SHAY, A. KEREN, G. KOREN, A. KANIGEL, O. SHAFIR, L. MARCIPAR, G. NIEUWENHUIS, E. MORENZONI, A. SUTER, T. PROKSCHA, M. DUBMAN, AND D. PODOLSKY
Interaction between the magnetic and superconducting order parameters in a $\text{La}_{1.94}\text{Sr}_{0.06}\text{CuO}_4$ wire studied via muon spin rotation
Physical Review B **80**, 144511 (2009).
Group(s): Morenzoni / Project(s): 1
- V. G. STORCHAK, O. E. PARFENOV, J. H. BREWER, P. L. RUSSO, S. L. STUBBS, R. L. LICHTI, D. G. ESHCHENKO, E. MORENZONI, T. G. AMINOV, V. P. ZLOMANOV, A. A. VINOKUROV, R. L. KALLAHER, AND S. VON MOLNÁR
Direct observation of the magnetic polaron
Physical Review B **80**, 235203 (2009).
Group(s): Morenzoni / Project(s): 1
- D. G. ESHCHENKO, V. G. STORCHAK, S. P. COTTRELL, AND E. MORENZONI
Electric-Field-Enhanced Neutralization of Deep Centers in GaAs
Physical Review Letters **103**, 216601 (2009).
Group(s): Morenzoni / Project(s): 1
- Group of A. Morpurgo**
- T. KAJI, T. TAKENOBU, A. F. MORPURGO, AND Y. IWASA
Organic Single-Crystal Schottky Gate Transistors

- Advanced Materials **21**, 3689 (2009).
Group(s): Morpurgo / Project(s): 2
- S. RUSSO, M. F. CRACIUN, M. YAMAMOTO, S. TARUCHA, AND A. F. MORPURGO
Double-gated graphene-based devices
New Journal of Physics **11**, 095018 (2009).
Group(s): Morpurgo / Project(s): 2
- ▶ H. XIE, H. ALVES, AND A. F. MORPURGO
Quantitative analysis of density-dependent transport in tetramethyltetraselenafulvalene single-crystal transistors: Intrinsic properties and trapping
Physical Review B **80**, 245305 (2009).
Group(s): Morpurgo / Project(s): 2
- X. LIU, J. B. OOSTINGA, A. F. MORPURGO, AND L. M. K. VANDERSYPEN
Electrostatic confinement of electrons in graphene nanoribbons
Physical Review B **80**, 121407 (2009).
Group(s): Morpurgo / Project(s): 2
- ▶ I. GUTIÉRREZ LEZAMA AND A. F. MORPURGO
Threshold Voltage and Space Charge in Organic Transistors
Physical Review Letters **103**, 066803 (2009).
Group(s): Morpurgo / Project(s): 2
- R. DANNEAU, F. WU, M. F. CRACIUN, S. RUSSO, M. Y. TOMI, J. SALMILEHTO, A. F. MORPURGO, AND P. J. HAKONEN
Shot noise measurements in graphene
Solid State Communications **149**, 1050 (2009).
Group(s): Morpurgo / Project(s): 2
- ▶ M. F. CRACIUN, S. RUSSO, M. YAMAMOTO, J. B. OOSTINGA, A. F. MORPURGO, AND S. TARUCHA
Trilayer graphene is a semimetal with a gate-tunable band overlap
Nature Nanotechnology **4**, 383 (2009).
Group(s): Morpurgo / Project(s): 2
- Group of Ch. Niedermayer**
- ▶ J. HOPPLER, J. STAHN, C. NIEDERMAYER, V. K. MALIK, H. BOUYANFIF, A. J. DREW, M. RÖSSLE, A. BUZDIN, G. CRISTIANI, H.-U. HABERMEIER, B. KEIMER, AND C. BERNHARD
Giant superconductivity-induced modulation of the ferromagnetic magnetization in a cuprate-manganite superlattice
Nature Materials **8**, 315 (2009).
Group(s): Bernhard, Niedermayer / Project(s): 1
- ▶ A. J. DREW, C. NIEDERMAYER, P. J. BAKER, F. L. PRATT, S. J. BLUNDELL, T. LANCASTER, R. H. LIU, G. WU, X. H. CHEN, I. WATANABE, V. K. MALIK, A. DUBROKA, M. RÖSSLE, K. W. KIM, C. BAINES, AND C. BERNHARD
Coexistence of static magnetism and superconductivity in $\text{SmFeAsO}_{1-x}\text{F}_x$ as revealed by muon spin rotation
Nature Materials **8**, 310 (2009).
Group(s): Bernhard, Niedermayer / Project(s): 4
- C. BERNHARD, A. J. DREW, L. SCHULZ, V. K. MALIK, M. RÖSSLE, C. NIEDERMAYER, T. WOLF, G. D. VARMA, G. MU, H.-H. WEN, G. WU, AND X. H. CHEN
Muon spin rotation study of magnetism and superconductivity in $\text{BaFe}_{2-x}\text{Co}_x\text{As}_2$ and $\text{Pr}_{1-x}\text{Sr}_x\text{FeAsO}$
New Journal of Physics **11**, 055050 (2009).
Group(s): Bernhard, Niedermayer / Project(s): 4
- J. STAHN, C. NIEDERMAYER, J. HOPPLER, AND C. BERNHARD
PNR studies of proximity and coupling effects in $\text{YBa}_2\text{Cu}_3\text{O}_7/\text{La}_{2/3}\text{Ca}_{1/3}\text{MnO}_3$ superlattices
Neutron News **20**, 13 (2009).
Group(s): Bernhard, Niedermayer / Project(s): 1
- ▶ D. HAUG, V. HINKOV, A. SUCHANECK, D. S. INOSOV, N. B. CHRISTENSEN, C. NIEDERMAYER, P. BOURGES, Y. SIDIS, J. T. PARK, A. IVANOV, C. T. LIN, J. MESOT, AND B. KEIMER
Magnetic-Field-Enhanced Incommensurate Magnetic Order in the Underdoped High-Temperature Superconductor $\text{YBa}_2\text{Cu}_3\text{O}_{6.45}$
Physical Review Letters **103**, 017001 (2009).
Group(s): Mesot, Niedermayer / Project(s): 4
- ▶ J. CHANG, N. B. CHRISTENSEN, C. NIEDERMAYER, K. LEFMANN, H. M. RÖNNOW, D. F. MCMORROW, A. SCHNEIDEWIND, P. LINK, A. HIESS, M. BOEHM, R. MOTTI, S. PAILHÉS, N. MOMONO, M. ODA, M. IDO, AND J. MESOT
Magnetic-Field-Induced Soft-Mode Quantum Phase Transition in the High-Temperature Superconductor $\text{La}_{1.855}\text{Sr}_{0.145}\text{CuO}_4$: An Inelastic Neutron-Scattering Study
Physical Review Letters **102**, 177006 (2009).
Group(s): Mesot, Niedermayer, Rønnow / Project(s): 4, 6
- L. UDBY, N. H. ANDERSEN, F. C. CHOU, N. B. CHRISTENSEN, S. B. EMERY, K. LEFMANN, J. W. LYNN, H. E. MOHOTTALA, C. NIEDERMAYER, AND B. O. WELLS
Magnetic ordering in electronically phase-separated $\text{La}_{2-x}\text{Sr}_x\text{CuO}_{4+y}$: Neutron diffraction experiments
Physical Review B **80**, 014505 (2009).
Group(s): Niedermayer / Project(s): 4

D. S. INOSOV, A. LEINWEBER, X. YANG, J. T. PARK, N. B. CHRISTENSEN, R. DINNEBIER, G. L. SUN, C. NIEDERMAYER, D. HAUG, P. W. STEPHENS, J. STAHN, O. KHVOSTIKOVA, C. T. LIN, O. K. ANDERSEN, B. KEIMER, AND V. HINKOV

Suppression of the structural phase transition and lattice softening in slightly underdoped $Ba_{1-x}K_xFe_2As_2$ with electronic phase separation

Physical Review B **79**, 224503 (2009).

Group(s): Niedermayer / Project(s): 4

- ▶ R. KHASANOV, D. V. EVTUSHINSKY, A. AMATO, H.-H. KLAUSS, H. LUETKENS, C. NIEDERMAYER, B. BÜCHNER, G. L. SUN, C. T. LIN, J. T. PARK, D. S. INOSOV, AND V. HINKOV

Two-Gap Superconductivity in $Ba_{1-x}K_xFe_2As_2$: A Complementary Study of the Magnetic Penetration Depth by Muon-Spin Rotation and Angle-Resolved Photoemission

Physical Review Letters **102**, 187005 (2009).

Group(s): Niedermayer / Project(s): 4

- ▶ J. T. PARK, D. S. INOSOV, C. NIEDERMAYER, G. L. SUN, D. HAUG, N. B. CHRISTENSEN, R. DINNEBIER, A. V. BORIS, A. J. DREW, L. SCHULZ, T. SHAPOVAL, U. WOLFF, V. NEU, X. YANG, C. T. LIN, B. KEIMER, AND V. HINKOV

Electronic Phase Separation in the Slightly Underdoped Iron Pnictide Superconductor $Ba_{1-x}K_xFe_2As_2$

Physical Review Letters **102**, 117006 (2009).

Group(s): Niedermayer / Project(s): 4

Group of H.-R. Ott

Z. FISK, H.-R. OTT, AND J. D. THOMPSON
Superconducting materials: What the record tells us

Philosophical Magazine **89**, 2111 (2009).

Group(s): Ott / Project(s): 6

Group of P. Paruch

- ▶ N. DIX, R. MURALIDHARAN, J. GUYONNET, B. WAROT-FONROSE, M. VARELA, P. PARUCH, F. SÁNCHEZ, AND J. FONTCUBERTA
On the strain coupling across vertical interfaces of switchable $BiFeO_3$ - $CoFe_2O_4$ multiferroic nanostructures

Applied Physics Letters **95**, 062907 (2009).

Group(s): Paruch / Project(s): 1

H. BÉA AND P. PARUCH
Multiferroics: A way forward along domain walls

Nature Materials **8**, 168 (2009).

Group(s): Paruch / Project(s): 1

- ▶ J. GUYONNET, H. BÉA, AND P. PARUCH
Lateral piezoelectric response across ferroelectric domain walls in thin films to be published in Journal of Applied Physics (2010).

Group(s): Paruch / Project(s): 1

- ▶ J. GUYONNET, H. BÉA, F. GUY, S. GARIGLIO, S. FUSIL, K. BOUZEHOANE, J.-M. TRISCONE, AND P. PARUCH

Shear effects in lateral piezoresponse force microscopy at 180° ferroelectric domain walls

Applied Physics Letters **95**, 132902 (2009).

Group(s): Paruch, Triscone (JM) / Project(s): 1

Group of G. Patzke

B. SIPOS, M. DUCHAMP, A. MAGREZ, L. FORRÓ, N. BARIŠIĆ, A. KIS, J. W. SEO, F. BIERI, F. KRUMEICH, R. NESPER, AND G. R. PATZKE

Mechanical and electronic properties of vanadium oxide nanotubes

Journal of Applied Physics **105**, 074317 (2009).

Group(s): Forró, Patzke / Project(s): 7, 3

- ▶ Y. ZHOU, K. VUILLE, A. HEEL, AND G. R. PATZKE
Studies on Nanostructured Bi_2WO_6 : Convenient Hydrothermal and TiO_2 -Coating Pathways

Zeitschrift für Anorganische und Allgemeine Chemie **635**, 1848 (2009).

Group(s): Patzke / Project(s): 3

Y. ZHOU, K. VUILLE, A. HEEL, B. PROBST, R. KONTIC, AND G. R. PATZKE
An inorganic hydrothermal route to photocatalytically active bismuth vanadate

Applied Catalysis A **375**, 140 (2010).

Group(s): Patzke / Project(s): 3

- ▶ Y. ZHOU, N. PIENACK, W. BENSCH, AND G. R. PATZKE
The Interplay of Crystallization Kinetics and Morphology in Nanostructured W/Mo Oxide Formation: An in situ Diffraction Study

Small **5**, 1978 (2009).

Group(s): Patzke / Project(s): 3

Group of Ch. Renner

J. H. G. OWEN
Competing interactions in molecular adsorption: NH_3 on $Si(001)$

Journal of Physics: Condensed Matter **21**, 443001 (2009).

Group(s): Renner / Project(s): 7

J. H. G. OWEN AND D. R. BOWLER

The origin of inter-dimer-row correlated adsorption for NH₃ on Si(001)

Surface Science **603**, 2902 (2009).

Group(s): Renner / Project(s): 7

Group of T. M. Rice

K. Y. YANG, H. B. YANG, P. D. JOHNSON, T. M. RICE, AND F. C. ZHANG

Quasiparticles in the pseudogap phase of underdoped cuprate

Europhysics Letters **86**, 37002 (2009).

Group(s): Rice, Sigrist / Project(s): 4

K. Y. YANG, W. Q. CHEN, T. M. RICE, M. SIGRIST, AND F. C. ZHANG

Nature of stripes in the generalized $t - J$ model applied to the cuprate superconductors

New Journal of Physics **11**, 055053 (2009).

Group(s): Rice, Sigrist / Project(s): 4, 5

▶ K. Y. YANG, W. Q. CHEN, T. M. RICE, AND F. C. ZHANG

Origin of the checkerboard pattern in scanning tunneling microscopy maps of underdoped cuprate superconductors

Physical Review B **80**, 174505 (2009).

Group(s): Rice, Sigrist / Project(s): 4

Group of N. de Rooij

D. ISARAKORN, A. SAMBRI, P. JANPHUANG, D. BRIAND, S. GARIGLIO, J.-M. TRISCONI, F. GUY, J. W. REINER, C. H. AHN, AND N. F. DE ROOIJ

Epitaxial piezoelectric MEMS on silicon

to be published in Journal of Micromechanics and Microengineering (2010).

Group(s): de Rooij, Triscone (JM) / Project(s): 1

Group of H. M. Rønnow

M. LE TACON, T. R. FORREST, C. RÜEGG, A. BOSAK, A. C. WALTERS, R. MITTAL, H. M. RØNNOW, N. D. ZHIGADLO, S. KATRYCH, J. KARPINSKI, J. P. HILL, M. KRISCH, AND D. F. MCMORROW

Inelastic x-ray scattering study of superconducting SmFeAsO_{1-x}F_y single crystals: Evidence for strong momentum-dependent doping-induced renormalizations of optical phonons

Physical Review B **80**, 220504 (2009).

Group(s): Karpinski, Rønnow / Project(s): 4, 6

▶ J. CHANG, N. B. CHRISTENSEN, C. NIEDERMAYER, K. LEFMAN, H. M. RØNNOW, D. F. MCMORROW, A. SCHNEIDEWIND, P. LINK, A. HIESS, M. BOEHM, R. MOTTL, S. PAILHÉS, N. MOMONO, M. ODA, M. IDO, AND J. MESOT

Magnetic-Field-Induced Soft-Mode Quantum Phase Transition in the High-Temperature Superconductor La_{1.855}Sr_{0.145}CuO₄: An Inelastic Neutron-Scattering Study

Physical Review Letters **102**, 177006 (2009).

Group(s): Mesot, Niedermayer, Rønnow / Project(s): 4, 6

▶ J. SCHLAPPA, T. SCHMITT, F. VERNAY, V. N. STROCOV, V. ILAKOVAC, B. THIELEMANN, H. M. RØNNOW, S. VANISHRI, A. PIAZZALUNGA, X. WANG, L. BRAICOVICH, G. GHIRINGHELLI, C. MARIN, J. MESOT, B. DELLEY, AND L. PATTHEY

Collective Magnetic Excitations in the Spin Ladder Sr₁₄Cu₂₄O₄₁ Measured Using High-Resolution Resonant Inelastic X-Ray Scattering

Physical Review Letters **103**, 047401 (2009).

Group(s): Mesot, Rønnow / Project(s): 6

▶ B. THIELEMANN, C. RÜEGG, H. M. RØNNOW, A. M. LÄUCHLI, J.-S. CAUX, B. NORMAND, D. BINER, K. W. KRÄMER, H.-U. GÜDEL, J. STAHN, K. HABICHT, K. KIEFER, M. BOEHM, D. F. MCMORROW, AND J. MESOT

Direct Observation of Magnon Fractionalization in the Quantum Spin Ladder

Physical Review Letters **102**, 107204 (2009).

Group(s): Mesot, Rønnow / Project(s): 6

Group of M. Sigrist

K. Y. YANG, H. B. YANG, P. D. JOHNSON, T. M. RICE, AND F. C. ZHANG

Quasiparticles in the pseudogap phase of underdoped cuprate

Europhysics Letters **86**, 37002 (2009).

Group(s): Rice, Sigrist / Project(s): 4

K. Y. YANG, W. Q. CHEN, T. M. RICE, M. SIGRIST, AND F. C. ZHANG

Nature of stripes in the generalized $t - J$ model applied to the cuprate superconductors

New Journal of Physics **11**, 055053 (2009).

Group(s): Rice, Sigrist / Project(s): 4, 5

▶ K. Y. YANG, W. Q. CHEN, T. M. RICE, AND F. C. ZHANG

Origin of the checkerboard pattern in scanning tunneling microscopy maps of underdoped cuprate superconductors

Physical Review B **80**, 174505 (2009).

Group(s): Rice, Sigrist / Project(s): 4

- P. M. R. BRYDON, C. INIOTAKIS, D. MANSKE, AND M. SIGRIST
Consequences of Broken Time-Reversal Symmetry in Triplet Josephson Junctions
Journal of Physics: Conference Series **150**, 052026 (2009).
Group(s): Sigris / Project(s): 4
- Y. YANASE AND M. SIGRIST
Antiferromagnetic order in the FFLO state
Journal of Physics: Conference Series **150**, 052287 (2009).
Group(s): Sigris / Project(s): 5
- ▶ Y. YANASE AND M. SIGRIST
Antiferromagnetic Order and π -triplet Pairing in the Fulde-Ferrel-Larkin-Ovchinnikov State
Journal of the Physical Society of Japan **78**, 114715 (2009).
Group(s): Sigris / Project(s): 5
- K. WAKABAYASHI, Y. TAKANE, M. YAMAMOTO, AND M. SIGRIST
Electronic transport properties of graphene nanoribbons
New Journal of Physics **11**, 095016 (2009).
Group(s): Sigris / Project(s): 2
- C. F. MICLEA, A. C. MOTA, M. SIGRIST, F. STEGLICH, T. A. SAYLES, B. J. TAYLOR, C. A. MCÉLROY, AND M. B. MAPLE
Vortex avalanches in the noncentrosymmetric superconductor $\text{Li}_2\text{Pt}_3\text{B}$
Physical Review B **80**, 132502 (2009).
Group(s): Sigris / Project(s): 5
- H. ADACHI AND M. SIGRIST
Probing the $d_{x^2-y^2}$ -wave Pomeranchuk instability by ultrasound
Physical Review B **80**, 155123 (2009).
Group(s): Sigris / Project(s): 5
- C. F. MICLEA, A. C. MOTA, M. NICKLAS, R. CARDOSO, F. STEGLICH, M. SIGRIST, A. PROKOFIEV, AND E. BAUER
Extreme vortex pinning in the noncentrosymmetric superconductor CePt_3Si
Physical Review B **81**, 014527 (2010).
Group(s): Sigris / Project(s): 5
- ▶ M. H. FISCHER AND M. SIGRIST
Effect of a staggered spin-orbit coupling on the occurrence of a nematic phase in $\text{Sr}_3\text{Ru}_2\text{O}_7$
Physical Review B **81**, 064435 (2010).
Group(s): Sigris / Project(s): 5
- ▶ D. F. AGTERBERG, M. SIGRIST, AND H. TSUNETSUGU
Order Parameter and Vortices in the Superconducting Q Phase of CeCoIn_5
Physical Review Letters **102**, 207004 (2009).
Group(s): Sigris / Project(s): 5
- A. RÜEGG AND M. SIGRIST
Role of Multiple Subband Renormalization in the Electronic Transport of Correlated Oxide Superlattices
in *Properties and Applications of Thermoelectric Materials - The Search for New Materials for Thermoelectric Devices*, V. ZLATIC AND A. C. HEWSON, eds. (Springer, Dordrecht, 2009), NATO Science for Peace and Security Series B: Physics and Biophysics, p. 181.
Group(s): Sigris / Project(s): 1
- Group of U. Staub**
- ▶ U. STAUB, Y. BODENTHIN, C. PIAMONTEZE, M. GARCÍA-FERNÁNDEZ, V. SCAGNOLI, M. GARGANOURAKIS, S. KOOHPAYEH, D. FORT, AND S. W. LOVESEY
Parity- and time-odd atomic multipoles in magnetoelectric GaFeO_3 as seen via soft x-ray Bragg diffraction
Physical Review B **80**, 140410 (2009).
Group(s): Staub / Project(s): 6
- ▶ U. STAUB, M. GARCÍA-FERNÁNDEZ, Y. BODENTHIN, V. SCAGNOLI, R. A. DE SOUZA, M. GARGANOURAKIS, E. POMJAKUSHINA, AND K. CONDER
Orbital and magnetic ordering in $\text{Pr}_{1-x}\text{Ca}_x\text{MnO}_3$ and $\text{Nd}_{1-x}\text{Sr}_x\text{MnO}_3$ manganites near half doping studied by resonant soft x-ray powder diffraction
Physical Review B **79**, 224419 (2009).
Group(s): Staub / Project(s): 6
- ▶ M. GARCÍA-FERNÁNDEZ, U. STAUB, Y. BODENTHIN, V. SCAGNOLI, V. POMJAKUSHIN, S. W. LOVESEY, A. MIRONE, J. HERREROMARTÍN, C. PIAMONTEZE, AND E. POMJAKUSHINA
Orbital Order at Mn and O Sites and Absence of Zener Polaron Formation in Manganites
Physical Review Letters **103**, 097205 (2009).
Group(s): Staub / Project(s): 6
- ▶ A. M. MULDER, S. M. LAWRENCE, U. STAUB, M. GARCÍA-FERNÁNDEZ, V. SCAGNOLI, C. MAZZOLI, E. POMJAKUSHINA, K. CONDER, AND Y. WANG
Direct Observation of Charge Order and an Orbital Glass State in Multiferroic LuFe_2O_4
Physical Review Letters **103**, 077602 (2009).
Group(s): Staub / Project(s): 6

Group of J.-M. Triscone

D. ISARAKORN, A. SAMBRI, P. JANPHUANG, D. BRIAND, S. GARIGLIO, J.-M. TRISCONE, F. GUY, J. W. REINER, C. H. AHN, AND N. F. DE ROOIJ

Epitaxial piezoelectric MEMS on silicon to be published in Journal of Micromechanics and Microengineering (2010).

Group(s): de Rooij, Triscone (JM) / Project(s): 1

- ▶ N. REYREN, S. GARIGLIO, A. D. CAVIGLIA, D. JACCARD, T. SCHNEIDER, AND J.-M. TRISCONE

Anisotropy of the superconducting transport properties of the LaAlO₃/SrTiO₃ interface
Applied Physics Letters **94**, 112506 (2009).

Group(s): Jaccard, Triscone (JM) / Project(s): 1

- ▶ J. GUYONNET, H. BÉA, F. GUY, S. GARIGLIO, S. FUSIL, K. BOUZEHOUE, J.-M. TRISCONE, AND P. PARUCH

Shear effects in lateral piezoresponse force microscopy at 180° ferroelectric domain walls
Applied Physics Letters **95**, 132902 (2009).

Group(s): Paruch, Triscone (JM) / Project(s): 1

- ▶ R. SCHERWITZL, P. ZUBKO, C. LICHTENSTEIGER, AND J.-M. TRISCONE

Electric-field tuning of the metal-insulator transition in ultrathin films of LaNiO₃
Applied Physics Letters **95**, 222114 (2009).

Group(s): Triscone (JM) / Project(s): 1

- ▶ S. GARIGLIO, N. REYREN, A. D. CAVIGLIA, AND J.-M. TRISCONE

Superconductivity at the LaAlO₃/SrTiO₃ interface
Journal of Physics: Condensed Matter **21**, 164213 (2009).

Group(s): Triscone (JM) / Project(s): 1

P. ZUBKO AND J.-M. TRISCONE

Applied physics: A leak of information
Nature **460**, 45 (2009).

Group(s): Triscone (JM) / Project(s): 1

T. SCHNEIDER, A. D. CAVIGLIA, S. GARIGLIO, N. REYREN, AND J.-M. TRISCONE

Electrostatically-tuned superconductor-metal-insulator quantum transition at the LaAlO₃/SrTiO₃ interface
Physical Review B **79**, 184502 (2009).

Group(s): Triscone (JM) / Project(s): 1

I. PALLECCHI, M. CODDA, E. GALLEANI D'AGLIANO, D. MARRÉ, A. D. CAVIGLIA, N. REYREN, S. GARIGLIO, AND J.-M. TRISCONE

Seebeck effect in the conducting LaAlO₃/SrTiO₃ interface

Physical Review B **81**, 085414 (2010).

Group(s): Triscone (JM) / Project(s): 1

- ▶ A. D. CAVIGLIA, M. GABAY, S. GARIGLIO, N. REYREN, C. CANCELLIERI, AND J.-M. TRISCONE

Tunable Rashba spin-orbit interaction at oxide interfaces

Physical Review Letters **104**, 126803 (2010).

Group(s): Triscone (JM) / Project(s): 1

S. GARIGLIO, M. GABAY, AND J.-M. TRISCONE
Oxide Materials: Superconductivity on the other side

Nature Nanotechnology **5**, 13 (2010).

Group(s): Triscone (JM) / Project(s): 1

H. J. A. MOLEGRAAF, J. HOFFMAN, C. A. F. VAZ, S. GARIGLIO, D. VAN DER MAREL, C. H. AHN, AND J. M. TRISCONE

Magnetoelectric Effects in Complex Oxides with Competing Ground States

Advanced Materials **21**, 3470 (2009).

Group(s): Triscone (JM), van der Marel / Project(s): 1

Group of M. Troyer

C. GILS

Ashkin–Teller universality in a quantum double model of Ising anyons

Journal of Statistical Mechanics p. P07019 (2009).

Group(s): Troyer / Project(s): 5

- ▶ B. BAUER, G. VIDAL, AND M. TROYER
Assessing the accuracy of projected entangled-pair states on infinite lattices

Journal of Statistical Mechanics p. P09006 (2009).

Group(s): Troyer / Project(s): 6

B. BAUER, E. GULL, S. TREBST, M. TROYER, AND D. A. HUSE

Optimized broad-histogram simulations for strong first-order phase transitions: droplet transitions in the large-Q Potts model

Journal of Statistical Mechanics p. P01020 (2010).

Group(s): Troyer / Project(s): 8

- ▶ C. GILS, S. TREBST, A. KITAEV, A. W. W. LUDWIG, M. TROYER, AND Z. WANG

Topology-driven quantum phase transitions in time-reversal-invariant anyonic quantum liquids

Nature Physics **5**, 834 (2009).

Group(s): Troyer / Project(s): 5

- S. V. ISAKOV, K. SENGUPTA, AND Y. B. KIM
Bose-Hubbard model on a star lattice
Physical Review B **80**, 214503 (2009).
Group(s): Troyer / Project(s): 6
- B. BAUER, M. TROYER, V. W. SCAROLA, AND K. B. WHALEY
Distinguishing phases with ansatz wave functions
Physical Review B **81**, 085118 (2010).
Group(s): Troyer / Project(s): 5, 6, 8
- V. GURARIE, L. POLLET, N. V. PROKOF'EV, B. V. SVISTUNOV, AND M. TROYER
Phase diagram of the disordered Bose-Hubbard model
Physical Review B **80**, 214519 (2009).
Group(s): Troyer / Project(s): 8
- V. W. SCAROLA, K. B. WHALEY, AND M. TROYER
Thermal canting of spin-bond order
Physical Review B **79**, 085113 (2009).
Group(s): Troyer / Project(s): 6
- A. F. ALBUQUERQUE, H. G. KATZGRABER, AND M. TROYER
ENCORE: An extended contractor renormalization algorithm
Physical Review E **79**, 046712 (2009).
Group(s): Troyer / Project(s): 6
- ▶ L. POLLET, N. V. PROKOF'EV, B. V. SVISTUNOV, AND M. TROYER
Absence of a Direct Superfluid to Mott Insulator Transition in Disordered Bose Systems
Physical Review Letters **103**, 140402 (2009).
Group(s): Troyer / Project(s): 8
- ▶ C. GILS, E. ARDONNE, S. TREBST, A. W. W. LUDWIG, M. TROYER, AND Z. WANG
Collective States of Interacting Anyons, Edge States, and the Nucleation of Topological Liquids
Physical Review Letters **103**, 070401 (2009).
Group(s): Troyer / Project(s): 5
- V. W. SCAROLA, L. POLLET, J. OITMAA, AND M. TROYER
Discerning Incompressible and Compressible Phases of Cold Atoms in Optical Lattices
Physical Review Letters **102**, 135302 (2009).
Group(s): Troyer / Project(s): 8
- ▶ I. V. KUKUSHKIN, J. H. SMET, V. W. SCAROLA, V. UMANSKY, AND K. VON KLITZING
Dispersion of the Excitations of Fractional Quantum Hall States
Science **324**, 1044 (2009).
Group(s): Troyer / Project(s): 5
- V. AMBEGAOKAR AND M. TROYER
Estimating errors reliably in Monte Carlo simulations of the Ehrenfest model
American Journal of Physics **78**, 150 (2010).
Group(s): Troyer / Project(s): 8
- Group of Ph. Willmott**
- ▶ M. SING, G. BERNER, K. GOSS, A. MÜLLER, A. RUFF, A. WETSCHEREK, S. THIEL, J. MANNHART, S. A. PAULI, C. W. SCHNEIDER, P. R. WILLMOTT, M. GORGOI, F. SCHÄFERS, AND R. CLAESSEN
Profiling the Interface Electron Gas of LaAlO₃/SrTiO₃ Heterostructures with Hard X-Ray Photoelectron Spectroscopy
Physical Review Letters **102**, 176805 (2009).
Group(s): Willmott / Project(s): 1
- D. MARTOCCIA, S. A. PAULI, T. BRUGGER, T. GREBER, B. D. PATTERSON, AND P. R. WILLMOTT
h-BN on Rh(111): Persistence of a commensurate 13-on-12 superstructure up to high temperatures
Surface Science **604**, L9 (2010).
Group(s): Willmott / Project(s): 1
- D. MARTOCCIA, T. BRUGGER, M. BJÖRCK, C. M. SCHLEPÜTZ, S. A. PAULI, T. GREBER, B. D. PATTERSON, AND P. R. WILLMOTT
h-BN/Ru(0001) nanomesh: A 14-on-13 superstructure with 3.5 nm periodicity
Surface Science **604**, L16 (2010).
Group(s): Willmott / Project(s): 1
- Group of A. Zheludev**
- ▶ T. HONG, A. ZHELUDEV, H. MANAKA, AND L.-P. REGNAULT
Evidence for a magnetic Bose glass in (CH₃)₂CHNH₃Cu(Cl_{0.95}Br_{0.05})₃ from neutron diffraction
Physical Review B **81**, 060410(R) (2010).
Group(s): Zheludev / Project(s): 6
- T. HONG, R. CUSTELCEAN, B. C. SALES, B. ROESSLI, D. K. SINGH, AND A. ZHELUDEV
Synthesis and structural characterization of 2Dioxane·2H₂O·CuCl₂: Metal-organic compound with Heisenberg antiferromagnetic S = 1/2 chains
Physical Review B **80**, 132404 (2009).
Group(s): Zheludev / Project(s): 6

- ▶ A. ZHELUDEV, V. O. GARLEA, A. TSVELIK, L.-P. REGNAULT, K. HABICHT, K. KIEFER, AND B. ROESSLI
Excitations from a chiral magnetized state of a frustrated quantum spin liquid
Physical Review B **80**, 214413 (2009).
Group(s): Zheludev / Project(s): 6

9.3.2 Scientific articles in journals without peer review

Group of Ph. Aebi

- ▶ C. MONNEY, E. F. SCHWIER, C. BATTAGLIA, M. G. GARNIER, N. MARIOTTI, C. DIDOT, H. BECK, P. AEBI, H. CERCELLIER, J. MARCUS, H. BERGER, AND A. N. TITOV

Temperature dependent photoemission on 1T-TiSe₂: Interpretation within the exciton condensate phase model

arXiv:0911.0327 (2009).

Group(s): Aebi / Project(s): 7

Group of G. Blatter

- A. U. THOMANN, V. B. GESHKENBEIN, AND G. BLATTER

Münchhausen effect: tunneling in an asymmetric SQUID

in *Advances in Theoretical Physics, Landau Memorial Conference*, V. LEBEDEV AND M. FEIGEL'MAN, eds. (American Institute of Physics, New York, 2009), AIP Conference Proceedings Vol. 1134, p. 63.

Group(s): Blatter / Project(s): 5

- F. HASSLER, B. KÜNG, G. B. LESOVIK, AND G. BLATTER

Single-Particle Excitations Generated by Voltage Pulses

in *Advances in Theoretical Physics, Landau Memorial Conference*, V. LEBEDEV AND M. FEIGEL'MAN, eds. (American Institute of Physics, New York, 2009), AIP Conference Proceedings Vol. 1134, p. 113.

Group(s): Blatter / Project(s): 2

- A. RÜEGG, S. D. HUBER, AND M. SIGRIST

A Z₂-slave-spin theory for strongly correlated fermions

arXiv:0912.3801 (2009).

Group(s): Sigrist, Blatter / Project(s): 4, 5, 8

Group of M. Büttiker

- M. BÜTTIKER

Edge-State Physics Without Magnetic Fields

Science **325**, 278 (2009).

Group(s): Büttiker / Project(s): 2

Group of L. Degiorgi

- ▶ M. LAVAGNINI, H.-M. EITER, L. TASSINI, B. MUSCHLER, R. HACKL, R. MONNIER, J.-H. CHU, I. R. FISHER, AND L. DEGIORGI

Raman scattering evidence for a cascade-like evolution of the charge-density-wave collective amplitude mode

arXiv:0909.1289 (2009).

Group(s): Degiorgi / Project(s): 7

Group of T. Esslinger

- ▶ N. STROHMAIER, D. GREIF, R. JÖRDENS, L. TARRUELL, H. MORITZ, T. ESSLINGER, R. SENSARMA, D. PEKKER, E. ALTMAN, AND E. DEMLER

Observation of elastic doublon decay in the Fermi-Hubbard model

arXiv:0905.2963 (2009).

Group(s): Esslinger / Project(s): 8

- ▶ R. JÖRDENS, L. TARRUELL, D. GREIF, T. UEHLINGER, N. STROHMAIER, H. MORITZ, T. ESSLINGER, L. DE LEO, C. KOLLATH, A. GEORGES, V. SCAROLA, L. POLLET, E. BUROVSKI, E. KOZIK, AND M. TROYER

Quantitative Determination of Temperature in the Approach to Magnetic Order of Ultracold Fermions in an Optical Lattice

arXiv:0912.3790 (2009).

Group(s): Esslinger, Troyer / Project(s): 8

Group of L. Forró

- ▶ N. P. ARMITAGE, R. TEDIOSI, F. LÉVY, E. GIANNINI, L. FORRÓ, AND D. VAN DER MAREL

An avoided Lifshitz-type semimetal-semiconductor transition: Infrared conductivity of elemental bismuth under pressure

arXiv:1002.4206 (2010).

Group(s): Forró, Giannini, van der Marel / Project(s): 5

Group of T. Giamarchi

- S. BUSTINGORRY, A. B. KOLTON, A. ROSSO, W. KRAUTH, AND T. GIAMARCHI

Thermal effects in the dynamics of disordered elastic systems

Physica B **404**, 444 (2009).

Group(s): Giamarchi / Project(s): 1

- T. GIAMARCHI

Deconstructing the electron

Physics **2**, 78 (2009).

Group(s): Giamarchi / Project(s): 7

Group of E. Giannini

- N. P. ARMITAGE, R. TEDIOSI, F. LÉVY, E. GIANNINI, L. FORRÓ, AND D. VAN DER MAREL
An avoided Lifshitz-type semimetal-semiconductor transition: Infrared conductivity of elemental bismuth under pressure
arXiv:1002.4206 (2010).
Group(s): Forró, Giannini, van der Marel / Project(s): 5

Group of V. Gritsev

- V. GRITSEV, T. ROSTUNOV, AND E. DEMLER
Exact methods in analysis of nonequilibrium dynamics of integrable models: application to the study of correlation functions in nonequilibrium 1D Bose gas
arXiv:0904.3221 (2009).
Group(s): Gritsev / Project(s): 8

- V. GRITSEV, P. BARMETTLER, AND E. DEMLER
Scaling approach to quantum non-equilibrium dynamics of many-body systems
arXiv:0912.2744 (2009).
Group(s): Gritsev / Project(s): 8

- T. KITAGAWA, S. PIELAWA, A. IMAMBEKOV, J. SCHMIEDMAYER, V. GRITSEV, AND E. DEMLER
Ramsey interference in one dimensional systems: The full distribution function of fringe contrast as a probe of many-body dynamics
arXiv:0912.4643 (2009).
Group(s): Gritsev / Project(s): 8

Group of D. van der Marel

- C.-C. CHEN, B. MORITZ, F. VERNAY, J. N. HANCOCK, S. JOHNSTON, C. J. JIA, G. CHABOT-COUTURE, M. GREVEN, I. ELFI-MOV, G. A. SAWATZKY, AND T. P. DEVEREAUX
Unraveling the Nature of Charge Excitations in La_2CuO_4 with Momentum-Resolved Cu K-edge Resonant Inelastic X-ray Scattering
arXiv:1002.4683 (2010).
Group(s): van der Marel / Project(s): 4

- N. P. ARMITAGE, R. TEDIOSI, F. LÉVY, E. GIANNINI, L. FORRÓ, AND D. VAN DER MAREL
An avoided Lifshitz-type semimetal-semiconductor transition: Infrared conductivity of elemental bismuth under pressure
arXiv:1002.4206 (2010).
Group(s): Forró, Giannini, van der Marel / Project(s): 5

- E. VAN HEUMEN, Y. HUANG, S. DE JONG, A. B. KUZMENKO, M. S. GOLDEN, AND D. VAN DER MAREL

- Optical properties of $\text{BaFe}_{2-x}\text{Co}_x\text{As}_2$*
arXiv:0912.0636 (2009).
Group(s): van der Marel / Project(s): 4

Group of A. Morpurgo

- A. F. MORPURGO
Dirac electrons broken to pieces
Nature **462**, 170 (2009).
Group(s): Morpurgo / Project(s): 2

Group of P. Paruch

- H. BÉA, P. PARUCH, M. BIBES, AND A. BARTHÉLÉMY
Nanoscale polarization switching mechanisms in multiferroic BiFeO_3 thin films
arXiv:0907.4568 (2009).
Group(s): Paruch / Project(s): 1

Group of Ch. Renner

- C. RENNER
Hands-on inspiration for science
Nature Materials **8**, 245 (2009).
Group(s): Renner / Project(s): Education

Group of H. M. Rønnow

- G. J. NILSEN, F. C. COOMER, M. A. DE VRIES, J. R. STEWART, P. P. DEEN, A. HARRISON, AND H. M. RØNNOW
Excitations and Short Range Order in the Quasi-Kagome Antiferromagnet Volborthite
arXiv:1001.2462 (2010).
Group(s): Rønnow / Project(s): 6

Group of M. Sigrist

- P. M. R. BRYDON, C. INIOTAKIS, D. MANSKE, AND M. SIGRIST
Functional superconductor interfaces from broken time-reversal symmetry
arXiv:0908.2975 (2009).
Group(s): Sigrist / Project(s): 4

- A. BOUHON AND M. SIGRIST
Influence of the domain walls on the Josephson effect in Sr_2RuO_4
arXiv:0909.3535 (2009).
Group(s): Sigrist / Project(s): 4

- H. KANEYASU AND M. SIGRIST
Nucleation of Vortex State in Ru-inclusion in Eutectic Ruthenium Oxide Sr_2RuO_4 -Ru
arXiv:1002.4793 (2010).
Group(s): Sigrist / Project(s): 5

A. RÜEGG, S. D. HUBER, AND M. SIGRIST
A Z_2 -slave-spin theory for strongly correlated fermions

arXiv:0912.3801 (2009).

Group(s): Sigrist, Blatter / Project(s): 4, 5, 8

Group of M. Troyer

▶ S. TROTZKY, L. POLLET, F. GERBIER, U. SCHNORRBERGER, I. BLOCH, N. V. PROKOF'EV, B. SVISTUNOV, AND M. TROYER

Suppression of the critical temperature for superfluidity near the Mott transition: validating a quantum simulator

arXiv:0905.4882 (2009).

Group(s): Troyer / Project(s): 8

▶ L. POLLET, J. D. PICON, H. P. BÜCHLER, AND M. TROYER

Supersolid phase with cold polar molecules on a triangular lattice

arXiv:0906.2126 (2009).

Group(s): Troyer / Project(s): 8

▶ E. KOZIK, K. VAN HOUCKE, E. GULL, L. POLLET, N. PROKOF'EV, B. SVISTUNOV, AND M. TROYER

Diagrammatic Monte Carlo for Correlated Fermions

arXiv:0907.0863 (2009).

Group(s): Troyer / Project(s): 5, 8

▶ B. CAPOGROSSO-SANSONE, S. GIORGINI, S. PILATI, L. POLLET, N. PROKOF'EV, B. SVISTUNOV, AND M. TROYER

Beliaev technique for a weakly interacting Bose gas

arXiv:0911.5383 (2009).

Group(s): Troyer / Project(s): 8

▶ R. JÖRDENS, L. TARRUELL, D. GREIF, T. UEHLINGER, N. STROHMAIER, H. MORITZ, T. ESSLINGER, L. DE LEO, C. KOLLATH, A. GEORGES, V. SCAROLA, L. POLLET, E. BUROVSKI, E. KOZIK, AND M. TROYER

Quantitative Determination of Temperature in the Approach to Magnetic Order of Ultracold Fermions in an Optical Lattice

arXiv:0912.3790 (2009).

Group(s): Esslinger, Troyer / Project(s): 8

Group of Ph. Willmott

D. MARTOCCIA, M. BJÖRCK, C. M. SCHLEPÜTZ, T. BRUGGER, S. A. PAULI, B. D. PATTERSON, T. GREBER, AND P. R. WILLMOTT

Graphene on Ru(0001): A corrugated and chiral structure

arXiv:0908.4517 (2009).

Group(s): Willmott / Project(s): 1

9.3.3 Publications involving several groups

- ▶ L. ANTOGNAZZA, M. THERASSE, M. DECROUX, F. ROY, B. DUTOIT, M. ABPLANALP, AND Ø. FISCHER
Comparison between the behavior of HTS thin film grown on sapphire and coated conductors for fault current limiter applications
 IEEE Transactions on Applied Superconductivity **19**, 1960 (2009).
 Group(s): Abplanalp, Decroux, Fischer / Project(s): 3
- C. MONNEY, H. CERCELLIER, F. CLERC, C. BATTAGLIA, E. F. SCHWIER, C. DIDIOT, M. G. GARNIER, H. BECK, P. AEBI, H. BERGER, L. FORRÓ, AND L. PATTHEY
Spontaneous exciton condensation in 1T-TiSe₂: BCS-like approach
 Physical Review B **79**, 045116 (2009).
 Group(s): Aebi, Forró / Project(s): 7
- M. HOESCH, X. CUI, K. SHIMADA, C. BATTAGLIA, S.-I. FUJIMORI, AND H. BERGER
Splitting in the Fermi surface of ZrTe₃: A surface charge density wave system
 Physical Review B **80**, 075423 (2009).
 Group(s): Aebi, Forró / Project(s): 7
- ▶ J. KARPINSKI, N. D. ZHIGADLO, S. KATRYCH, Z. BUKOWSKI, P. MOLL, S. WEYENETH, H. KELLER, R. PUZNIAK, M. TORTELLO, D. DAGHERO, R. GONNELLI, I. MAGGIO-APRILE, Y. FASANO, Ø. FISCHER, K. RO-GACKI, AND B. BATLOGG
Single crystals of LnFeAsO_{1-x}F_x (Ln = La, Pr, Nd, Sm, Gd) and Ba_{1-x}Rb_xFe₂As₂: Growth, structure and superconducting properties
 Physica C **469**, 370 (2009).
 Group(s): Batlogg, Fischer, Karpinski, Keller / Project(s): 4
- A. BELOUSOV, S. KATRYCH, J. JUN, J. ZHANG, D. GÜNTHER, R. SOBOLEWSKI, J. KARPINSKI, AND B. BATLOGG
Bulk single-crystal growth of ternary Al_xGa_{1-x}N from solution in gallium under high pressure
 Journal of Crystal Growth **311**, 3971 (2009).
 Group(s): Batlogg, Karpinski / Project(s): 4
- ▶ Z. BUKOWSKI, S. WEYENETH, R. PUZNIAK, P. MOLL, S. KATRYCH, N. D. ZHIGADLO, J. KARPINSKI, H. KELLER, AND B. BATLOGG
Superconductivity at 23 K and low anisotropy in Rb-substituted BaFe₂As₂ single crystals
 Physical Review B **79**, 104521 (2009).
 Group(s): Batlogg, Karpinski, Keller / Project(s): 4
- ▶ J. HOPPLER, J. STAHN, C. NIEDERMAYER, V. K. MALIK, H. BOUYANFIE, A. J. DREW, M. RÖSSLE, A. BUZDIN, G. CRISTIANI, H.-U. HABERMEIER, B. KEIMER, AND C. BERNHARD
Giant superconductivity-induced modulation of the ferromagnetic magnetization in a cuprate-manganite superlattice
 Nature Materials **8**, 315 (2009).
 Group(s): Bernhard, Niedermayer / Project(s): 1
- C. BERNHARD, A. J. DREW, L. SCHULZ, V. K. MALIK, M. RÖSSLE, C. NIEDERMAYER, T. WOLF, G. D. VARMA, G. MU, H.-H. WEN, G. WU, AND X. H. CHEN
Muon spin rotation study of magnetism and superconductivity in BaFe_{2-x}Co_xAs₂ and Pr_{1-x}Sr_xFeAsO
 New Journal of Physics **11**, 055050 (2009).
 Group(s): Bernhard, Niedermayer / Project(s): 4
- ▶ A. J. DREW, C. NIEDERMAYER, P. J. BAKER, F. L. PRATT, S. J. BLUNDELL, T. LANCASTER, R. H. LIU, G. WU, X. H. CHEN, I. WATANABE, V. K. MALIK, A. DUBROKA, M. RÖSSLE, K. W. KIM, C. BAINES, AND C. BERNHARD
Coexistence of static magnetism and superconductivity in SmFeAsO_{1-x}F_x as revealed by muon spin rotation
 Nature Materials **8**, 310 (2009).
 Group(s): Bernhard, Niedermayer / Project(s): 4
- J. STAHN, C. NIEDERMAYER, J. HOPPLER, AND C. BERNHARD
PNR studies of proximity and coupling effects in YBa₂Cu₃O₇/La_{2/3}Ca_{1/3}MnO₃ superlattices
 Neutron News **20**, 13 (2009).
 Group(s): Bernhard, Niedermayer / Project(s): 1
- D. ISARAKORN, A. SAMBRI, P. JANPHUANG, D. BRIAND, S. GARIGLIO, J.-M. TRISCONE, F. GUY, J. W. REINER, C. H. AHN, AND N. F. DE ROOIJ
Epitaxial piezoelectric MEMS on silicon to be published in Journal of Micromechanics and Microengineering (2010).
 Group(s): de Rooij, Triscone (JM) / Project(s): 1
- N. CURTZ, E. KOLLER, H. ZBINDEN, M. DECROUX, L. ANTOGNAZZA, Ø. FISCHER, AND N. GISIN
Patterning of ultrathin YBCO nanowires using a new focused-ion-beam process
 Superconductor Science & Technology **23**, 045015 (2010).
 Group(s): Decroux, Fischer / Project(s): 3

- F. PFUNER, L. DEGIORGI, H. BERGER, AND L. FORRÓ
Infrared investigation of the phonon spectrum in the frustrated spin cluster compound $\text{FeTe}_2\text{O}_5\text{Cl}$
 Journal of Physics: Condensed Matter **21**, 375401 (2009).
 Group(s): Degiorgi, Forró / Project(s): 6, 7
- ▶ A. SACCHETTI, C. L. CONDRON, S. N. GVASALIYA, F. PFUNER, M. LAVAGNINI, M. BALDINI, M. F. TONEY, M. MERLINI, M. HANFLAND, J. MESOT, J.-H. CHU, I. R. FISHER, P. POSTORINO, AND L. DEGIORGI
Pressure-induced quenching of the charge-density-wave state in rare-earth tritellurides observed by x-ray diffraction
 Physical Review B **79**, 201101(R) (2009).
 Group(s): Degiorgi, Mesot / Project(s): 7
- ▶ A. P. PETROVIĆ, Y. FASANO, R. LORTZ, C. SENATORE, A. DEMUER, A. B. ANTUNES, A. PARÉ, D. SALLOUM, P. GOUGEON, M. POTEL, AND Ø. FISCHER
Real-Space Vortex Glass Imaging and the Vortex Phase Diagram of SnMo_6S_8
 Physical Review Letters **103**, 257001 (2009).
 Group(s): Fischer, Flükiger / Project(s): 2, 5
- ▶ N. JENKINS, Y. FASANO, C. BERTHOD, I. MAGGIO-APRILE, A. PIRIOU, E. GIANNINI, B. W. HOOGENBOOM, C. HESS, T. CREN, AND Ø. FISCHER
Imaging the Essential Role of Spin Fluctuations in High- T_c Superconductivity
 Physical Review Letters **103**, 227001 (2009).
 Group(s): Fischer, Giamarchi, Giannini / Project(s): 4
- ▶ B. M. WOJEK, E. MORENZONI, D. G. ESHCHENKO, A. SUTER, T. PROKSCHA, E. KOLLER, E. TREBOUX, O. FISCHER, AND H. KELLER
Magnetism and superconductivity in cuprate heterostructures studied by low energy μSR
 Physica B **404**, 720 (2009).
 Group(s): Fischer, Keller, Morenzoni / Project(s): 1, 4
- A. UBALDINI, E. GIANNINI, C. SENATORE, AND D. VAN DER MAREL
 BiOCuS : A new superconducting compound with oxypnictide-related structure
 Physica C (2010), doi:10.1016/j.physc.2009.11.164.
 Group(s): Flükiger, Giannini, van der Marel / Project(s): 4
- G. GHIRINGHELLI, A. PIAZZALUNGA, X. WANG, A. BENDOUNAN, H. BERGER, F. BOTTEGONI, N. CHRISTENSEN, C. DALLERA, M. GRIONI, J.-C. GRIVEL, M. MORETTI SALA, L. PATHEY, J. SCHLAPPA, T. SCHMITT, V. STROCOV, AND L. BRAICOVICH
Crystal field and low-energy excitations measured by high resolution RIXS at the L_3 edge of Cu, Ni and Mn
 The European Physical Journal – Special Topics **169**, 199 (2009).
 Group(s): Forró, Grioni / Project(s): 7
- B. SIPOS, M. DUCHAMP, A. MAGREZ, L. FORRÓ, N. BARIŠIĆ, A. KIS, J. W. SEO, F. BIERI, F. KRUMEICH, R. NESPER, AND G. R. PATZKE
Mechanical and electronic properties of vanadium oxide nanotubes
 Journal of Applied Physics **105**, 074317 (2009).
 Group(s): Forró, Patzke / Project(s): 7, 3
- I. PALLECCHI, G. LAMURA, M. TROPEANO, M. PUTTI, R. VIENNOIS, E. GIANNINI, AND D. VAN DER MAREL
Seebeck effect in $\text{Fe}_{1+x}\text{Te}_{1-y}\text{Se}_y$ single crystals
 Physical Review B **80**, 214511 (2009).
 Group(s): Giannini, van der Marel / Project(s): 4
- R. VIENNOIS, E. GIANNINI, D. VAN DER MAREL, AND R. ČERNÝ
Phase diagram of single-crystalline tetragonal iron chalcogenides
 Physica C (2010), doi:10.1016/j.physc.2009.11.126.
 Group(s): Giannini, van der Marel / Project(s): 4
- R. VIENNOIS, E. GIANNINI, J. TEYSSIER, J. ELIA, J. DEISENHOFER, AND D. VAN DER MAREL
Two-dimensional orbital ordering in d^1 Mott insulator Sr_2VO_4
 Journal of Physics: Conference Series **200**, 012219 (2010).
 Group(s): Giannini, van der Marel / Project(s): 4
- J. TEYSSIER, R. VIENNOIS, V. GURITANU, E. GIANNINI, AND D. VAN DER MAREL
Kondo effect and quantum critical point in $\text{Mn}_{(1-x)}\text{Co}_x\text{Si}$
 Journal of Physics: Conference Series **200**, 032076 (2010).
 Group(s): Giannini, van der Marel / Project(s): 5
- R. VIENNOIS, E. GIANNINI, D. VAN DER MAREL, AND R. ČERNÝ
Effect of Fe excess on Structural, Magnetic and Superconducting Properties of Single-Crystalline $\text{Fe}_{1+x}\text{Te}_{1-y}\text{Se}_y$
 Journal of Solid State Chemistry (2010), doi:10.1016/j.jssc.2010.01.024.
 Group(s): Giannini, van der Marel / Project(s): 4

- M. MEDARDE, C. DALLERA, M. GRIONI, B. DELLEY, F. VERNAY, J. MESOT, M. SIKORA, J. A. ALONSO, AND M. J. MARTÍNEZ-LOPE
Charge disproportionation in RNiO₃ perovskites (R = rare earth) from high-resolution x-ray absorption spectroscopy
Physical Review B **80**, 245105 (2009).
Group(s): Grioni, Mesot / Project(s): 7
- N. REYREN, S. GARIGLIO, A. D. CAVIGLIA, D. JACCARD, T. SCHNEIDER, AND J.-M. TRISCONE
Anisotropy of the superconducting transport properties of the LaAlO₃/SrTiO₃ interface
Applied Physics Letters **94**, 112506 (2009).
Group(s): Jaccard, Triscone (JM) / Project(s): 1
- T. KONDO, R. KHASANOV, Y. SASSA, A. BENDOUNAN, S. PAILHES, J. CHANG, J. MESOT, H. KELLER, N. D. ZHIGADLO, M. SHI, Z. BUKOWSKI, J. KARPINSKI, AND A. KAMINSKI
Anomalous asymmetry in the Fermi surface of the high-temperature superconductor YBa₂Cu₄O₈ revealed by angle-resolved photoemission spectroscopy
Physical Review B **80**, 100505 (2009).
Group(s): Karpinski, Keller, Mesot / Project(s): 4
- M. LE TACON, T. R. FORREST, C. RÜEGG, A. BOSAK, A. C. WALTERS, R. MITTAL, H. M. RØNNOW, N. D. ZHIGADLO, S. KATRYCH, J. KARPINSKI, J. P. HILL, M. KRISCH, AND D. F. MCMORROW
Inelastic x-ray scattering study of superconducting SmFeAsO_{1-x}F_y single crystals: Evidence for strong momentum-dependent doping-induced renormalizations of optical phonons
Physical Review B **80**, 220504 (2009).
Group(s): Karpinski, Rønnow / Project(s): 4, 6
- P. S. HÄFLIGER, R. KHASANOV, R. LORTZ, A. PETROVIĆ, K. TOGANO, C. BAINES, B. GRANALI, AND H. KELLER
Muon-Spin Rotation Study of the Ternary Noncentrosymmetric Superconductors Li₂Pd_xPt_{3-x}B
Journal of Superconductivity and Novel Magnetism **22**, 337 (2009).
Group(s): Keller, Fischer / Project(s): 4
- R. KHASANOV, M. BENDELE, A. AMATO, P. BABKEVICH, A. T. BOOTHROYD, A. CERVELLINO, K. CONDER, S. N. GVASALIYA, H. KELLER, H.-H. KLAUSS, H. LUETKENS, V. POMJAKUSHIN, E. POMJAKUSHINA, AND B. ROESSLI
Coexistence of incommensurate magnetism and superconductivity in Fe_{1+y}Se_xTe_{1-x}
Physical Review B **80**, 140511(R) (2009).
Group(s): Keller, Kenzelmann / Project(s): 4, 5
- D. HAUG, V. HINKOV, A. SUCHANECK, D. S. INOSOV, N. B. CHRISTENSEN, C. NIEDERMAYER, P. BOURGES, Y. SIDIS, J. T. PARK, A. IVANOV, C. T. LIN, J. MESOT, AND B. KEIMER
Magnetic-Field-Enhanced Incommensurate Magnetic Order in the Underdoped High-Temperature Superconductor YBa₂Cu₃O_{6.45}
Physical Review Letters **103**, 017001 (2009).
Group(s): Mesot, Niedermayer / Project(s): 4
- J. CHANG, N. B. CHRISTENSEN, C. NIEDERMAYER, K. LEFMAN, H. M. RØNNOW, D. F. MCMORROW, A. SCHNEIDEWIND, P. LINK, A. HIESS, M. BOEHM, R. MOTT, S. PAILHÉS, N. MOMONO, M. ODA, M. IDO, AND J. MESOT
Magnetic-Field-Induced Soft-Mode Quantum Phase Transition in the High-Temperature Superconductor La_{1.855}Sr_{0.145}CuO₄: An Inelastic Neutron-Scattering Study
Physical Review Letters **102**, 177006 (2009).
Group(s): Mesot, Niedermayer, Rønnow / Project(s): 4, 6
- J. SCHLAPPA, T. SCHMITT, F. VERNAY, V. N. STROCOV, V. ILAKOVAC, B. THIELEMANN, H. M. RØNNOW, S. VANISHRI, A. PIAZZALUNGA, X. WANG, L. BRAICOVICH, G. GHIRINGHELLI, C. MARIN, J. MESOT, B. DELLEY, AND L. PATTHEY
Collective Magnetic Excitations in the Spin Ladder Sr₁₄Cu₂₄O₄₁ Measured Using High-Resolution Resonant Inelastic X-Ray Scattering
Physical Review Letters **103**, 047401 (2009).
Group(s): Mesot, Rønnow / Project(s): 6
- B. THIELEMANN, C. RÜEGG, H. M. RØNNOW, A. M. LÄUCHLI, J.-S. CAUX, B. NORMAND, D. BINER, K. W. KRÄMER, H.-U. GÜDEL, J. STAHN, K. HABICHT, K. KIEFER, M. BOEHM, D. F. MCMORROW, AND J. MESOT
Direct Observation of Magnon Fractionalization in the Quantum Spin Ladder
Physical Review Letters **102**, 107204 (2009).
Group(s): Mesot, Rønnow / Project(s): 6
- J. GUYONNET, H. BÉA, F. GUY, S. GARIGLIO, S. FUSIL, K. BOUZEHOUE, J.-M. TRISCONE, AND P. PARUCH
Shear effects in lateral piezoresponse force microscopy at 180° ferroelectric domain walls
Applied Physics Letters **95**, 132902 (2009).
Group(s): Paruch, Triscone (JM) / Project(s): 1
- K. Y. YANG, W. Q. CHEN, T. M. RICE, M. SIGRIST, AND F. C. ZHANG

- Nature of stripes in the generalized $t - J$ model applied to the cuprate superconductors*
New Journal of Physics **11**, 055053 (2009).
Group(s): Rice, Sigrist / Project(s): 4, 5
- K. Y. YANG, W. Q. CHEN, T. M. RICE, AND F. C. ZHANG
Origin of the checkerboard pattern in scanning tunneling microscopy maps of underdoped cuprate superconductors
Physical Review B **80**, 174505 (2009).
Group(s): Rice, Sigrist / Project(s): 4
- K. Y. YANG, H. B. YANG, P. D. JOHNSON, T. M. RICE, AND F. C. ZHANG
Quasiparticles in the pseudogap phase of underdoped cuprate
Europhysics Letters **86**, 37002 (2009).
Group(s): Rice, Sigrist / Project(s): 4
- H. J. A. MOLEGRAAF, J. HOFFMAN, C. A. F. VAZ, S. GARIGLIO, D. VAN DER MAREL, C. H. AHN, AND J. M. TRISCONE
Magnetoelectric Effects in Complex Oxides with Competing Ground States
Advanced Materials **21**, 3470 (2009).
Group(s): Trisone (JM), van der Marel / Project(s): 1
- A. RÜEGG, S. D. HUBER, AND M. SIGRIST
A Z_2 -slave-spin theory for strongly correlated fermions
arXiv:0912.3801 (2009).
Group(s): Sigrist, Blatter / Project(s): 4, 5, 8
- R. JÖRDENS, L. TARRUELL, D. GREIF, T. UEHLINGER, N. STROHMAIER, H. MORITZ, T. ESSLINGER, L. DE LEO, C. KOLLATH, A. GEORGES, V. SCAROLA, L. POLLET, E. BUROVSKI, E. KOZIK, AND M. TROYER
Quantitative Determination of Temperature in the Approach to Magnetic Order of Ultracold Fermions in an Optical Lattice
arXiv:0912.3790 (2009).
Group(s): Esslinger, Troyer / Project(s): 8
- N. P. ARMITAGE, R. TEDIOSI, F. LÉVY, E. GIANNINI, L. FORRÓ, AND D. VAN DER MAREL
An avoided Lifshitz-type semimetal-semiconductor transition: Infrared conductivity of elemental bismuth under pressure
arXiv:1002.4206 (2010).
Group(s): Forró, Giannini, van der Marel / Project(s): 5

11 Finance

Contents

11.1 Finance NCCR Overview	178
11.2 Funding sources	182
11.3 Allocation to projects	183
11.4 Expenditures	186
11.5 Comments on finances	190

NCCR: MaNEP
 Director: Fischer Oystein
 Home Institution: Université de Genève - GE
 Start Date: 01.07.2001

Report: Year 9 Intermediate Report
 Period: 01.07.2009 - 30.06.2013
 Year: 9 - 12
 Status: in preparation

Criteria:

Finance NCCR Overview

Project leader	Institution	Project title	Group leader	Start of project	Duration	Total SNSF-funding	Total other funding	Total
Management								
Fischer Øystein	Université de Genève	Office		01.07.2001	156	1'644'168	4'035'780	5'679'948
Fischer Øystein	Université de Genève	Education / Women		01.07.2001	156	609'571	1'049'443	1'659'014
Fischer Øystein	Université de Genève	Knowledge and Technology Transfer		01.07.2001	156	374'208	1'080'190	1'454'398
Fischer Øystein	Université de Genève	Communication		01.07.2001	156	460'885	772'626	1'233'511
Fischer Øystein	Université de Genève	Communication		01.07.2001	156	199'504	1'133'520	1'333'024
Reserve								
Fischer Øystein		Change of reserve - Budget				1'927'949	0	1'927'949
Fischer Øystein		Change of reserve - Forecast				450'000	0	450'000
Fischer Øystein		Change of reserve - Effective				1'477'949	0	1'477'949
						0	0	0
						0	0	0
Project(s) without workpackage								
Cors Jorge		Economic stimulus package - Cut-and-coat process by wire-EDM	Cors Jorge	01.11.2009	24	142'326	194'279	336'605
Flükiger Rene	Université de Genève	Economic stimulus package - Development of MgB2 wires		01.10.2009	24	33'201	145'579	178'780
Cors Jorge		Economic stimulus package - Electrochemical sensors with higher resolution	Cors Jorge	01.10.2009	24	39'144	86'699	125'843
Kenzelmann Michel		Economic stimulus package - Neutron optical devices for small samples		01.10.2009	24	76'754	52'070	128'824

Signature of NCCR Director:.....

Project leader	Institution	Project title	Group leader	Start of project	Duration	Total SNSF-funding	Total other funding	Total
Fischer Øystein	Université de Genève	Techniques Know-How		01.07.2009	48	200'000	3'429'271	3'629'271
Fischer Øystein	Université de Genève	Equipment Geneva		01.07.2001	144	694'750	1'075'000	1'769'750
Triscone Jean-Marc	Université de Genève	Project 1 - Novel phenomena at interfaces and in superlattices	Aebi Philipp A.; Bernhard Christian; Giamarchi Thierry; Giannini Enrico; Keller Hugo; Morenzoni Elvezio; Morpurgo Alberto; Niedermayer Christoph; Paruch Patrycja; Sigrist Manfred; Triscone Jean-Marc; Willmott Phillip	01.07.2009	48	600'231	5'510'801	6'111'032
Fischer Øystein	Université de Genève	Project 3 - Electronic materials for energy systems and other applications	de Rooij Nico; Decroux Michel; Fischer Øystein; Kenzelmann Michel; Renner Christoph; Triscone Gilles; Triscone Jean-Marc; Yvon Klaus	01.07.2009	48	1'465'553	1'165'173	13'117'326
Van der Marel Dirk	Université de Genève	Project 4 - Electronic properties of oxide superconductors and related materials	Baeriswyl Dionys; Batlogg Bertram; Bernhard Christian; Fischer Øystein; Giamarchi Thierry; Giannini Enrico; Karpinski Janusz; Keller Hugo; Mesot Joël; Morenzoni Elvezio; Niedermayer Christoph; Sigrist Manfred; Van der Marel Dirk	01.07.2009	48	992'663	9'387'272	10'379'934

Project leader	Institution	Project title	Group leader	Start of project	Duration	Total SNSF-funding	Total other funding	Total
Sigrist Manfred	ETH Zürich	Project 5 - Novel electronic phases in strongly correlated electron systems	Baeriswyl Dionys; Blatter Johann; Giannini Enrico; Kenzelmann Michel; Sigrist Manfred; Troyer Matthias; Van der Marel Dirk	01.07.2009	48	600'118	3'539'664	4'139'781
Forro Laszlo	EPF Lausanne	Project 7 - Electronic materials with reduced dimensionality	Aebi Philipp A.; Degiorgi Leonardo; Fischer Øystein; Forro Laszlo; Giamarchi Thierry; Griani Marco	01.07.2009	48	767'017	6'788'711	7'555'728
Giamarchi Thierry	Université de Genève	Project 8 - Cold atomic gases as novel quantum simulators for condensed matter	Blatter Johann; Esslinger Tilman; Giamarchi Thierry; Sigrist Manfred; Troyer Matthias	01.07.2009	48	599'999	4'686'772	5'286'771
Morpurgo Alberto	Université de Genève	Project 2 - Materials for future electronics	Batlogg Bertram; Büttiker Markus; Forro Laszlo; Giamarchi Thierry; Morpurgo Alberto; Paruch Patrycja; Renner Christoph; Sigrist Manfred; Triscone Jean-Marc; Van der Marel Dirk	01.07.2009	48	600'647	7'163'044	7'763'690
Mila Frederic	EPF Lausanne	Project 6 - Magnetism and competing interactions in bulk materials	Forro Laszlo; Giamarchi Thierry; Kenzelmann Michel; Mesot Joël; Mila Frederic; Niedermayer Christoph; Renner Christoph; Staub Urs; Troyer Matthias	01.07.2009	48	774'999	5'856'863	6'631'863

Project leader	Institution	Project title	Group leader	Start of project	Duration	Total SNSF-funding	Total other funding	Total
Total:								
								11'159'518
								63'603'577
								74'763'095

Year 9 Intermediate Report
 01.07.2009 - 30.06.2013
 9 - 12
 in preparation

MaNEP
 Fischer Oystein
 Université de Genève - GE
 01.07.2001

Report:
 Period:
 Year:
 Status:

Criteria:

Funding sources

Funding source	Year 9	Year 10	Year 11	Year 12	Total Cash Total in Kind	% %	Total	%
SNSF-funding	Cash in Kind 3'045'362 0	4'656'128 0	2'546'580 0	911'448 0	11'159'518 0	18.3 0.0	11'159'518	14.9
Self-funding from Home Institution	Cash in Kind 1'423'290 0	4'034'713 0	4'462'624 0	5'889'072 0	15'809'699 0	26.0 0.0	15'809'699	21.1
Self-funding from groups	Cash in Kind 277'949 13'073'119	10'161'750 0	10'092'350 0	8'799'350 0	29'331'399 13'073'119	48.2 93.8	42'404'518	56.7
Self-funding other	Cash in Kind 0 619'000	496'200 0	496'200 0	121'200 0	1'113'600 619'000	1.8 4.4	1'732'600	2.3
3rd party-funding	Cash in Kind 232'145 250'000	1'058'205 0	1'058'205 0	1'058'205 0	3'406'760 250'000	5.6 1.8	3'656'760	4.9
Total:	Cash in Kind 4'978'745 13'942'119	20'406'996 0	18'655'959 0	16'779'275 0	60'820'975 13'942'119		74'763'094.94	100.0

Signature of NCCR Director:.....

NCCR: MaNEP **Year 9 Intermediate Report**
Director: Fischer Oystein **Report:** 01.07.2009 - 30.06.2013
Home Institution: Université de Genève - GE **Period:** 9 - 12
Start Date: 01.07.2001 **Status:** in preparation

Criteria:

Allocation to projects

Project leader	Project title	Year 9	Year 10	Year 11	Year 12	SNSF Funded	Total Funded	Total Not SNSF Funded	Total	%
Management										
Fischer Øystein	Office	605'059	1'670'726	1'689'790	1'714'373	1'644'168	4'035'780	5'679'948	7.6	
		109'800	492'817	471'930	466'967	609'571	931'943	1'659'014	2.2	
		117'500	0	0	0	0	117'500			
Fischer Øystein	Education / Women	75'308	443'030	443'030	443'030	374'208	1'030'190	1'454'398	1.9	
		50'000	0	0	0	0	50'000			
Fischer Øystein	Knowledge and Technology Transfer	169'211	341'164	361'568	361'568	460'885	772'626	1'233'511	1.6	
		0	0	0	0	0	0			
Fischer Øystein	Communication	83'239	393'715	413'262	442'808	199'504	1'133'520	1'333'024	1.8	
		0	0	0	0	0	0			
Reserve										
Fischer Øystein	Change of reserve - Budget	1'477'949	250'000	0	200'000	1'927'949	0	1'927'949	2.6	
		0	250'000	0	200'000	450'000	0	450'000	0.6	
Fischer Øystein	Change of reserve - Forecast	1'477'949	0	0	0	1'477'949	0	1'477'949	2.0	
		0	0	0	0	0	0	0	0.0	
Project(s) without workpackage										
Cors Jorge	Economic stimulus package - Cut-and-coat process by	16'837'857	18'486'270	16'966'169	14'864'902	7'587'401	59'567'797	67'155'198	89.8	
		299'105	0	0	0	142'326	156'779	336'605	0.5	
		37'500	0	0	0	0	37'500			

Signature of NCCR Director:.....

Project leader	Project title	Year 9	Year 10	Year 11	Year 12	Total		%
						SNSF Funded	Not SNSF Funded	
Flükiger Rene	Economic stimulus package - Development of MgB2	178'780 0	0 0	0 0	0 0	33'201	145'579 0	178'780 0.2
Cors Jorge	Economic stimulus package - Electrochemical sensors	598'10 66'033	0 0	0 0	0 0	39'144	20'666 66'033	125'843 0.2
Kenzelmann Michel	Economic stimulus package - Neutron optical devices for	78'824 50'000	0 0	0 0	0 0	76'754	2'070 50'000	128'824 0.2
Fischer Øystein	Equipment Geneva	0 25'000	794'750 0	400'000 0	550'000 0	694'750	1'050'000 25'000	1'769'750 2.4
Triscone Jean-Marc	Project 1 - Novel phenomena at interfaces and in	288'015 1'800'923	1'462'412 0	1'391'933 0	1'167'749 0	600'231	3'709'878 1'800'923	6'111'032 8.2
Morpurgo Alberto	Project 2 - Materials for future electronics	182'519 2'032'567	1'860'227 0	1'778'108 0	1'910'269 0	600'647	5'130'477 2'032'567	7'763'690 10.4
Fischer Øystein	Project 3 - Electronic materials for energy systems	615'502 2'035'617	3'805'882 0	3'492'107 0	3'168'218 0	1'465'553	9'616'156 2'035'617	13'117'326 17.5
Van der Marel Dirk	Project 4 - Electronic properties of oxide	521'104 2'304'716	2'720'255 0	2'645'488 0	2'188'371 0	992'663	7'082'556 2'304'716	10'379'934 13.9
Sigrist Manfred	Project 5 - Novel electronic phases in strongly correlated	211'507 1'102'137	1'082'860 0	1'030'678 0	712'600 0	600'118	2'437'527 1'102'137	4'139'781 5.5
Mila Frederic	Project 6 - Magnetism and competing interactions in	319'778 1'861'758	1'780'465 0	1'680'161 0	989'700 0	774'999	3'995'105 1'861'758	6'631'863 8.9

Project leader	Project title	Year 9	Year 10	Year 11	Year 12	SNSF Funded		Total	%
						SNSF Funded	Not SNSF Funded		
Forro Laszlo	Project 7 - Electronic materials with reduced	219'437 1'308'364	2'131'527 0	2'028'200 0	1'868'200 0	767'017 0	5'480'347 1'308'364	7'555'728	10.1
Giamarchi Thierry	Project 8 - Cold atomic gases as novel quantum	88'856 1'125'005	1'635'329 0	1'455'213 0	982'368 0	599'999 0	3'561'767 1'125'005	5'286'771	7.1
Fischer Øystein	Techniques Know-How	0 25'000	1'212'563 0	1'064'281 0	1'327'427 0	200'000 0	3'404'271 25'000	3'629'271	4.9
Total		18'920'865	20'406'996	18'655'959	16'779'275	11'159'518	63'603'577	74'763'095	100.0

NCCR: MaNEP **Year 9 Intermediate Report**
Director: Fischer Oystein **Report:** 01.07.2009 - 30.06.2013
Home Institution: Université de Genève - GE **Year:** 9 - 12
Start Date: 01.07.2001 **Status:** in preparation

Criteria:

Expenditures

Project	Group leader / Research group	Gross salaries	Social charges	Equipment	Consumables	Travel	Miscellaneous	Credit	Total Cash Total in Kind	Total
Management		3'690'311	699'637	0	670'000	0	620'000	0		5'679'948
Office		Cash 838'761	167'753	0	190'000	0	345'000	0	1'541'514	1'659'014
		in Kind 117'500	0	0	0	0	0	0	117'500	
Education / Women		Cash 882'831	176'567	0	70'000	0	275'000	0	1'404'398	1'454'398
		in Kind 50'000	0	0	0	0	0	0	50'000	
Knowledge and Technology Transfer		Cash 898'408	175'103	0	160'000	0	0	0	1'233'511	1'233'511
		in Kind 0	0	0	0	0	0	0	0	
Communication		Cash 902'811	180'213	0	250'000	0	0	0	1'333'024	1'333'024
		in Kind 0	0	0	0	0	0	0	0	
Reserve										1'927'949
Change of reserve - Budget	Fischer Øystein	Cash								450'000
Change of reserve - Forecast		Cash								1'477'949
Change of reserve - Effective		Cash								0
Project(s) without workpackage		53'714'294	2'315'683	2'938'204	2'616'237	810'531	4'760'249	0		67'155'198
Economic stimulus package	Cors Jorge	Cash 65'457	9'792	90'491	2'682	1'170	129'513	0	299'105	336'605
- Cut-and-coat process by wire-EDM		in Kind 37'500	0	0	0	0	0	0	37'500	

Signature of NCCR Director:.....

Project	Group leader / Research group	Cash in Kind	Gross salaries	Social charges	Equipment	Consumables	Travel	Miscellaneous	Credit	Total Cash Total in Kind	Total
Economic stimulus package - Development of MgB2 wires		Cash in Kind	0	0	24'231	30'000	0	124'549	0	178'780	178'780
Economic stimulus package - Neutron optical devices for small samples		Cash in Kind	67'348	9'405	570	0	1'500	0	0	78'824	128'824
Techniques Know-How		Cash in Kind	2'477'558	495'512	0	120'000	0	511'201	0	3'604'271	3'629'271
			25'000	0	0	0	0	0	0	25'000	
Economic stimulus package - Electrochemical sensors with higher resolution	Cors Jorge	Cash in Kind	0	0	51'155	2'655	0	6'000	0	59'810	125'843
			66'033	0	0	0	0	0	0	66'033	
Project 8 - Cold atomic gases as novel quantum simulators for condensed matter	Blatter Johann; Esslinger Tilman; Giamarchi Thierry; Sigrist Manfred; Troyer Matthias	Cash in Kind	3'561'793	114'583	100'000	150'000	92'500	142'891	0	4'161'766	5'286'771
			1'125'005	0	0	0	0	0	0	1'125'005	
Project 5 - Novel electronic phases in strongly correlated electron systems	Baeriswyl Dionys; Blatter Johann; Giannini Enrico; Kenzelmann Michel; Sigrist Manfred; Troyer Matthias; Van der Marel Dirk	Cash in Kind	2'681'938	75'723	96'000	79'500	57'000	47'484	0	3'037'645	4'139'781
			1'102'137	0	0	0	0	0	0	1'102'137	
Project 3 - Electronic materials for energy systems and other applications	de Rooij Nico; Decroux Michel; Fischer Øystein; Kenzelmann Michel; Renner Christoph; Triscone Gilles; Triscone Jean-Marc; Yvon Klaus	Cash in Kind	7'860'231	586'404	80'000	529'800	66'500	1'958'775	0	11'081'709	13'117'326
			2'035'617	0	0	0	0	0	0	2'035'617	

Project	Group leader / Research group	Cash	Gross salaries	Social charges	Equipment	Consumables	Travel	Miscellaneous	Credit	Total Cash Total in Kind	Total
Project 4 - Electronic properties of oxide superconductors and related materials	Baeriswyl Dionys; Batlogg Bertram; Bernhard Christian; Fischer Øystein; Giamarchi Thierry; Giannini Enrico; Karpinski Janusz; Keller Hugo; Mesot Joël; Morenzoni Elvezio; Niedermayer Christoph; Sigrist Manfred; Van der Marel Dirk	Cash	6'732'373	403'036	144'000	336'000	149'200	310'609	0	8'075'218	10'379'934
		in Kind	2'304'716	0	0	0	0	0	0	0	2'304'716
Project 1 - Novel phenomena at interfaces and in superlattices	Aebi Philipp A.; Bernhard Christian; Giamarchi Thierry; Giannini Enrico; Keller Hugo; Morenzoni Elvezio; Morpurgo Alberto; Niedermayer Christoph; Paruch Patrycja; Sigrist Manfred; Triscone Jean-Marc; Willmott Philip	Cash	3'323'170	211'998	105'000	185'000	64'200	420'741	0	4'310'109	6'111'032
		in Kind	1'800'923	0	0	0	0	0	0	0	1'800'923
Equipment Geneva		Cash	0	0	1'444'757	0	0	299'993	0	1'744'750	1'769'750
		in Kind	25'000	0	0	0	0	0	0	25'000	
Project 7 - Electronic materials with reduced dimensionality	Aebi Philipp A.; Degiorgi Leonardo; Fischer Øystein; Forro Laszlo; Giamarchi Thierry; Griioni Marco	Cash	4'753'601	84'136	615'000	520'000	100'200	174'427	0	6'247'364	7'555'728
		in Kind	1'308'364	0	0	0	0	0	0	0	1'308'364

Project	Group leader / Research group	Cash in Kind	Gross salaries	Social charges	Equipment	Consumables	Travel	Miscellaneous	Credit	Total Cash Total in Kind	Total
Project 2 - Materials for future electronics	Batlogg Bertram; Büttiker Markus; Forro Laszlo;	Cash	4753'103	236'620	112'000	428'800	76'000	124'601	0	5731'123	7763'690
	Giamarchi Thierry; Morpurgo Alberto; Paruch Patrycja; Renner Christoph; Sigrüst Manfred; Triscone Jean-Marc; Van der Marel Dirk	in Kind	2032'567	0	0	0	0	0	0	2032'567	
Project 6 - Magnetism and competing interactions in bulk materials	Forro Laszlo; Giamarchi Thierry; Kenzelmann Michel; Mesot Joëli; Milla Frederic; Niedermayer Christoph; Renner Christoph; Staub Urs; Troyer Matthias	Cash in Kind	3'663'104 1'861'758	88'475 0	75'000 0	231'800 0	202'261 0	509'465 0	0 0	4770'104 1'861'758	6'631'863
	Total		57'404'605	3'015'320	2'938'204	3'286'237	810'531	5'380'249	0		74'763'095

11.5 Comments on finances

The present list extracted from NIRA 2.0 shows the overall financial situation and gives a global picture close to reality. However, the finance of the individual projects as they appear for Year 9 is far from reality. We have no real means of understanding why this discrepancy occurs. However, we suspect that this is linked to the extremely complex manner in which NIRA 2.0 collects the financial data.

Please note that the problem is not that MaNEP does not have full control of the financial situation. Using our traditional and very efficient tools we have all the necessary financial information. We are able to produce an overview of the situation for the SNSF if requested. The problem resides in the fact that the SNSF requires us to report financially through NIRA 2.0, which we have to do in addition to our standard accounting systems which function well and give the necessary control.

The transition from NIRA to NIRA 2.0 implies an increase of an order of magnitude in complexity and this change has hit us fully for this report. Combined with the large number of new researchers in MaNEP, it has resulted in a situation in which there was not enough time between completion of the financial report for Year 8 and the establishment of the present report to verify all the data in NIRA 2.0.

In fact, MaNEP's administrative manager has been working almost 100% of her time on NIRA 2.0 since September on the accounting report Year 8. She has been working on the




present report since February. Within this process she has also been helping SNSF to find numerous structural errors in the version which was released last autumn. The administrative manager has many other tasks related to the organization including research, meetings, events and human resources etc. which have unfortunately been neglected during this time. Therefore we cannot continue to run MaNEP in this way and the only possibility in order to comply with the SNSF's request for using NIRA 2.0 is to search for a full time employee who would be able to start in May. The employee's job will be to keep the MaNEP NIRA 2.0 file up to date. We propose then to submit a corrected version as soon as this person will be able to be trained on NIRA 2.0 and has had the possibility of making the necessary corrections to the intermediate report.

This difficulty has another aspect. That is, that NIRA 2.0 asks for a huge amount of detail from the persons paid by the self-funding groups which put an enormous strain on MaNEP members around Switzerland. In Phase III each group leader receives on average CHF 40'000 per year. This is much less than the amount the same members receive from other funding sources who do not ask for the same detailed information. This situation is clearly a factor that will discourage MaNEP members from staying within the network. There should be a balance between the amount distributed and the administrative effort requested.





























12 Appendix: milestones of the MaNEP projects

The tables of milestones allow one to follow the time evolution of MaNEP scientific activities. The tables below are drawn from the situation given in the MaNEP Phase III Proposal and display the changes for Year 9.

Color code

Milestones unchanged since the Proposal	
Milestones added this year	
Milestones suppressed this year	

Project 1: Novel phenomena at interfaces and in superlattices

	Milestones	Year 9	Year 10	Year 11	Year 12
1.	Conducting interfaces				
	Growth and characterization of oxide interfaces (LaAlO ₃ /SrTiO ₃) [Triscone, Willmott, Niedermayer]				
	Study of the electronic properties of conducting oxide interface systems (transport properties) [Jaccard, Triscone, van der Marel]				
	Structure of LAO/STO interface [Aebi, Willmott]				
	Control of interface conductivity by interface doping [Triscone, Willmott]				
	Fabrication of novel 2D electron gases not based on SrTiO ₃ [Triscone, Willmott]				
	Structural studies using SXRD on the SC interface between under- and overdoped LSCO [Willmott]				
	Optical probes of metallic interface states in oxide heterostructures [Bernhard, van der Marel]				

	Milestones (Project 1, continued)	Year 9	Year 10	Year 11	Year 12
	<p>Oxygen diffusion studies in thin films [Niedermayer]</p> <p>Electronic properties of ¹⁸O exchanged interfaces [Niedermayer]</p> <p>Resistivity and Hall effect of the LAO/STO interface in pressurized liquid [Jaccard, Triscone]</p> <p>Multi-probe investigation of the LAO/STO interface in various pressure media [Jaccard, Triscone]</p> <p>Aspects of mechanisms [Sigrist]</p> <p>Aspects of non-centrosymmetry [Sigrist]</p> <p>Investigate the atomic environment at surfaces and interfaces close to the surface [Aebi, Triscone]</p> <p>PES/ARPES of oxide interfaces [Grioni, Triscone]</p> <p>RIX of interfaces and superlattices [Grioni, Triscone]</p> <p>Spectroscopic studies (Raman, optical studies) [Niedermayer]</p> <p>Magneto-transmission in the THz range [van der Marel, Triscone]</p>	<p>Grey</p> <p>Grey</p> <p>Grey</p> <p>Grey</p> <p>Grey</p> <p>Grey</p> <p>Grey</p> <p>Grey</p> <p>Grey</p> <p>Grey</p> <p>Yellow</p>	<p>Grey</p> <p>Grey</p> <p>Grey</p> <p>Grey</p> <p>Grey</p> <p>Grey</p> <p>Grey</p> <p>Yellow</p> <p>Grey</p> <p>Grey</p> <p>Grey</p>	<p>Grey</p> <p>Grey</p> <p>Green</p> <p>Grey</p> <p>Green</p> <p>Grey</p> <p>Green</p> <p>Grey</p> <p>Grey</p> <p>Grey</p> <p>Grey</p>	<p>Grey</p> <p>Grey</p> <p>Grey</p> <p>Green</p> <p>Grey</p> <p>Grey</p> <p>Grey</p> <p>Grey</p> <p>Grey</p> <p>Grey</p> <p>Grey</p> <p>Green</p> <p>Grey</p> <p>Grey</p>
2.	Coupling of instabilities at insulating interfaces				
	<p>Growth and characterization of oxide interfaces (PbTiO₃/SrTiO₃ and novel systems) [Aebi, Paruch Triscone]</p> <p>Structural studies using SXRD of improper FE lattices [Triscone, Willmott]</p> <p>XPD measurement of tetragonality in ultra-thin PTO films as a function of temperature [Aebi, Triscone]</p> <p>Investigate the atomic environment at surfaces and interfaces close to the surface [Aebi, Triscone]</p> <p>Study of the electronic properties of insulating oxide systems (dielectric, ferroelectric, multiferroic) [Paruch, Triscone]</p>	<p>Grey</p> <p>Grey</p> <p>Grey</p> <p>Grey</p> <p>Grey</p>	<p>Grey</p> <p>Grey</p> <p>Green</p> <p>Grey</p> <p>Grey</p>	<p>Grey</p> <p>Grey</p> <p>Grey</p> <p>Grey</p> <p>Grey</p>	<p>Grey</p> <p>Grey</p> <p>Grey</p> <p>Grey</p> <p>Grey</p>

	Milestones (Project 1, continued)	Year 9	Year 10	Year 11	Year 12
3.	Magnetic/superconducting interfaces				
	μ SR and optical experiments on Y123/Pr123 [Fischer, Morenzoni, Bernhard , Keller]				
	μ SR experiments in 214 superlattices (Interface superconductivity and magnetism) [Morenzoni, Keller]				
	Experiments on LSCO tri- and bilayers (study of proximity effects in UD and OD layers) [Morenzoni, Keller]				
	Magnetic interface states in oxide heterostructures from paramagnetic materials [Bernhard]				
	Spectroscopic studies (Raman, optical studies) [Niedermayer, Bernhard]				
	Study electronic properties at magnetic/superconducting interfaces close to the surface [Aebi, Bernhard]				
	Superconductivity induced changes in magnetic states of high T_c -manganite multilayers [Bernhard, Niedermayer]				
4.	Electronic properties of organic charge transfer interfaces				
	Identification of new materials for charge-transfer interfaces [Morpurgo]				
	Magneto-transmission in the THz range [Morpurgo, van der Marel]				
	Low-temperature transport through metallic charge transfer interfaces [Morpurgo]				
5.	Domain walls in ferroelectrics/multiferroics: a model interface system				
	Domains with internal degrees of freedom [Giamarchi, Paruch]				
	Response to oscillatory fields [Giamarchi, Paruch]				
	AFM studies of magnetoelectric coupling in nanocomposite multiferroic materials [Paruch, Triscone]				
	Nanoscale variable temperature studies of ferroelectric domain walls in $\text{PbZr}_{0.2}\text{Ti}_{0.8}\text{O}_3$ [Paruch, Triscone]				

	Milestones (Project 1, continued)	Year 9	Year 10	Year 11	Year 12
	Nanoscale variable temperature studies of ferroelectric domain walls in BiFeO ₃ [Paruch]				
	Effects of atmosphere and surface chemical modification on ferroelectric polarization [Aebi, Paruch]				
6.	Crystal growth of new substrates with tuned structural and physical properties				
	Preliminary growth experiments of SrTiO ₃ crystals with the existing equipment [Giannini]				
	Growth of various oxide substrates with the improved Czocharlski technique [Giannini]				
	Development of new substrates with tuned structural and electronic properties [Giannini]				

Project 2: Materials for future electronics

	Milestones	Year 9	Year 10	Year 11	Year 12
1.	Oxide heterostructures				
	Nano-patterned top gates on LaAlO ₃ /SrTiO ₃ heterostructures [Triscone, Morpurgo]				
	Electrostatically controlled Josephson junctions [Triscone, Morpurgo]				
	Interplay of superconductivity and confinement in LaAlO ₃ /SrTiO ₃ heterostructures [Triscone, Morpurgo]				
	Nanostructures for the investigation of spin-orbit interaction [Triscone, Morpurgo]				
	Atomic force microscopy writing of nanostructures at the LaAlO ₃ /SrTiO ₃ interface [Paruch, Triscone]				
	Atomic force microscopy reading (conducting AFM and capacitive) of nanostructures at the LaAlO ₃ /SrTiO ₃ interface [Paruch, Triscone]				
	Transport properties of AFM written nanostructures at the LaAlO ₃ /SrTiO ₃ interface at room temperature [Paruch, Triscone]				

	Milestones (Project 2, continued)	Year 9	Year 10	Year 11	Year 12
	Low temperature investigations of AFM written nanostructures at the LaAlO ₃ /SrTiO ₃ interface [Paruch, Triscone]				
2.	Carbon based materials				
2.1	Graphene				
	Optimisation of sample preparation and atomic scale imaging of single layer and bilayer graphene [Renner]				
	Implementation of combined AFM/STM imaging/spectroscopy on graphene [Renner]				
	Structural and spectroscopic characterisation of few-layer graphene [Renner]				
	Spectroscopy on doped/intercalated few-layer graphene devices [Renner]				
	Edge-state tunneling spectroscopy of single layer graphene [Renner]				
	Spin dependent tunneling spectroscopy of graphene [Renner]				
	Nature of transport gap in graphene nano-ribbons [Morpurgo]				
	Magnetoresistance of graphene nano-ribbons [Morpurgo]				
	Comparison of transport in few-layer graphene of different thickness [Morpurgo]				
	Transport through suspended graphene [Morpurgo]				
	Magnetotransport in high-mobility graphene [Morpurgo]				
	Transport through graphene on high-k dielectrics or ferroelectric substrates [Paruch, Morpurgo, Triscone]				
	Gate-dependent spectroscopy of bi-layer graphene [van der Marel]				
	Spectroscopy of few-layer graphene in different dielectric environments [van der Marel]				

Milestones (Project 2, continued)		Year 9	Year 10	Year 11	Year 12
	<p>Magneto-optical spectroscopy of epitaxial graphene [van der Marel]</p> <p>ESR on exfoliated graphene [Forró]</p>				
2.2	<p>Carbon Nanotubes</p> <p>Ferroelectric field-effect modulation of carbon nanotube resistivity [Paruch]</p> <p>Controlled manipulation of carbon nanotubes on ferroelectric substrates [Paruch]</p> <p>Non-destructive AFM measurements of polarization around carbon nanotubes [Paruch]</p> <p>Mechanism of domain switching and growth using carbon nanotubes [Paruch]</p>				
2.3	<p>Organic semiconductors</p> <p>New molecular materials for the study of intrinsic transport [Morpurgo]</p> <p>Mechanisms of threshold voltage shift and drift [Morpurgo]</p> <p>Low-temperature transport measurements [Morpurgo]</p> <p>Comparison of intrinsic transport properties in different organic semiconductors [Morpurgo]</p> <p>Infrared spectroscopy of organic semiconductor interfaces [van der Marel]</p>				
3.	<p>Theory</p> <p>Unpaired spins and Aharonov-Bohm effect: Scattering formalism [Büttiker]</p> <p>Unpaired spins and Aharonov-Bohm effect: Results for graphene [Büttiker]</p> <p>Edge conductance in gapped bilayer graphene [Büttiker]</p>				

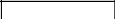
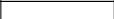
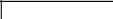

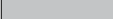












Milestones (Project 2, continued)	Year 9	Year 10	Year 11	Year 12
Topological properties of gapped bilayer graphene [Büttiker]				
Shot-noise and pre-formed pairs: High T_c -normal junction [Büttiker]				
Shot-noise and pre-formed pairs: Analysis of shot noise [Büttiker]				
Effect of electron-phonon coupling on transport through graphene nano-ribbons [Sigrist]				
Ordered phases in heterostructures of correlated electrons [Sigrist]				
Transport properties of heterostructures of correlated electrons [Sigrist]				
Exploring new directions in heterostructures of correlated electrons [Sigrist]				
Luttinger liquids with an external bath [Giamarchi]				

Project 3: Electronic materials for energy systems and other applications

Milestones	Year 9	Year 10	Year 11	Year 12
1. Applied superconductivity				
Development of a new method to fabricate MgB ₂ wires with higher critical current [Flükiger]				
Development of lengths of MgB₂ wires [Flükiger]				
Investigation of relaxation in inhomogenous YBCO [Flükiger]				
Study of contact resistance between coated conductors and other superconductors [Flükiger, Bruker]				
Development and calibration of an experimental setup for the measurement of thermal conductivity of coated conductors [Decroux]				

	Milestones (Project 3, continued)	Year 9	Year 10	Year 11	Year 12
	Study of the influence of the substrate thickness on the thermal behavior of coated conductors [Decroux] Measurement of propagation velocities on coated conductors [Decroux]				
2.	Oxides for energy harvesting				
	Optimization and full characterization of ultra-thin SrTiO ₃ epitaxial buffer layers on silicon [J.-M. Triscone, G. Triscone] Growth of epitaxial Pb(Zr,Ti)O ₃ , 50/50, with high piezoelectric coefficient on silicon with metallic oxide electrodes [J.-M. Triscone, G. Triscone] Growth of epitaxial PMN-PT on silicon with giant piezoelectric response [J.-M. Triscone, G. Triscone] Realization and mechanical and electrical characterization of membranes based on fully epitaxial oxide materials [J.-M. Triscone, N. de Rooij] Realization and characterization of nano -beams based on fully epitaxial oxide materials [J.-M. Triscone, N. de Rooij] Realization of an energy harvesting demonstrator based on piezoelectric materials [J.-M. Triscone, N. de Rooij] Investigation of the thermoelectric properties of the 2-DEG electron gas at the LaAlO ₃ /SrTiO ₃ interface [J.-M. Triscone] Investigation of the thermoelectric properties of LaAlO ₃ /SrTiO ₃ superlattices [J.-M. Triscone] Investigation of the thermoelectric properties of thin doped SrTiO ₃ layers on silicon [J.-M. Triscone] Identification of new promising thermoelectric oxides and synthesis of performing polycrystalline thermoelectric materials of a new generation [Weidenkaff] Modeling of energy conversion based on data from the material specification [Weidenkaff] Synthesis of single crystalline materials [Weidenkaff]	[Grey] [Grey] [Grey] [Grey] [Grey] [Green] [Green] [Green] [Green] [Green] [Green] [Grey] [Grey] [Grey] [Grey] [Grey] [Grey] [Green] [Green]	[Grey] [Grey] [Grey] [Grey] [Grey] [Grey] [Grey] [Grey] [Grey] [Grey] [Grey] [Grey] [Grey] [Grey] [Grey] [Grey] [Grey] [Grey] [Grey]	[Grey] [Grey] [Grey] [Grey] [Grey] [Grey] [Grey] [Grey] [Grey] [Grey] [Grey] [Grey] [Grey] [Grey] [Grey] [Grey] [Grey] [Grey] [Grey]	[Grey] [Grey] [Grey] [Grey] [Grey] [Grey] [Grey] [Grey] [Grey] [Grey] [Grey] [Grey] [Grey] [Grey] [Grey] [Grey] [Grey] [Grey] [Grey]

	Milestones (Project 3, continued)	Year 9	Year 10	Year 11	Year 12
	<p>Evaluation of candidate materials and decision about which to use for the p and n type legs of a ceramic converter [Weidenkaff]</p> <p>Assembling of a first generation oxide thermoelectric converter based on the news materials [Weidenkaff]</p> <p>Second generation thermoelectric convertor as demonstrator [Weidenkaff]</p>				
3.	Application of artificial superlattices				
	<p>Investigation of the growth process of Ni/Ti layers to achieve lower roughness as well as an improved homogeneity of the layers [Kenzelmann]</p> <p>Systematic characterization of various substrate materials in order to find a tool for selecting substrates experiencing the required surface quality [Kenzelmann]</p> <p>Developing polishing processes to manufacture metal substrates with a very low roughness [Kenzelmann]</p> <p>Improvement of polarizing supermirrors, i.e. extending the critical angle of reflection [Kenzelmann]</p> <p>Develop Co-free, remanent magnetic layers for polarizing supermirrors [Kenzelmann]</p>				
4.	Hydrogen detectors and other sensors				
	<p>Setup of experimental tools for conductance measurements in H₂ atmosphere [Yvon, Fischer/Cors]</p> <p>Identification of hydrogen sensitive intermetallic compounds, fabrication of thin films [Yvon, Fischer/Cors]</p> <p>Performance validation [Asulab, Yvon, Fischer/Cors]</p> <p>Design of the resistive detector electronics layout and fabrication of first prototype devices [Asulab, Yvon, Fischer/Cors]</p>				

Milestones (Project 3, continued)	Year 9	Year 10	Year 11	Year 12
Benchmarking against the performance of commercial devices [Asulab, Yvon, Fischer/Cors]				
Fine tuning of device design [Asulab]				
Fabrication of a large number of devices and testing/homologisation at sensor performance facility (NL) [Asulab, Yvon, Fischer/Cors]				
Study and optimization of cantilever surface passivation for optimal piezo-resistive effect. Functional cantilever using piezo-resistive deflection readout for AFM [Renner]				
Deflection and torsion mode AFM cantilever using piezo-resistive readout [Renner]				
Development and optimization of one-step hydrothermal approaches to functionalized oxidic nanorods and nanowires for sensor applications: W/Mo-oxide nanorods and Bi ₂ O ₃ /SnO ₂ composite nanowires as major preparative targets [Patzke]				
Setup of gas sensor construction [Patzke, Phasis, Fischer/Cors]				
Preparative exploration of advanced ternary and higher oxide systems with sensor activity, e.g. ZnGa ₂ O ₄ -based spinel nanorods and targeted modification of MoO ₃ nanowires [Patzke, Phasis, Fischer/Cors]				
Development of market-ready gas phase sensors with special emphasis on new portable devices for environmental applications and industrial process control [Patzke, Phasis, Fischer/Cors]				
Development of bio-sensors operating with nanowires: technical setup [Patzke, Phasis, Fischer/Cors]				
Industrial implementation and marketing optimization of the gas sensor devices [Patzke, Phasis, Fischer/Cors]				
Fabrication of portable bio-sensors based on oxidic nanomaterials (QCM and FET techniques) for commercial bio-medicinal applications [Patzke, Phasis, Fischer/Cors]				

	Milestones (Project 3, continued)	Year 9	Year 10	Year 11	Year 12
5.	New surface treatments for microcomponents				
	Experimental investigation of compounds suitable for chemical marking on stainless steel, brass, gold and platinum [Fischer/Cors, Phasis, Vacheron Constantin]	■			
	Definition of the identification tools for reliable identification of the microscopic marks [Fischer/Cors, Phasis, Vacheron Constantin]	■			
	Design and construction of an automatic marking prototype [Fischer/Cors, Phasis, Vacheron Constantin]		■		
	Experimental validation of the ability to mark 20'000 parts/year [Fischer/Cors, Phasis, Vacheron Constantin]	■	■		
	Research of visually attractive surface effects using the marking technology at a macroscopic scale [Fischer/Cors, Phasis]	■	■	■	
	Selective coating of watch cases and other parts with transition metal carbides and nitrides. [Fischer/Cors, Phasis]	■	■	■	
	Implementation and measurement of tribological nanomaterial-based coatings on selected substrates [Fischer/Cors, Phasis]		■	■	■

Project 4: Electronic properties of oxide superconductors and related materials

	Milestones	Year 9	Year 10	Year 11	Year 12
1.	Optical conductivity, ARPES, RIXS, STM, muons, neutrons studies of cuprate superconductors				
1.1	What is the nature of the pseudo-gap?				
	ARPES studies of SC and pseudo-gaps in $(\text{La,Nd})_{2-x}\text{Sr}_x\text{CuO}_4$ [Mesot]	■	■	■	
	Muon spectroscopy and influence of isotope substitution on the gap in cuprate high T_c [Keller]	■	■		
1.2	How does the spectrum of collective spin excitations evolve from anti-ferromagnetic state to the high-T_c phase?				
	STM studies of strongly overdoped Bi2201 [Fischer]	■	■	■	

	Milestones (Project 4, continued)	Year 9	Year 10	Year 11	Year 12
	STM studies of tunneling asymmetry in $Y_{1-x}Pr_xBa_2Cu_3O_7$ [Fischer]				
	Resonant inelastic soft X-ray scattering (RIXS) at the SLS [Grioni]				
1.3	What is the mechanism of superconductivity pairing in the cuprates: is there a pairing glue?				
	Calculation of spin susceptibility from ARPES spectral function [Mesot]				
	Electron-boson scattering in optical- and single particle spectral functions [van der Marel]				
2.	New materials and crystal growth				
2.1	Iron pnictide high-T_c superconductors				
	STM studies of iron-pnictides [Fischer]				
	Processing and crystal growth of Sb-based ternary and quaternary pnictides [Giannini]				
	Crystal growth of superconducting Fe-chalcogenides and related materials [Giannini]				
	Processing and growth of new binary pnictides with a tetrahedral structure [Giannini]				
	Crystal growth of $LnFeAsO$ and $A(Me)As_2Fe_2$ [Karpinski]				
	Substitutions in $LnFeAsO$ and $A(Me)As_2Fe_2$ [Karpinski]				
	Muon spectroscopy of the multiple-gap behavior in pnictide superconductors [Morenzoni, Keller]				
	Optical investigations of pnictides [van der Marel]				
2.2	Other non-cuprate high-T_c superconductors				
	Development of hydrothermal growth technique and application to the Sr_2VO_4 system [Giannini]				
	Searching for new superconductors [Karpinski]				

	Milestones (Project 4, continued)	Year 9	Year 10	Year 11	Year 12
	Optical investigations of Sr ₂ VO ₄ [van der Marel]				
2.3	Cuprate high-<i>T_c</i> superconductors Growth of TI-based cuprates [Giannini] Cuprates with reduced lattice parameter [Jaccard] investigations on the 122 FeAs compounds [Degiorgi] Interaction of localized <i>f</i> electrons with superconductivity [Morenzoni]				
3.	Microscopic theories for cuprate superconductivity and novel superconductors				
3.1	Variational many-body wavefunctions Coexistence of hot spots and superconductivity [Baeriswyl] Superconductivity and ferromagnetism (multilayers), superfluid density [Baeriswyl]				
3.2	The chiral <i>p</i>-wave (spin triplet) state of Sr₂RuO₄ study of the 3K phase in Sr ₂ RuO ₄ [Sigrist] study of Josephson effect in Sr ₂ RuO ₄ [Sigrist] study of Sr ₂ RuO ₄ in magnetic field [Sigrist] study of exotic vortices in Sr ₂ RuO ₄ [Sigrist]				

Project 5: Novel electronic phases in strongly correlated electron systems

	Milestones	Year 9	Year 10	Year 11	Year 12
1.	Unconventional superconductivity in heavy fermion metals				
1.1	Superconductivity and magnetism				
	Study of influence of FFLO phase of CeCoIn ₅ on flux lattice of fields along <i>c</i> -axis [Kenzelmann]	█			
	Symmetry of flux lattice in CeCoIn ₅ for fields in basal plane (in Q-phase) [Kenzelmann]		█		
	Form factor of flux lattice in CeCoIn ₅ for fields in the basal plane [Kenzelmann]			█	
	Microscopic measurements of magnetism in superconducting phase [Kenzelmann]	█	█	█	
	Temperature dependence of the flux lattice in CeCoIn ₅ for fields in the basal plane [Kenzelmann]	█			█
	Theoretical discussion of Q-phase of CeCoIn ₅ [Sigrist]	█	█		
	Investigation of CeRhIn ₅ [Jaccard, Morenzoni]		█	█	
1.2	Superconductivity and valence fluctuations				
	Hall and Nernst effect in CeCu ₂ Si ₂ [Jaccard]	█	█		
	Investigation of CeNi ₂ Ge ₂ [Jaccard]			█	█
1.3	Non-centrosymmetric superconductors				
	Phenomenology and microscopic theory [Sigrist]	█	█	█	
	Processing of polycrystal and crystal growth of CeCo(Ge,Si) ₃ [Giannini]	█	█		
1.4	Vortex matter in superconductors				
	Study of pinning-depinning transition [Blatter]	█	█		

	Milestones (Project 5, continued)	Year 9	Year 10	Year 11	Year 12
2.	Novel quantum phases and phase transitions in 4f- and 5f-electron systems				
	NMR under pressure and at low temperatures on Ce intermetallics [Ott]				
	Optical studies of (Eu,Ba)Si [Degiorgi]				
	Optical studies on the hidden phase of URu ₂ Si ₂ [van der Marel]				
3.	Magnetic, optical and transport properties in TM Si/Ge and Bi				
	Optical studies of Co-doped FeSb ₂ [Degiorgi]				
	Growth of 3d- and 4d-TM silicides [Giannini]				
	High-pressure synthesis of TM germanides [Giannini]				
	Optical and transport studies of TM silicides [van der Marel]				
	Optical studies of TM germanides [van der Marel]				
	Theoretical discussion of transition metal silicides/germanides [Sigrist]				
	Sb-tuning in Bi _{1-x} Sb _x crystals [Giannini]				
	Optical studies of topological band-edge insulators [van der Marel]				
4.	Theoretical and computational developments for strongly correlated electrons				
	Characterization of crossover phenomena [Baeriswyl]				
	Competition between (positional) disorder and (electron-electron) interaction [Baeriswyl]				
	Development of new QMC algorithms [Troyer]				

Project 6: Magnetism and competing interactions in bulk materials

Milestones	Year 9	Year 10	Year 11	Year 12
1. Spin chains and ladders				
Excitations experimental [Rønnow, Mesot, Ott]	█	█	█	
NMR/NQR on low-dimensional systems – shifted from Project 5 [Mesot, Ott]	█		█	
Theoretical [Giamarchi, Troyer]	█	█	█	
Quenched disorder [Zheludev]		█	█	
μSR [Morenzoni, Zheludev]		█	█	
1D spin chains (KTi(SO ₄)H ₂ O, NaV ₂ O ₄) – shifted from paragraph 3 [Degiorgi, Rønnow]	█	█	█	
2. Spin-dimer physics				
Exotic phases in Shastry-Sutherland model [Mila, Troyer]	█	█	█	
High-pressure studies of SrCu ₂ (BO ₃) ₂ [Rønnow]	█	█		
Frustration effects in Han Purple [Mila, Rønnow]	█	█		
3. Spin-liquids				
Quadrupolar order in NiGaS ₄ [Mila]	█			
Kagome spin-1/2 theory [Mila]	█	█	█	█
Kagome spin-1/2 experimental realizations [Rønnow]	█			
4. Multiferroics and helimagnets				
Resonant X-ray diffraction [Staub]	█	█	█	█

	Milestones (Project 6, continued)	Year 9	Year 10	Year 11	Year 12
	Magnetic structures in multiferroic and magneto-electric model materials [Kenzelmann]				
	Topological phases in helimagnets [Staub, Zheludev]				
5.	Magneto-resistive materials				
	STM on perovskite manganites [Fischer]				
	Spin-polarized STM on bi-layer manganites [Renner]				
6.	Resonant inelastic X-ray scattering				
	Theory of light scattering in frustrated magnets [Mila]				
	Experiments on collective excitations [Rønnow]				

Project 7: Electronic materials with reduced dimensionality

	Milestones	Year 9	Year 10	Year 11	Year 12
1.	Investigation of the electronic properties of TiSe₂ and related dichalcogenides				
	T dependence of ARPES in TiSe ₂ [Aebi]				
	ARPES study of intercalated TiSe ₂ [Aebi]				
	High pressure study of TiSe ₂ and related compounds [Forró]				
2.	Spectroscopic and structural investigation of RTe₃				
	Optical spectroscopy of RTe ₃ [Degiorgi]				
	X-ray and neutron scattering measurements of rare-earth tritellurides [Rønnow]				

	Milestones (Project 7, continued)	Year 9	Year 10	Year 11	Year 12
3.	ESR, ARPES and transport study of organic charge transfer salts				
	ESR and transport study of ET-based salts [Forró, Giamarchi, Groni, Mila]				
4.	Study of quasi-1D vanadates				
	ARPES and RIXS of BaVS ₃ [Groni]				
	Magnetic measurements of BaVS ₃ [Forró, Ott]				
5.	Study of other low-dimensional materials				
	ESR study of quasi 1-D organic conductors [Forró, Giamarchi]				
	Transport and STM study of Chevrel phases [Fischer]				
	Spin and charge degrees of freedom in Sr ₁₄ Cu ₂₄ O ₄₁ [Rønnow, Mila, Giannini, Degiorgi]				

Project 8: Cold atomic gases as novel quantum simulators for condensed matter

	Milestones	Year 9	Year 10	Year 11	Year 12
1.	Model Systems and novel phases				
	Strongly correlated quantum states of cold atoms and light [Gritsev]				
	Phase diagram of two-dimensional dipolar gases on a square- lattice substrate potential [Blatter]				
	Observation of anti-ferromagnetic order in an optical lattice [Esslinger]				
	Quantitative comparison between experiment and theory on spin ordering [Esslinger]				
	Study of the two-dimensional Hubbard model in the low entropy regime [Esslinger]				
	Numerical simulations of cold atomic systems [Troyer]				

	Milestones (Project 8, continued)	Year 9	Year 10	Year 11	Year 12
	<p>Equation of state of 3D Fermi gases [Troyer]</p> <p>Mott transition and antiferromagnetism in cold atomic gases [Giamarchi]</p> <p>Bose mixture [Giamarchi]</p>				
2.	Probe and Thermometry				
	<p>Validation of cold atomic systems [Troyer]</p> <p>Bragg spectroscopy [Giamarchi]</p>				
3.	Dynamics and novel Phases				
	<p>Nonequilibrium dynamics [Gritsev]</p> <p>Dynamics and strong correlation of condensates for precision measurements [Gritsev]</p> <p>Quantum phase transition and non-equilibrium dynamics of polaritons in an array of coupled QED cavities [Blatter]</p> <p>Non-equilibrium physics in the Mott-insulating phase [Esslinger]</p> <p>Disordered Bosonic and Fermionic systems [Giamarchi]</p>				